A Feedforward Tracking Filter

Aumen Kwok-keung Lee

A Thesis

in

The Department

of

Electrical Engineering

Presented in Partial Fulfillment of the Requirements
for the Degree of Master of Engineering at
Concordia University
Montréal, Québec, Canada

December 1984

ABSTRACT

A Feedforward Tracking Filter

Aumen Kwok-keung Lee

A feedforward tracking filter (FTF) adopting two matched (identical) bandpass filters (BPF) and feedforward control to provide fast and reliable acquisition, phase and frequency tracking ability is proposed. As opposed to feedback tracking filters, the FTF is unconditionally stable, free from hang-up and only needs a unity gain. Various analog and digital BPF configurations are used in the analysis of the continuous and discrete FTF transient and steady-state behaviour. The results show that for the same noise bandwidth, the FTF using two identical double-tuned BPF's provides the best performance, and that the acquisition is not degraded by inter-burst-interference (IBI). Acquisition of the discrete FTF can be achieved in no longer than twice the delay of the digital BPF. Symmetrical transversal filters with apodized weight coefficients achieve the fastest acquisition. The effect of the mis-matched BPF's on the tracking performance are studied analytically and experimentally.

To characterize the nonlinear FTF bandpass system, the spectrum and the signal-to-noise ratio (SNR) of the FTF upon the excitation of signal plus noise are investigated. The

experimental and theoretical results are in agreement, which show that tracking ability using feedforward compensation scheme is achieved at the expense of the SNR. The lowpass equivalent model of the FTF is strictly linear such that the phase noise performance of the FTF is found to have the same characteristics as that of the PLL.

Comparison of FTF with a PLL and an AFC loop indicates that FTF has superior frequency tracking performance and fast acquisition without being impaired by the hangup phenomenon. An illustrative application of the FTF to a coherent TDMA/QPSK carrier recovery circuit is presented.

ACKNOWLEDGEMENTS

I would like to express my deep gratitude to my thesis supervisors, Dr. Tho Le-Ngoc and Dr. Vijay K. Bhargava, for their invaluable assistance and constant guidance throughout this research, and for their advice and constructive criticism during the preparation of this thesis.

I would also like to express my appreciation to Mr. Michael Morris, Vice-president of Engineering of SR Telecom. Inc., for his interest and support.

I am grateful to the development engineers of SR Telecom. Inc., specially to Mr. Michel Roux and Mr. Claudio Lucente for their helpful discussions and assistance in obtaining the laboratory measurements.

I would also like to thank Miss Frances Woo for proof reading this thesis.

TABLE OF CONTENTS

LIST OF FIGURES

LIST OF TABLES

CHAPTER 1

INTRODUCTION

In coherent, synchronous communication systems, signals carrying information are usually transmitted with suppressed carrier for efficient use of transmitted power. The receiver must regenerate a properly phased local carrier for coherent demodulation. Otherwise the performance of the communication system will be degraded. In the worst case, the undesirable phase error between the local and regenerated carriers will cause loss of information. In practice, the regenerated carrier is accompanied with a large amount of noise, and its phase varies randomly in time. Therefore, circuitry or a tracking bandpass filter must be provided in the receiver to keep track of the change of this random, noisy input phase information. For this special purpose, the tracking bandpass filter is a narrowband bandpass filter with a constant phase response over a certain range of input frequency offset.

1.1 Tracking bandpass filters

Conventionally, the phase tracking ability is achieved by feeding back the output signal and comparing its phase to that of the input signal to produce an error signal which is, in turn, used to correct the output phase. Phase-locked loop (PLL) in Fig.1.1 is an example of a conventional tracking bandpass filter (BPF): the output of the phase detector

(PD) represents the phase difference (error) between the input and output signals. This phase error signal is filtered by a lowpass filter (LPF) and fed to drive a Voltage Controlled Oscillator (VCO) which generates a signal according to the magnitude of the error signal. By successively looping and correcting, the error signal will vanish and the VCO output phase will eventually equal the phase of the input signal. The characteristics of the loop filter has a considerable influence on the properties of the loop. The second order PLL with high gain active LPF is shown to have good steady-state tracking performance and narrow noise bandwidth [1,2].

It is well known that there is always a tradeoff between acquisition (pull-in) time and equivalent noise bandwidth of a tracking BPF. In the particular case of PLL, the pull-in time is inversely related to the bandwidth of the loop. Under a certain narrow bandwidth requirement, the PLL is too slow to respond (e.g. in the Time Division Multiple Access (TDMA) digital communication systems). Moreover, there is another significant problem associated with PLL if fast acquisition of a signal is a requirement. This problem is known as 'hang-up' which gives occasional prolonged phase transient and thus causes very long acquisition time [1,3].

The feedback configuration of the PLL may account for

the above drawbacks although the advantage of the feedback configuration has been extensively demonstrated [5]. Gardner in his report [4] has suggested the use of a high-Q single-tuned BPF centered at the nominal frequency of the input signal to achieve fast acquisition and solve the hang-up problem. However, the input frequency offset will cause changes in the phase difference between the input and output signals due to the steep slope of the phase response of the high-Q filter. An Automatic Frequency Control (AFC) loop has to be used to regulate the input frequency offset and resultant phase shift through the filter. An AFC using a high-Q BPF centered at the input nominal frequency w_o is shown in Fig.1.2. For an input frequency step, the phase difference between the input and output of the BPF produces an error signal to correct the VCO frequency. The modified VCO signal is then fed back to adjust the input frequency of the BPF to w_o. Simultaneously, the VCO signal is fed forward to maintain the constant phase difference of the input and output of the BPF.

Regarding this circuit (Fig.1.2), the high-Q filter is restricted to have total phase change less than π or 2π in order to have a desirable error signal characteristic with only one zero crossing at the center frequency w_o. The restriction arises from the periodic characteristic of the phase detector having zero crossing at every $k\pi$ of phase. Besides, the linearity of the phase response of the filter and the output characteristic of the phase detector are also

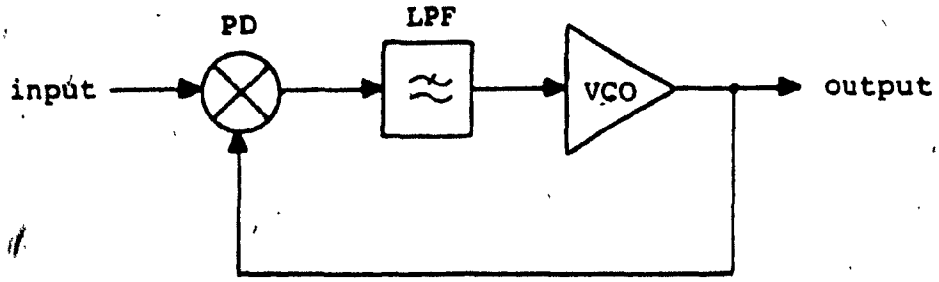

Fig. 1.1: Phase-locked Loop (PLL)

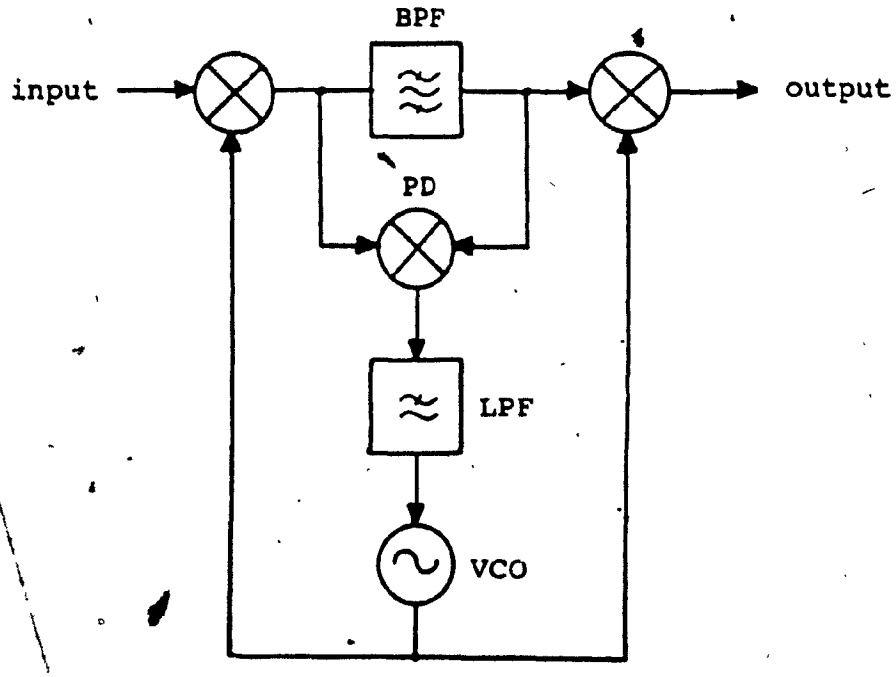

Fig. 1.2: AFC loop with high-Q BPF

required to give a linear characteristic of the error signal.

1.2 Feedforward Tracking Bandpass Filter

In essence, the conventional feedback correction scheme is adopted to obtain the tracking effect in both the PLL and AFC loop using high-Q BPF. In contrast to this 'feedback' approach, a novel approach of using 'feedforward' compensation scheme to attain the tracking ability is used in a quadrupler of TDMA/QPSK* demodulator [7]. It was shown that the feedforward approach can also achieve fast acquisition time and good tracking performance. The circuit used in [7] is designed particularly for the quadrupler configuration. Its application to other carrier recovery (CR) circuit using remodulator technique is hindered, and its increased cycle skipping rate introduced by the phase ambiguity of the divider in this circuit is also a problem. To extend the feedforward concept, a generalized Feedforward Tracking Bandpass Filter (FTF) shown in Fig.2.1 is proposed and studied in this thesis. FTF consists of two identical BPF's tuned at the nominal frequency of the input signal and two non-linear elements, namely, a doubler and a multipler. It will be shown that, in addition to the fast acquisition and good tracking performance, FTF is free from hang-up and from the restrictions found in the BPF with AFC.

---

* Quadrature Phase Shifting Keying (QPSK)

1.3 Scope of thesis

Following this introductory chapter, the basic operation of the FTF is explained and an equivalent baseband model of FTF is presented in Chapter 2.

The equivalent baseband model is used in Chapter 3 to investigate the transient behaviour of the FTF with phase and frequency step input signals. Various bandpass filter configurations are considered and compared in the investigation. Experiments are performed to verify the analytical results. The discussion of the phase transient due to the Inter-Burst-Interference are also included in Chapter 3.

The steady-state behaviour of the FTF is examined in Chapter 4. The effects of the mis-matched BPF's on the tracking performance is analytically and experimentally illustrated. The tradeoff between the bandwidth and steady-state/acquisition performance is presented.

In Chapter 5, the performance of the FTF in an additive white Gaussian noise environment is studied. An analytical evaluation of the spectrum of the FTF using ideal BPF's is given. The analytical results are verified by performing experiments with sharp surface-wave-acoustic (SAW) bandpass filters. The expressions of the input and output signal-to-noise ratio of the continuous and discrete FTF are derived. The effect of the phase noise on the FTF and the probability

of the phase error caused by the phase noise are studied. Finally, a brief discussion of the cycle skipping of the FTF is presented in Chapter 5.

In Chapter 6, the FTF is compared with other tracking filters such as a PLL and an AFC loop.

Chapter 7 describes an illustrative application of the FTF in the CR circuit of a coherent QPSK demodulator. The effect of the FTF on the bit error rate performance of the modulator/demodulator are experimentally investigated.

Finally, Chapter 8 contains the conclusion and suggestions for further study.

1.4 Research contributions

A generalized Feedforward Tracking Bandpass Filter (FTF) is proposed and studied in this thesis. The main theme of this thesis is to introduce a feedforward scheme which can provide superior performance than some schemes such as PLL and AFC loop, namely, faster acquisition, zero steady-state error for both phase and frequency step inputs, and no hang-up problem. The major contributions of our research can be summarized below:

* Investigation of the best type of BPF used in the feedforward compensation scheme in order to achieve

the fastest acquisition.

* Investigation of the phase and frequency tracking behaviour of the feedforward compensation scheme.

* Investigation of the nonlinear behaviour of the feedforward compensation scheme in an additive white Gaussian noise.

CHAPTER 2

GENERAL ANALYSIS OF FTF

2.1 Principle of operation

The basic operation of the FTF is different from that of the conventional feedback tracking BPF.

Refering to the Fig.2.1, a high-Q BPF (BPF1) centered at the nominal input frequency is used to filter the noise accompaning the input signal. The phase shift θ at the output of the BPF1 due to the input frequency offset is compensated by

* forwarding the frequency offset to another identical high-Q BPF (BPF2) to induce a total phase of 2θ,
* forwarding the frequency offset to a doubler to produce a phase shift of 2θ at twice the frequency of the signal, and
* subtracting the output phase of BPF2 from that of the doubler.

The input signal with unaltered phase is replicated at the output of the multiplier. From this scheme, the tracking ability, in effect, is obtained although the output is not fed back to track the input signal.

The linear phase characteristics of the BPF is not

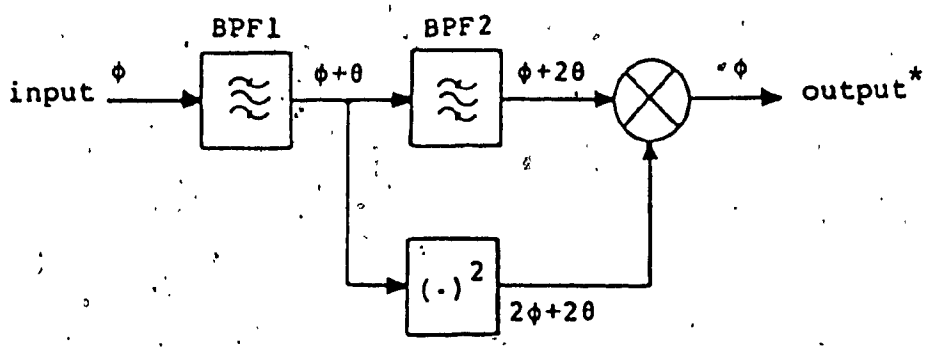

Fig. 2.1: Bandpass model of FTF

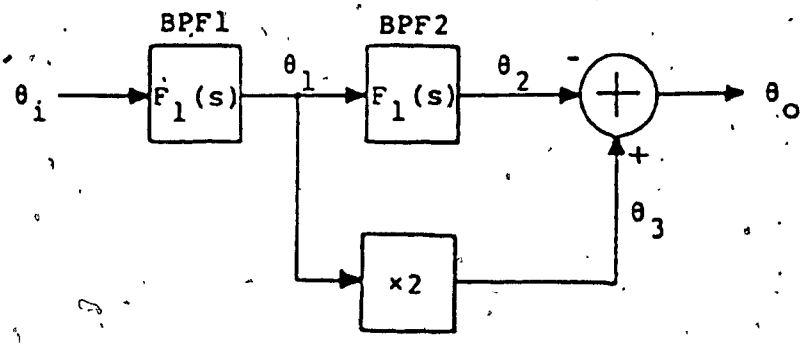

Fig. 2.2: Lowpass equivalent model of FTF

---

* FTF is followed by a bandpass filter which removes the high frequency components due to multiplication and amplification.

required in general. In fact, any type of BPF can be employed into the FTF. This broad choice of BPF leads us to the investigation of the best BPF which will give the fastest acquisition of the FTF. In short, FTF adopts a feedforward phase compensation scheme to achieve the tracking capability and this scheme gives the name to this particular tracking BPF.

2.2 Loop model

To study the transient and steady-state behaviour of the FTF, an equivalent baseband model of the FTF in a noise-free environment shown in Fig.2.2 is used. The BPF's are replaced by their equivalent lowpass models and the bandpass input is replaced by its baseband phase input. K_d and K_m are the gain of the doubler and the multiplier respectively.

Assuming the two BPF's have the same transfer function $F_1(s)$, a set of transfer functions of the FTF can be found as

$$\frac{\theta_1(s)}{\theta_i(s)} = F_1(s) \tag{2.1a}$$

$$\frac{\theta_2(s)}{\theta_i(s)} = [F_1(s)]^2 \tag{2.1b}$$

$$\frac{\theta_3(s)}{\theta_i(s)} = 2K_d F_1(s) \tag{2.1c}$$

$$\frac{\theta_o(s)}{\theta_i(s)} = K_m F_1(s)[2K_d - F_1(s)] \triangleq H(s) \qquad (2.1d)$$

and the error transfer function is found to be

$$\frac{\theta_e(s)}{\theta_i(s)} \triangleq \frac{\theta_i(s)-\theta_o(s)}{\theta_i(s)}$$

$$= 1 - H(s) = 1 - 2K_m K_d F_1(s) + K_m F_1^2(s) \qquad (2.2)$$

If $K_d=K_m=1$, Eq.(2.2) becomes

$$\frac{\theta_e(s)}{\theta_i(s)} = [1 - F_1(s)]^2 \qquad (2.3)$$

which is the error function that will be used to analyze the transient and steady-state behaviour of the FTF. The justification of unit gain doubler and multiplier is given in Chapter 4.

Note that two BPF's are assumed to have the same transfer function in the analysis. In practice, it is difficult to have two designed filters which have exactly identical characteristics. The consideration of the mismatching of the transfer functions of the BPF's will be discussed in detail in Chapter 4.

CHAPTER 3

TRANSIENT BEHAVIOUR OF FTF

3.1 Introduction

For fast and reliable acquisition of a tracking filter, it is important to know the transient behaviour of the tracking filter in response to a step input. The rate of diminishing of the transient response determines an important parameter, the acquisition time of a tracking filter. In order to know how fast the FTF can acquire the input phase and how it behaves before acquisition, a study of the transient responses of the FTF with phase and frequency step inputs is undertaken.

In this chapter, various BPF configurations are employed in the comparative study of the transient behaviour. FTF is thereafter categorized into Continuous and Discrete FTF according to analog or digital (discrete) filters used. The analog filters, synchronously tuned and Butterworth filters, are chosen for their hardware simplicity and their inherent short transient delay [4]. Because of the approximate brick-wall and linear phase characteristic, different surface-acoustic-wave (SAW) BPF's are chosen as the digital filters used in the discrete FTF. The comparisons in continuous FTF, based on the same noise equivalent bandwidth B_1 of the BPF, determine an analog BPF configuration that can give the fastest acquisition. The acquisition of the dis-

crete FTF is then related to that of the continuous FTF under the same noise bandwidth constraint. The above transient analysis, in terms of system terminology, is a zero-state response. As far as the speed is concerned, the non-zero initial state of the BPF has a significant influence on the acquisition [4]. The transient behaviour including the initial state or equivalently the Inter-Burst-Interference transient behaviour of the FTF is subsequently investigated. Finally, the prolonged transient caused by the hang-up phenomenon is shown not to be present in the FTF.

3.2 Transient behaviour of Continuous FTF

In this section, the lowpass equivalent model of the FTF is used to simulate the bandpass model of the FTF. Accordingly, the various analog BPF's under consideration will be replaced by their lowpass equivalent transfer functions which are listed in Table 3.1. The BPF's are chosen to have the same noise bandwidth for white noise. Besides, each filter is designed to have a unity gain in order to obtain zero steady-state error as shown in Chapter 4. The parameter τ is the time constant of the single-tuned BPF, which is determined by

$$\tau = 2Q/w_o \qquad (3.1)$$

where Q and w_o are the quality factor and the resonance

Order	Lowpass Equivalent BPF	$F_1(s)$	B_1
First	Single-tuned	$\frac{1}{s\tau+1}$	$\frac{1}{2\tau}$
	Lag-lead	$\frac{s\tau_2+1}{s\tau_1}$	--
Second	Double-tuned (Synchronous)	$\frac{(\frac{2}{\tau})^2}{(s+\frac{2}{\tau})^2}$	$\frac{1}{2\tau}$
	Butterworth	$\frac{\frac{2}{\tau^2}}{s^2+\frac{2}{\tau}s+\frac{2}{\tau^2}}$	
Third	Synchronous	$\frac{(\frac{8}{3\tau})^3}{(s+\frac{8}{3\tau})^3}$	$\frac{1}{2\tau}$
	Butterworth	$\frac{(\frac{3}{2\tau})^3}{(s+\frac{3}{2\tau})[s^2+\frac{3}{2\tau}s+(\frac{3}{2\tau})^2]}$	
Fourth	Synchronous	$\frac{(\frac{16}{5\tau})^4}{(s+\frac{16}{5\tau})^4}$	$\frac{1}{2\tau}$

Table 3.1: Equivalent lowpass transfer functions of various BPF's

angular frequency of the single-tuned BPF respectively.

The transient responses of the FTF due to a phase step $\Delta\theta$ and frequency step Δw is calculated by substituting

$$\theta_i(s) = \Delta\theta/s \tag{3.2a}$$

and $$\theta_i(s) = \Delta w/s^2 \tag{3.2b}$$

into the error function in Eq.(2.3) respectively. The equations of the transient responses of various FTF's are given in the sequel.

3.2.1 FTF using First-order BPF

(a) Single-tuned BPF

Substituting the transfer function of the single-tuned BPF into Eq.(2.3), the transfer function H(s) of the first order FTF* is found as

$$H(s) = \frac{(2s/\tau) + 1/\tau^2}{s^2 + (2s/\tau) + 1/\tau^2} \tag{3.3}$$

and the error transfer function is

$$\frac{\theta_e(s)}{\theta_i(s)} = \frac{s^2}{s^2 + (2s/\tau) + 1/\tau^2} \tag{3.4}$$

---

* For convenience, the "order" of the FTF is designated by the order of the lowpass equivalent BPF used. The actual order of the FTF is twice the order of the BPF in use.

Note that this is the same expression as the error transfer function of the second order PLL with infinite DC loop gain [1,2]. In this case, the damping factor is 1 and the natural frequency is $1/\tau$. This result indicates that FTF using single-tuned BPF without negative feedback path can achieve the characteristics of the second order PLL.

The transient phase errors of a phase step and a frequency step are respectively computed as

$$\theta_e(t') = \Delta\theta(1-t')\exp(t') \qquad (3.5a)$$

$$\theta_e(t') = \Delta w\tau[t'\exp(t')] \qquad (3.5b)$$

where $t' = t/\tau$.

(b) Lag-lead BPF

When this BPF is used, the transfer function of the FTF is

$$H(s) = [s^2(2\tau_1\tau_2-\tau_2^2)+2s(\tau_1-\tau_2)-1]/(s^2\tau_1^2) \qquad (3.6)$$

and the transient phase errors are

$$\theta_e(t) = (\Delta\theta/\tau_1^2)\{(\tau_1-\tau_2)^2 - 2(\tau_1-\tau_2)t + t^2\}$$

$$\theta_e(t) = (\Delta w/\tau_1^2)\{(\tau_1-\tau_2)^2 - 2(\tau_1-\tau_2)t^2 + t^3\} \qquad (3.7)$$

Eq.(3.7) shows that the error increases as time increases. Hence, the FTF using lag-lead BPF is not stable. Although lag-lead filters give a better performance in negative feedback loop, the pole at s=0 of the filter causes

instability in the feedforward loop. This is a difference between the conventional PLL and the FTF.

3.2.2 FTF using second-order BPF

Generally, the transfer function of the second order lowpass equivalent BPF is represented by

$$F_1(s) = \frac{w_c^2}{s^2 + 2\zeta w_c s + w_c^2} \tag{3.8}$$

where ζ is the damping factor and w_c is the cutoff frequency. The corresponding transfer function of the FTF is

$$H(s) = \frac{2w_c^2 s^2 + 4\zeta w_c^3 s + w_c^4}{s^4 + 4\zeta w_c s^3 + (2\zeta^2+1)2w_c^2 s^2 + 4\zeta w_c^3 s + w_c^4} \tag{3.9}$$

and the error function is

$$\frac{\theta_e(s)}{\theta_i(s)} = \frac{s^4 + 4\zeta w_c s^3 + 4\zeta^2 w_c^2 s^2}{s^4 + 4\zeta w_c s^3 + (2\zeta^2+1)2w_c^2 s^2 + 4\zeta w_c^3 s + w_c^4} \tag{3.10}$$

Likewise, these transfer functions have expressions similar to non-ideal fourth order PLL's. The transfer function of fourth order PLL with imperfect integrators is [8]

$$H(s) = \frac{cw_o s^3 + bw_o^2 s^2 + aw_o^3 s + w_o^4}{s^4 + (cw_o+\lambda_1)s^3 + (bw_o^2+\lambda_2)s^2 + (aw_o^3+\lambda_3)s + w_o^4} \tag{3.11}$$

where $\lambda_1 = \tau_1 + \tau_2 + \tau_3$

$$\lambda_2 = \tau_1\tau_2 + \tau_1\tau_3 + \tau_2\tau_3$$

$$\lambda_3 = \tau_1\tau_2\tau_3$$

and a,b,c are constants, w_o is the natural frequency; τ_1, τ_2 and τ_3 are the inverse of the time constants associated with the imperfect integrators. Comparing Eqs.(3.9) and (3.11), the constants have the following values:

$$a = 4\zeta \ , \quad b = 2 \ , \quad c = 0$$

and $\tau_2 = \tau_3 = 2\zeta w_c$ if $w_o = w_c$ and $\tau_1 = 0$.
This indicates that if a second order BPF is used in the FTF, the FTF will have the characteristics of a fourth order PLL with imperfect integrators.

The phase step and frequency step responses are given in Table 3.2 and plotted in Figs.3.1 and 3.2. $\zeta = 1$ corresponds to the critical damping case which is shown to have the fastest decay. $\zeta < 1$ is the underdamped case and $\zeta > 1$ is the overdamped case. Their curves are characterized by the oscillation and the slow decay. In all cases of ζ, the error tends to zero steady-state error when time approaches infinity. As far as the transient phase error is concerned, it is not recommended to use a second order BPF with ζ larger than 1 because the instantaneous error is large and the acquisition time is long. Neither is the case of $\zeta < 1/\sqrt{2}$ recommended. The best range is thus within $1/\sqrt{2}$ and 1.

Let us consider the poles and zeros of the FTF. There

	Phase step ($\Delta\theta$ rad)	Frequency step (Δw rad/sec.)
$\zeta>1$	$\Delta\theta e^{-\zeta w_c t}\left\{\frac{\zeta(2\zeta^2-1)}{2(\sqrt{\zeta^2-1})^3}\sinh(w_c\sqrt{\zeta^2-1}t)\right.$ $-w_c t\left[\frac{\sinh(w_c\sqrt{\zeta^2-1}t)}{2\sqrt{\zeta^2-1}}+\frac{\cosh(w_c\sqrt{\zeta^2-1}t)}{2(\zeta^2-1)}\right]$ $\left.+\cosh(w_c\sqrt{\zeta^2-1}t)\right\}$	$\frac{\Delta w}{w_c}e^{-\zeta w_c t}\left\{w_c t\left[\frac{(2\zeta^2-1)}{2(\zeta^2-1)}\cosh(w_c\sqrt{\zeta^2-1}t)\right.\right.$ $\left.+\frac{\zeta\sinh(w_c\sqrt{\zeta^2-1}t)}{\sqrt{\zeta^2-1}}\right]-\frac{\sinh(w_c\sqrt{\zeta^2-1}t)}{2(\sqrt{\zeta^2-1})^3}\Big\}$
$\zeta=1$	$\Delta\theta e^{-w_c t}\left[1+w_c t-\frac{(w_c t)^2}{2}-\frac{(w_c t)^3}{6}\right]$	$\frac{\Delta w}{w_c}e^{-w_c t}w_c t\left[1+w_c t+\frac{(w_c t)^2}{6}\right]$
$\zeta<1$	$\Delta\theta e^{-\zeta w_c t}\left\{\frac{\zeta(1-2\zeta^2)}{2(\sqrt{1-\zeta^2})^3}\sin(w_c\sqrt{1-\zeta^2}t)\right.$ $-w_c t\left[\frac{\sin(w_c\sqrt{1-\zeta^2}t)}{2\sqrt{1-\zeta^2}}-\frac{\cos(w_c\sqrt{1-\zeta^2}t)}{2(1-\zeta^2)}\right]$ $\left.+\cos(w_c\sqrt{1-\zeta^2}t)\right\}$	$\frac{\Delta w}{w_c}e^{-\zeta w_c t}\left\{w_c t\left[\frac{(1-2\zeta^2)}{2(1-\zeta^2)}\cos(w_c\sqrt{1-\zeta^2}t)\right.\right.$ $\left.+\frac{\zeta\sin(w_c\sqrt{1-\zeta^2}t)}{\sqrt{1-\zeta^2}}\right]-\frac{\sin(w_c\sqrt{1-\zeta^2}t)}{2(\sqrt{1-\zeta^2})^3}\Big\}$

Table 3.2: Transient phase error of second order FTF

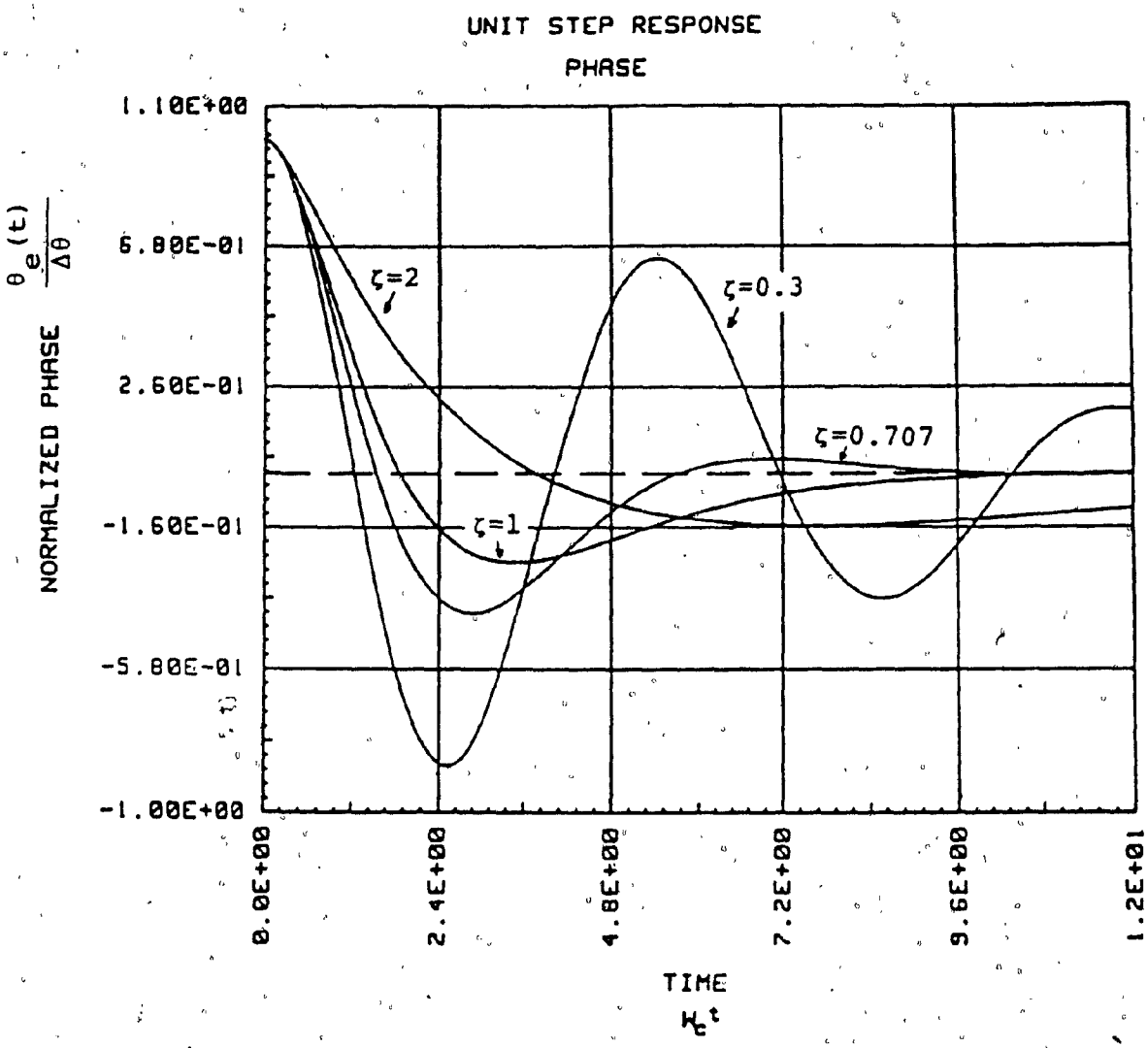

Fig. 3.1: Phase step transient phase error of second order FTF

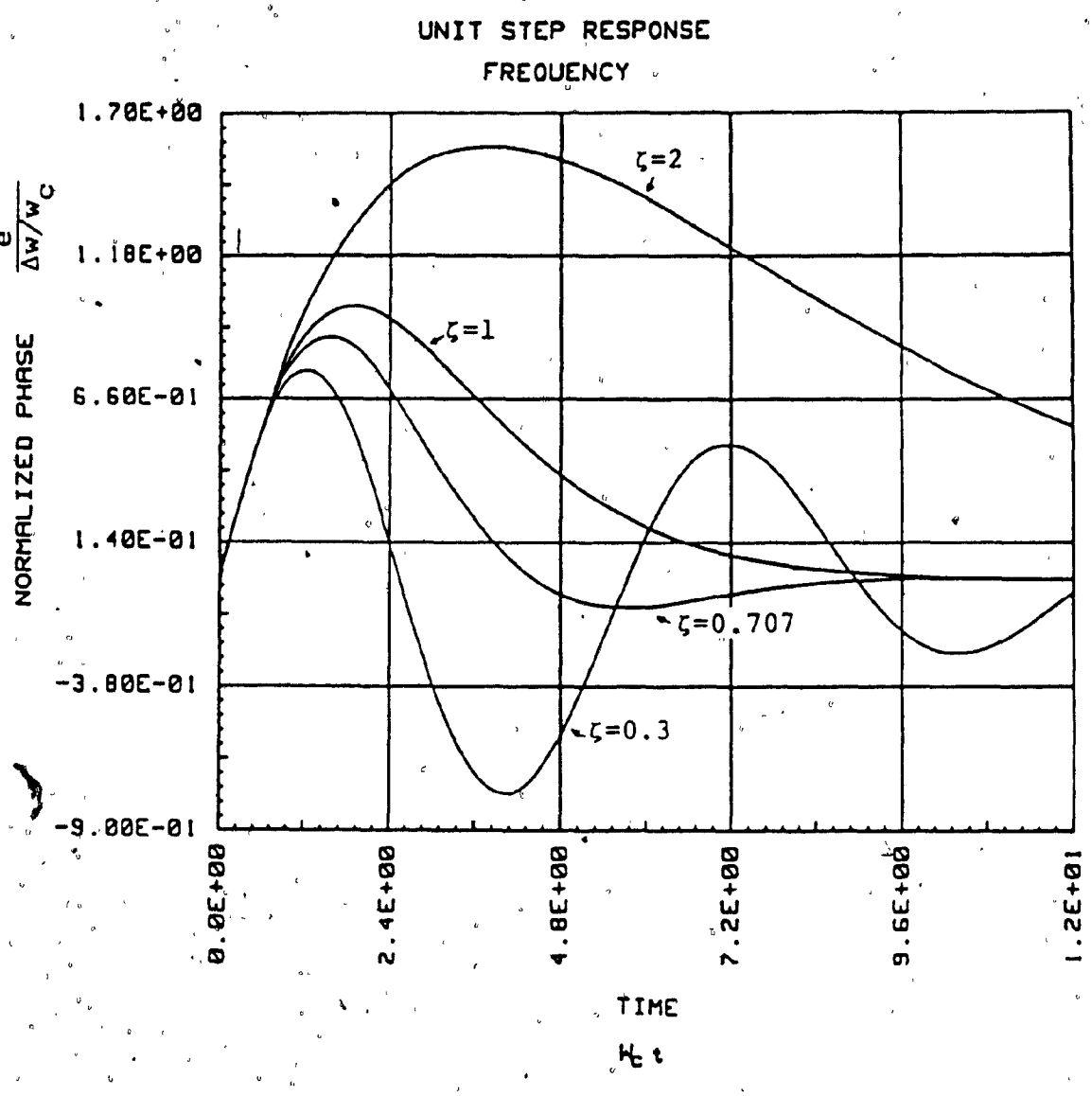

Fig. 3.2: Frequency step transient phase error of second order FTF

are two simple zeros,

$$z_{1,2} = -\zeta w_c \pm w_c\sqrt{\zeta^2-\tfrac{1}{2}} \qquad (3.12)$$

and two poles of multiplicity 2,

$$p_{1,2} = -\zeta w_c \pm w_c\sqrt{\zeta^2-1} \qquad (3.13)$$

These poles and zeros determine, in addition to the stability, the transient behaviour of the FTF. It is known that complex zeros and complex poles of the transfer function are harmful to the transient behaviour and the stability of the high order PLL [9]. This statement is also applicable to the FTF since FTF has PLL characteristics. However, the second order FTF is stable for every value of ζ as the poles always lie in the left half plane of the s-plane as shown in the root locus plot in Fig.3.3. Since the root locus of all values of ζ never crosses the right half plane, the stability of the FTF is superior to the probable instability caused by the parameter variations (in abnormal conditions) of the high order PLL. In fact, the stability of the FTF can be determined by the BPF used because the poles of the BPF are exactly the same as the FTF. Further, the complex poles or zeros cause poor transient response of the second order FTF as illustrated in Figs.3.1 and 3.2.

Two special cases, doubled-tuned (synchronous) and Butterworth, of the second order lowpass equivalent BPF are taken for the comparative study. Their respective transient phase error equations are given in Table 3.3 and compared

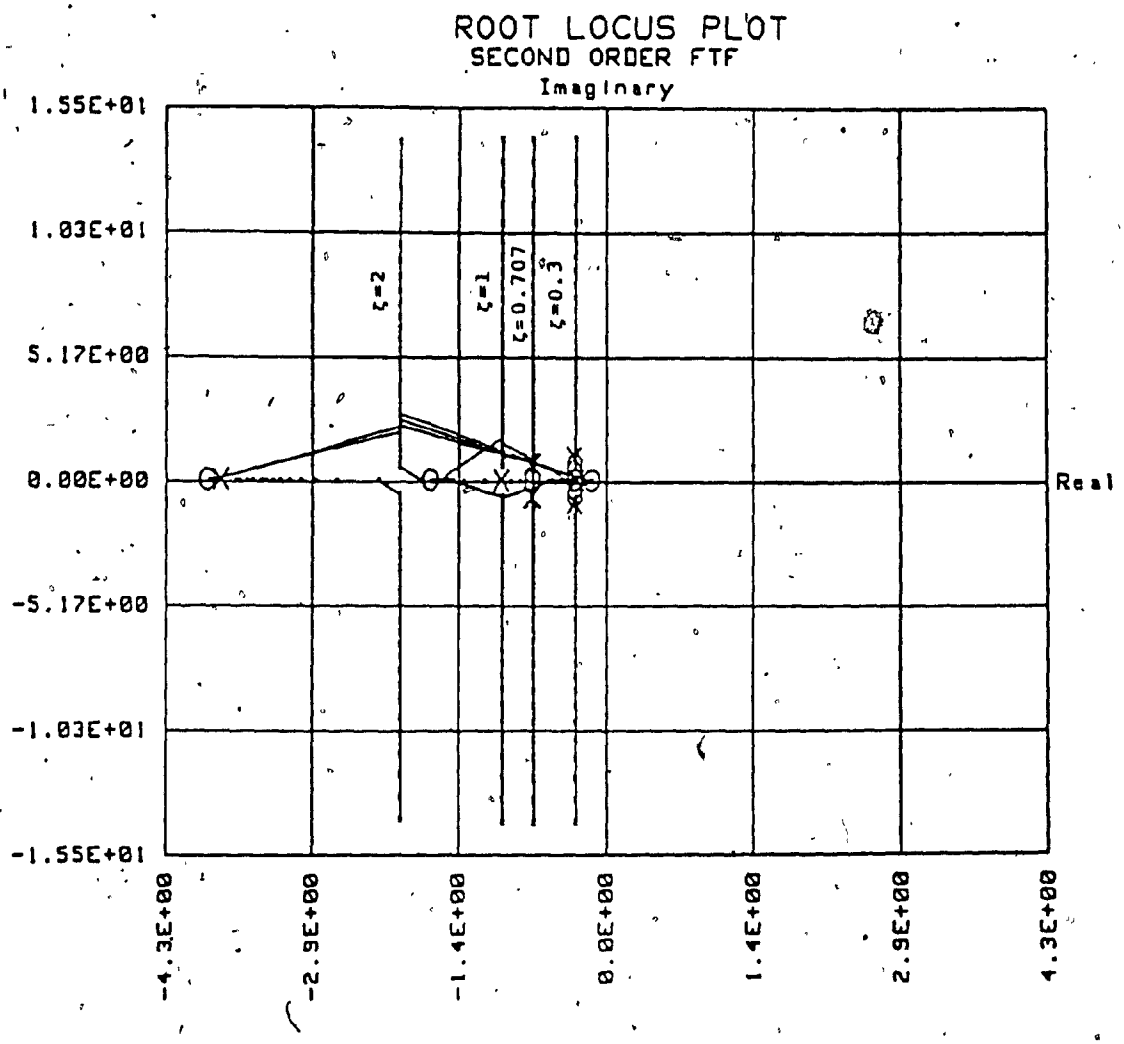

Fig. 3.3: Root locus plot of second order FTF

FTF with	Phase step ($\Delta\theta$ rad)	frequency step (Δw rad/s)
Double-tuned BPF $w_c = 2/\tau$ $\zeta = 1$	$\Delta\theta e^{-2t'}\left[1+2t'+\frac{(2t')^2}{2}-\frac{(2t')^3}{6}\right]$	$\Delta w\tau e^{-2t'}\ t'\left[1+2t'+\frac{(2t')^2}{6}\right]$
Second order Butterworth BPF $w_c = \sqrt{2}/\tau$ $\zeta = 1/\sqrt{2}$	$\Delta\theta e^{-t'}(\cos(t')-t'[\sin(t')$ $-\cos(t')])$	$\Delta w\tau e^{-t'}\ t'(1+t')\sin(t')$
$t' = t/\tau$		

Table 3.3: Transient phase error of a double-tuned and second order Butterworth FTF

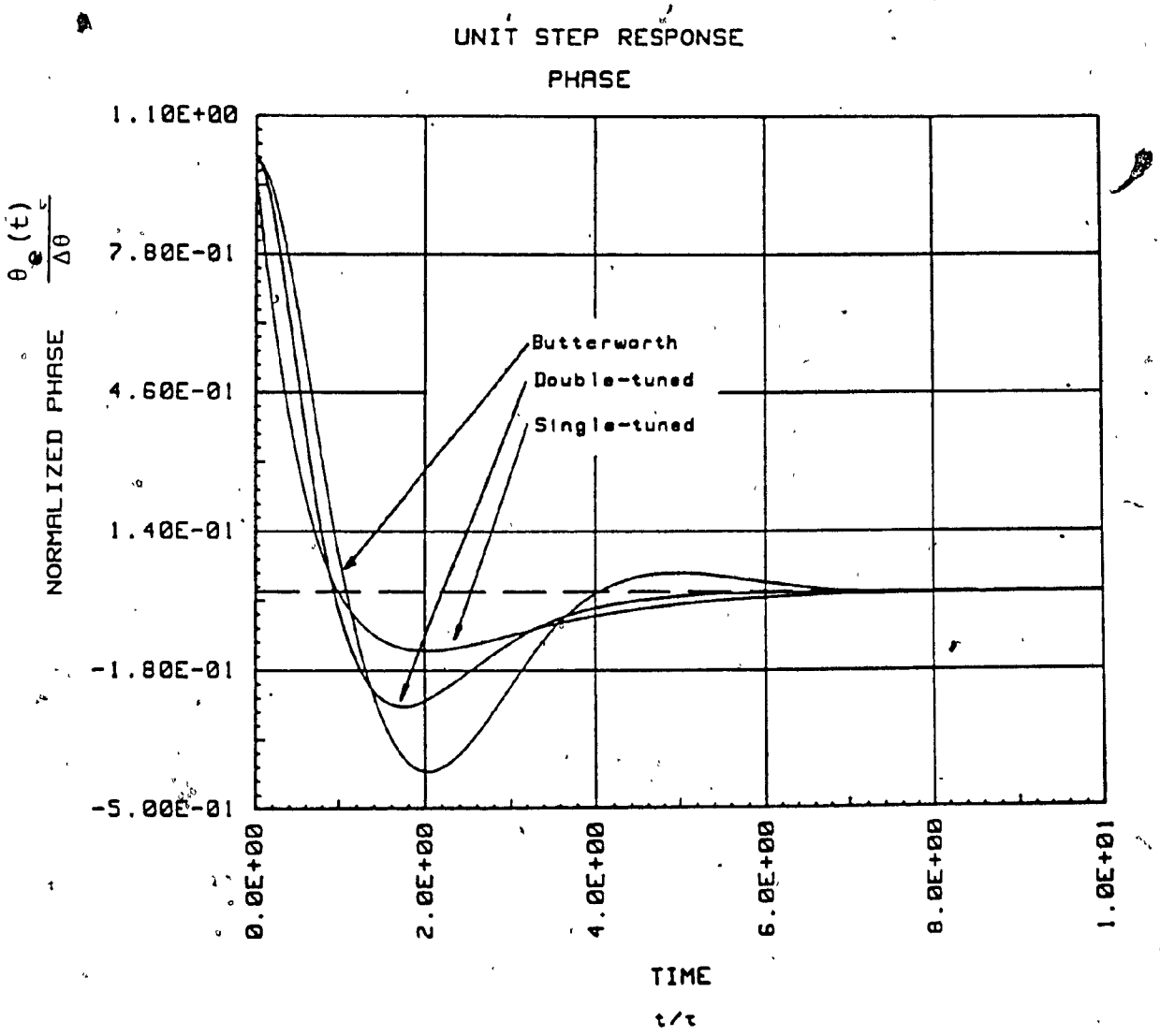

Fig. 3.4: Phase step transient phase error of first and second order FTF

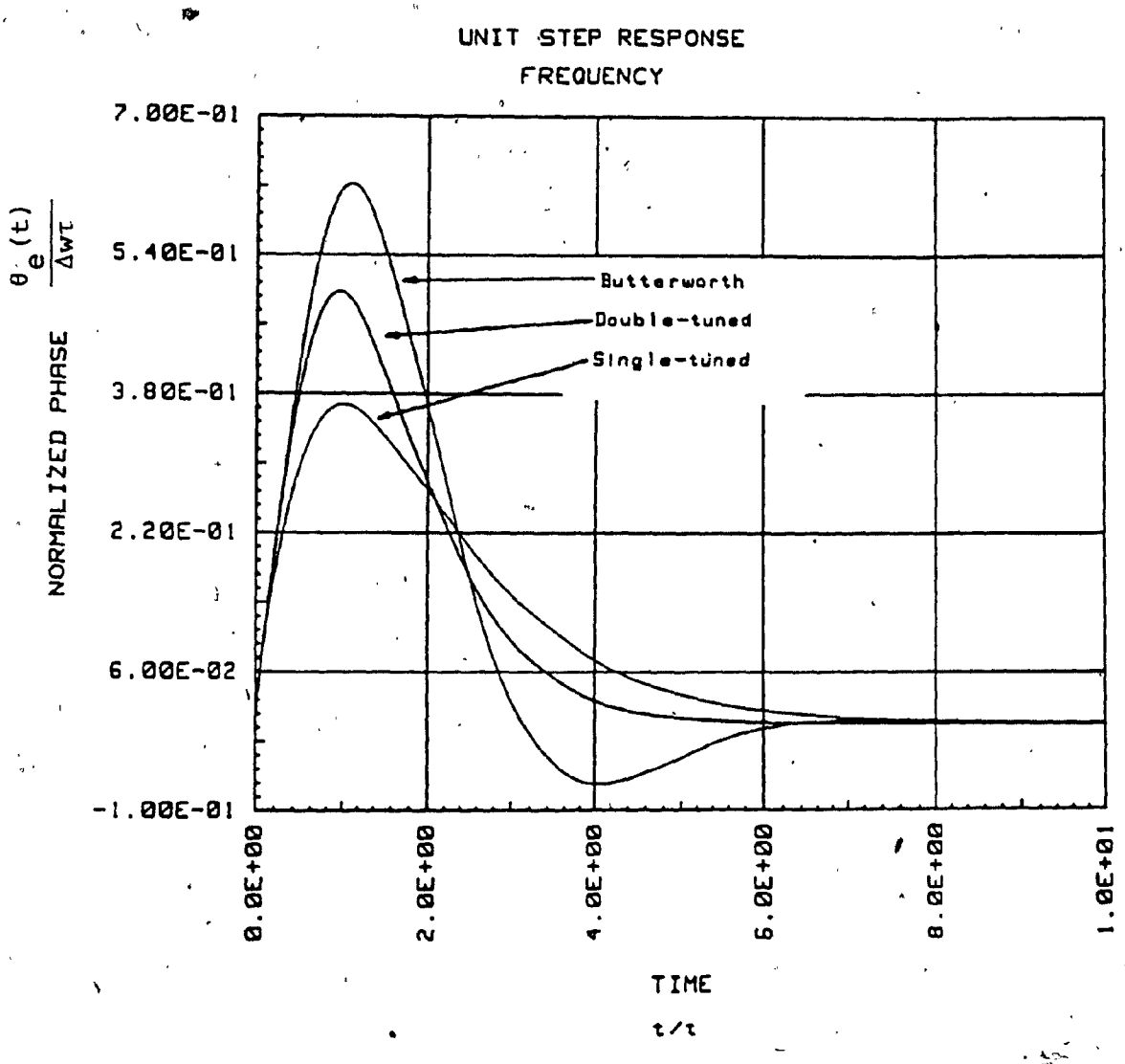

Fig. 3.5: Frequency step transient phase error of first and second order FTF

with that of the single-tuned FTF in Figs.3.4 and 3.5. In case of the doubled-tuned BPF, all the poles and zeros are real and negative whereas there is one real zero of multiplicity 2 and two complex poles of multiplicity 2 in the Butterworth BPF. It can be seen that the transient response of the second order Butterworth FTF is worse than that of the double-tuned FTF under the same noise bandwidth. The discrepancy, as mentioned before, is due to the complex poles existing in the transfer function of the BPF. The effect of complex poles in higher order filters, as described in the following section, is more prominent. The result also shows that the double-tuned FTF has significant improvement in the acquisition time over the single-tuned FTF for the same noise bandwidth B_1. Since the equivalent noise bandwidth B_L of the double-tuned FTF is wider than that of the single-tuned FTF (Table 5.2). A shorter acquisition time is thus resulted.

3.2.3 FTF using Third order BPF

The effect of the complex poles on the transient behaviour can be illustrated more clearly in the third order FTF. Similarly, the transient phase error equations of the FTF using synchronous and Butterworth filters are computed and presented in Table 3.4. The poles of the synchronous BPF are real but there are two complex poles of multiplicity 2 in the third order Butterworth BPF. Compared to the responses of the double-tuned FTF shown in Figs.3.6 and 3.7,

FTF with	phase step ($\Delta\theta$ rad)	frequency step (Δw rad/s)
Synchronous BPF	$\Delta\theta\ e^{-T}(1+T+\frac{T^2}{2}-\frac{T^3}{6}-\frac{T^4}{24}-\frac{T^5}{120})$	$\Delta w\tau t' e^{-T}(1+T+\frac{T^2}{2}+\frac{T^3}{12}+\frac{T^4}{120})$
Third order Butterworth BPF	$\Delta\theta\{e^{-\frac{3t'}{4}}[(2+\frac{t'}{2})\cos(\frac{3\sqrt{3}t'}{4}) + (\frac{\sqrt{3}t'}{2}+\frac{4}{3\sqrt{3}})\sin(\frac{3\sqrt{3}t'}{4})] - e^{-\frac{3t'}{2}}(1+\frac{3t'}{2})\}$	$\Delta w\tau\{e^{-\frac{3t'}{4}}[\frac{20}{9\sqrt{3}}\sin(\frac{3\sqrt{3}t'}{4}) -(\frac{4}{3}+\frac{2t'}{3})\cos(\frac{3\sqrt{3}t'}{4})] + e^{-\frac{3t'}{2}}(\frac{4}{3}+t')\}$
$T=\frac{8}{3}t'$, $t'=\frac{t}{\tau}$		

Table 3.4: Transient phase error of third order FTF

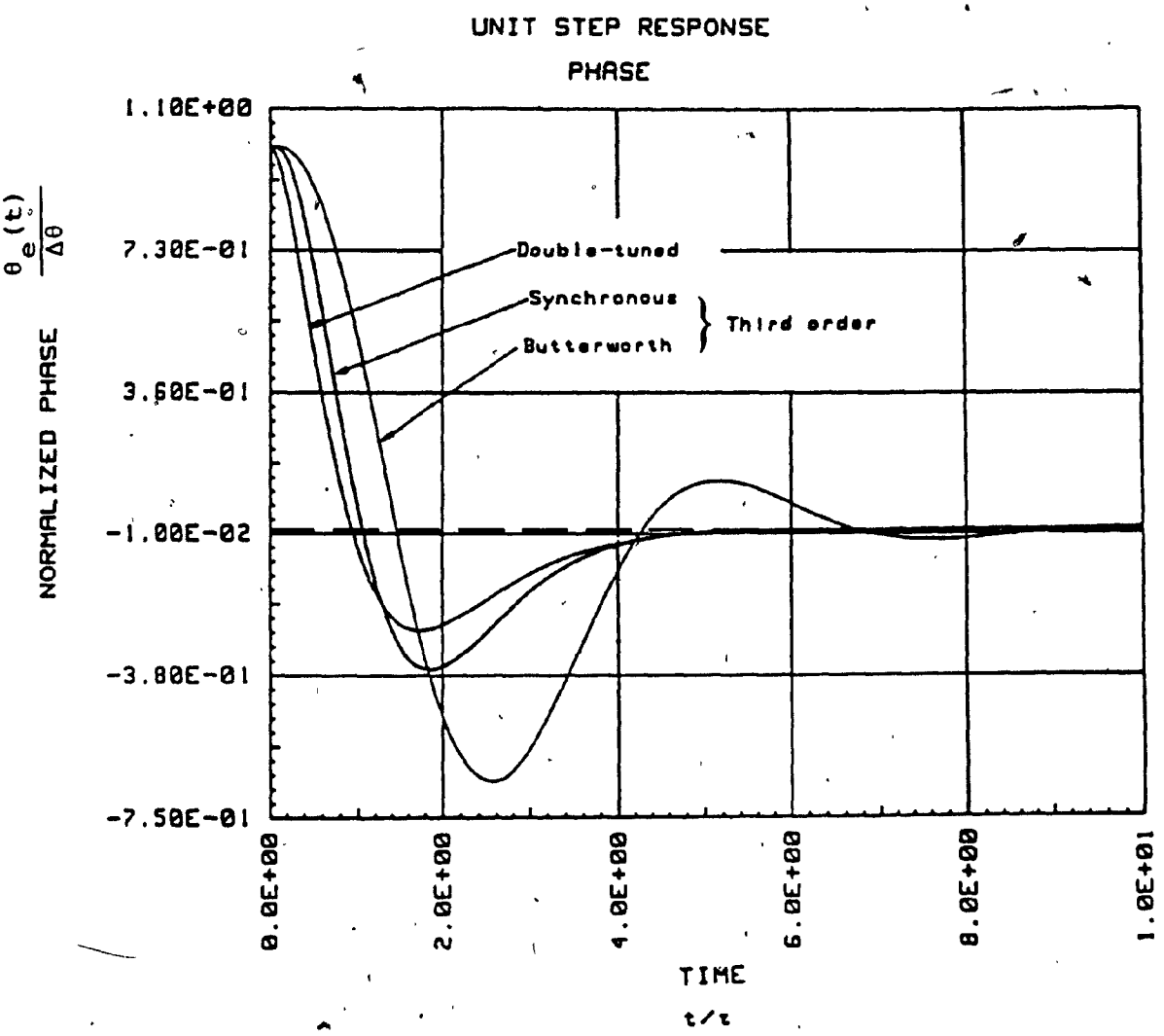

Fig. 3.6: Phase step transient phase error of double-tuned and third order FTF

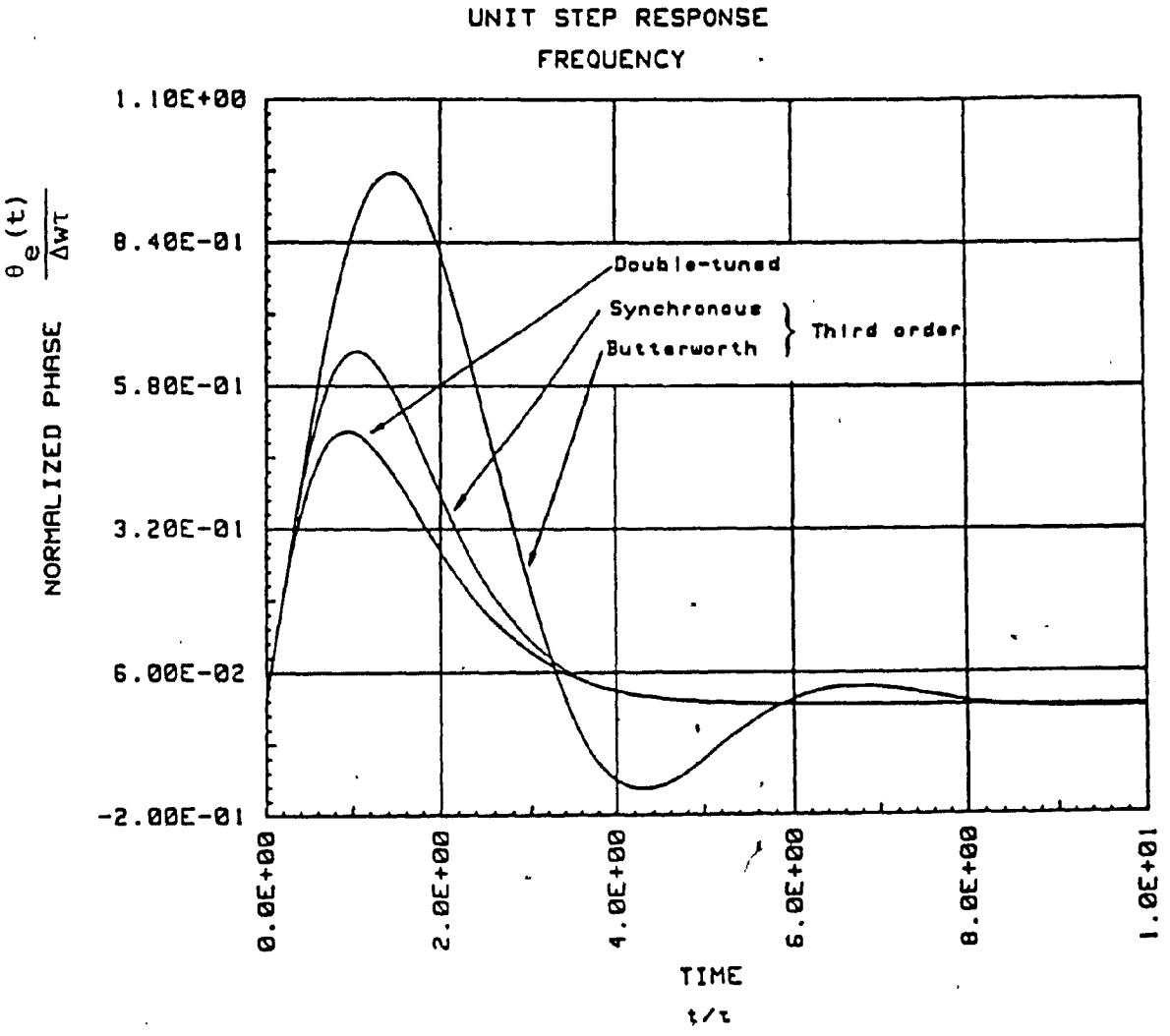

Fig. 3.7: Frequency step transient phase error of double-tuned and third order FTF

it is noticed that the transient response is increasingly bad as the order of the transfer function increases, especially when complex poles are present (in the Butterworth BPF case). Although the instantaneous transient phase error of the third order synchronous FTF is larger than the second order FTF, the transient error decreases rapidly. The acquisition time, as a result, is not significantly decreased. Up to this point, if fast acquisition is a requirement, the comparison can lead to a conclusion that the synchronous BPF is the best type of BPF to be used in the FTF under a certain noise bandwidth.

3.2.4 FTF using Fourth order BPF

The purpose of dealing with fourth order FTF is to justify the implication that the higher the order of the FTF the better the performance.

$$\theta_e(t') = \Delta\theta \exp(-T)\left[1+T+\frac{T^2}{2}+\frac{T^3}{6}-\frac{T^4}{24}-\frac{T^5}{120}-\frac{T^6}{720}-\frac{T^7}{5040}\right] \quad (3.14)$$

$$\theta_e(t') = \Delta w\tau t'\exp(-T)\left[1+T+\frac{T^2}{2}+\frac{T^3}{6}+\frac{T^4}{40}+\frac{T^5}{360}+\frac{T^6}{5040}\right] \quad (3.15)$$

where $T = (16/5)t'$. Eqs.(3.14) and (3.15) give the transient phase error of the fourth order synchronous FTF which is plotted in Figs.3.8 and 3.9. It is surprising that no further improvement in acquisition time is found in the third and fourth order FTF's. The fact is that the high order BPF's increase their cutoff frequency w_c (or bandwidth) in order to achieve the same noise equivalent

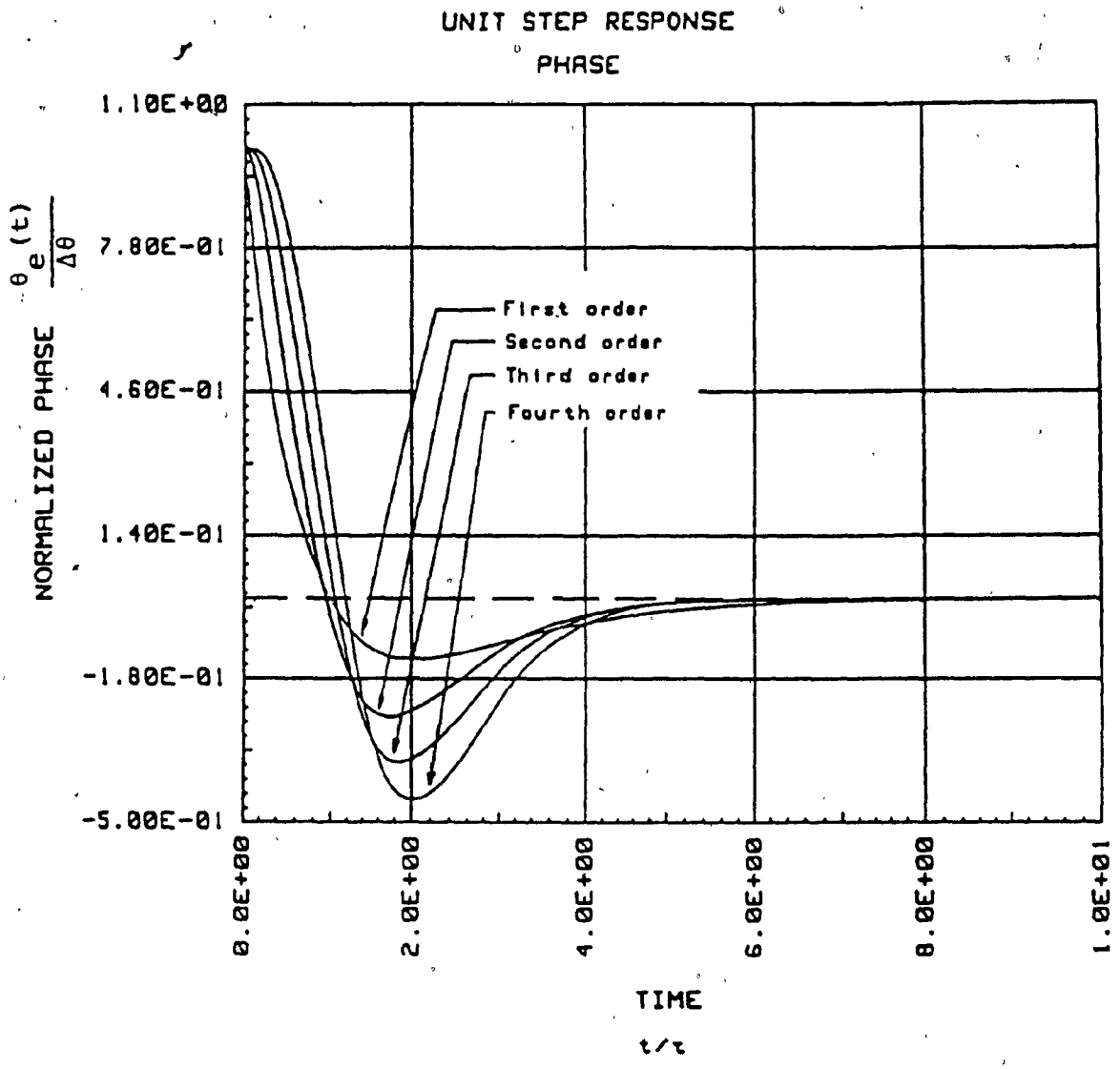

Fig. 3.8: Phase step transient phase error of four synchronous FTF's with the same B_1

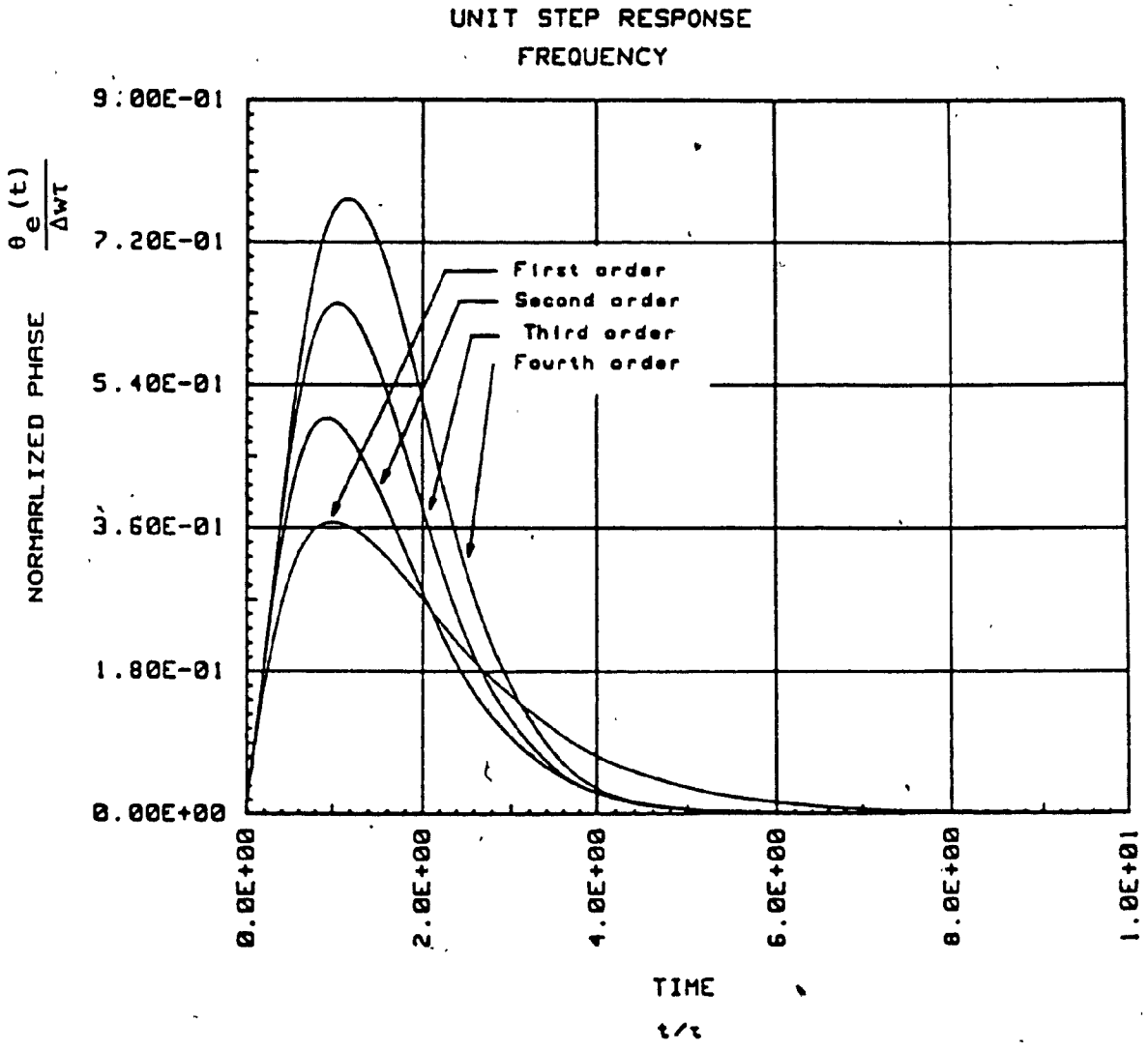

Fig. 3.9: Frequency step transient phase error of four synchronous FTF's with the same B_1

bandwidth $1/2\tau$. This expansion in the frequency domain leads to faster decay of the transient responses in the time domain. The equations in Table 3.2 reveal the fact that the exponential decaying factor depends on w_c and ζ. However, the faster decay of the transient response is counteracted by the increasingly large transient phase error due to the increase in the multiplicity of the real pole of the FTF. For this reason, the high order FTF's may not shorten the acquisition time. Moreover, Table 3.5 shows that the increase in w_c is decelerated, and hence, it is possible that the acquisition time is extended when the increase in transient phase error is faster than the decay. Figs.3.8 and 3.9 illustrates that as the transient responses of the fourth order synchronous FTF shifts to the right, it is plausible that FTF higher than fourth order may have a longer acquisition time than that of the second order FTF.

To further show the tradeoffs between the acquisition time and the bandwidth of the FTF, the transient phase errors of the four synchronous FTF's with different B_1 (B_1 increases with order) are depicted in Figs.3.10 and 3.11. The acquisition time is obviously extended as the order increases. The reason is that the bandwidth is narrower as more filters are cascaded. Therefore, rapid acquisition has to pay for the increase in bandwidth. This is also the reason that the narrow bandwidth of the PLL, improved by the negative feedback, accounts for the sluggishness of the PLL.

BPF	w_c	Δw_c
First order	$1/\tau$	$1/\tau$
Second order	$2/\tau$	$0.6/\tau$
Third order	$8/3\tau$	$0.53/\tau$
Fourth order	$16/5\tau$	

Table 3.5: Cutoff frequencies of four synchronously-tuned BPF's with the same noise bandwidth

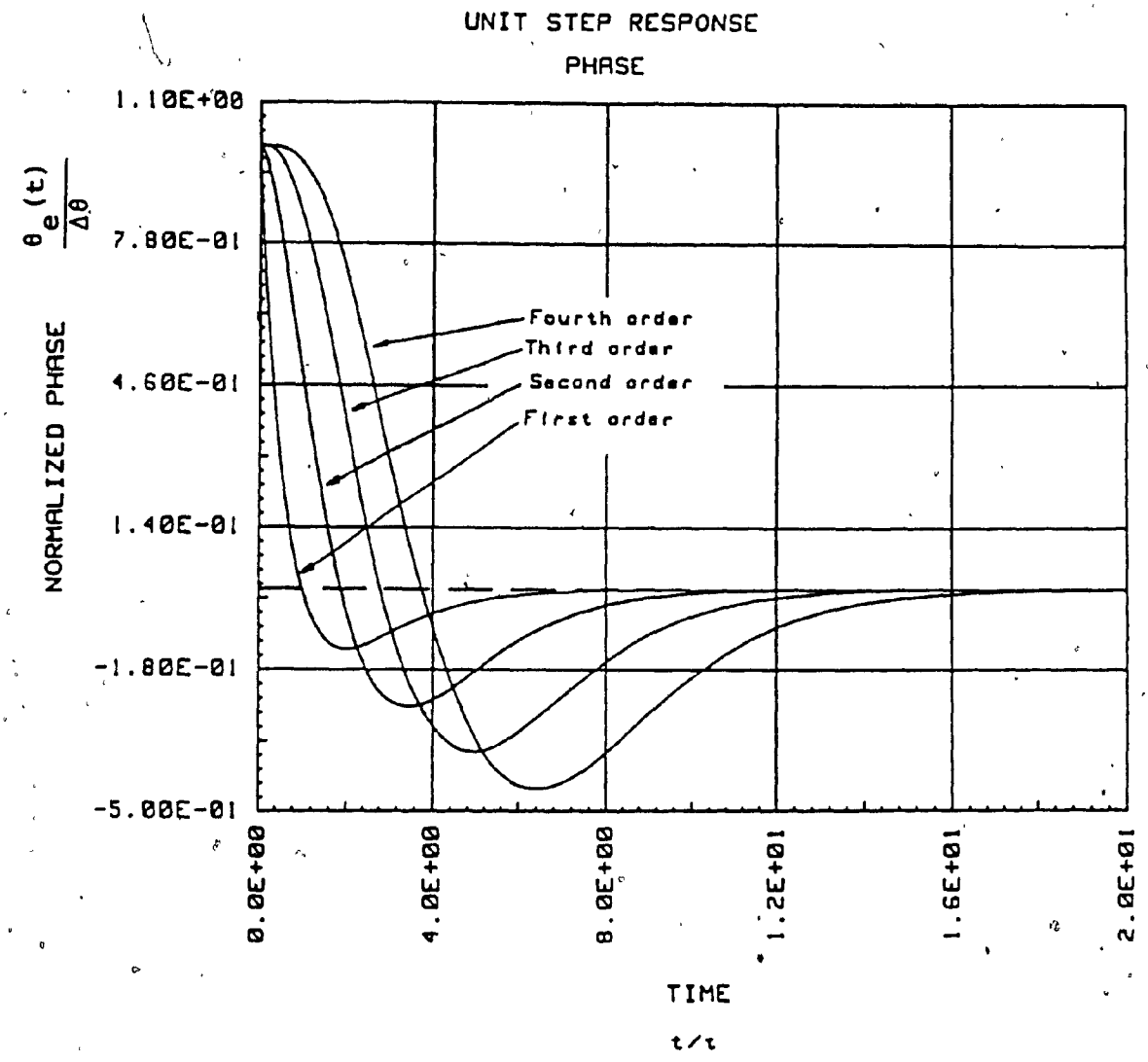

Fig. 3.10: Phase step transient phase error of four synchronous FTF's (B_1 increases with order)

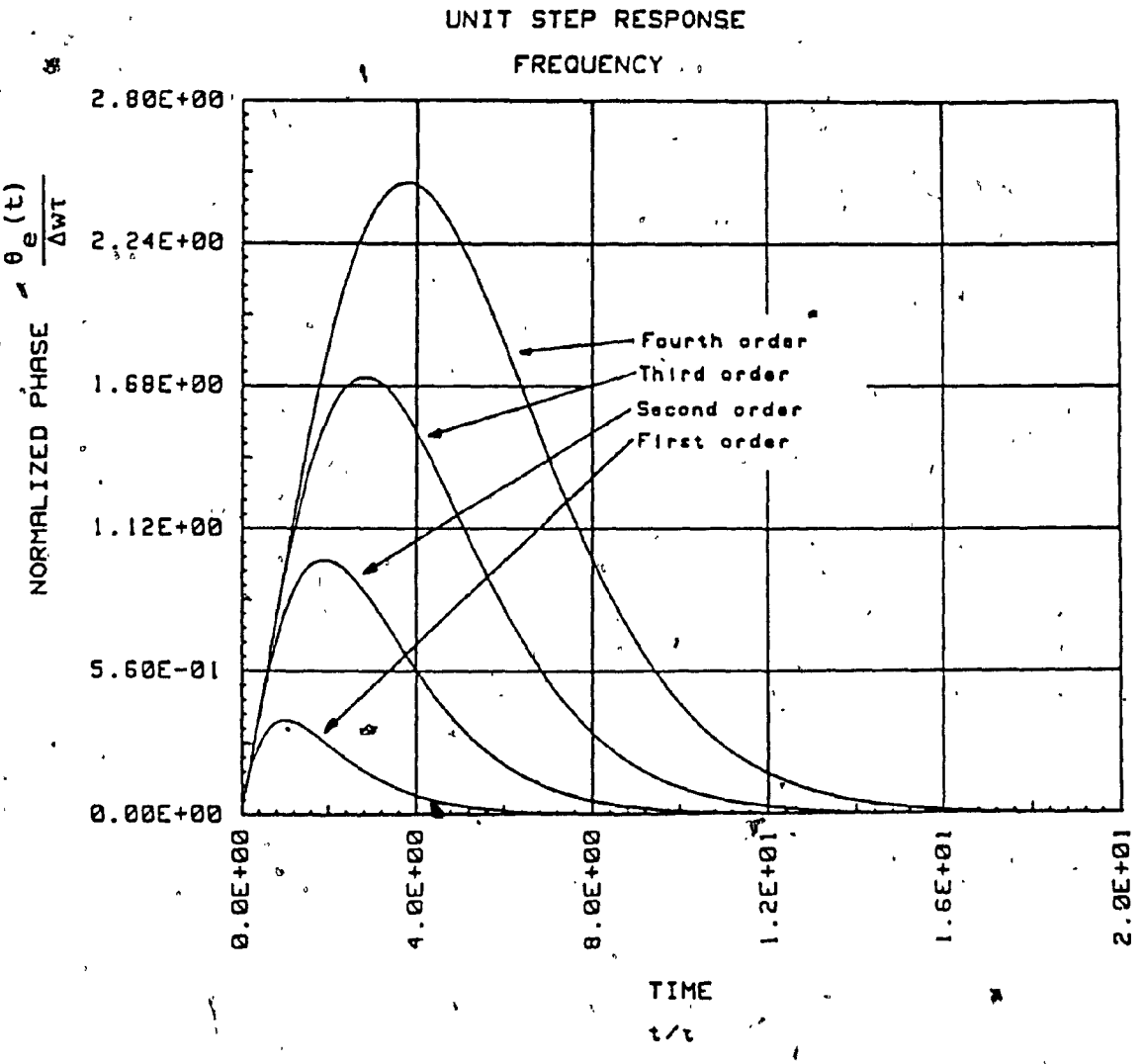

Fig. 3.11: Frequency step transient phase error of four synchronous FTF's (B_1 increases with order)

3.2.5 Experimental results

Two single-tuned BPF's with Q=60 at f_o=10MHz ($\tau \simeq 2\mu s$) were used in an experimental first order FTF. In response to a phase step input, the predicted exponential decay (Appendix C.1) of the transient phase error of the single-tuned and double-tuned BPF's is shown in Fig.3.12. An error of 36% is found after an elapsed time τ in Fig.3.12a. There is no steady-state error found in both cases as expected, since the signal is at the resonant frequency of the BPF's. Moreover, the time required to settle in double-tuned BPF is twice as long as the single-tuned BPF. It is the same acquisition time, 9 μs (approximately 4.5τ), required for the first order FTF shown in Fig.3.13. Certainly, no steady-state error is found in the FTF. The resultant output of the FTF is effectively obtained by subtracting twice of the output in Fig.3.12a from that in Fig.3.12b.

The results of the transient response of the single-tuned and double-tuned BPF's due to a frequency step of 40kHz are shown in Figs.3.14 and 3.15. A steady-state error of 50mV (equivalently 25 degrees) is found in the single-tuned BPF while 100mV or 50 degrees of error is obtained in double-tuned BPF. Therefore, doubling the output of the single-tuned BPF and substracting by the output of the double-tuned BPF, a zero steady-state error is obtained at the output of the FTF, after 9 μs, as shown in Fig.3.16.

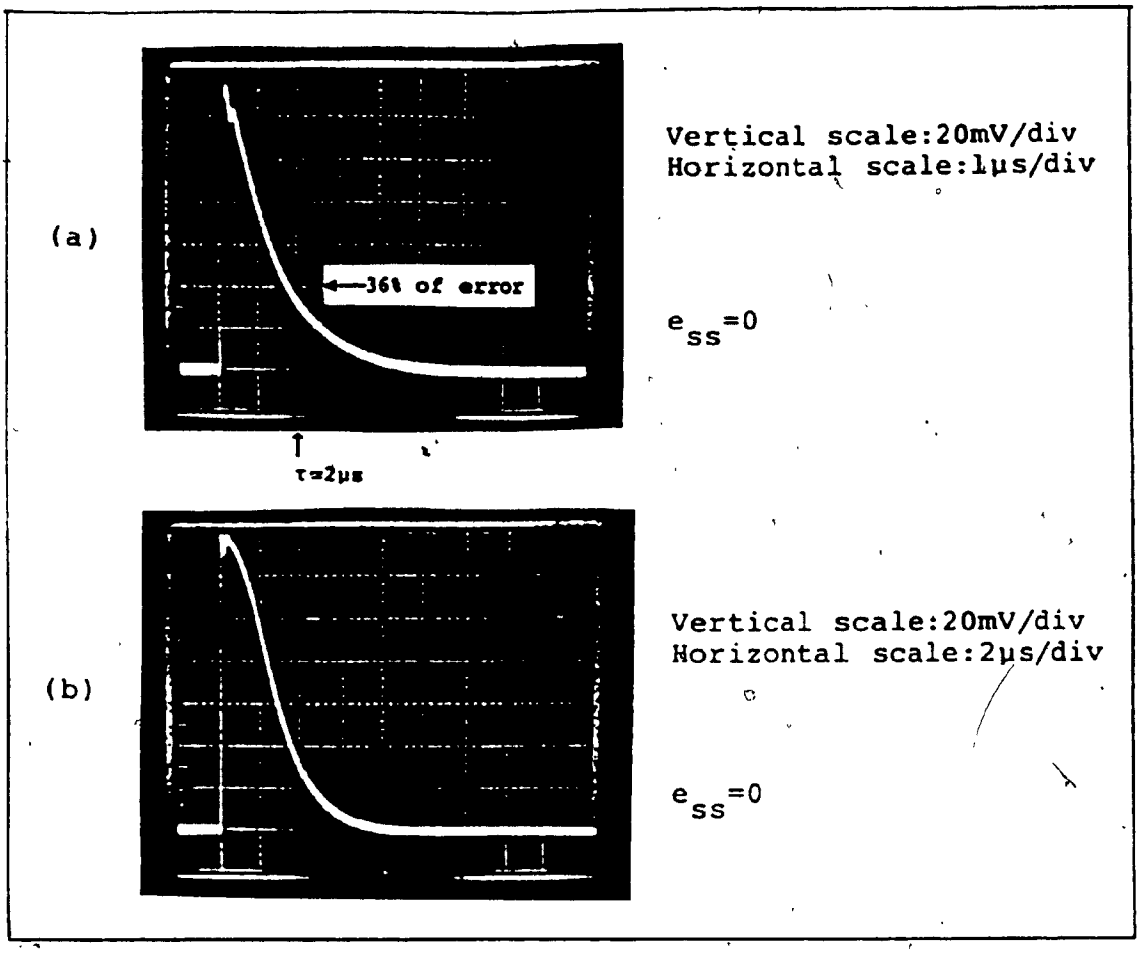

Fig. 3.12: Measured phase step transient phase error of a single-tuned BPF (a) and of a double-tuned BPF (b)

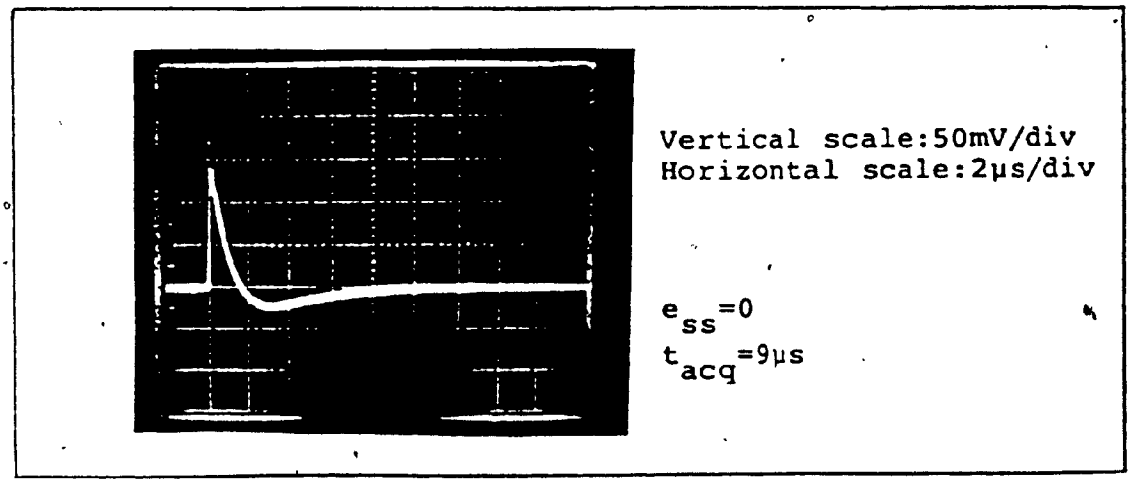

Fig. 3.13: Measured phase step transient phase error of a single-tuned FTF

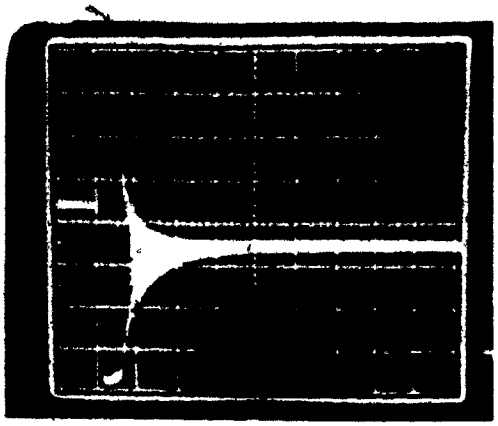

Vertical scale:50mV/div
Horizontal scale:2μs/div

(a) Multiple traces *

e_{ss} = 50mV (25°)

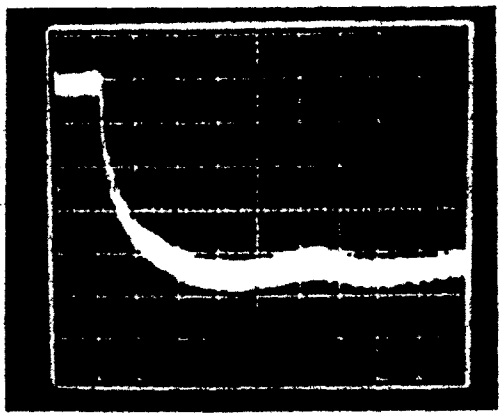

Vertical scale:10mV/div
Horizontal scale:2μs/div

(b) Single trace

Fig. 3.14: Measured frequency step transient phase error of a single-tuned BPF

---

* Multiple traces are obtained due to the all possible phase differences of the two signal generators in the experiment (Appendix D).

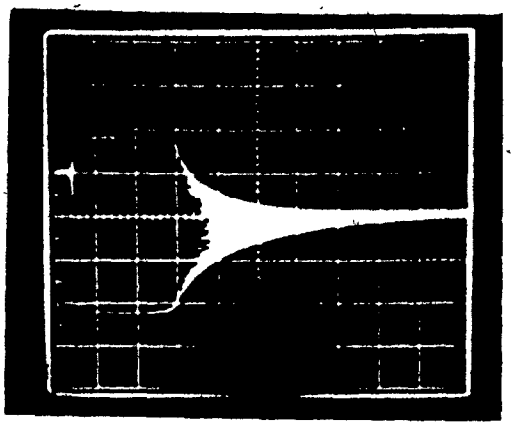

Vertical scale:.1V/div
Horizontal scale:1μs/div

(a) Multiple traces

e_{ss}=100mV (50°)

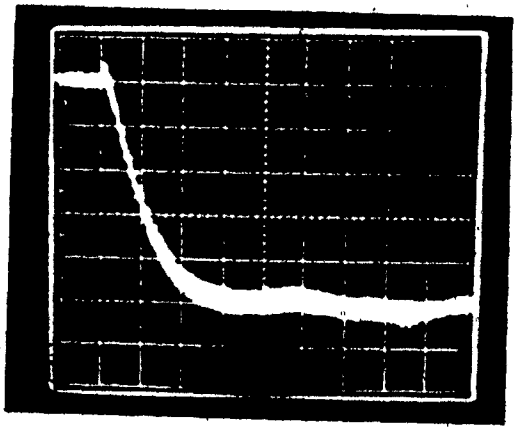

Vertical scale:20mV/div
Horizontal scale:2μs/div

(b) Single trace

Fig. 3.15: Measured frequency step transient phase error of a double-tuned BPF

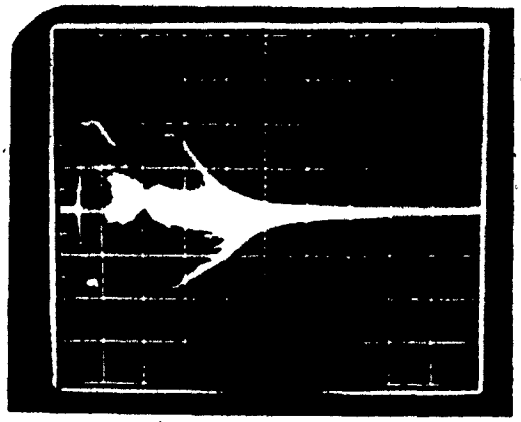

Vertical scale:.1V/div
Horizontal scale:1μs/div

(a) Multiple traces

$e_{ss}=0$

$t_{acq}=9\mu s$

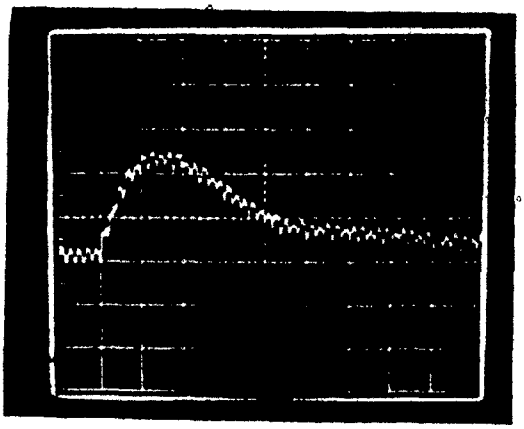

Vertical scale:10mV/div
Horizontal scale:1μs/div

(b) Single trace

Fig. 3.16: Measured frequency step transient phase error of a single-tuned FTF

3.3 Transient behaviour of Discrete FTF

The application of surface-acoustic-wave (SAW) filters or symmetrical transversal filters in the FTF has two advantages, namely, fast spectral rolloff and good noise rejection, and stability (since they are passive devices). The passivity of the SAW filters also guarantees the stability of the FTF.

The lowpass equivalent of the transfer function of a unit gain SAW filter in z-transform is given by (Appendix C.2)

$$F_l(z) = \frac{\sum_{n=0}^{N-1} a_n z^{-n}}{\sum_{n=0}^{N-1} a_n}, \quad a_i = a_{N-1-i} \text{ for } i<N-1 \tag{3.16}$$

where a_i is the weight coefficient of i^{th} tap and N is the total number of taps. Substituting this transfer function into Eq.(2.3), the error transfer function becomes

$$\frac{\theta_e(z)}{\theta_i(z)} = 1 - \frac{2\sum_{n=0}^{N-1} a_n z^{-n}}{\sum_{n=0}^{N-1} a_n} + \frac{\sum_{n=0}^{2(N-1)} \sum_{i=0}^{n} a_i a_{n-i} z^{-n}}{\left(\sum_{n=0}^{N-1} a_n\right)^2}, \quad a_i=0 \text{ for all } i \geq N-1 \tag{3.17}$$

The last term in Eq.(3.17) is the square of Eq.(3.16), which corresponds to the transfer function of the cascaded SAW filters. The expression shows that cascaded SAW filters act as a single SAW filter of different characteristic and the

symmetrical property of its coefficients still holds.

Applying the phase step input $\theta_i(k)=\Delta\theta u(k)$ and using the translation property of z-transform, the phase error is found to be a delayed version of the step input as shown in Eq.(3.18).

$$\theta_e(k)=\Delta\theta\left[u(k)-\frac{2\sum_{n=0}^{N-1}a_n u(k-n)}{\sum_{n=0}^{N-1}a_n}+\frac{\sum_{n=0}^{2(N-1)}\sum_{i=0}^{n}a_i a_{n-i}u(k-n)}{\left(\sum_{n=0}^{N-1}a_n\right)^2}\right], a_i=0 \text{ for all } i\geq N-1 \tag{3.18}$$

Assuming the step functions $u(k-m)=1$ for $0\leq m\leq N-1$, then

$$\theta_e(k)=\Delta\theta\left[1-\frac{2\sum_{n=0}^{N-1}a_n}{\sum_{n=0}^{N-1}a_n}+\frac{\sum_{n=0}^{2(N-1)}\sum_{i=0}^{n}a_i a_{n-i}}{\left(\sum_{n=0}^{N-1}a_n\right)^2}\right] \tag{3.19}$$

The last term of Eq.(3.19) is simply 1 since it is the unity gain of $[F_1(z)]^2$ at DC (w=0). As a result, the phase error is

$$\theta_e(k) = \Delta\theta(1-2+1) = 0 \tag{3.20}$$

This result indicates that the phase error of the FTF, using symmetrical transversal filter, due to a phase step, vanishes after 2(N-1) tap delays for all N.

Similarly, if we apply a frequency step input, $\theta_i(k)=\Delta wku(k)$, the phase error is

$$\theta_e(k) = \Delta w\left[ku(k) - \frac{2\sum_{n=0}^{N-1} a_n (k-n)u(k-n)}{\sum_{n=0}^{N-1} a_n}\right.$$

$$\left. + \frac{\sum_{n=0}^{2(N-1)} \sum_{i=0}^{n} a_i a_{n-i} (k-n)u(k-n)}{\left(\sum_{n=0}^{N-1} a_n\right)^2}\right], \quad a_i = 0 \text{ for all } i \geq N-1 \tag{3.21}$$

Assuming unit step functions (i.e. $u(k)=1$, $k \geq 0$), Eq.(3.21) becomes

$$\theta_e(k) = \Delta w\left\{k\left[1 - \frac{2\sum_{n=0}^{N-1} a_n}{\sum_{n=0}^{N-1} a_n} + \frac{\sum_{n=0}^{2(N-1)} \sum_{i=0}^{n} a_i a_{n-i}}{\left(\sum_{n=0}^{N-1} a_n\right)^2}\right]\right.$$

$$\left. + \frac{2\sum_{n=0}^{N-1} n a_n}{\sum_{n=0}^{N-1} a_n} - \frac{\sum_{n=0}^{2(N-1)} \sum_{i=0}^{n} n a_i a_{n-i}}{\left(\sum_{n=0}^{N-1} a_n\right)^2}\right\}, \quad a_i = 0 \text{ for all } i \geq N-1 \tag{3.22}$$

Applying the symmetrical property, we can obtain

$$2\sum_{n=0}^{N-1} n a_n = (N-1)\sum_{n=0}^{N-1} a_n \tag{3.23}$$

and

$$2\sum_{n=0}^{2(N-1)} \sum_{i=0}^{n} n a_i a_{n-i} = 2(N-1)\sum_{n=0}^{2(N-1)} \sum_{i=0}^{n} a_i a_{n-i} \tag{3.24}$$

Substituting these two equations and Eq.(3.19) into Eq.(3.22), the phase error is

$$\theta_e(k) = \Delta w[(N-1) - (N-1)] = 0 \tag{3.25}$$

After 2(N-1) tap delays, the phase error of the discrete FTF due to a frequency step Δw also vanishes. Consequently, a FTF employing symmetrical transversal filter can acquire a phase or a frequency step input after 2(N-1) tap delays.

Each tap delay is equal to the total delay T_d of the filter divided by N-1 intervals. Hence the delay D of the discrete FTF using the symmetrical transversal filter is

$$D = 2(N-1)[T_d/(N-1)] = 2T_d \tag{3.26}$$

Numerically, if the delay of the filter is 6μs, then the acquisition time is 12μs. Shorter acquisition time can be attained by choosing a SAW filter with faster response. Faster response in return needs a wider bandwidth, which is clearly illustrated in Figs.C.9 to C.11. The bandwidth of the filter is inversely proportional to the delay T_d.

To illustrate that the transient phase errors of the discrete FTF due to a phase and a frequency step vanish after 2(N-1) tap delays, a computer simulation of the transient responses in Eqs.(3.18) and (3.21) was carried out. SAW filters were chosen with 127 taps and the following 3 different sets of weight coefficients:

1) apodized coefficients of [sin(k/2)]/(k/2) (Fig.C.6),

2) apodized coefficients of [sin(k/6)]/(k/6) (Fig.C.7),

and 3) normalized uniform coefficients (Fig.C.8)

The results are shown in Figs.3.17 to 3.22.

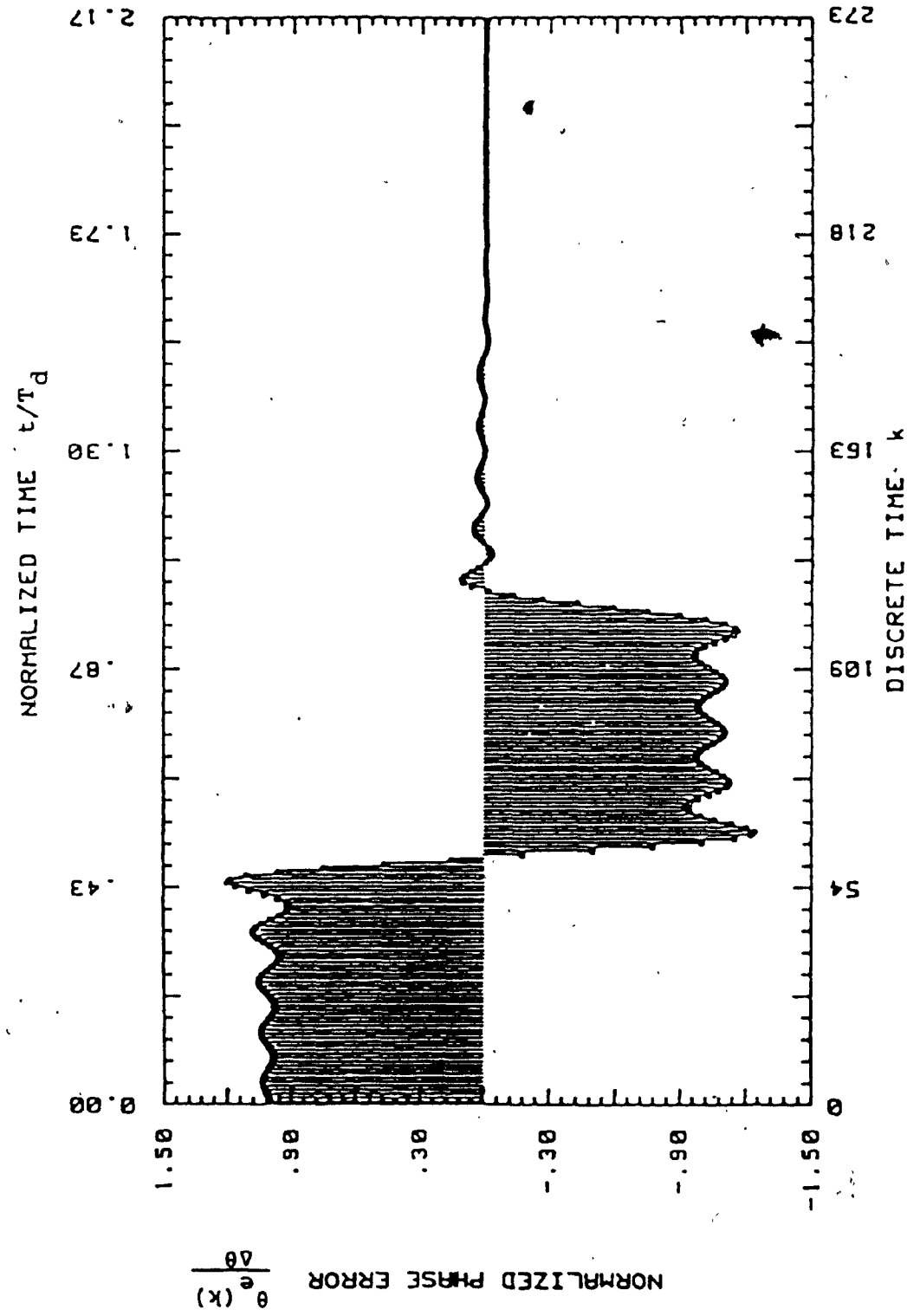

Fig. 3.17: Phase step transient phase error of discrete FTF using transversal filter with apodized coefficients $[\sin(k/2)/(k/2)]$

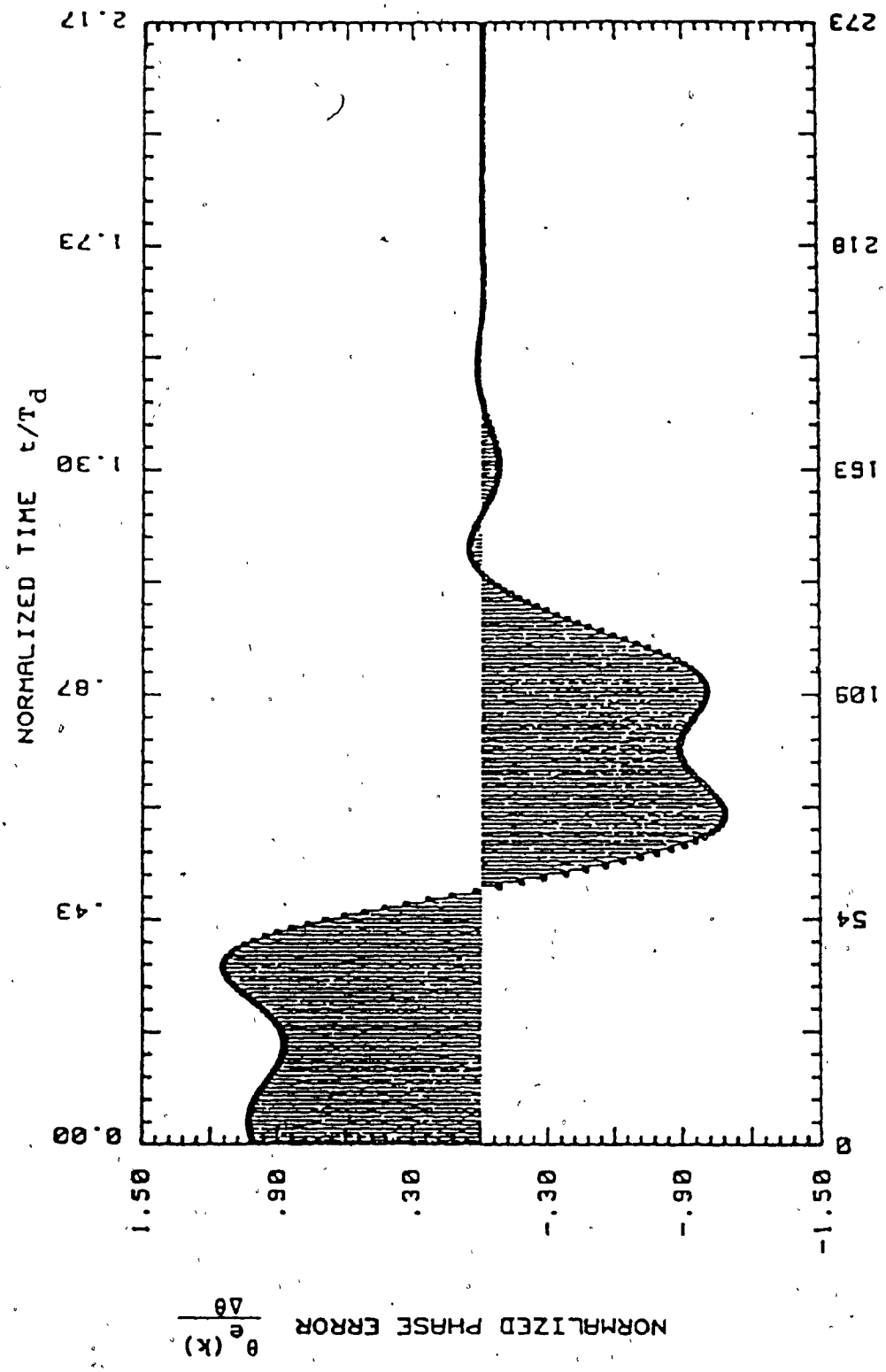

Fig. 3.18: Phase step transient phase error of discrete FTF using transversal filter with apodized coefficients $|\sin(k/6)|/(k/6)|$

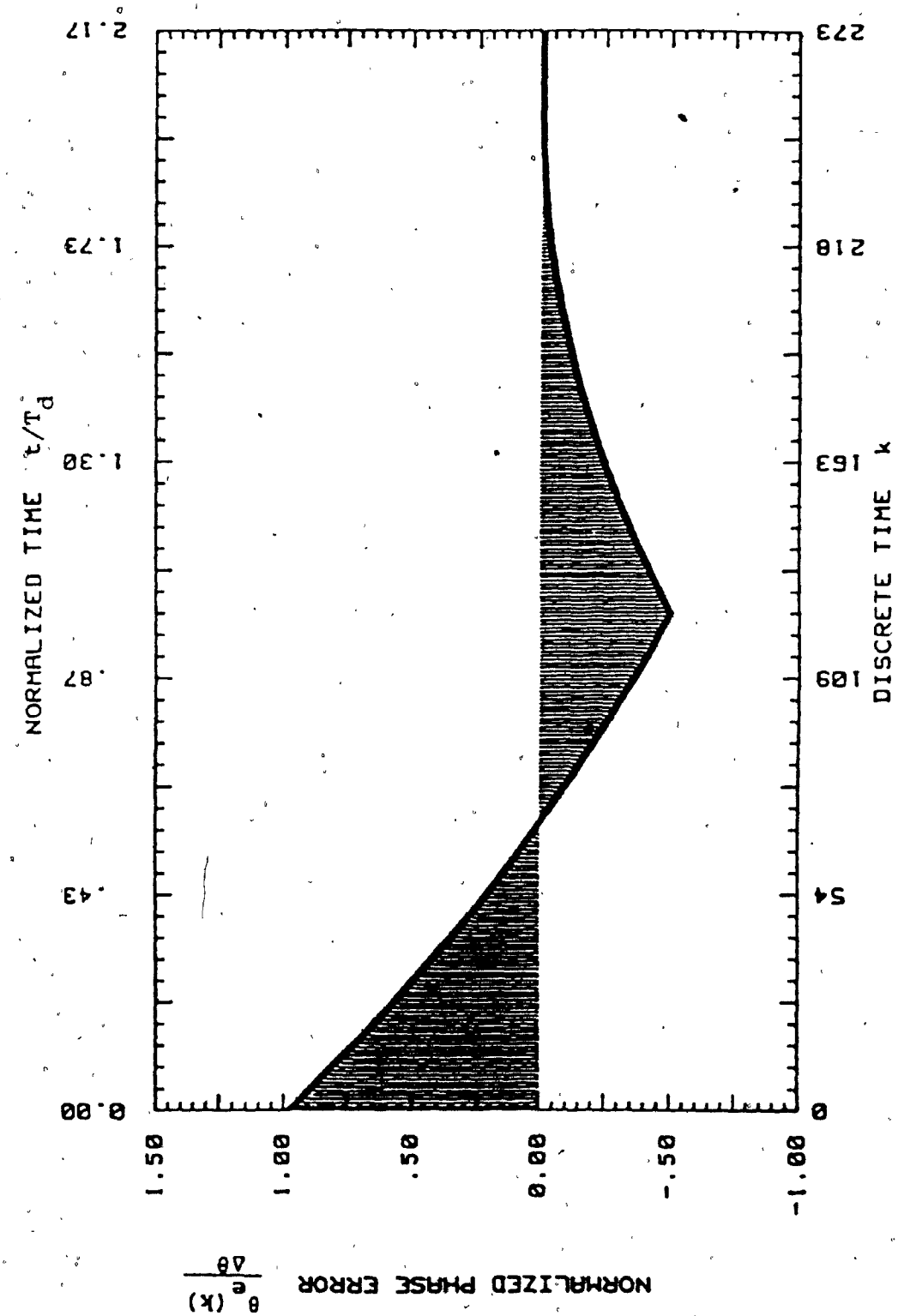

Fig. 3.19: Phase step transient phase error of discrete FTF using transversal filter with uniform coefficients

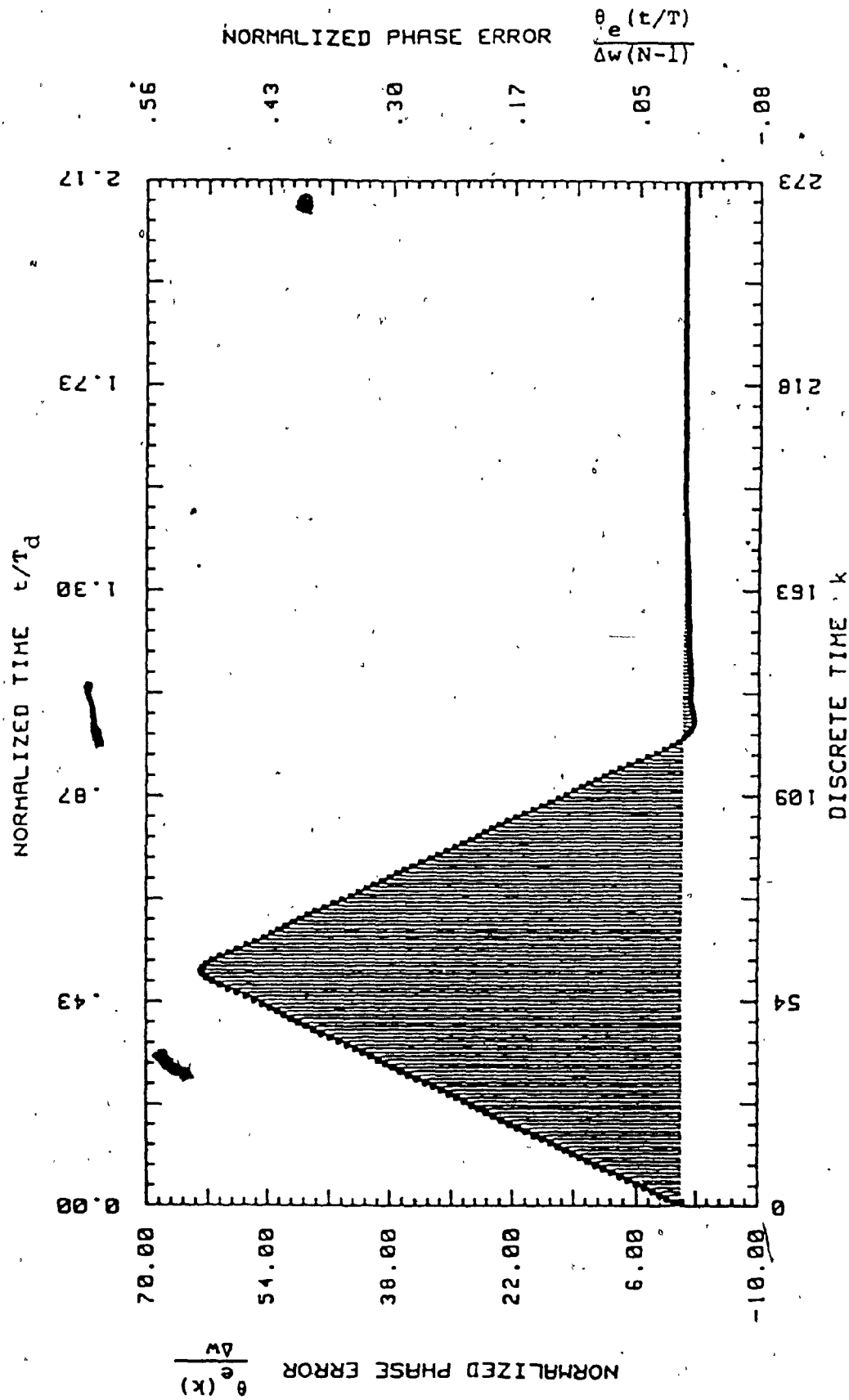

Fig. 3.20: Frequency step transient phase error of discrete FTF using transversal filter with apodized coefficients $|\sin(k/2)/(k/2)|$

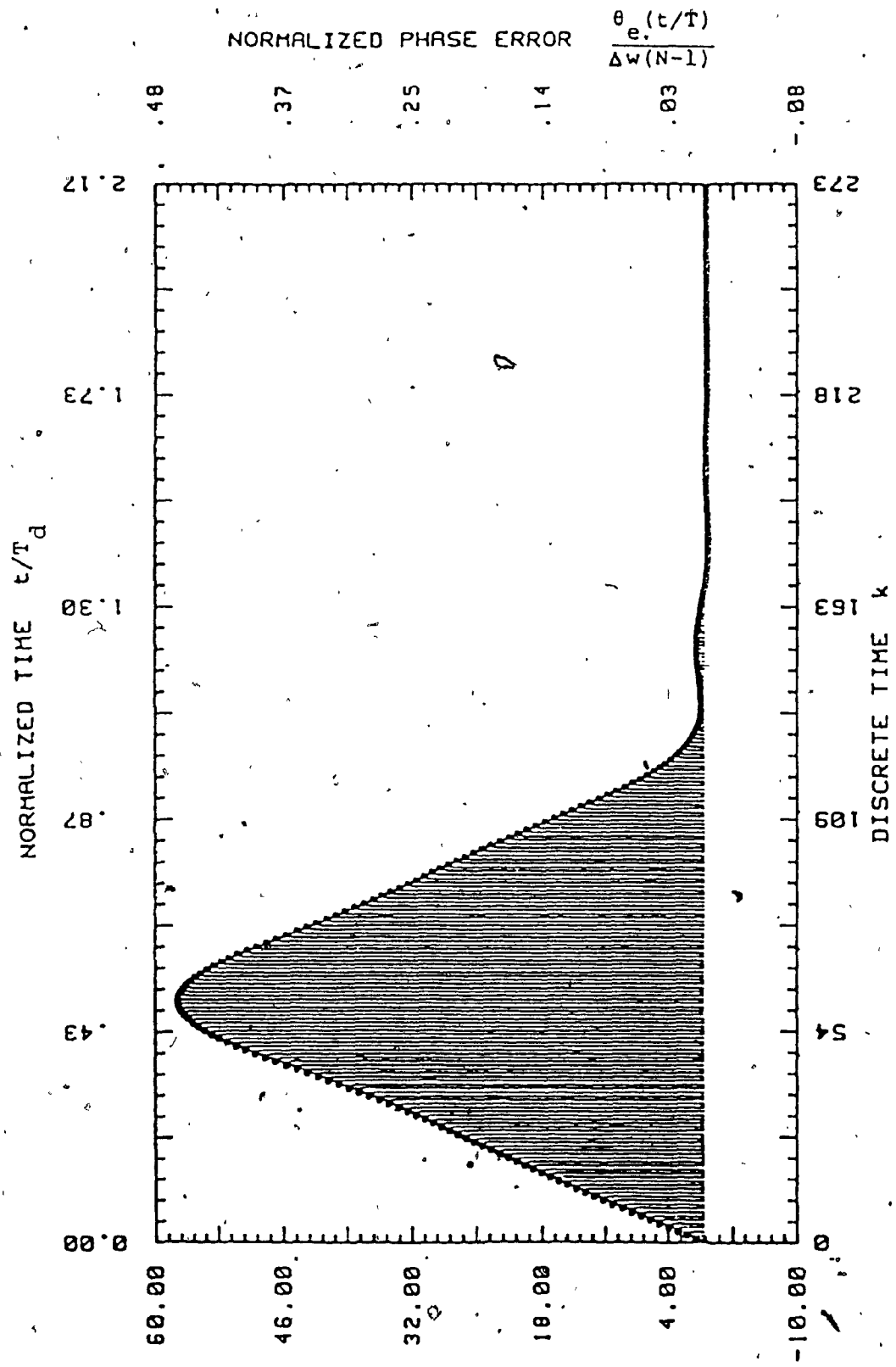

Fig. 3.21: Frequency step transient phase error of discrete FTF using transversal filter with apodized coefficients $|\sin(k/6)/(k/6)|$

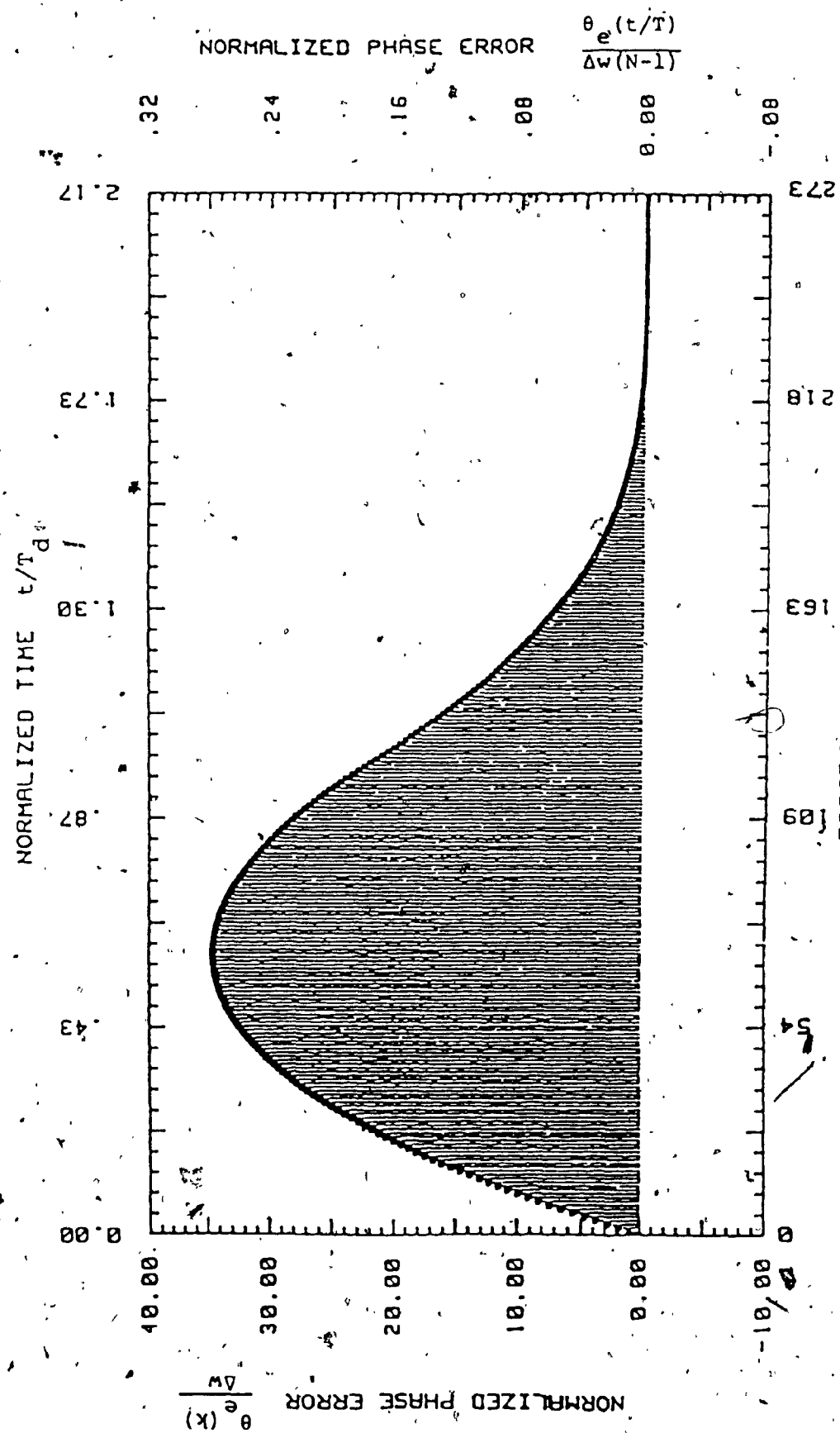

Fig. 3.22: Frequency step transient phase error of discrete FTF using transversal filter with uniform coefficients

It is found that both phase and frequency step transient phase error responses vanish after 2(N-1) = 2(126) = 252 tap delays in all three cases. In fact, the responses decay to a negligible error before 252 tap delays. The longest acquisition time is obtained with the filter having uniform coefficients because this case has the narrowest bandwidth among the three cases. As the sinc function of the apodized coefficients expands in the time domain, its corresponding rectangular characteristics shrinks in the frequency domain. In other words, the bandwidth decreases. Uniform coefficients is the extreme case when the sinc function spreads over the 127 or N taps and its bandwidth becomes the narrowest (Figs.C.11 and C.14). In Figs.3.17 and 3.20, the case with coefficients of [sin(k/2)]/(k/2) having a wider bandwidth gives a faster acquisition. The shortest acquisition time, in the simulation example, is 126 tap delays when the coefficients are zero except the 63rd coefficient.

Assuming that a SAW filter with apodized coefficient of Fig.C.7 is used, its noise equivalent bandwidth is approximately $6.3/T_d$ in Fig.C.10. Therefore, under the same noise bandwidth, it is found that

$$T_d = 12.6\tau \qquad (3.27)$$

and the total delay of the FTF will be 25.2τ. From the computer simulation result, the acquisition time of this discrete FTF is less than 25.2τ and approximately equals

18τ. Comparing with the acquisition time of the continuous second order FTF, 6τ, the acquisition performance of the discrete FTF seems to be degraded. This result is expected as the signal has to pass through each tap delay in order to achieve filtering effect.

A SAW BPF with apodized coefficients, centered at 70MHz, is used in an experimental discrete FTF. As in the case with the first order continuous FTF, no phase error occurs at the output of the BPF's (Fig.3.23) if a phase step input is applied. The measured results shown in Fig.3.23a indicate the delay of one SAW BPF to be around 11μs. The acquisition time of the discrete FTF is found to be 20μs, less than 22μs, as shown in Fig.3.24. Compared to the simulated result in Fig.3.18, the experimental result bears a close resemblance.

The transient responses of the discrete FTF due to a frequency step of 40 kHz are shown in Figs.3.25 to 3.27. The error induced by the frequency offset at the output of one single SAW and cascaded SAW are 37.5 degrees and 80 degrees respectively. These errors are corrected at the output of the discrete FTF after 20μs. The experimental result also agrees with the simulated result in Fig.3.21.

In summary, fast acquisition is achieved in both Continuous and Discrete FTF. Compromise is always required between fast acquisition and narrow bandwidth. Under the

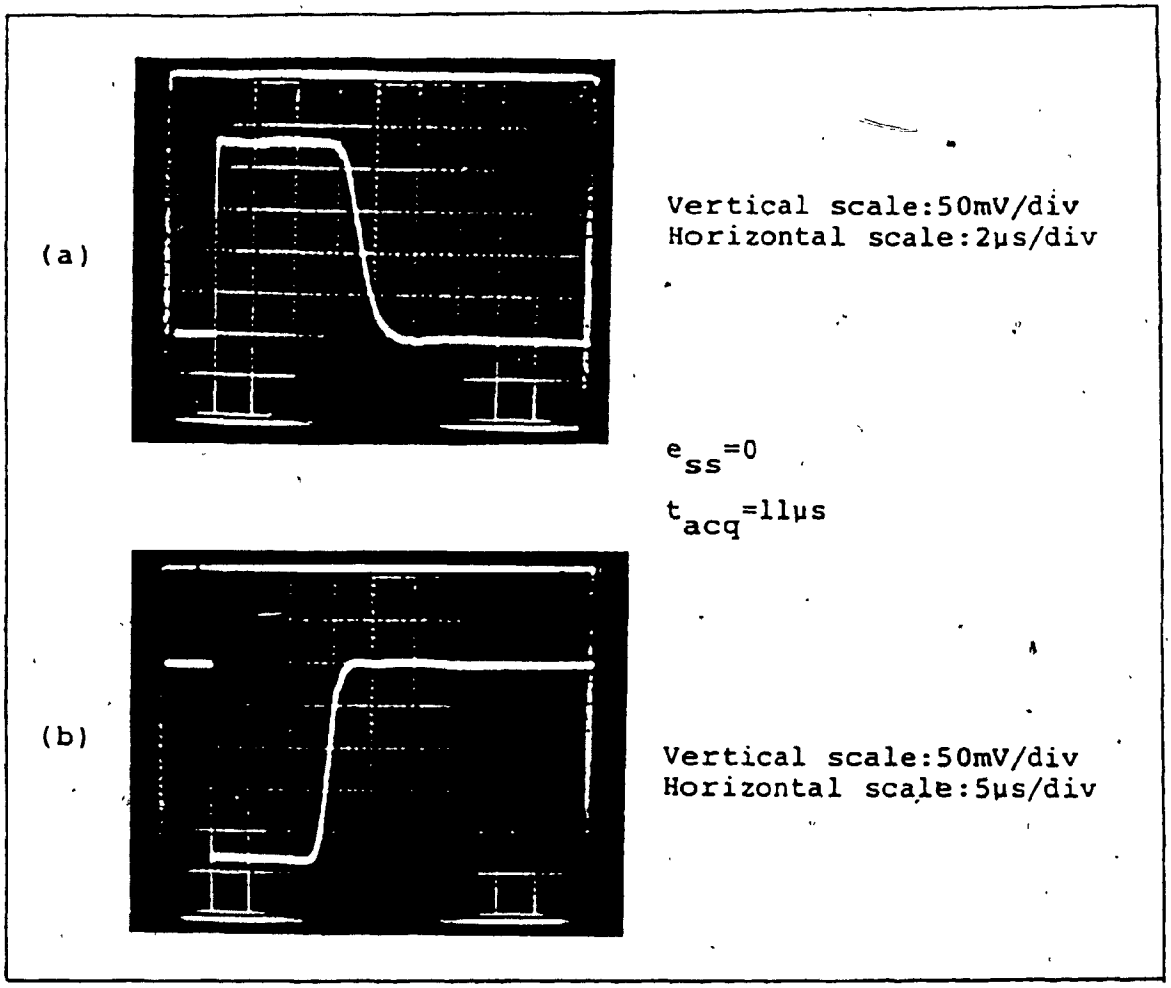

Fig. 3.23: Measured phase step transient phase error of a single SAW BPF (a), and two SAW BPF's in cascade (b)

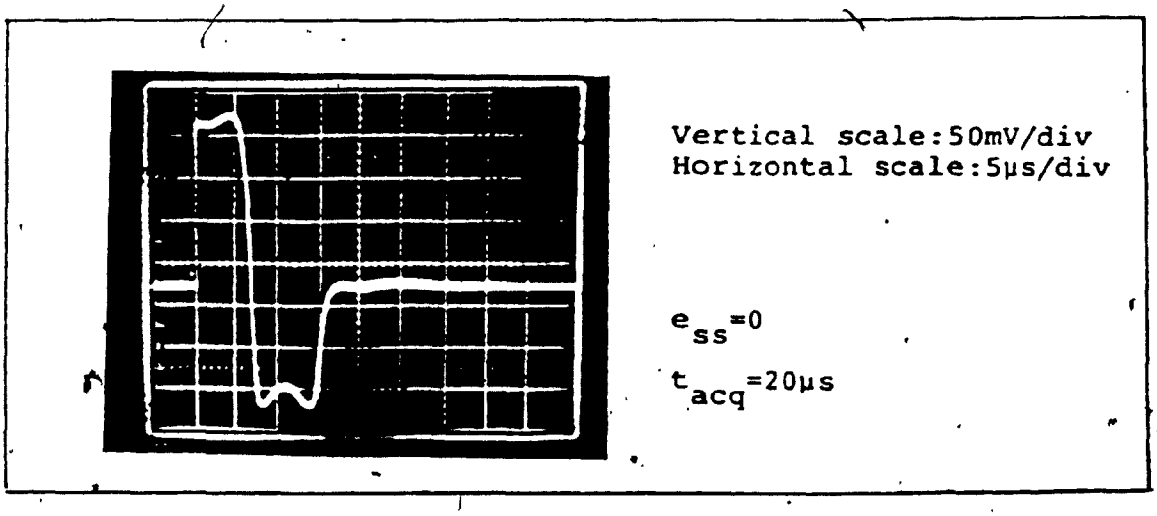

Fig. 3.24: Measured phase step transient phase error of a discrete FTF using SAW BPF's

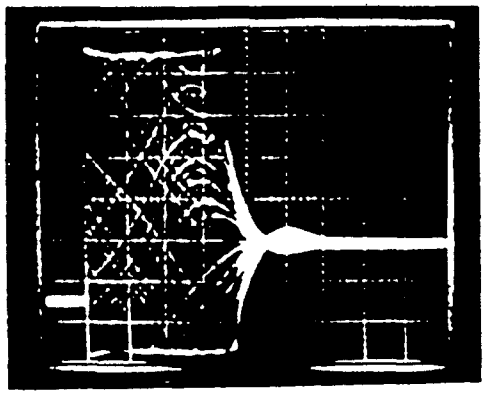

Vertical scale:50mV/div
Horizontal scale:2μs/div

(a) Multiple traces

e_{ss}=37.5°

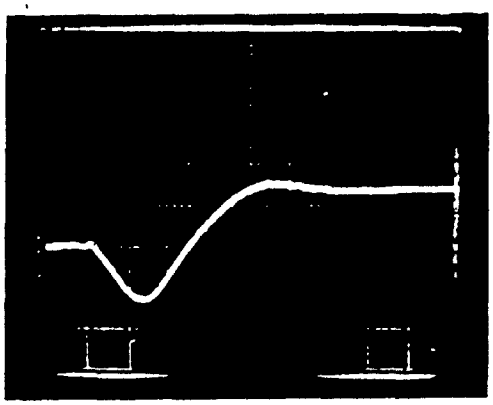

(b) Single trace

Fig. 3.25: Measured frequency step transient phase error of a single SAW BPF

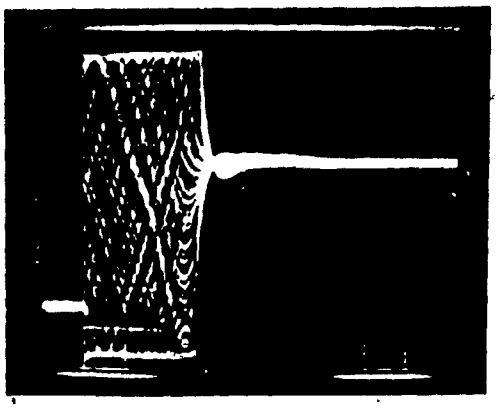

Vertical scale:50mV/div
Horizontal scale:5μs/div

(a) Multiple traces

e_{ss}=80°

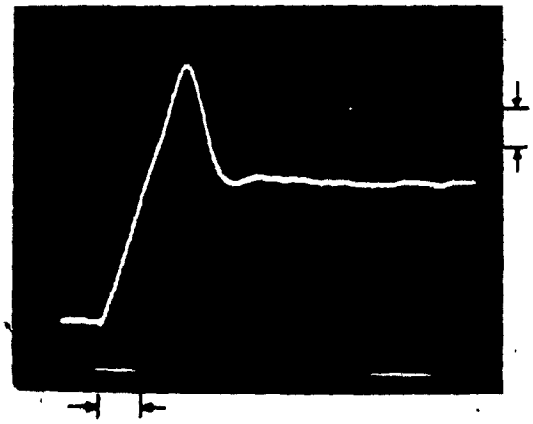

(b) Single trace

Fig. 3.26: Measured frequency step transient phase error of of two SAW BPF's in cascade

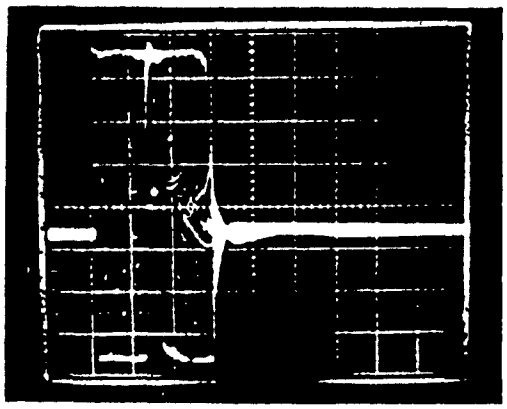

Vertical scale:50mV/div
Horizontal scale:5μs/div

(a) Multiple traces

$e_{ss}=0$

$t_{acq}=20\mu s$

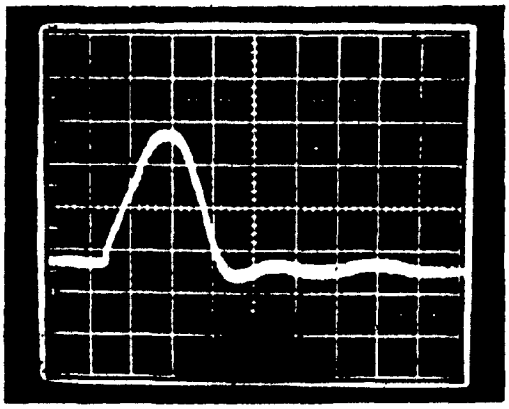

(b) Single trace

Fig. 3.27: Measured frequency step transient phase error of a discrete FTF using SAW BPF's

constraint of the equivalent noise bandwidth of the BPF, the second order synchronous FTF can achieve the same or better acquisition performance than the higher order FTF. In the case of the discrete FTF, similar acquisition performance with minor degradation in acquisition time is obtained. The symmetrical transversal filter with apodized coefficients assures that the FTF acquires the phase and frequency within two times of the BPF delay.

3.4 Interburst transient behaviour of the FTF

The foregoing discussion assumes that the FTF is in zero initial state. This assumption is valid if there is sufficient time allowed for the BPF's to decay their residual voltage of the previous excitation before a new input is received. However, in some applications, for example, the TDMA carrier recovery circuit, the signal changes swiftly from one burst to the next and results in two types of effects [4,6]:

1) signal level at the filter output rises asymptotically, causing the signal-to-noise ratio to rise accordingly,
2) the interaction of the decaying signal from the previous burst with the increasing signal in the present burst.

The transient due to these effects, called interburst transient or Inter-Burst-Interference (IBI), depends upon

the initial phase difference between the signal of each burst. The phase perturbation due to this transient effect is of interest, especially its effect on the acquisition performance of the FTF.

To analyze the IBI behaviour, the carrier frequency of the two bursts are assumed to be identical. Both BPF's are then tuned to this frequency. It is also assumed that the preceding burst has a phase of $\Delta\theta$ while the present burst has a zero phase. Moreover, no gap between the bursts (the worst case) is assumed.

With these assumptions, the bandpass signal of the preceding burst can be represented as

$$v_{-1}(t) = \mathrm{Re}[c_{-1}(t)e^{jw_o t}] \tag{3.28}$$

where $c_{-1}(t) = \alpha A e^{j\Delta\theta} u(-t)$

which is the equivalent lowpass signal of $v_{-1}(t)$. α is the voltage ratio of the amplitude A between the preceding and the current bursts, and u(t) is the unit step function. Similarly, the present burst signal is represented as

$$v_i(t) = \mathrm{Re}[c_i(t)e^{jw_o t}] \tag{3.29}$$

where $c_i(t) = Au(t)$.

The analog filters regarded as linear bandpass systems can also be expressed in terms of their equivalent lowpass analog, i.e. the impulse response of the bandpass filter is

$$f(t) = 2\mathrm{Re}[f_1(t)e^{jw_o t}] \tag{3.30}$$

where $f_1(t)$ is the impulse response of the equivalent lowpass filter. By superposition, the desired phase output of the BPF due to the excitation of the preceding and the present bursts is computed by

$$\theta(t) = \int_{-\infty}^{\infty} f_1(\lambda)[c_1(t-\lambda)+c_{-1}(t-\lambda)]d\lambda \tag{3.31}$$

Explicitly, the convolution of Eq.(3.31) can be written as

$$\theta(t) = A\int_0^t f_1(\lambda)d\lambda + \alpha Ae^{j\Delta\theta}\int_t^{\infty} f_1(\lambda)d\lambda \tag{3.32}$$

With the aid of Eq.(3.32), the phase output of BPF1 and BPF2 (Fig.2.2) of a single-tuned, a double-tuned and a second order Butterworth FTF are given in Table 3.6. The phase output of the FTF's is then computed with

$$\theta_o(t') = 2\theta_1(t') - \theta_2(t') \tag{3.33}$$

where $t' = t/\tau$. The results are illustrated separately in Figs.3.28, 3.29 and 3.30 with different initial phase difference between two successive bursts. It is noted that the maximum phase error is ±180 degrees while it is ±45 degrees in [7]. The two "divide-by-two" devices in [7] cause the phase error to be reduced by a factor of 4. Moreover, these three figures show that the residual voltage due to the preceding burst does not degrade the acquisition performance of the FTF. The phase output of the FTF settles to the input phase of the present burst as fast as is the case without initial phase error.

FTF with	θ_1	θ_2
Single-tuned BPF	$\tan^{-1}\{a\sin(\Delta\theta)e^{-t'}/(1-[1-a\cos(\Delta\theta)]e^{-t'})\}$	$\tan^{-1}\{a\sin(\Delta\theta)(1+t')e^{-t'}/(1-[1-a\cos(\Delta\theta)](1+t')e^{-t'})\}$
Double-tuned BPF	$\tan^{-1}\{a\sin(\Delta\theta)(1+2t')e^{-2t'}/(1-[1-a\cos(\Delta\theta)](1+2t')e^{-2t'})\}$	$\tan^{-1}\{a\sin(\Delta\theta)[1+2t'+\frac{(2t')^2}{2}+\frac{(2t')^3}{6}]e^{-2t'}/(1-[1-a\cos(\Delta\theta)][1+2t'+\frac{(2t')^2}{2}+\frac{(2t')^3}{6}]e^{-2t'})\}$
Second order Butterworth BPF	$\tan^{-1}\{a\sin(\Delta\theta)[\sin(t')+\cos(t')]e^{-t'}/(1-[1-a\cos(\Delta\theta)][\sin(t')+\cos(t')]e^{-t'})\}$	$\tan^{-1}\{a\sin(\Delta\theta)[(1-t')\cos(t')+(2+t')\sin(t')]e^{-t'}/(1-[1-a\cos(\Delta\theta)][(1-t')\cos(t')+(2+t')\sin(t')]e^{-t'})\}$
$t'=t/\tau$		

Table 3.6: Transient phase errors, $\theta_1(t)$ and $\theta_2(t)$, of first-order and second-order FTF due to IBI

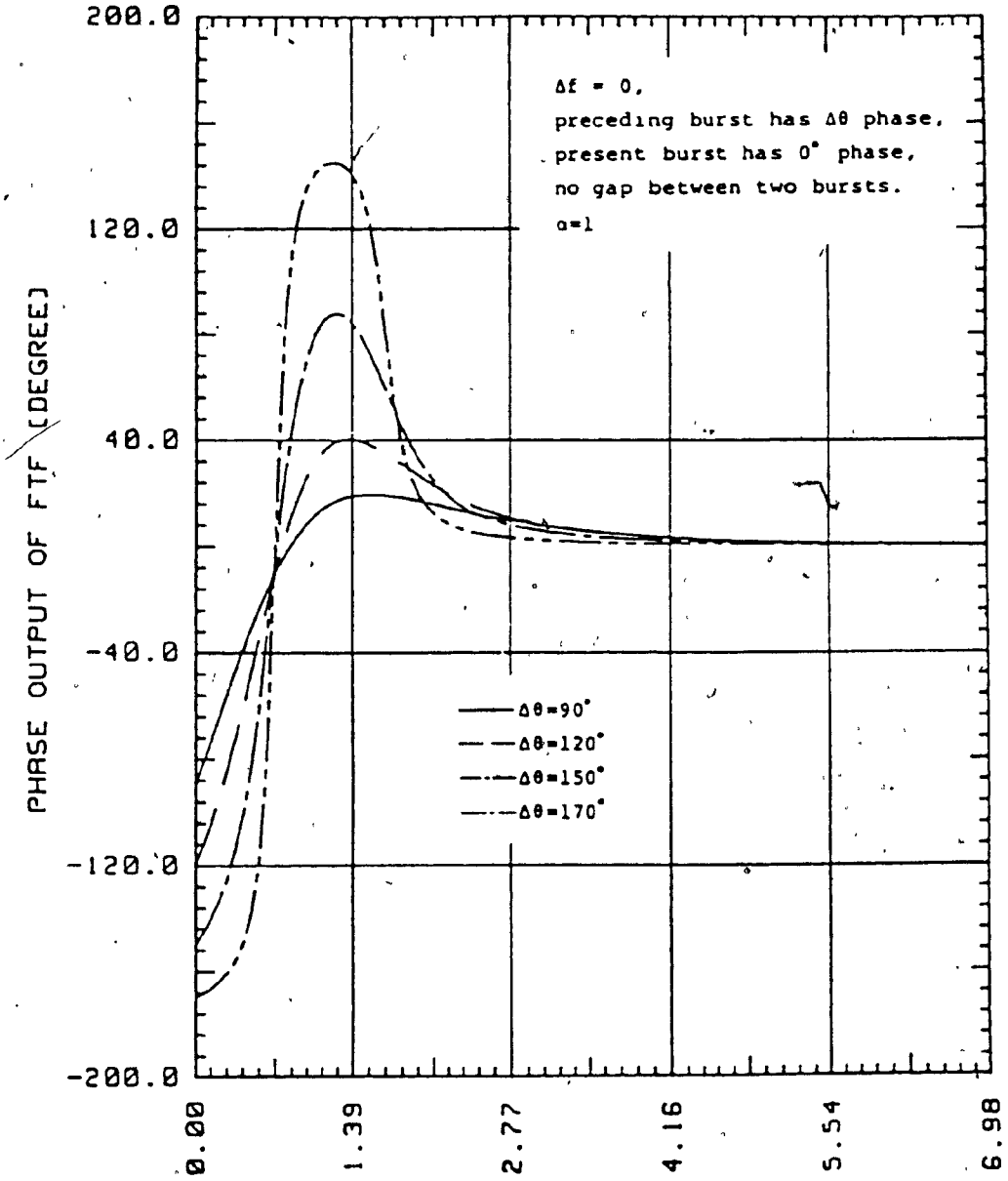

Fig. 3.28: Transient phase output of single-tuned FTF due to IBI

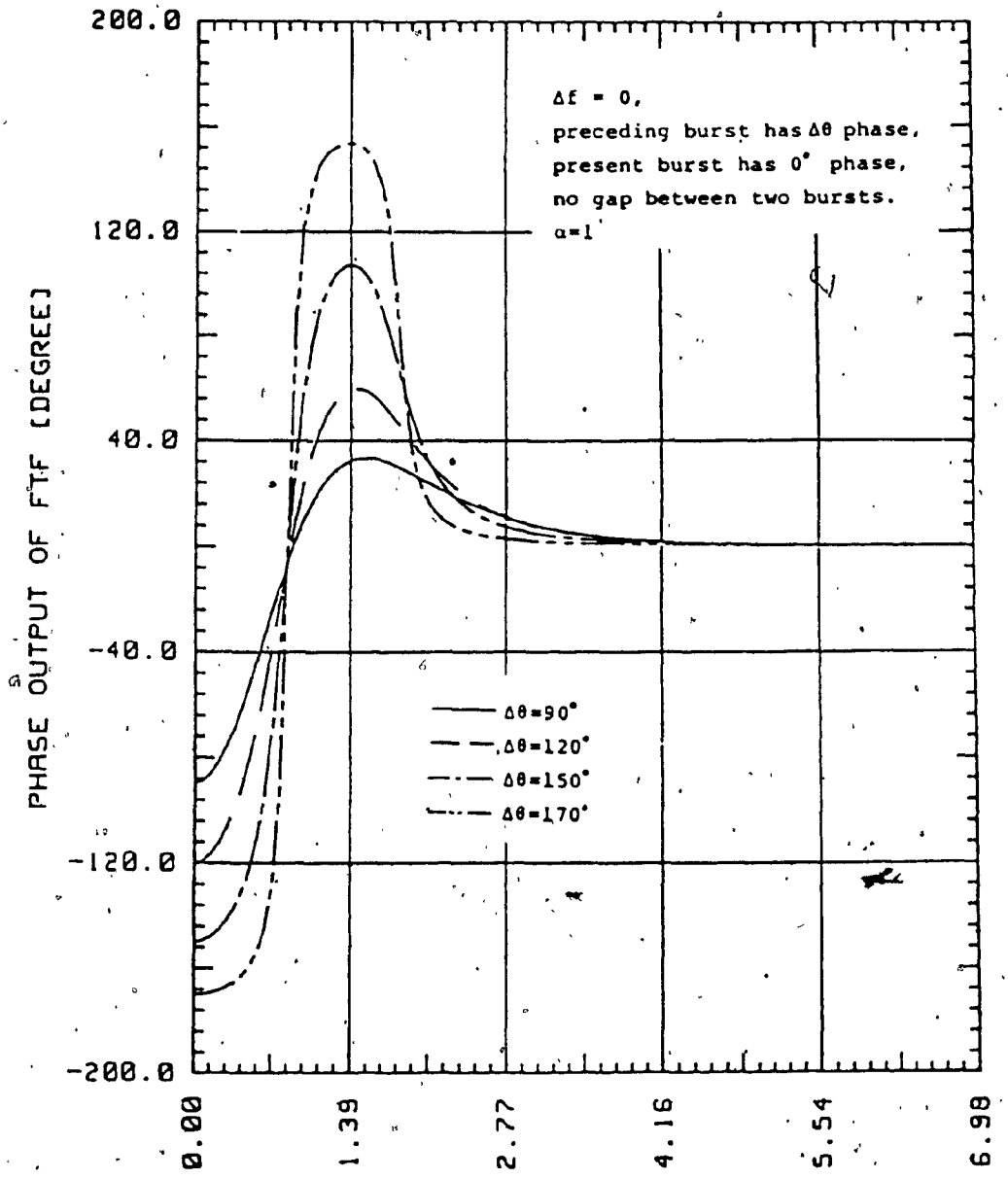

Fig. 3.29: Transient phase output of double-tuned FTF due to IBI

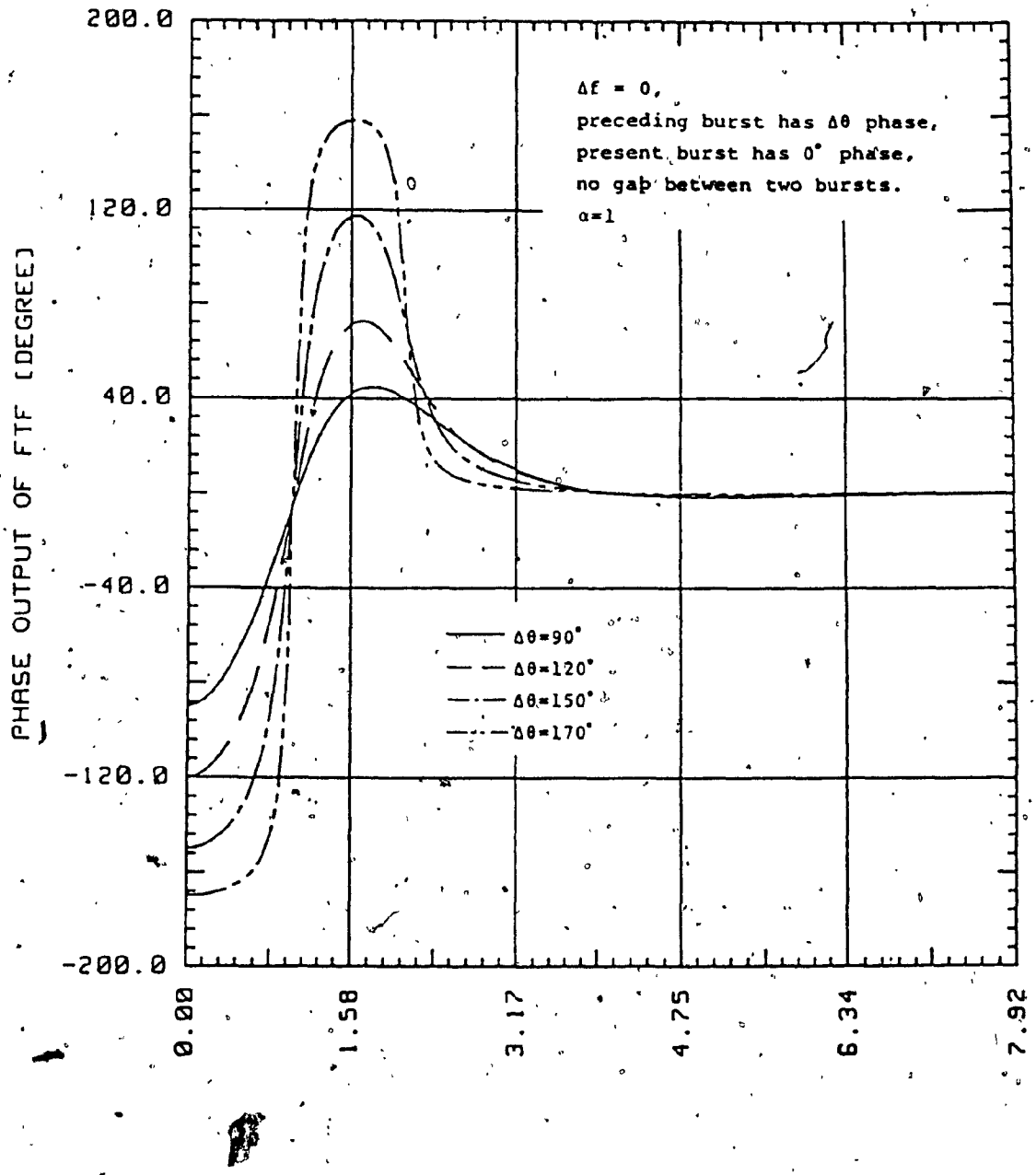

Fig: 3.30: Transient phase output of a second-order Butterworth FTF due to IBI

3.5 "Hang-up-free" characteristics

As mentioned before, PLL occasionally exhibits prolonged phase transient and this phenomenon is called 'hang up'. Hangup is a serious problem in fast acquisition applications. The fundamental cause of this problem is due to the feedback configuration and the nonlinear periodic characteristics of the phase detectors (so far all of the well known phase detectors have a periodic characteristics versus the phase error). In the first order PLL, hangup can be visualized when the initial phase error falls on the vicinity of the unstable null of the phase error characteristics. The error voltage or the restoring force at this unstable null is small so that the loop converges very slowly towards the stable null [1,3]. It has been investigated that the presence of noise worsen this problem. Noise can introduce equivocation and cause the loop to wander about this null.

Using the phase plane point of view, the hangup will occur in a second order PLL if the state trajectory of the loop comes near the saddle point or the unstable equilibrium node in the phase plane [10]. From Fig.3.31, there are alternate stable and unstable nodes in the phase plane resulting from the periodic characteristics of the phase detector. When the phase error rate $\dot{\theta}_e$ comes near the separatrix (the line passes through the unstable node), a longer time is needed to reach the stable node and hence,

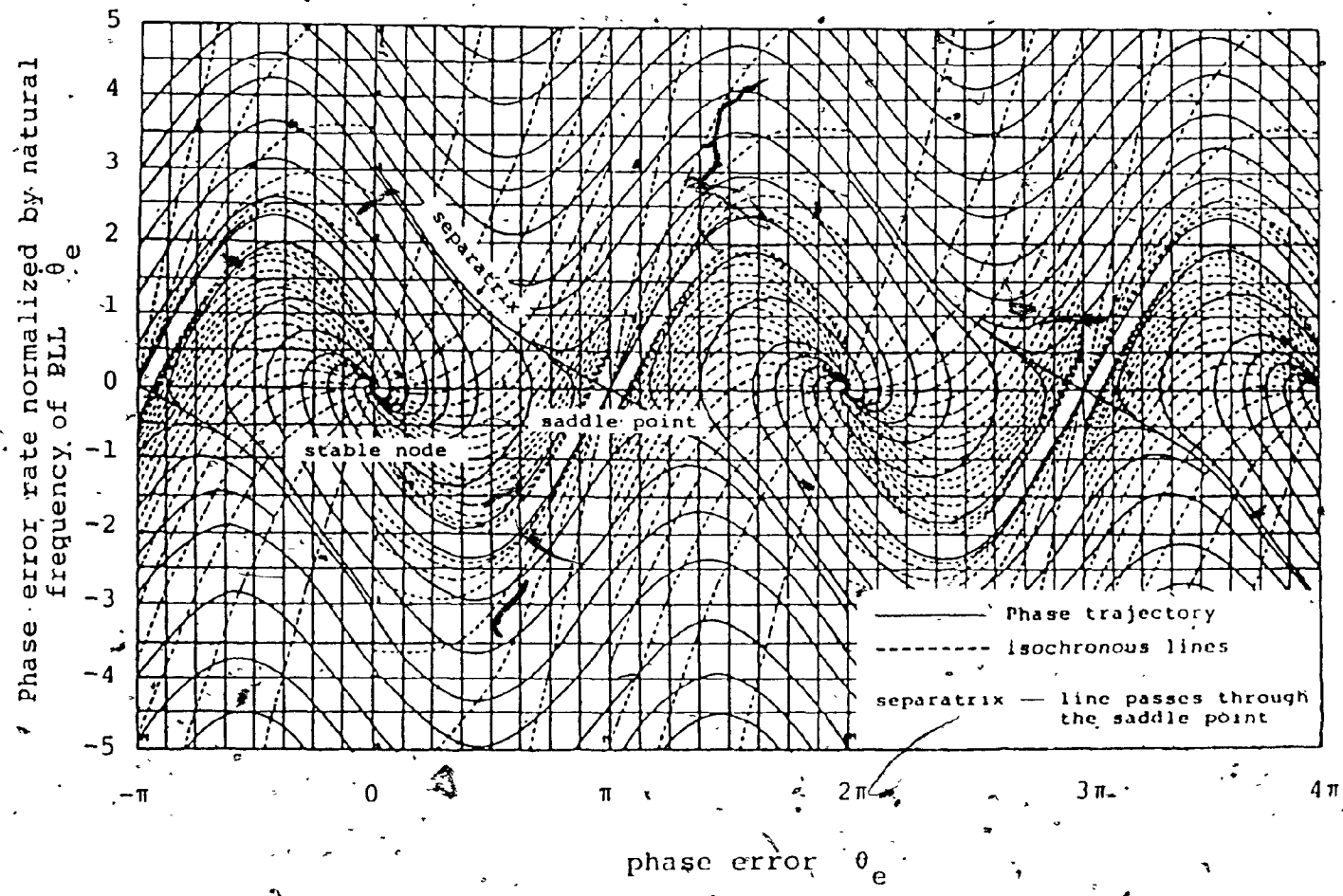

Fig. 3.31: Phase plane trajectories of a second order PLL with sinusoidal phase detector (from [22])

hangup is likely to occur.

It is difficult to solve the hangup problem as it is a natural feature of the PLL [3]. If the nonlinear periodic characteristics is removed, the hangup problem can be solved. This is exactly the solution inherently provided by the FTF. Phase detector is not used in the FTF and its lowpass equivalent model is strictly linear. In fact, if the PLL is assumed to operate as a linear system, the hangup phenomenon will not occur.

Consider the first order FTF using single-tuned BPF's. The differential equation of the phase error from Eq.(3.4) is derived as

$$\ddot{\theta}_e + \frac{2}{\tau}\dot{\theta}_e + \frac{1}{\tau}\theta_e = 0 \tag{3.34}$$

which is an ordinary differential equation that can be rewritten in matrix form as

$$\dot{\underline{U}} = \underline{A}\underline{U} \tag{3.35}$$

by defining two variables

$$u_1 = \theta_e \tag{3.36a}$$

$$u_2 = \dot{\theta}_e \tag{3.36b}$$

where the matrix $\underline{A}$ is

$$\underline{A} = \begin{bmatrix} 0 & 1 \\ -\frac{1}{\tau^2} & -\frac{2}{\tau} \end{bmatrix} \tag{3.37}$$

The eigenvalues of Eq.(3.35) are found to be real and equal with the value of $-1/\tau$. For a system specified by Eq.(3.35), there is only one equilibrium point at $(\theta_e=0, \dot{\theta}_e=0)$ and it is stable because the eigenvalues are real and negative [16]. This result is expected since the nonlinearity and the periodicity are removed. The result also means that the phase error and the phase error rate approach asympotically the stable equilibrium node as the time approaches infinity without passing any saddle point. Assigning two arbitrary constants c_1 and c_2, the exact state trajectory can be found as

$$\frac{\dot{\theta}_e}{\theta_e} = \frac{c_2 + (\frac{c_1}{\tau} + c_2)\ln \frac{\frac{1}{\tau}\theta_e + \dot{\theta}_e}{\frac{c_1}{\tau} + c_2}}{c_1 - (\frac{c_1}{\tau} + c_2)\tau \ln \frac{\frac{1}{\tau}\theta_e + \dot{\theta}_e}{\frac{c_1}{\tau} + c_2}} \qquad (3.38)$$

This shows that the stable node is at (0;0) and that the trajectories asympotically converge to this node. Therefore, the first order FTF is free from hangup by successfully removing the nonlinear periodicity inherent in the PLL. These results are also applicable for higher order FTF. It can be concluded that the best method to solve the hangup problem is eliminating the saddle point in the phase plane, in other words, a scheme other than PLL has to be used. Feedforward compensation scheme is one of the schemes that has this potential.

CHAPTER 4

STEADY-STATE BEHAVIOUR OF FTF

It is known that superior steady-state performance of a tracking BPF is achieved at the expense of the bandwidth of the BPF. The tradeoff between these two conflicting requirements of the FTF is studied in this chapter. Before this investigation, a thorough analysis of the steady-state behaviour of the FTF in a noise-free environment is presented. Its behaviour in an additive white Gaussian noise environment will be studied in chapter 5. The analysis in the absence of noise provides an understanding of the tracking capability and limitation of both continuous and discrete FTF's. In practice, it is quite difficult to realize two perfectly identical BPF's due to component variations. Effects of mismatched synchronously tuned BPF's and transversal BPF's on the tracking behaviour of the FTF are analytically and experimentally investigated. Measured frequency responses of an experimental continuous FTF are also included to illustrate the signal processing mechanism of the bandpass model of the FTF. It is found that a narrower output bandwidth is measured if the conventional method of sweeping the input signal across the bandwidth of interest is used. However, this illusive narrower bandwidth is not beneficial for a nonlinear system when noise comes into effect.

4.1 Steady-state analysis of FTF

For the purpose of illustration, the error function of Eq. (2.2) is rewritten as

$$\theta_e(s) = [1 - 2K_m K_d F_1(s) + K_m F_1^2(s)]\, \theta_i(s) \qquad (4.1)$$

With respect to a frequency step input, the steady-state error of FTF can be obtained by using the final value theorem of the Laplace transform, that is

$$\lim_{s\to 0} s\theta_e(s) = \lim_{s\to 0} [1-2K_m K_d F_1(s)+K_m F_1^2(s)]\frac{\Delta w}{s} \qquad (4.2)$$

The limit exists if the quantity inside the square bracket equals to zero. The same concept is applied for a phase step input. The DC gain of the lowpass equivalent of the BPF is then found to be dependent upon the doubler gain K_d and the multipler gain K_m,

$$F_1(0) = K_d \quad \text{and} \quad F_1(0) = 1/\sqrt{K_m}$$

The simplest solution is when both doubler and multiplier have unity gain. Under this criteria, a BPF with unity gain is necessary for FTF to achieve tracking. The sufficiency depends on the transfer function and it is investigated henceforth.

4.1.1 Tracking of Continuous FTF

From the previous discussion in Chapter 3, it is clear that the FTF of any order is capable of tracking any phase

step or frequency step input signal. Consider the case of general second order FTF. The steady-state error, e_{ss}, is found by applying the final value theorem, i.e.

$$e_{ss} = \lim_{t\to\infty} \theta_e(t) = \lim_{s\to 0} s\theta_e(s)$$

$$= \lim_{s\to 0} \frac{s(s^4+4\zeta w_c s^3+4\zeta^2 w_c^2 s^2)}{s^4+4\zeta w_c s^3+(2\zeta^2+1)2w_c^2 s^2+4\zeta w_c^3 s+w_c^4} \cdot \frac{\Delta\dot{w}}{s^3}$$

$$= \frac{4\zeta^2 \Delta\dot{w}}{w_c^2} \qquad (4.3)$$

if the input $\theta_i(s) = \Delta\dot{w}/s^3$.

Eq.(4.3) is the steady-state error or dynamic tracking error of the second order FTF if the input frequency varies linearly with time (frequency velocity). The error can be reduced either by decreasing ζ or by increasing w_c. However, decreasing ζ will cause instability of the loop and poor acquisition. On the other hand, increasing w_c implies increasing the bandwidth of the BPF and hence increasing the unwanted noise power. Moreover, the steady-state error is unbounded if the inputs have frequency acceleration ($\theta_i(s) = \Delta\ddot{w}/s^4$).

Similarly, it can be proved that higher order FTF's also cannot track frequency velocity and frequency acceleration inputs. However, this limitation is not serious since frequency velocity or frequency acceleration of an input seldom occurs in practice.

4.1.2 Tracking of Discrete FTF

In case of discrete FTF, the final value theorem of z-transform,

$$e_{ss} = \lim_{k\to\infty} \theta_e(k) = \lim_{z\to 1} (z-1)\theta_e(z) \tag{4.4}$$

is used to find the steady-state error. e_{ss} is evaluated by substituting different types of input into Eq.(4.4). Three types of inputs are interesting and their z-transform pairs are given in Table 4.1.

For the first case, we obtain the steady-state error of the discrete FTF upon an input with a phase step as

$$e_{ss} = \lim_{z\to 1} \left\{1-2F_1(z)+[F_1(z)]^2\right\} z\Delta\theta \tag{4.5}$$

where $F_1(z)$ is defined in Eq.(3.16). Since $F_1(1)=1$, e_{ss} in Eq.(4.5) is zero. For a frequency step input,

$$e_{ss} = \lim_{z\to 1}\left[1- \frac{2\sum_{n=0}^{N-1} a_n z^{-n}}{\sum_{n=0}^{N-1} a_n} + \frac{\sum_{n=0}^{2(N-1)} \sum_{i=0}^{n} a_i a_{n-i} z^{-n}}{\left(\sum_{n=0}^{N-1} a_n\right)^2}\right] \frac{z}{z-1}\,\Delta w \tag{4.6}$$

where $a_i = 0$ for all $i > N-1$.

Applying the L'Hôpital's rule, the limit becomes

$$e_{ss} = \lim_{z\to 1}\left[1- \frac{2\sum_{n=0}^{N-1} a_n z^{-n}(-n+1)}{\sum_{n=0}^{N-1} a_n} + \frac{\sum_{n=0}^{2(N-1)} \sum_{i=0}^{n} a_i a_{n-i} z^{-n}(-n+1)}{\left(\sum_{n=0}^{N-1} a_n\right)^2}\right] \Delta w$$

which is simiplified by using Eq.(3.23) and (3.24), i.e.

$$e_{ss} = \left[\frac{2\sum_{n=0}^{N-1} n a_n}{\sum_{n=0}^{N-1} a_n} - \frac{\sum_{n=0}^{2(N-1)} \sum_{i=0}^{n} n a_i a_{n-i}}{\left(\sum_{n=0}^{N-1} a_n \right)^2} \right] \Delta\dot{w} = 0 \qquad (4.7)$$

This shows that the discrete FTF also can track phase and frequency step input signals. This result agrees with the result obtained from the transient analysis in Chapter 3.

Further, e_{ss} is evaluated by applying frequency velocity to the FTF. After using L'Hôpital's rule twice and simplifying the expression with Eqs.(3.23) and (3.24), we get

$$e_{ss} = \left[\frac{1}{2} - \frac{2\sum_{n=0}^{N-1} a_n n^2}{\sum_{n=0}^{N-1} a_n} + \frac{\sum_{n=0}^{2(N-1)} \sum_{i=0}^{n} a_i a_{n-i} n^2}{\left(\sum_{n=0}^{N-1} a_n \right)^2} \right] \Delta\dot{w} \qquad (4.8)$$

Eq.(4.8) is the steady-state error of the discrete FTF using symmetrical transversal BPF when frequency velocity is applied. Instead of depending on ζ and cutoff frequency w_c, the phase error depends on two parameters in the time domain, namely the weight coefficient and the number of taps. Large error will result if a umiform coefficient transversal BPF is used. On the contrary, a smaller error will result if an apodized coefficient transversal BPF is used because the alternate signed coefficient values provide cancellation of error. Reducing the number of taps N, is another way to minimize the error. Both methods, however,

need a wider bandwidth and hence suffer from increased noise power. From this analysis, the incapability of tracking frequency velocity, and frequency acceleration is also shown to be a limitation of the discrete FTF.

4.2 FTF with mismatched BPF's

Due to the component tolerance and variation, perfectly matched* filters are practically difficult to realize. Effects of mismatched BPF's on the tracking performance of the FTF are investigated by representing BPF2 as $G_1(s)$ as depicted in Fig.4.1. The error function of Eq.(2.3) is subsequently modified as

$$E(s) = 1-2F_1(s)+F_1(s)G_1(s) \tag{4.9}$$

Although the two BPF's have different characteristics, the FTF can still track a phase step input as long as the BPF's have unity gain, i.e.

$$e_{ss} = \lim_{s\to 0} [1-2F_1(s)+F_1(s)G_1(s)]\Delta\theta = 0 \tag{4.10}$$

for $F_1(0) = G_1(0) = 1$.

For a frequency step input, e_{ss} becomes

$$e_{ss} = \lim_{s\to 0} [1-2F_1(s)+F_1(s)G_1(s)]\frac{\Delta w}{s}$$

$$= [G'_1(0) - F'_1(0)]\Delta w \tag{4.11}$$

---

* "Matched" filters in this case means that the filters are identical

	time domain	z-domain
phase step	$\Delta\theta u(k)$	$\Delta\theta\frac{z}{z-1}$
frequency step	$\Delta w k u(k)$	$\Delta w\frac{z}{(z-1)^2}$
frequency velocity	$\Delta \dot{w} k^2 u(k)$	$\Delta \dot{w}\frac{z(z+1)}{(z-1)^3}$

Table 4.1: z-transform pairs of three inputs for steady-state analysis of discrete FTF

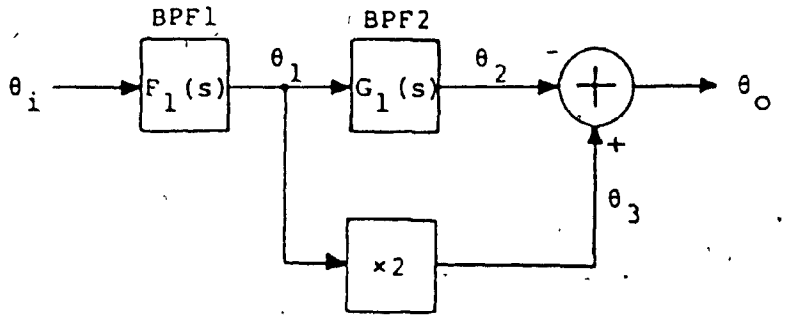

Fig. 4.1: Equivalent lowpass model of FTF with mismatched BPF's

after using the L'Hôpital's rule. If the synchronously tuned circuit is used, the equivalent lowpass transfer functions of the BPF's are

$$F_1(s) = \prod_{i=1}^{n} \frac{w_{ci}}{s + w_{ci}} \tag{4.12a}$$

$$G_1(s) = \prod_{i=1}^{n} \frac{w_{gi}}{s + w_{gi}} \tag{4.12b}$$

where w_{ci}'s and w_{gi}'s are the cutoff frequencies of the individual single-tuned BPF's of the $F_1(s)$ and $G_1(s)$ respectively. Note that $F_1(0)=G_1(0)=1$. The derivative of $F_1(s)$ and $G_1(s)$ at s=0 can be derived as

$$F_1'(0) = -\sum_{i=1}^{n} \frac{1}{w_{ci}} = -\frac{1}{w_c} \tag{4.13a}$$

$$G_1'(0) = -\sum_{i=1}^{n} \frac{1}{w_{gi}} = -\frac{1}{w_g} \tag{4.13b}$$

where w_c and w_g are the overall cutoff frequency of $F_1(s)$ and $G_1(s)$ respectively. Substituting Eqs.(4.13) into Eq.(4.11) yields

$$e_{ss} = \left(\frac{w_g - w_c}{w_g w_c}\right) \Delta w \tag{4.14}$$

Let $\delta w = w_g - w_c$ denote the mismatch. Usually $\delta w << w_c$, and the error can be approximated as

$$e_{ss} \approx \frac{\delta w}{w_c^2} \Delta w \tag{4.15}$$

Clearly the steady-state phase error increases as the mismatch δw increases. The result also shows the conflict between the minimization of steady-state error and the reduction of bandwidth. The e_{ss} caused by mismatch can be improved by widening the bandwidth of the synchronously-tuned BPF. This effectively decreases the steepness of the slope of the phase response of the filter. Hence the same mismatch gives a less variation in phase than a steeper slope of a narrower bandwidth BPF. Nevertheless, the error due to the mismatch is small since $w_c^2 >> \delta w$ and as expected the error vanishes as $\delta w \rightarrow 0$.

In short, steady-state tracking performance of the FTF depends on the similarity of the two BPF's in use. As illustrated in Fig.4.2, two experimental single-tuned BPF's with f_o=10MHz and Q=62.5 have discrepancies in phase response within $\pm 0.5°$ over 500kHz. Applying these two single-tuned BPF's into the FTF, a steady-state phase error of $\pm 0.2°$ over a range of $\pm$40kHz is obtained as shown in Fig.4.3a. The flat phase response of the FTF in Figs.4.3b and 4.4b reveals the tracking behaviour of the FTF. The tracking range of the FTF covers the 3dB bandwidth of the FTF. Outside the passband, FTF loses the tracking ability due to the attenuation of the signal by the BPF. The phase of the signal becomes ambiguous when the signal power is low and as a consequence, the phase error increases.

The frequency response of an experimental double-tuned

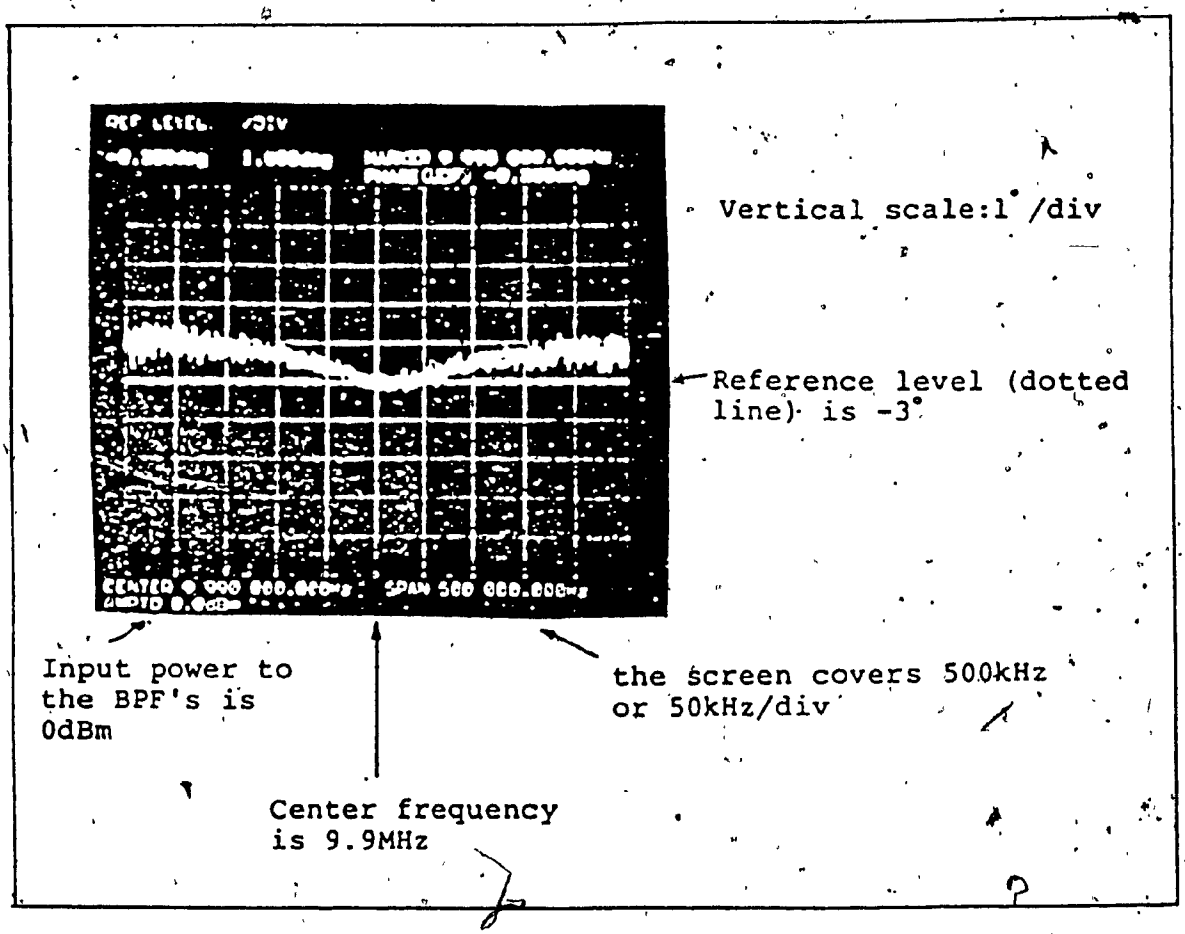

Fig. 4.2: Steady-state phase error of two experimental single-tuned BPF's

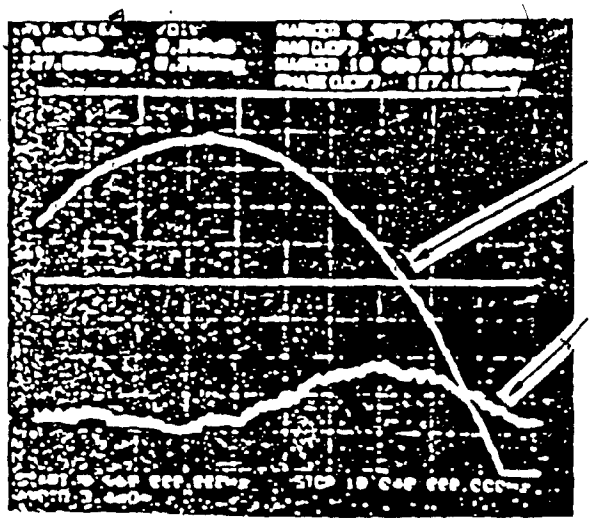

Input amplitude: 3.4 dBm

Amplitude response:
Vertical scale:0.2dB/div.
Horizontal scale:8kHz/div

Phase response:
Vertical scale:0.2°/div
Horizontal scale:8kHz/div

Center frequency:10MHz.

(a) Near field

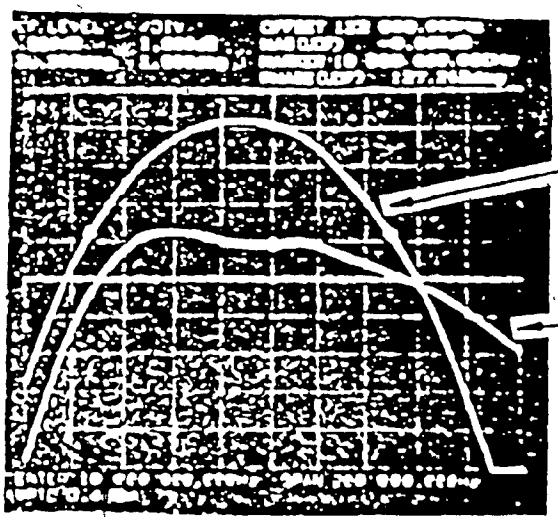

Input amplitude: 3.4 dBm

Amplitude response:
Vertical scale:1dB/div
Horizontal scale:20kHz/div

Phase response:
Vertical scale:1°/div
Horizontal scale:20kHz/div

Center frequency:10MHz

(b) Far field

Fig. 4.3: Frequency response of a single-tuned FTF

FTF is displayed in Fig.4.4 which shows a total of 4° tracking error within ±40kHz. There are two explainations for this larger steady-state error as compared to the single-tuned FTF. Firstly, the mismatch increases due to the difficulty of aligning four single-tuned BPF's simultaneouly. Secondly, the bandwidth of the double-tuned BPF decreases. Both contributions can easily be understood with Eq.(4.15). As a result of narrower bandwidth, the tracking range of a double-tuned FTF (115kHz) is narrower than that of a single-tuned FTF (122kHz). Therefore, the tracking range of the FTF depends on the bandwidth of the BPF's in use.

Following the same treatment, a similar expression of Eq.(4.11) for discrete FTF is derived as

$$e_{ss} = [G'_1(1) - F'_1(1)]\,\Delta w \tag{4.16}$$

where $F'_1(1) = \left.\frac{dF_1(z)}{dz}\right|_{z=1}$, $G'_1(1) = \left.\frac{dG_1(z)}{dz}\right|_{z=1}$

$F_1(z)$ and $G_1(z)$ are the z-transforms of the symmetrical transversal bandpass filters BPF1 and BPF2 in Fig.4.1. Taking into account the variation of weight coefficients and delay tap in the realizaion of a practical transversal filter, $F_1(z)$ and $G_1(z)$ are represented by

$$F_1(z) = \frac{\sum_{n=0}^{N-1} a_n z^{-n}}{\sum_{n=0}^{N-1} a_n} \tag{4.17a}$$

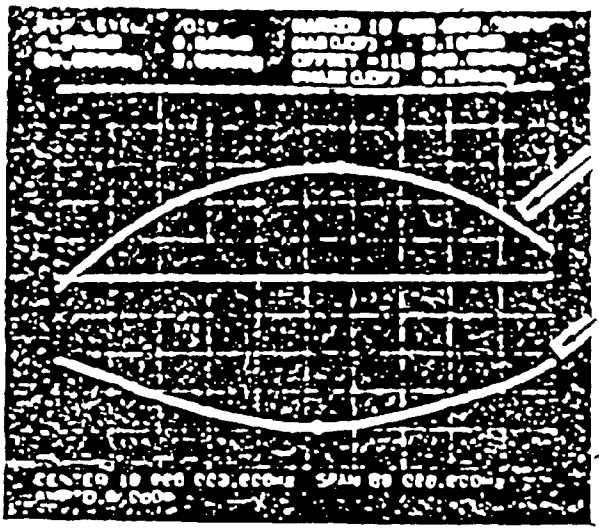

Input amplitude: 6 dBm

Amplitude response:
Vertical scale:0.5dB/div
Horizontal scale:8kHz/div

Phase response:
Vertical scale:2°/div
Horizontal scale:8kHz/div

Center frequency:10MHz

(a) Near field

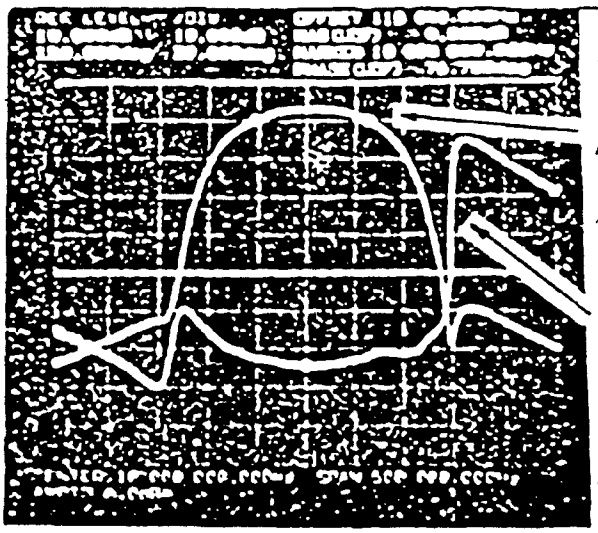

Input amplitude: 6 dBm

Amplitude response:
Vertical scale:10dB/div
Horizontal scale:50kHz/div

Phase response:
Vertical scale:20°/div
Horizontal scale:50kHz/div

Center frequency:10MHz

(b) Far field

Fig. 4.4: Frequency response of a double-tuned FTF

$$\text{and} \quad G_1(z) = \frac{\sum_{n=0}^{N-1} (a_n+\Delta a_n) z^{-(n+\Delta t_n)}}{\sum_{n=0}^{N-1} (a_n+\Delta a_n)} \tag{4.17b}$$

Therefore, Δa_n represents the imperfectness appended to the weight coefficients a_n while Δt_n is the variation added to the delay n. These two discrepancies, in fact, account for the slight non-linear phase characteristics of the practical transversal filters. From Eq.(4.17b), the derivative of $G_1(z)$ at z=1 can be found as

$$G_1'(1) = \frac{-\sum_{n=0}^{N-1} na_n - \sum_{n=0}^{N-1} (a_n+\Delta a_n)\Delta t_n + n\Delta a_n}{\sum_{n=0}^{N-1} (a_n+\Delta a_n)} \tag{4.18}$$

Usually $\Delta a_n \ll a_n$, thus

$$G_1'(1) = F_1'(1) - \frac{\sum_{n=0}^{N-1} (\Delta t_n a_n + n\Delta a_n)}{\sum_{n=0}^{N-1} a_n} \tag{4.19}$$

where

$$F_1'(1) = \frac{\sum_{n=0}^{N-1} -na_n}{\sum_{n=0}^{N-1} a_n} \tag{4.20}$$

Substituting Eq.(4.19) into Eq.(4.16), yields

$$e_{ss} = \frac{\sum_{n=0}^{N-1} -(\Delta t_n a_n + n\Delta a_n)}{\sum_{n=0}^{N-1} a_n} \Delta w \qquad (4.21)$$

which is the tracking error of discrete FTF caused by the mismatch of the weight coefficients and delay taps of the transversal BPF's. It is quite hard to predict this error as it depends on the trend of the deviation of individual mismatch. It is possible that there is cancellation among the mismatch. However, it is certain that the error increases if bandwidth of the BPF decreases because the length of delay n increases.

Figs.4.5 and 4.6 show the difference in characteristics of BPF1 and BPF2 of an experimental discrete FTF. As a result of the mismatch, the overall phase response of the discrete FTF, in Fig.4.7b, shows ±1.5° error over ±40kHz about the center frequency at 70MHz.

In summary, smaller the mismatch of the BPF's in use, the lesser the tracking error of the FTF. For the continuous FTF, this error depends on the mismatch of the cutoff frequencies of the BPF's. In the case of discrete FTF, this error depends on the mismatch of the parameters in time domain, a_n and n.

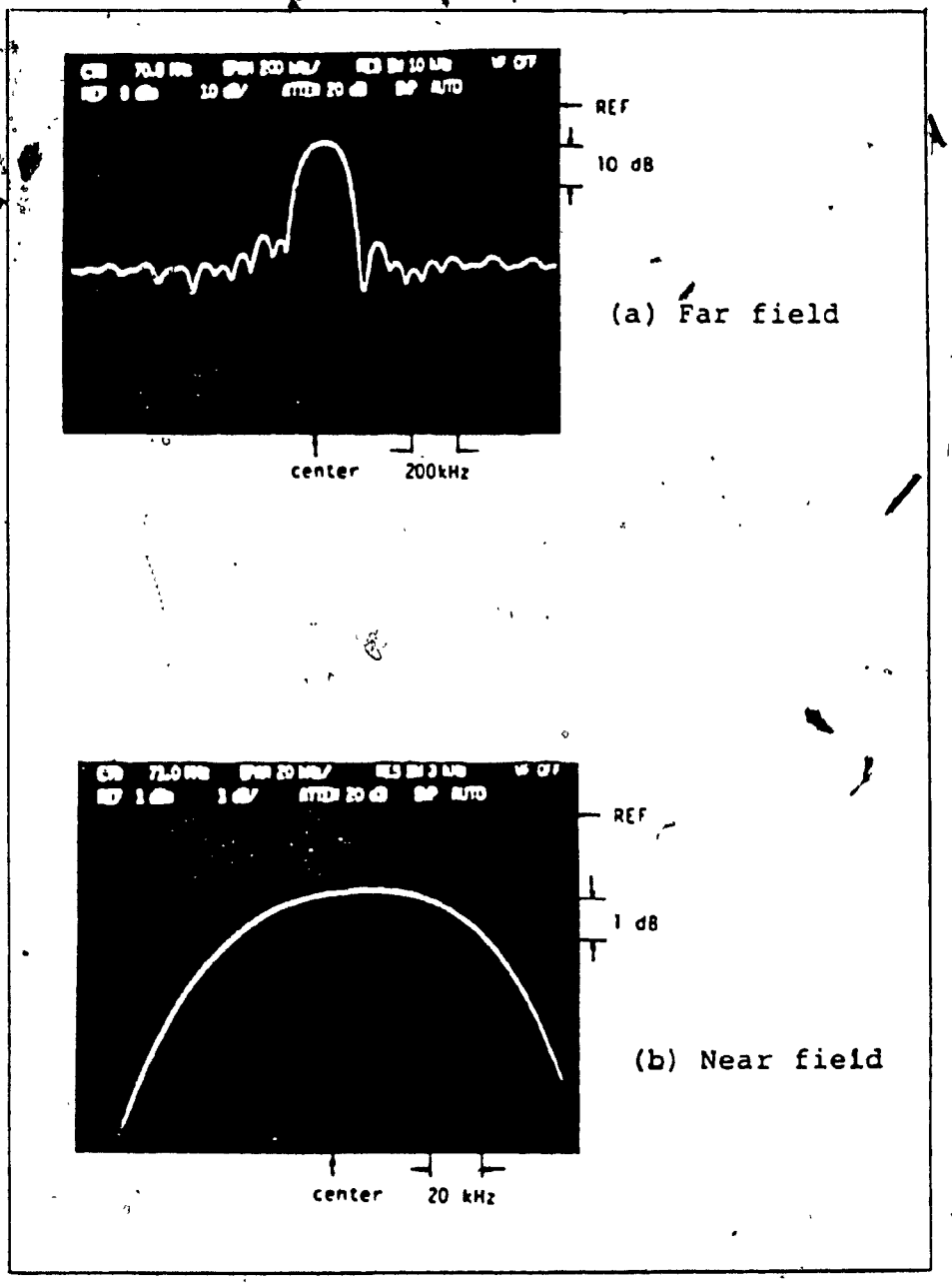

Fig. 4.5: Amplitude response of a SAW BPF

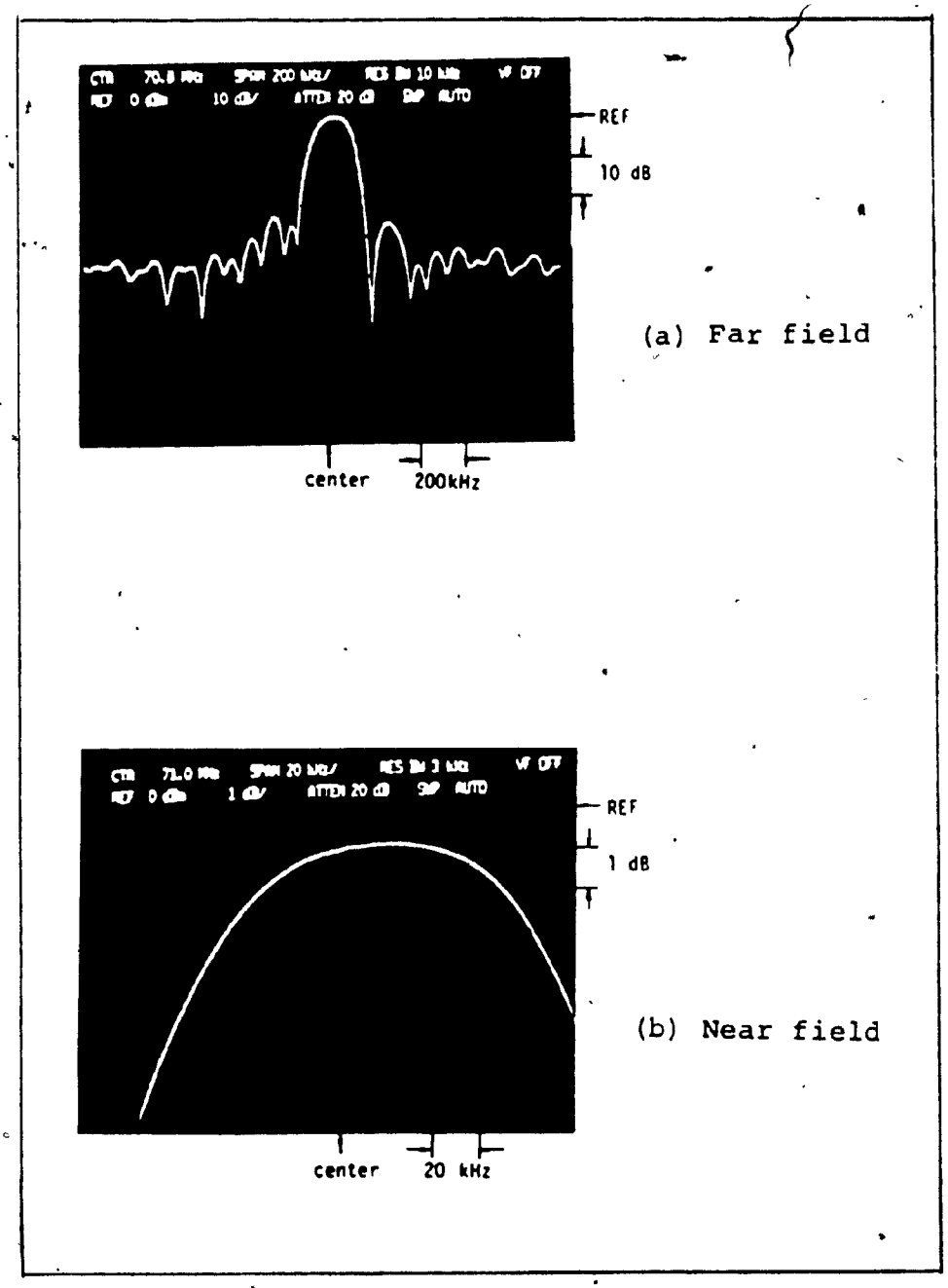

Fig. 4.6: Amplitude response of two SAW BPF's in cascade

(a) Amplitude response

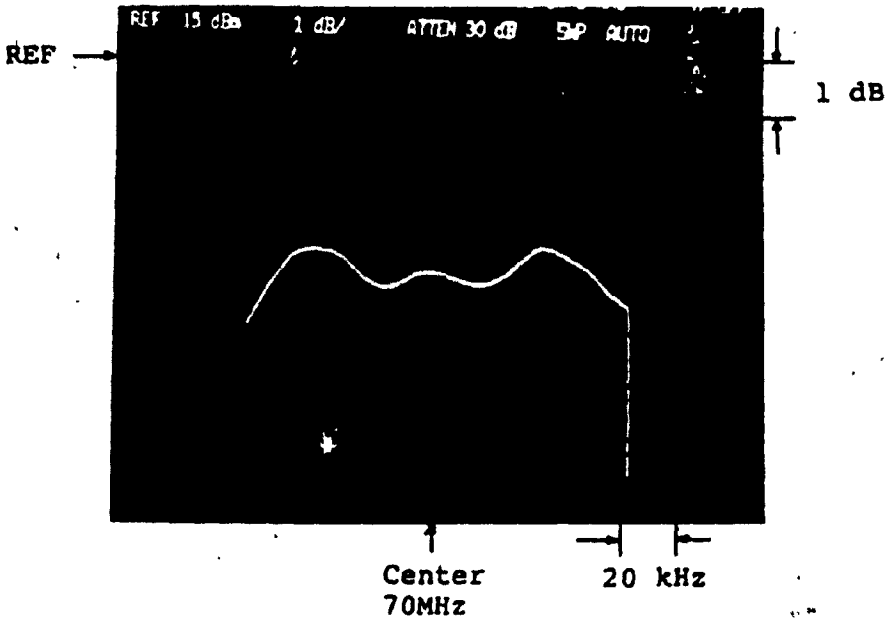

(b) Phase response

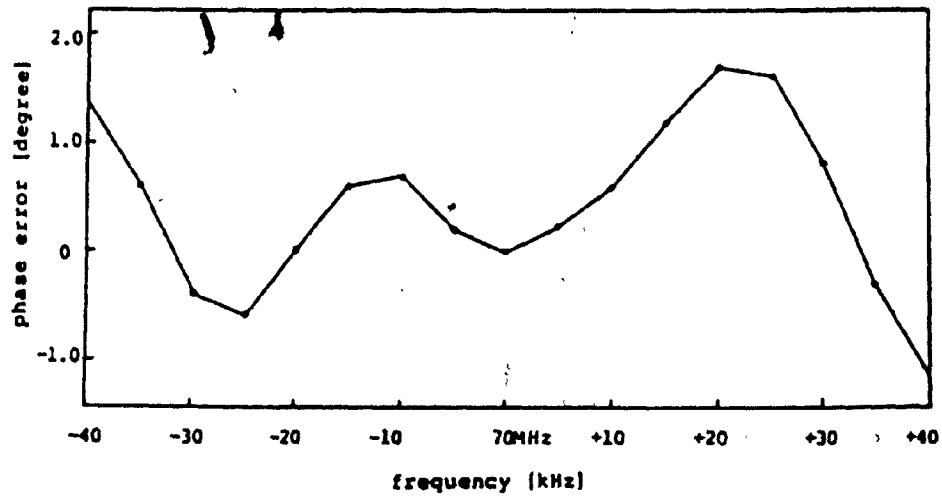

Fig. 4.7: Frequency response of an experimental discrete FTF using SAW BPF's

4.3 Frequency Response of an Experimental Continuous FTF

Fig.4.8 shows the experimental set-up to measure the frequency response of the continuous FTF. This experiment also illustrates the signal processing mechanism of the FTF. The mixer and the BPF's are driven by proper input power levels such that they operate linearly. An amplifier is needed to turn on the doubler at this low input level.

The measured frequency responses of the first single-tuned BPF (point Ⓐ of Fig.4.8) and of the cascaded single-tuned BPF's (point Ⓑ of Fig.4.8) are compared in Fig.4.9. The bandwidth of the cascaded single-tuned BPF's is certainly narrower than that of a single-tuned BPF. In fact, the 3dB bandwidth of a single-tuned BPF corresponds to the 6dB bandwidth of the cascaded single-tuned BPF's. Conversely, the doubler spreads the spectrum as shown in Fig.4.10 in which the doubler output Ⓒ overlays on the output Ⓐ. The effect of the doubler is to double the frequency of the input and the 3dB bandwidth.

Multiplying the output of the doubler in Fig.4.10 by that of cascaded single-tuned BPF's in Fig.4.9, the frequency response of the FTF output is obtained and recorded in Figs.4.11. It is surprising that the output of FTF has a "narrower bandwidth" than that of the cascaded BPF's. The narrowing effect is due to the slow rolloff of the single-tuned BPF. After multiplication with another slow rolloff

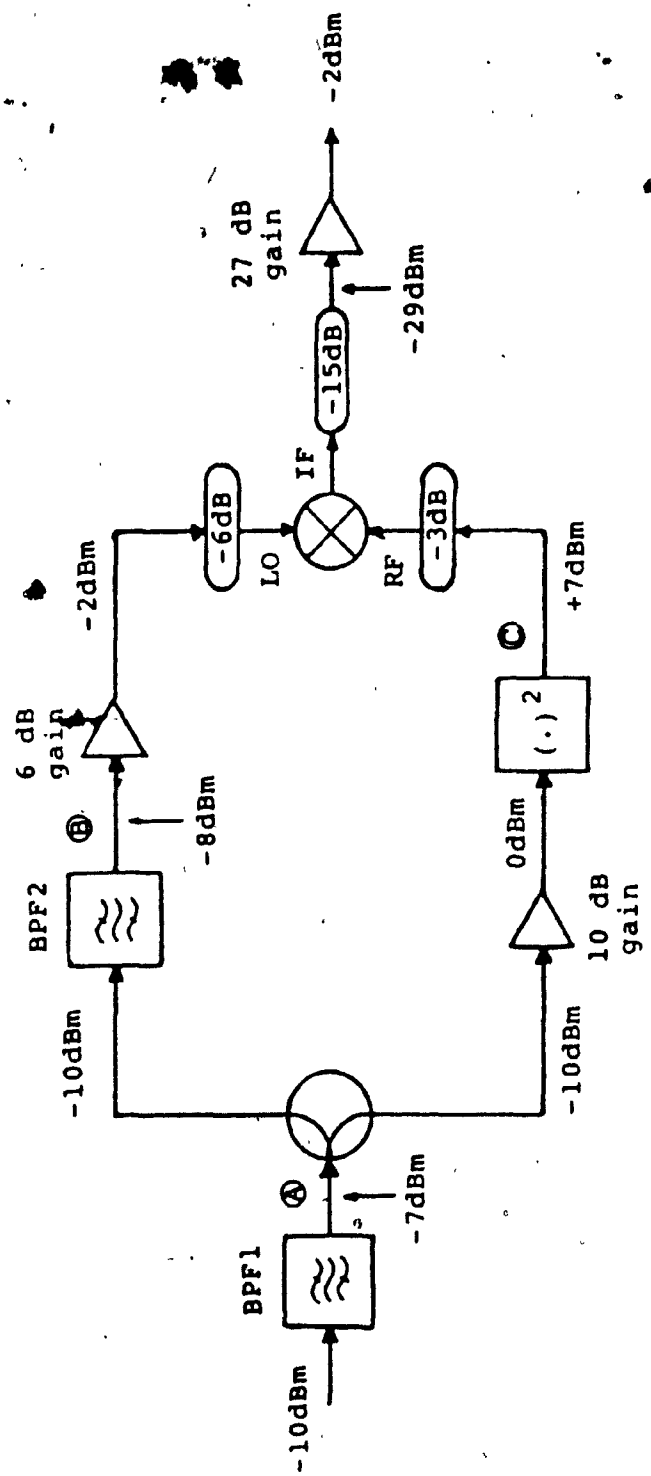

Fig. 4.8: Experimental set-up for the frequency response measurement of a single-tuned FTF

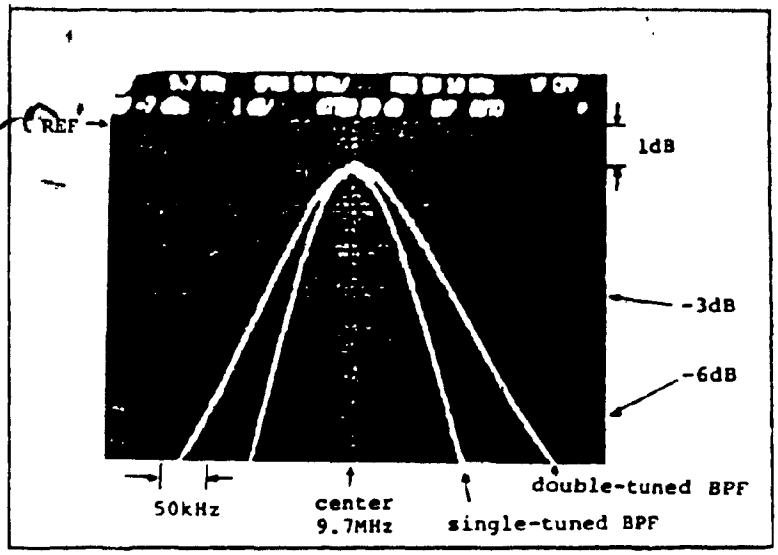

Fig. 4.9: Comparision of amplitude response of a single-tuned and double tuned BPF's

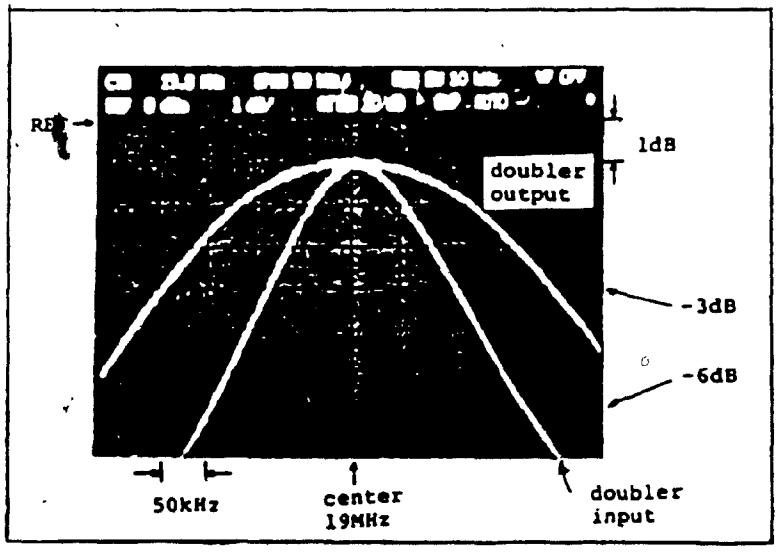

Fig. 4.10: Amplitude response of doubler in response to the output of a single-tuned BPF's

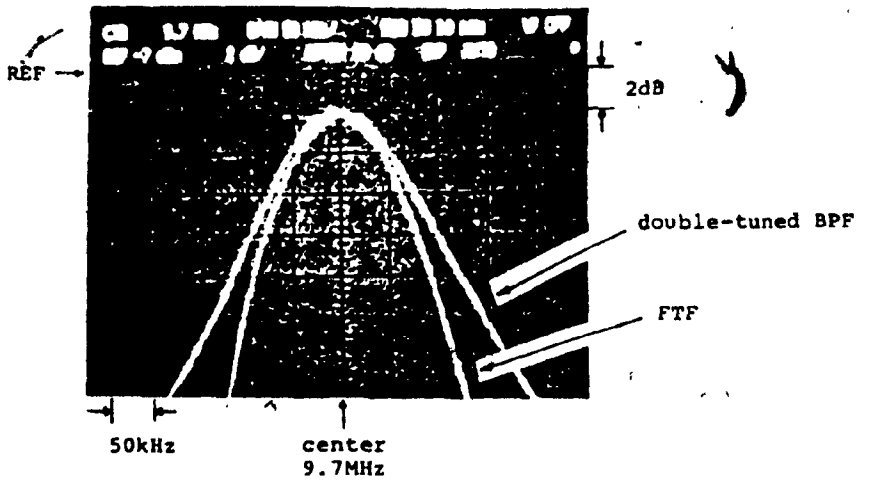

(a) Compared to double-tuned BPF

input level:-10dBm

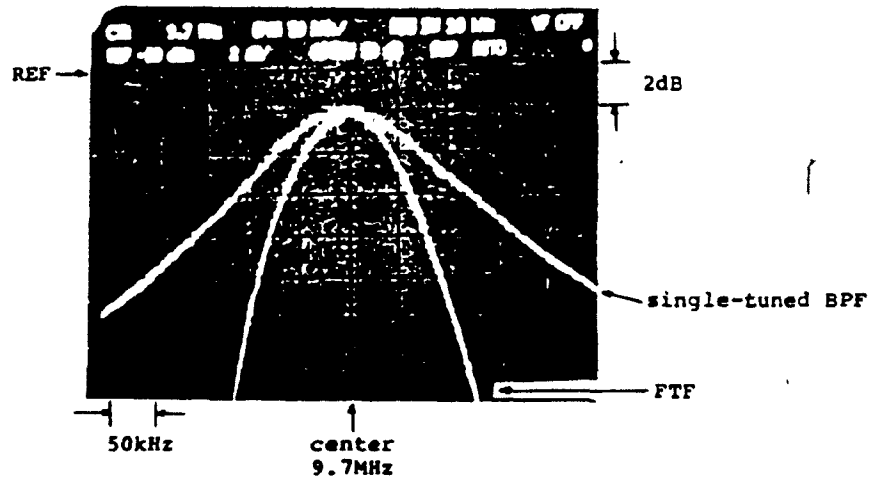

(b) Compared to single-tuned BPF

Fig. 4.11: Amplitude response of a single-tuned FTF to illustrate the "narrower" bandwidth

frequency response, an output with faster rolloff than the inputs is obtained.

The narrowed bandwidth shown in the frequency response for a single-tone, noise-free input signal will not lead to an improvement of the equivalent noise bandwidth of the FTF. On the contrary, as will be shown in Chapter 5, the output signal-to-noise ratio is degraded due to the nonlinear effect. It is noted that the conventional approach to determine the bandwidth of a linear BPF by sweeping the input frequency is not applicable in the nonlinear system nor is it applicable in the bandpass model of the FTF.

It is further investigated that the "narrower bandwidth" is quite harmful practically in a sense that the fluctuations of the amplitude causes amplitude modulation (AM) to phase modulation (PM) of certain components in the circuit. Hence, limiters are used to minimize this effect in practice. The improved amplitude response by the limiters has a drawback of increasing the bandwidth at the output of the FTF. Fig.4.12 shows that the bandwidth of the FTF increases significantly when the mixer and the BPF's operate in the saturated region. The saturation acts as a limiter to spread the spectrum accordingly.

As a final remark, this frequency response is measured in the absence of noise. Since FTF employs nonlinear elements, the frequency response of the FTF in the presence

of noise cannot be predicted easily. The narrower bandwidth of FTF output will no longer be obtained if noise is added or if limiters are used. The interaction of noise with the FTF will be shown later in Chapter 5, to clarify this point.

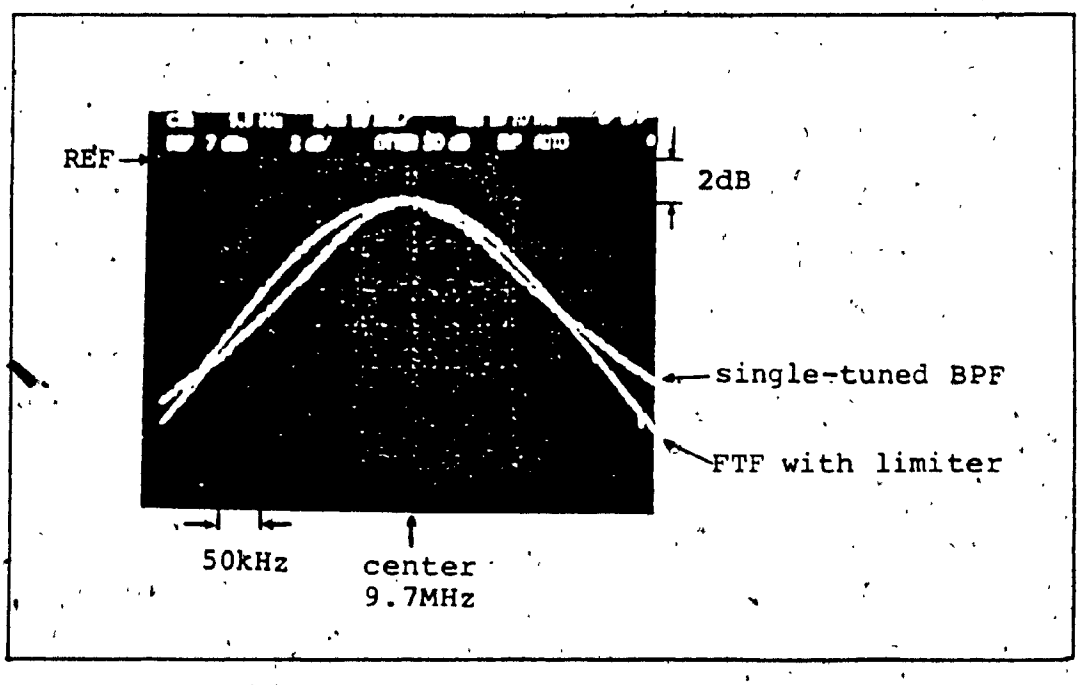

Fig. 4.12: Effect of the limiter on FTF output

CHAPTER 5

PERFORMANCE OF FTF IN AN AWGN ENVIRONMENT

A major requirement of the tracking filter is its ability to filter the noise accompaning the input signal. Analysis of the effect of the noise on the FTF is presented in this chapter. The nonlinear behaviour of the bandpass model of the FTF in an additive white Gaussian noise (AWGN) environment is first studied. There are two criteria characterizing a nonlinear system like FTF [11]. The first one is the output statistics which will be investigated in the first section. In the second section, another criterion of a nonlinear system, the input and output signal-to-noise ratio (SNR) relationship is derived. Following the non-linear analysis, the phase jitter performance of the linear baseband model of the FTF is presented in the third section.

5.1 Spectral Analysis

Unlike the linear system, the output signal and noise of the non-linear bandpass model of the FTF will not have a simple linear combination of the input signal and noise. It will be shown later that the resulting output consists of a mixture of signal intermodulation product and of noise product terms, which are not combined linearly and have lost the statistical character of the original input.

Fig.5.1 shows a block diagram of the FTF in an AWGN

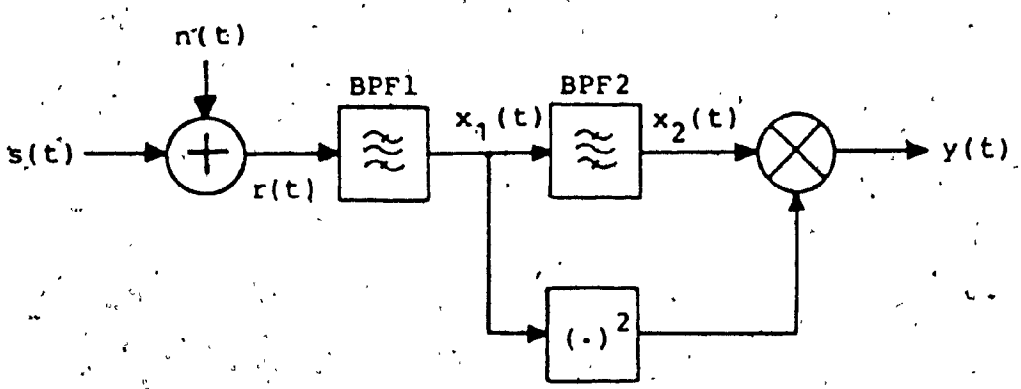

Fig. 5.1: Bandpass model of FTF in AWGN

environment. The input signal is

$$r(t) = s(t) + n(t) \tag{5.1}$$

The desired signal s(t) is a noise-free sinusoidal signal,

$$s(t) = A\cos(w_o t+\theta) \tag{5.2}$$

where amplitude A is a constant, and θ is a random phase uniformly distributed over the range $(-\pi,\pi)$. The additive noise n(t) is a white Gaussian random process with zero mean and power density $N_o/2$. s(t) and n(t) are assumed to be stationary and statistically independent.

The output of BPF1 and BPF2 are given respectively by

$$x_1(t) = \underbrace{\int_{-\infty}^{\infty} f(\lambda)s(t-\lambda)d\lambda}_{s_{x_1}(t)} + \underbrace{\int_{-\infty}^{\infty} f(\lambda)n(t-\lambda)d\lambda}_{n_1(t)} \tag{5.3a}$$

$$x_2(t) = \underbrace{\int_{-\infty}^{\infty} c(\lambda)s(t-\lambda)d\lambda}_{s_{x_2}(t)} + \underbrace{\int_{-\infty}^{\infty} c(\lambda)n(t-\lambda)d\lambda}_{n_2(t)} \tag{5.3b}$$

where f(t) is the impulse response of the BPF, and c(t) is the impulse response of the cascaded BPF's. Mathematically, c(t) is written as

$$c(t) = \int_{-\infty}^{\infty} f(\lambda)f(t-\lambda)d\lambda \tag{5.4}$$

that is the convolution of the impulse responses of BPF1 and BPF2. From Eqs.(5.3), $n_1(t)$ and $n_2(t)$ become bandpass

Gaussian random processes and are independent of s(t).

As the input is a pure sinusoidal signal, $s_{x_1}(t)$ and $s_{x_2}(t)$ are sinusoidal signals with phase delays, θ_1 and θ_2, respectively. Therefore,

$$s_{x_1}(t) = A_1\cos(w_o t+\theta+\theta_1) \tag{5.5a}$$

$$s_{x_2}(t) = A_2\cos(w_o t+\theta+\theta_2) \tag{5.5b}$$

where A_1 and A_2 are the amplitudes modified by the BPF's. To simplify the calculation, s(t) is assumed to fall in the centre frequency of the BPF's so that $\theta_1=\theta_2=0$ and $A_1=A_2=A$. The desired equality

$$s_{x_1}(t) = s_{x_2}(t) = s(t) \tag{5.6}$$

is then valid. As a result, the Eqs.(5.3) are rewritten as

$$x_1(t) = s(t) + n_1(t) \tag{5.7a}$$

$$x_2(t) = s(t) + n_2(t) \tag{5.7b}$$

After obtaining the essential properties of the inputs, the 'direct method' in [11,12] is adopted to determine the autocorrelation of the output of the FTF. To proceed, the output of the FTF in response to the received signal of Eq.(5.1) is first computed, i.e.

$$\begin{aligned} y(t) &= [x_1(t)]^2 x_2 \\ &= [s(t)+n_1(t)]^2[s(t)+n_2(t)] \end{aligned} \tag{5.8}$$

Multiplying out the expression, the output contains five

product terms:

$$y(t) = y_{sxs}(t) + y_{sxn_1}(t) + y_{sxn_2}(t) + y_{sxn_1xn_2}(t) + y_{n_1xn_2}(t) \quad (5.9a)$$

where $y_{sxs}(t) = s^3(t)$ (5.9b)

$$y_{sxn_1}(t) = 2s^2(t)n_1(t) + s(t)n_1^2(t) \quad (5.9c)$$

$$y_{sxn_2}(t) = s^2(t) + n_2(t) \quad (5.9d)$$

$$y_{sxn_1xn_2}(t) = 2s(t)n_1(t)n_2(t) \quad (5.9e)$$

$$y_{n_1xn_2}(t) = n_1^2(t)n_2(t) \quad (5.9f)$$

The first product term represents the desired signal. The rest are noise-product terms, either due to the interaction between signal with noise or due to the interaction between noise itself. The noise-product terms are generated by the nonlinear characteristics of the FTF.

Applying the stationary property of s(t), n(t), $n_1(t)$ and $n_2(t)$, the autocorrelation function of y(t) is found to be a function of the time difference, i.e.

$$R_{yy}(\varepsilon) = E[y(t_1)y(t_2)], \quad t_2 = t_1 + \varepsilon$$

$$= E\left[\sum_{\substack{i,j,k,l,p,q \\ i+j+k+l+p+q=6}}^{3} \Omega_{i,j,k,l,p,q}\, s_1^i s_2^j n_{11}^k n_{12}^l n_{21}^p n_{22}^q\right] \quad (5.10)$$

where $s_1 = s(t_1)$, $s_2 = s(t_2)$

$n_{11} = n_1(t_1)$, $n_{12} = n_1(t_2)$

$$n_{21} = n_2(t_1), \quad n_{22} = n_2(t_2),$$

and E[x] is the expectation of a random variable x. Since s(t) is statistically independent of $n_1(t)$ and $n_2(t)$, from Table 5.1 and Appendix A.3, the moment functions in Eq.(5.10) are non-zero only if

(i+j) is even and (k+l+p+q) is even.

Grouping into five product terms, the non-zero terms in Eq.(5.10) can be shown to be

$$R_{yy}(\varepsilon) = R_{sxs}(\varepsilon) + R_{sxn_1}(\varepsilon) + R_{sxn_2}(\varepsilon) + R_{sxn_1xn_2}(\varepsilon) + R_{n_1xn_2}(\varepsilon) \tag{5.11a}$$

where

$$R_{sxs}(\varepsilon) = E[s_1^3 s_2^3] \tag{5.11b}$$

$$R_{sxn_1}(\varepsilon) = E[s_1^3 s_2] E[n_{12}^2] + 4E[s_1^2 s_2^2] E[n_{11}n_{12}] + E[s_1 s_2^3] E[n_{11}^2] + E[s_1 s_2] E[n_{11}^2 n_{12}^2] \tag{5.11c}$$

$$R_{sxn_2}(\varepsilon) = E[s_1^2 s_2^2] E[n_{21}n_{22}] \tag{5.11d}$$

$$\begin{aligned} R_{sxn_1xn_2}(\varepsilon) = {} & 2E[s_1^3 s_2] E[n_{12}n_{22}] + 2E[s_1^2 s_2^2] E[n_{11}n_{22}] \\ & + 2E[s_1^2] E[n_{11}n_{12}^2 n_{22}] + 2E[s_1 s_2] E[n_{11}^2 n_{12} n_{22}] \\ & + 2E[s_1^2 s_2^2] E[n_{12}n_{21}] + E[s_1^2] E[n_{12}^2 n_{21} n_{22}] \\ & + 2E[s_1 s_2^3] E[n_{11}n_{21}] + 2E[s_1 s_2] E[n_{11}n_{12}^2 n_{21}] \\ & + 4E[s_1 s_2] E[n_{11}n_{12}n_{21}n_{22}] \\ & + 2E[s_2^2] E[n_{11}^2 n_{12} n_{21}] \\ & + E[s_2^2] E[n_{11}^2 n_{21} n_{22}] \end{aligned} \tag{5.11e}$$

$E[x_1^i, x_2^j]$	x = s sinusoid
$E[x_1]$	0
$E[x_1, x_2]$	$\frac{1}{2}A^2 \cos w_o \varepsilon$
$E[x_1^2]$	$\frac{1}{2}A^2$
$E[x_1, x_2^2]$	0
$E[x_1, x_2^3]$	$\frac{3}{8}A^4 \cos w_o \varepsilon$
$E[x_1^2, x_2^2]$	$\frac{1}{4}A^4 (1+\frac{1}{2}\cos 2w_o \varepsilon)$
$E[x_1^3, x_2^3]$	$\frac{1}{32}A^6 (9\cos w_o \varepsilon + \cos 3w_o \varepsilon)$

Table 5.1: Moments of a sinusoidal function with uniformly distributed phase angle

$$R_{n_1 x n_2}(\varepsilon) = E[n_{11}^2 n_{12}^2 n_{21} n_{22}] \tag{5.11f}$$

Substituting the appropriate moments into Eqs.(5.11), the autocorrelation function of the product terms becomes

$$R_{sxs}(\varepsilon) = \frac{A^6}{32}(9\cos w_o\varepsilon + \cos 3w_o\varepsilon) \tag{5.12a}$$

$$R_{sxn_1}(\varepsilon) = (\tfrac{3}{4}A^4 N_o B_1 + \tfrac{1}{2}N_o^2 A^2 B_1^2)\cos w_o\varepsilon + A^4(1+\tfrac{1}{2}\cos 2w_o\varepsilon)R_{n_1 n_1}(\varepsilon) + A^2 R_{n_1 n_1}^2(\varepsilon)\cos w_o\varepsilon \tag{5.12b}$$

$$R_{sxn_2}(\varepsilon) = \frac{A^4}{4}(1+\tfrac{1}{2}\cos 2w_o\varepsilon)R_{n_2 n_2}(\varepsilon) \tag{5.12c}$$

$$\begin{aligned} R_{sxn_1 xn_2}(\varepsilon) = {} & (\tfrac{3}{2}A^4 N_o B_c + 2A^2 N_o^2 B_1 B_c + 2A^2 N_o^2 B_c^2)\cos w_o\varepsilon \\ & + 4A^2 N_o B_c R_{n_1 n_1}(\varepsilon) + A^2 N_o B_1 R_{n_2 n_2}(\varepsilon) \\ & + (A^2 N_o B_1 + A^2 N_o B_c + \tfrac{A^4}{2})[R_{n_1 n_2}(\varepsilon) + R_{n_2 n_1}(\varepsilon)] \\ & + \tfrac{A^4}{4}\cos 2w_o\varepsilon[R_{n_1 n_2}(\varepsilon) + R_{n_2 n_1}(\varepsilon)] \\ & + 2A^2\cos w_o\varepsilon R_{n_1 n_1}(\varepsilon)[R_{n_1 n_2}(\varepsilon) + R_{n_2 n_1}(\varepsilon)] \\ & + 2A^2\cos w_o\varepsilon R_{n_1 n_1}(\varepsilon)R_{n_2 n_2}(\varepsilon) \\ & + 2A^2\cos w_o\varepsilon R_{n_1 n_2}(\varepsilon)R_{n_2 n_1}(\varepsilon) \end{aligned} \tag{5.12d}$$

$$\begin{aligned} R_{n_1 x n_2}(\varepsilon) = {} & 4N_o^2 B_c^2 R_{n_1 n_1}(\varepsilon) + N_o^2 B_1^2 R_{n_2 n_2}(\varepsilon) \\ & + 2N_o^2 B_1 B_c[R_{n_1 n_2}(\varepsilon) + R_{n_2 n_1}(\varepsilon)] + 2R_{n_1 n_1}^2(\varepsilon)R_{n_2 n_2}(\varepsilon) \\ & + 4R_{n_1 n_1}(\varepsilon)R_{n_1 n_2}(\varepsilon)R_{n_2 n_1}(\varepsilon) \end{aligned} \tag{5.12e}$$

where

$$R_{n_1 n_1}(\varepsilon) = E[n_1(t_1)n_1(t_2)] = E[n_{11}n_{12}] \tag{5.13a}$$

$$R_{n_2 n_2}(\varepsilon) = E[n_{21}n_{22}] \tag{5.13b}$$

$$R_{n_1 n_2}(\varepsilon) = E[n_{11}n_{22}] \tag{5.13c}$$

$$R_{n_2 n_1}(\varepsilon) = E[n_{21}n_{12}] \tag{5.13d}$$

and $$R_{n_1n_1}(0) = N_oB_1 \qquad (5.14a)$$

$$R_{n_2n_2}(0) = N_oB_2 \qquad (5.14b)$$

$$R_{n_1n_2}(0) = \hat{R}_{n_2n_1}(0) = N_oB_c \qquad (5.14c)$$

where B_1 and B_2 are one-sided equivalent noise bandwidth of F(w) and C(w) respectively. B_c is the one-sided equivalent noise correlation bandwidth (Appendix A).

Note that cross-correlation terms $R_{n_1n_2}(\varepsilon)$ and $R_{n_2n_1}(\varepsilon)$ are present in Eqs.(5.12d) and (5.12e). Since $n_1(t)$ and $n_2(t)$ are derived from the same source, they are correlated as demonstrated in Appendix A.2. Due to the cross-correlation of $n_1(t)$ and $n_2(t)$, the $R_{sxn_1xn_2}(\varepsilon)$ term becomes the major contribution to the noise power.

Taking the Fourier transform of the autocorrelation function, $R_{yy}(\varepsilon)$, the spectral density of the output of the FTF is obtained as

$$S_{yy}(f) = S_{sxs}(f) + S_{sxn_1}(f) + S_{sxn_2}(f) + S_{sxn_1xn_2}(f) + S_{n_1xn_2}(f) \qquad (5.15a)$$

where

$$S_{sxs}(f) = \frac{A^6}{64}[\,9\delta(f-f_o)+9\delta(f+f_o)+\delta(f-3f_o)+\delta(f+3f_o)\,] \qquad (5.15b)$$

$$S_{sxn_1}(f) = (\tfrac{3}{8}A^4N_oB_1+\tfrac{1}{4}A^2N_o^2B_1^2)[\,\delta(f-f_o)+\delta(f+f_o)\,]+A^4S_{n_1n_1}(f) + \frac{A^4}{4}[\,S_{n_1n_1}(f-2f_o)+S_{n_1n_1}(f+2f_o)\,] + \frac{A^2}{2}[\,W(f-f_o)+W(f+f_o)\,] \qquad (5.15c)$$

$$S_{sxn_2}(f) = \frac{A^4}{4}S_{n_2n_2}(f)+\frac{A^4}{16}[S_{n_2n_2}(f-2f_o)+S_{n_2n_2}(f+2f_o)] \quad (5.15d)$$

$$\begin{aligned} S_{sxn_1xn_2}(f) = {} & (\tfrac{3}{4}A^4N_oB_c+A^2N_o^2B_1B_c+A^2N_o^2B_c^2)[\delta(f-f_o)+\delta(f+f_o)] \\ & +4A^2N_oB_cS_{n_1n_1}(f)+A^2N_oB_1S_{n_2n_2}(f) \\ & +(A^2N_oB_1+\frac{A^4}{2}+A^2N_oB_c)\ 2S^{real}_{n_1n_2}(f) \\ & +\frac{A^4}{4}[S^{real}_{n_1n_2}(f-2f_o)+S^{real}_{n_1n_2}(f+2f_o)] \\ & +A^2[2U(f-f_o)+2U(f+f_o)+V(f-f_o)+V(f+f_0)] \\ & +A^2[Z(f-f_o)+Z(f+f_o)] \end{aligned} \quad (5.15e)$$

$$\begin{aligned} S_{n_1xn_2}(f) = {} & 4N_o^2B_c^2S_{n_1n_1}(f)+N_o^2B_1^2S_{n_2n_2}(f)+4N_o^2B_1B_cS^{real}_{n_1n_2}(f) \\ & +2W(f)*S_{n_2n_2}(f)+4S_{n_1n_1}(f)*Z(f) \end{aligned} \quad (5.15f)$$

and

$$W(f) = S_{n_1n_1}(f)*S_{n_1n_1}(f) \quad (5.16a)$$

$$U(f) = S_{n_1n_1}(f)*S^{real}_{n_1n_2}(f) \quad (5.16b)$$

$$V(f) = S_{n_1n_1}(f)*S_{n_2n_2}(f) \quad (5.17c)$$

$$Z(f) = S_{n_1n_2}(f)*S_{n_1n_2}(f)^* \quad (5.17d)$$

where * denotes convolution and x^* is the complex conjugate of x, and $S^{real}_{n_1n_2}(f)$ is the real part of $S_{n_1n_2}(f)$. Eqs.(5.15a-f) and (5.16a-d) show that the FTF output spectral density, $S_{yy}(f)$, depends on the convolutions of three bandpass functions, $S_{n_1n_2}(f)$, $S_{n_1n_1}(f)$ and $S_{n_2n_2}(f)$. The results of the convolutions are expected to be bandpass functions and their spectral information are confined in the vicinity of f_o and of $3f_o$. To understand the distribution of this spectral information, it is always instructive to examine the output spectrum graphically.

It can be seen that the characteristics of the BPF's in use determine the FTF spectral density. For the simplest case of an ideal BPF having brick wall amplitude response and linear phase characteristics, the spectral density of $n_1(t)$ and $n_2(t)$ are equivalent since $B_1=B_2=B$. Therefore,

$$S_{n_1n_1}(f) = S_{n_2n_2}(f) = \begin{cases} \frac{N_o}{2}, & f_o - \frac{B}{2} < |f| < f_o + \frac{B}{2} \\ 0, & \text{otherwise} \end{cases} \tag{5.17}$$

Eq.(5.17) represents a rectangular spectrum centred at f_o as shown in Fig.5.2a.

The cross-correlation spectral density $S_{n_1n_2}(f)$ is evaluated by separating into its real and imaginary parts (see Appendix A). In this ideal BPF case, we may write the real part of $S^{real}_{n_1n_2}(f)$ as

$$S^{real}_{n_1n_2}(f) = \begin{cases} \frac{N_o}{2}\cos[b(|f|-f_o)], & f_o - \frac{B}{2} < |f| < f_o + \frac{B}{2} \\ 0, & \text{otherwise} \end{cases} \tag{5.18a}$$

and the imaginary part is

$$S^{imag}_{n_1n_2}(f) = \begin{cases} \frac{N_o}{2}\sin[b(|f|-f_o)], & f_o - \frac{B}{2} < |f| < f_o + \frac{B}{2} \\ 0, & \text{otherwise} \end{cases} \tag{5.18b}$$

where "b" is a coefficient representing the slope of the linear phase response. This coefficient determines the shape of the truncated sinusoidal spectra, $S^{real}_{n_1n_2}(f)$ and $S^{imag}_{n_1n_2}(f)$, in Eq.(5.18). For convenience, it is chosen to be

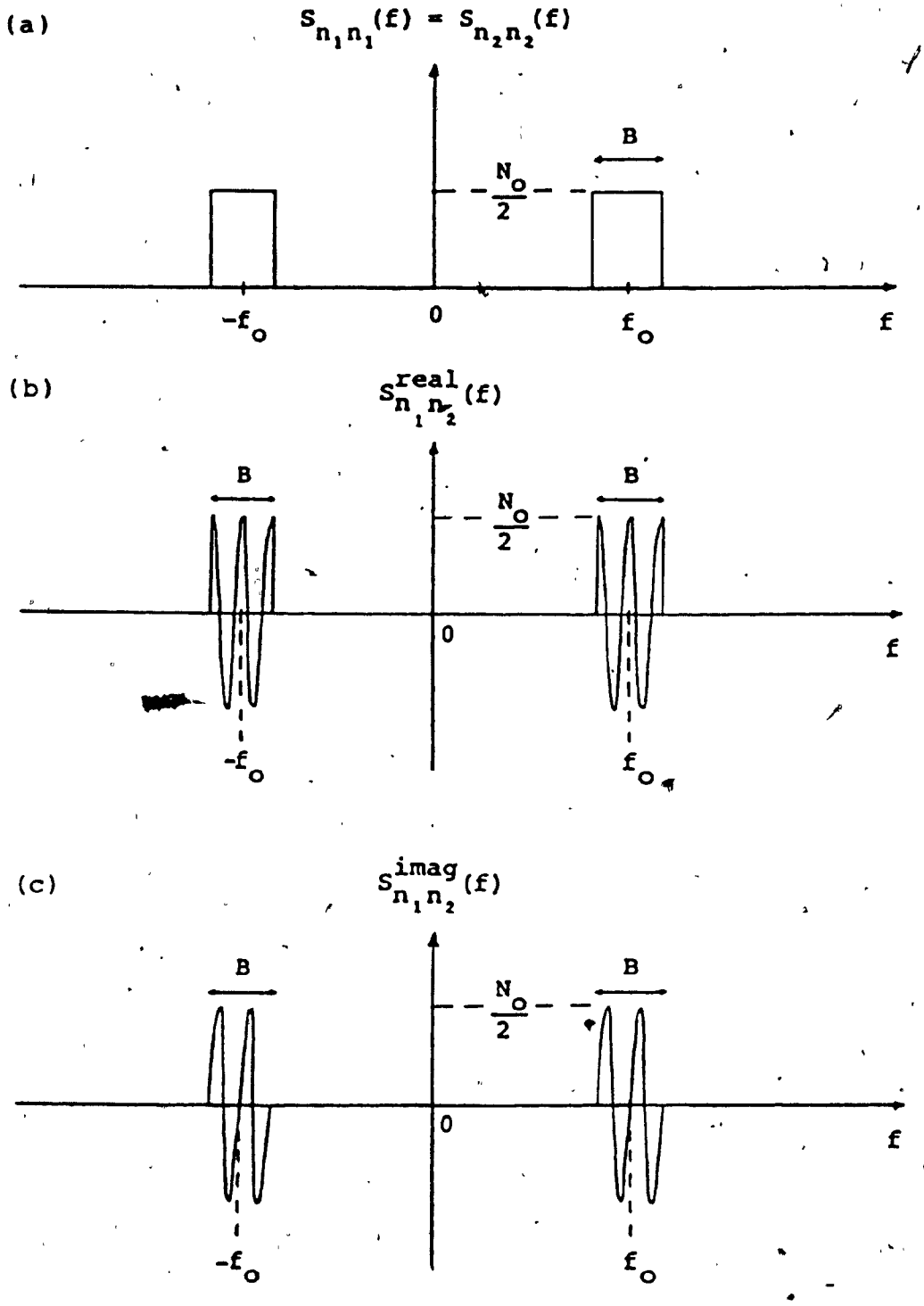

Fig. 5.2: Spectral densities of $S_{n_1n_1}(f)$, $S_{n_2n_2}(f)$ and $S_{n_1n_2}(f)$ in the presence of AWGN

$$b = -4\pi/B \tag{5.19}$$

to closely conform to the slope of the linear phase of the experimental SAW filter. The respective spectral densities of $S^{real}_{n_1n_2}(f)$ and $S^{imag}_{n_1n_2}(f)$ are shown in Figs.5.2b and 5.2c. It is noted that $S^{real}_{n_1n_2}(f)$ is an even function of f about f_o while $S^{imag}_{n_1n_2}(f)$ is an odd function of f about f_o.

Performing the appropriate convolution of Eqs.(5.16) and using the results developed in Appendix B, the spectra of W(f), U(f), V(f) and Z(f) are obtained as follows. Both W(f) and V(f) have a simple triangular shape as shown in Eq.(5.20a).

$$W(f) = V(f) = \begin{cases} \frac{N_o}{2}(B-|f|) & , \quad 0<|f|\leq B \\ \frac{N_o}{4}(B-||f|-2f_o|), & 2f_o-B<|f|<2f_o+B \\ 0 & , \quad \text{otherwise} \end{cases} \tag{5.20a}$$

U(f) turns out to be a truncated sinusoidal spectrum depending on the value of the coefficient b, which is represented in Eq.(5.20b).

$$U(f) = \begin{cases} \frac{N_o^2}{2b}\left\{\sin[b(\frac{B}{2}-|f|)]+\sin\frac{bB}{2}\right\} & , \quad 0<|f|\leq B \\ \frac{N_o^2}{4b}\left\{\sin[b(\frac{B}{2}-||f|-2f_o|)]+\sin\frac{bB}{2}\right\}, & 2f_o-B<|f|<2f_o+B \\ 0 & , \quad \text{otherwise} \end{cases} \tag{5.20b}$$

Z(f) is also found to be dependent of b, which is described by

$$Z(f) = \begin{cases} \frac{N_o}{2b}\sin[b(B-|f|)] & , 0<|f|\leq B \\ \frac{N_o^2}{4b}\sin[b(B-||f|-2f_o|)] & , 2f_o-B<|f|<2f_o+B \\ 0 & , \text{otherwise} \end{cases} \quad (5.20c)$$

The spectra of these four functions are plotted in Figs.5.3 for the case $b=-4\pi/B$.

The spectrum of each product term in Eq.(5.15) are approximately displayed in Figs.(5.4) following the substitution of Eqs.(5.7), (5.8) and (5.20). It is clearly noticeable that there are some spectral components outside the vicinity of f_o in each of the output spectral density terms. There is no component around 0Hz and $2f_o$, because, the doubler and the multiplier are memoryless devices. The doubler shifts the input at f_o to 0Hz and $2f_o$ whereas the multiplier shifts the frequency components at f_o back to the vicinity around f_o and $3f_o$.

From these spectra, the output signal and noise do not possess a linear combination of the input signal and noise. The nonlinear operation of the FTF scrambles the input signal and input noise to produce the complex output spectrum in which the input signal and noise cannot be isolated independently. The output spectral density term resulting from the interaction of the input signal with itself is shown to contain a pair of impulses. The one situated at f_o is the desired output signal while the one at

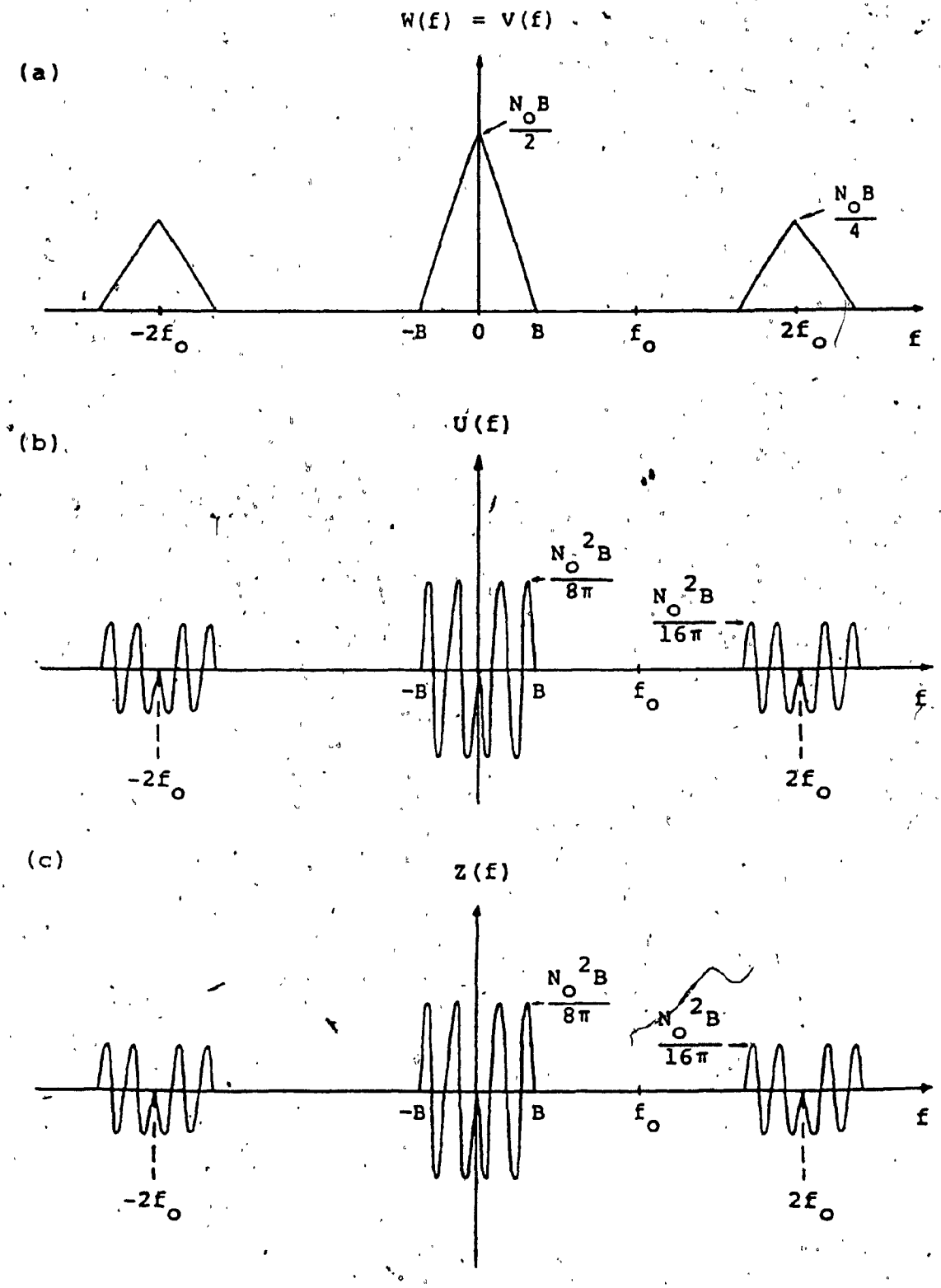

Fig. 5.3: Spectral densities of W(f), V(f), U(f) and Z(f) in the presence of AWGN

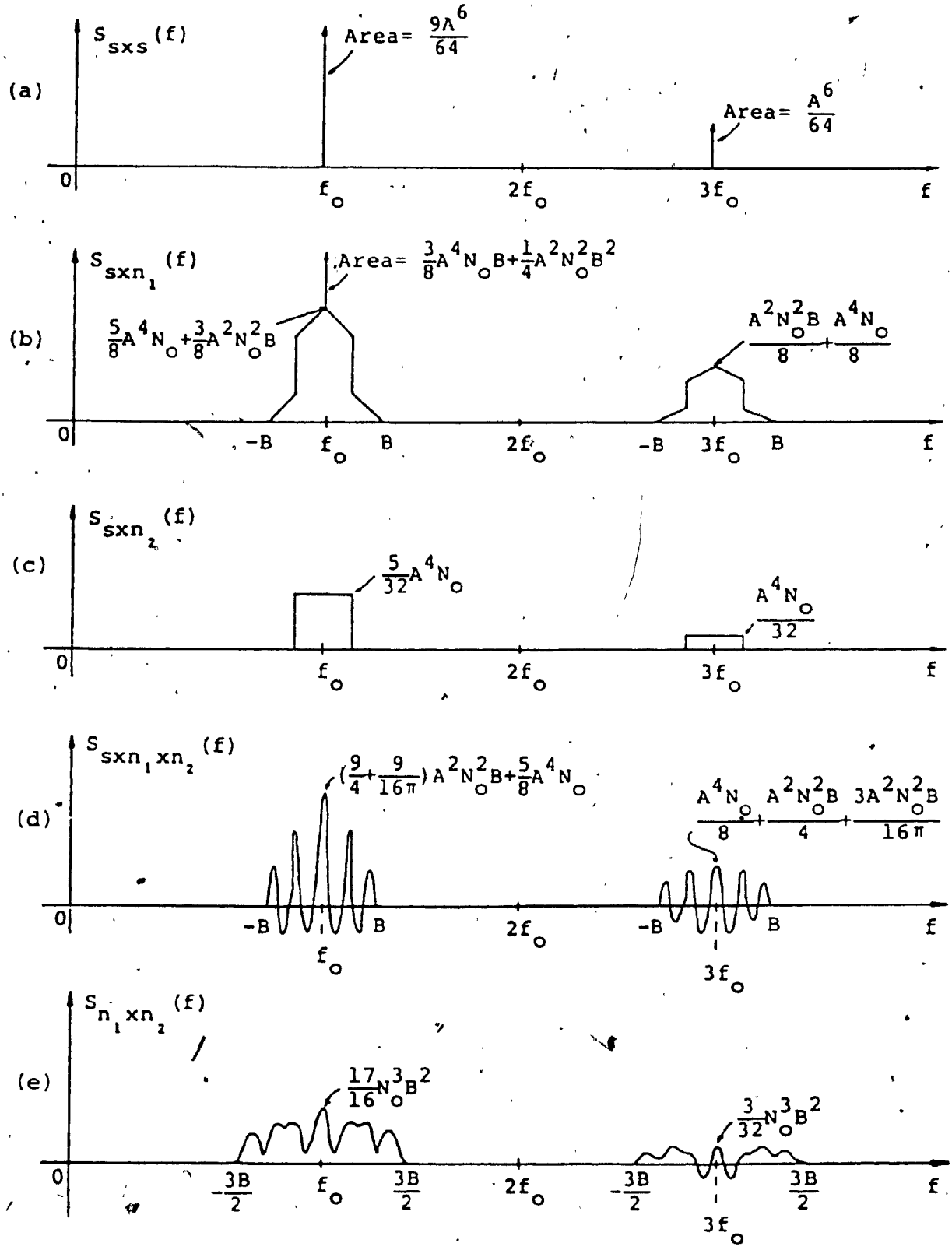

Fig. 5.4: Spectral densities of individual product terms of the FTF output in the presence of AWGN

$3f_o$ will be the interference as a result of intermodulation.

The output spectral density due to the interaction of signal and $n_1(t)$, is found to contain an impulse in addition to the continuous spectrum. Usually, a continuous spectrum is generated by the interaction of signal and noise. The discrete line present in $S_{sxn_1}(f)$ is due to the nonlinear operation of the doubler on the signal and $n_1(t)$. Conversely, without the action of the doubler, the discrete line is absent in the spectrum of $S_{sxn_2}(f)$. The impulse also exists in the spectrum of $S_{sxn_1xn_2}(f)$ for the same reason (Eq.(5.15c)), although it does not appear in the Fig.5.4d. The null result of the one-sided noise equivalent correlation bandwidth as shown in Eq.(5.21) accounts for the disappearance of the impulse in this special ideal BPF case.

$$B_c = \int_{-\frac{B}{2}+f_o}^{\frac{B}{2}+f_o} \cos[-\frac{4\pi}{B}(f-f_o)]df = \frac{B}{2\pi} \sin 2\pi = 0 \qquad (5.21)$$

The zero result of the B_c is desirable as it helps to reduce slightly the noise power due to the $S_{sxn_1xn_2}(f)$ and $S_{n_1xn_2}(f)$ terms appearing at the FTF output.

The doubler has another effect that it doubles the bottom of the output spectrum of the BPF's. This effect can be found in the spectra of $S_{sxn_1}(f)$ and $S_{sxn_1xn_2}(f)$ in Figs.5.4b and 5.4d. A detailed analysis of the doubler has been given in [12] from which the spectrum of a unit gain

doubler in response to the output of BPF1 is found to be

$$S_z(f) = \begin{cases} \frac{A^4}{16}[\delta(f-f_o)+\delta(f+f_o)] & \\ + \frac{A^2 N_o}{2} & 2f_o-\frac{B}{2}<|f|<2f_o+\frac{B}{2} \\ + \frac{N_o^2}{4}(B-||f|-2f_o|) & , \quad 2f_o-B<|f|<2f_o+B \\ 0 & , \quad \text{otherwise} \end{cases} \qquad (5.22)$$

This is the output of the doubler centered at $2f_o$. It is drawn in Fig.5.5 that the bottom of the spectrum is doubled when it is compared to its input.

The undulating shape of $S_{sxn_1xn_2}(f)$ is due to the addition of three truncated sinusoidal spectra of different periods. This irregular shape plus $S_{n_1xn_2}(f)$, characterizes the shape of the overall output spectrum of the FTF in Fig.5.6.

The spectrum due to the interaction of $n_1(t)$ and $n_2(t)$ is continuous. It represents the output spectrum of the FTF when the input is noise alone. The discrete spectral component due to the sinusoidal signal, should not be present. Moreover, the bottom of this spectrum is three times wider than the bandwidth of the BPF. This spreading effect is due to the multiplier and the doubler.

The overall output spectral density of FTF, by summing the product terms, is drawn in Fig.5.6. The undulating

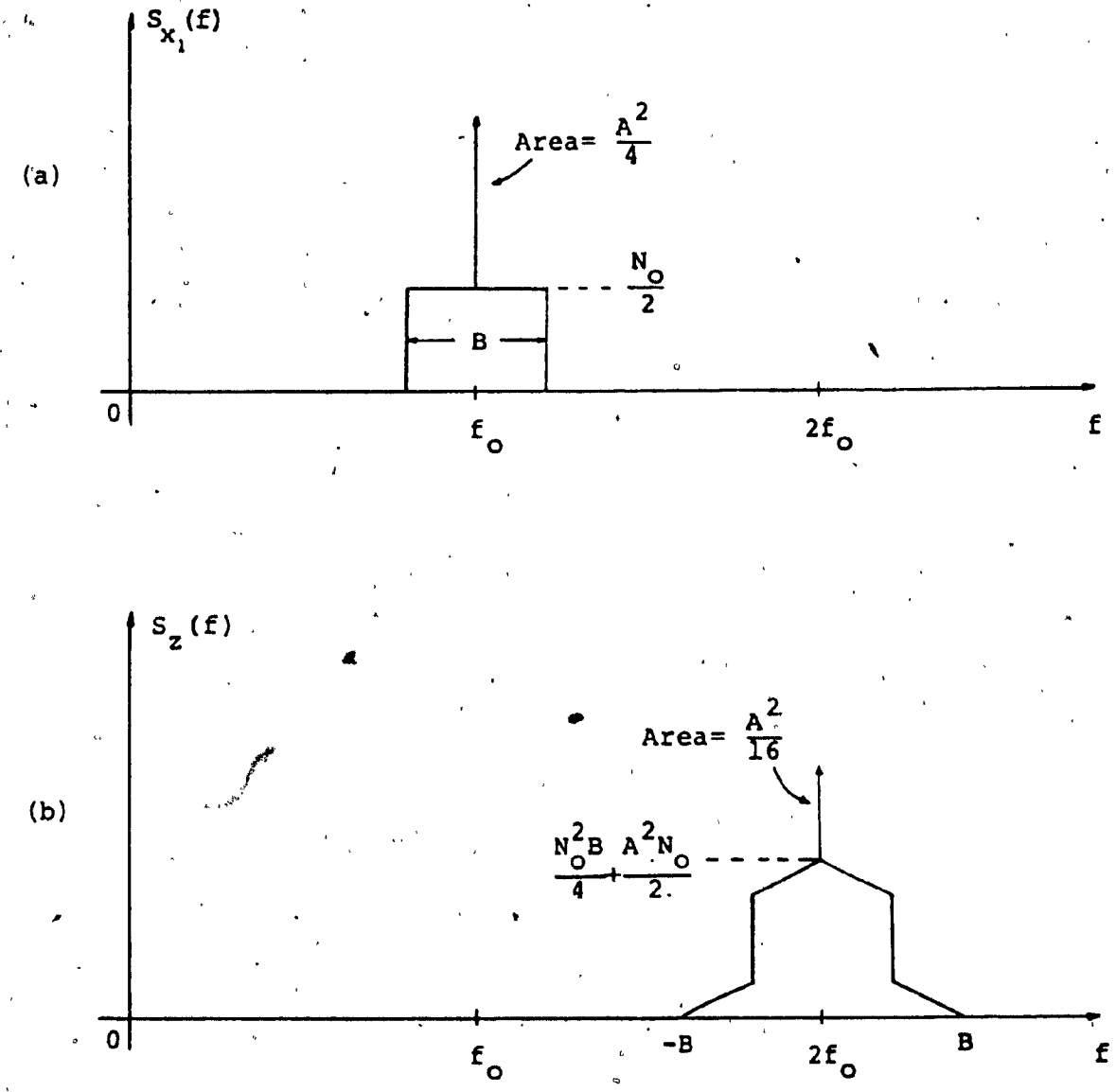

Fig. 5.5: Spectral density of a doubler in response to the output of BPF1

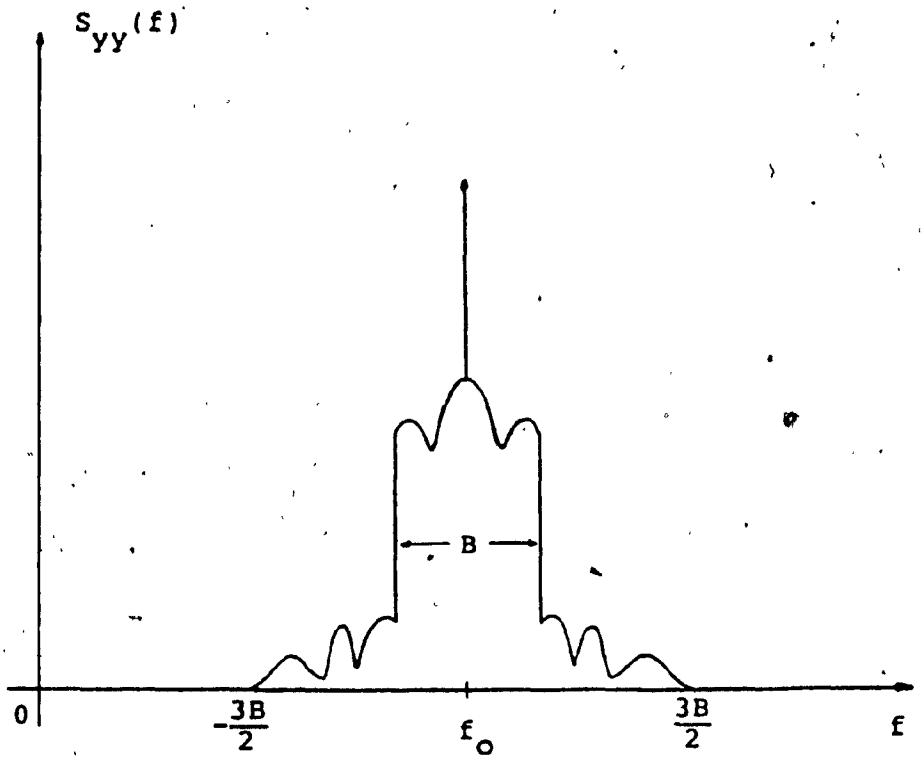

Fig. 5.6: Overall output spectral density of FTF using ideal BPF's with sinusoidal signal plus AWGN

pattern and the spreading are retained in the overall spectrum.

Experimentally, a discrete FTF is used to verify the theoretical results since SAW BPF's have very similar characteristics to ideal BPF's. The results of the output of each element of the FTF in Fig.5.1 are measured. Fig.5.7 displays a single-tone signal and the accompanied noise before and after the first SAW filter, r(t) and $x_1(t)$. The filtering of the SAW BPF is clearly seen, and the sharp rolloff of the spectrum approximates the brick wall characteristics of an ideal BPF. The output at the second SAW BPF, $x_2(t)$, is shown along with $x_1(t)$ in Fig.5.8. A narrower bandwidth is obtained as expected. This improvement is not considered in the theory for the sake of simplicity. Fig.5.9 is the output of a doubler, z(t), overlaying on its input $x_1(t)$. It is noted that the output SNR of the doubler is lower than the input SNR. The degradatiion of SNR of the doubler is predicted in theory [12]. Due to this degradation, the output SNR of the FTF also degrades as will be seen in a later section. The spreading effect of the doubler is approximately shown in the picture. The final output of the FTF, y(t), is compared respectively with $x_1(t)$ and $x_2(t)$ in Figs.5.10. As mentioned before, the output SNR is degraded. The overall spectrum agrees closely with the special case of the theorectical result obtained in Fig.5.6. The undulating close-in noise and the spreading effect at the bottom of the spectrum are both recorded in the picture.

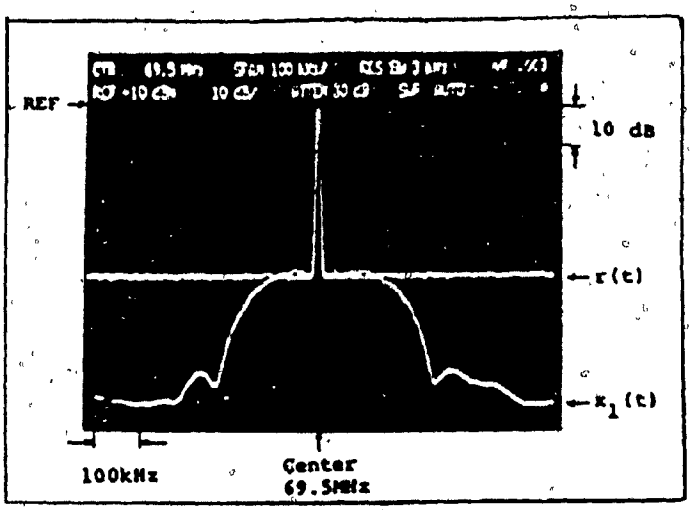

Fig. 5.7:
Measured output of BPF1, $x_1(t)$, in response to sinusoidal input plus AWGN, r(t)

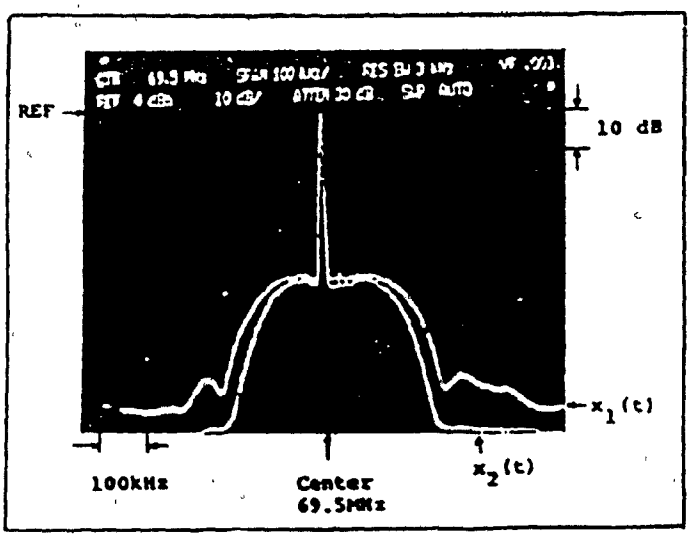

Fig. 5.8:
Measured output of BPF2, $x_2(t)$, in response to sinusoidal input plus AWGN

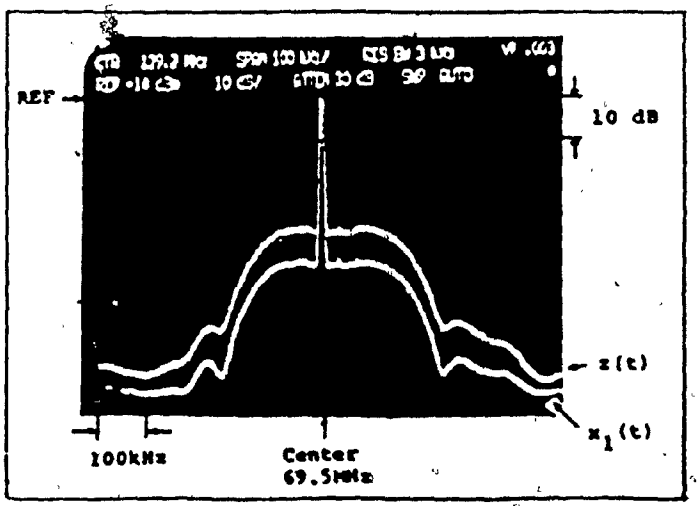

Fig. 5.9:
Measured output of doubler, z(t), in response to output of BPF1, $x_1(t)$

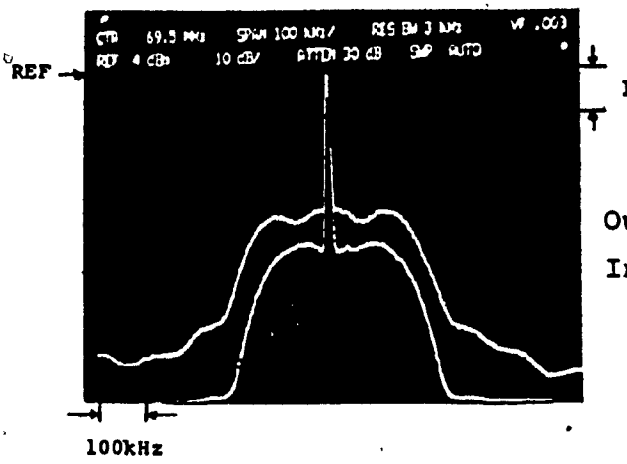

Outer display: y(t)
Inner display: $x_2(t)$

(a) Compared to BPF2 output, $x_2(t)$

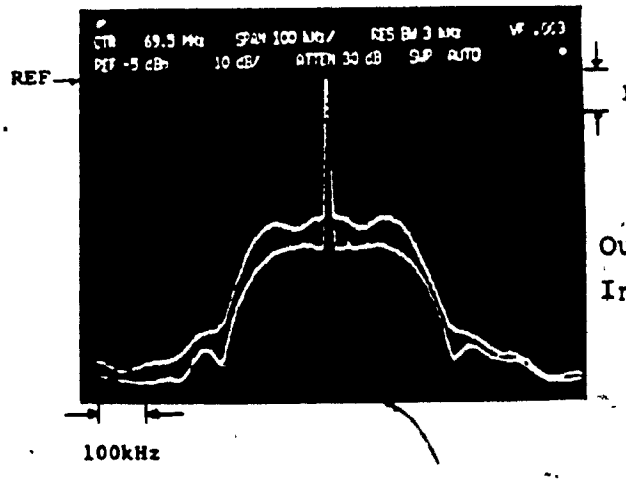

Outer display: y(t)
Inner display: $x_1(t)$

(b) Compared to BPF1 output, $x_1(t)$

Fig. 5.10: Measured output of FTF using SAW BPF's in response to sinusoidal signal plus AWGN

Comparing the spectral analysis of FTF in AWGN environment to that in noise-free environment, it is found that the improvement of bandwidth in the latter is no longer found in the former. This result indicates that the nonlinear effect on the signal plus noise is different from that on the single-tone, noise-free signal. Therefore, due to slow roll-off of the single-tuned BPF, the "narrower bandwidth" measured by sweeping the input frequency is not the true bandwidth of the FTF. The performance of the FTF thus cannot be measured by the bandwidth but by the SNR which is studied in the next section.

5.2 Signal-to-noise ratios

In this section, the relation of the input and output signal-to-noise power ratios of the bandpass model of the discrete and continuous FTF's is investigated.

From the expression for the autocorrelation function of the output of the FTF in Eq.(5.12a) and confining our interest in the vicinity of f_o, the signal power at the FTF output is evaluated to be

$$S_T = R_{sxs}(0) = \frac{9A^6}{32} \qquad (5.23)$$

Similarly, from Eqs.(5.12b-e), the total noise power at the FTF output is equal to

$$N_T = R_{sxn_1}(0)+R_{sxn_2}(0)+R_{sxn_1xn_2}(0)+R_{n_1xn_2}(0) \qquad (5.24)$$

where

$$R_{sxn_1}(0) = \frac{3}{4}A^4N_oB_1+\frac{1}{2}A^2N_o^2B_1^2+A^4(1+\frac{1}{2}\cdot\frac{1}{2})R_{n_1n_1}(0)+\frac{3}{4}A^2R_{n_1}^2{}_{n_1}(0)$$

$$= 2A^4N_oB_1 + \frac{5}{4}A^2N_o^2B_1^2 \qquad (5.25a)$$

The factor of 1/2 arises in the third term because half of the power of $R_{n_1n_1}(\varepsilon)\cos w_o\varepsilon$ is centered at f_o whereas the other half is at $3f_o$. The same reason applies to the factor of 3/4 in the last term, three quarters of power is centered at f_o, and the rest is centered at $3f_o$.

$$R_{sxn_2}(0) = \frac{5}{16}A^4N_oB_2 \qquad (5.25b)$$

$$R_{sxn_1xn_2}(0) = \frac{11}{4}A^4N_oB_c+11A^2N_o^2B_1B_c+\frac{11}{2}A^2N_o^2B_c^2$$

$$+\frac{5}{2}A^2N_o^2B_1B_2 \qquad (5.25c)$$

$$R_{n_1xn_2}(0) = 11N_o^3B_c^2B_1+\frac{5}{2}N_o^3B_1^2B_2 \qquad (5.25d)$$

Summing the individual noise power in Eqs.(5.25a-d), the total noise power in Eq.(5.24) is computed as

$$N_T = 2A^4N_oB_1+\frac{5}{16}A^4N_oB_2+\frac{11}{4}A^4N_oB_c+\frac{5}{4}A^2N_o^2B_1^2+\frac{5}{2}A^2N_o^2B_1B_2$$

$$+11A^2N_o^2B_1B_c+\frac{11}{2}A^2N_o^2B_c^2+\frac{5}{2}N_o^3B_1^2B_2+11N_o^3B_c^2B_1 \qquad (5.26)$$

5.2.1 SNR of FTF using ideal BPF's

For ideal BPF, the total noise power is modified as

$$N_T = \frac{37}{16}A^4N_oB + \frac{11}{4}A^4N_oB_c + \frac{15}{4}A^2N_o^2B^2 + 11A^2N_o^2B_cB + \frac{11}{2}A^2N_o^2B_c^2 + \frac{5}{2}N_o^3B^3 + 11N_o^3BB_c^2 \quad (5.27)$$

since $B_1 = B_2 = B$.

Defining the input signal-to-noise ratio, SNR_i, to be

$$SNR_i \triangleq \eta = \frac{A^2}{2N_oB_1} \quad (5.28)$$

which is the output signal-to-noise ratio of the BPF1 in Fig.5.1, the output signal-to-noise ratio, SNR_o, of the FTF can be derived as

$$SNR_o \triangleq \frac{S_T}{N_T} = \frac{9}{4}\eta^3B^3 \Big/ \left(\frac{37}{4}\eta^3B^3+11\eta^2B^2B_c+\frac{15}{2}\eta B^3+22\eta B^2B_c + 11\eta BB_c^2+\frac{5}{2}B^3+11BB_c^2\right) \quad (5.29)$$

Expressing the one-sided noise equivalent correlation bandwidth B_c in terms of B as shown in Eq.(5.30),

$$B_c = \int_{f_o-\frac{B}{2}}^{f_o+\frac{B}{2}} \cos[b(f-f_o)]\,df = \frac{2}{b}\sin\frac{bB}{2} \quad (5.30)$$

the SNR_o in Eq.(5.29) is then simplified as

$$SNR_o = \frac{9\eta^3}{37\eta^2+30\eta+10+44\eta(\eta+2)\,\mathrm{sinc}(x)+44(\eta+1)\,\mathrm{sinc}^2(x)} \quad (5.31)$$

where $\mathrm{sinc}(x)=\sin(x\pi)/(x\pi)$ is the sinc function of x, and

$$x = -bB/2\pi. \tag{5.32}$$

This can be rearranged as

$$b = -2\pi x/B \quad , \quad x \geq 1/2 \tag{5.33}$$

Eq.(5.33) represents the slope of the linear phase response of the BPF. The variable x can be any real number less than zero. It is unrealistic to have x=0 as there is no filter having zero input-output phase relationship unless it is a tracking filter or FTF. In essence, x is assigned arbitrarily to lie in the domain $x>1/2$ based on the fact that a single-tuned BPF gives approximately a phase difference of π over its entire 3dB bandwidth. Figs.5.11 and 5.12 are the input-output SNR relationship of FTF using ideal BPF's for three different coefficients. The small signal suppression, inherent from the doubler, is evidently shown. At high input SNR, a linear characteristic is obtained, which can be approximated by

$$SNR_o = \frac{9\eta}{37 + 44\,\mathrm{sinc}(x)} \quad , \quad x \geq \frac{1}{2} \tag{5.34}$$

and thus the output SNR generally suffers 6 to 7 dB degradation. The significance of comparing the output SNR of the FTF with that of the first BPF is that a certain price has to be paid in order to achieve tracking capability in a feedforward fashion, i.e. degradation in SNR and increased complexity of the circuit.

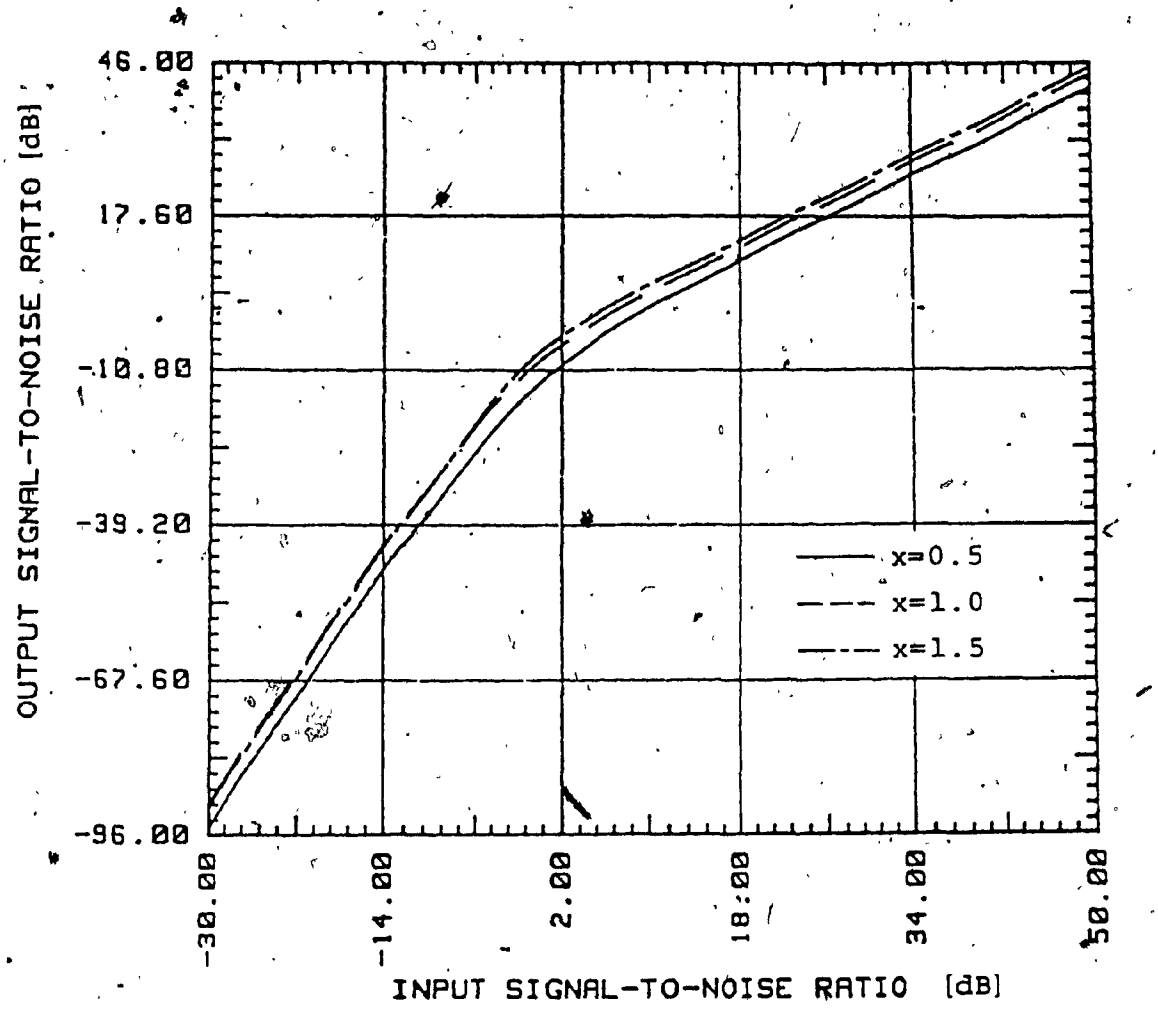

Fig. 5.11: Output SNR of FTF using ideal BPF's vs output SNR of BPF1 (general case)

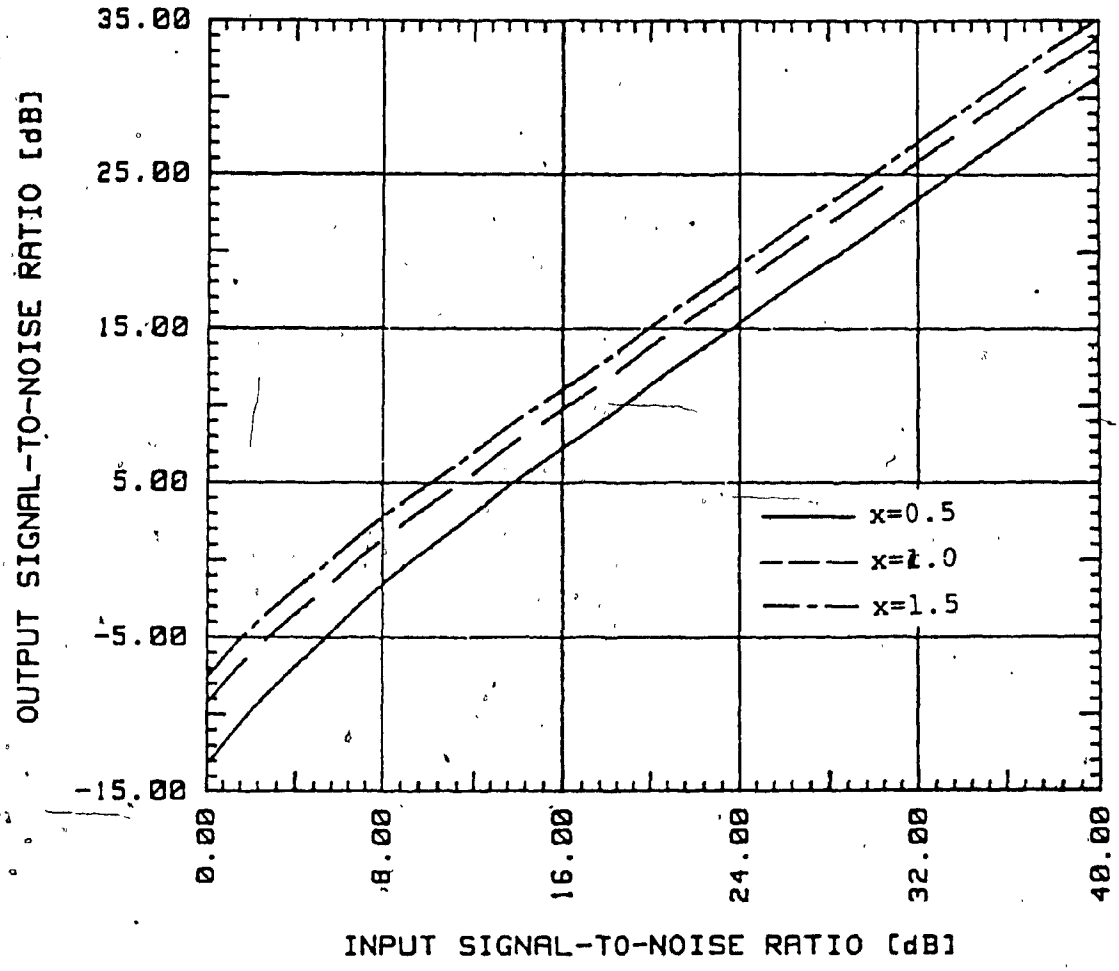

Fig. 5.12: Output SNR of FTF using ideal BPF's vs output SNR of BPF1 at high SNR

Given a fixed SNR_i, the SNR_o improves at zero-crossing points of the sinc function, i.e. when x is an integer. The corresponding SNR_o is

$$SNR_o = \frac{9\eta^3}{37\eta^2 + 50\eta + 10} \tag{5.35}$$

The result in Eq.(5.35) can also be obtained if x is large because the value of sinc(x) approaches to zero as $x \to \infty$. Nevertheless, the improvement of the SNR_o resulting from the property of the sinc function is not significant. As shown in Fig.5.13, the difference only varies within 1dB for $x>1/2$. The figure illustrates the pattern of the sinc function. The highest output SNR is found at x=1.2 where the value of sinc(x) is a minimum.

5.2.2 SNR of FTF using synchronous-tuned BPF

The Eq.(5.23-26) are also applicable for high-Q synchronously-tuned BPF (Q>10). Therefore, we can use the approach in the previous section to find the SNR's for this case.

Here, B_c is calculated by using Eqs.(A.12) and (A.16), i.e.

$$N_o B_c = R_{n_1 n_2}(0) \tag{5.36}$$

where

$$R_{n_1 n_2}(0) = \int_{-\infty}^{\infty} S_{n_1 n_2}(f)\,df = \mathcal{F}^{-1}[F(jw)c^*(jw)]\Big|_{\epsilon=0} \cdot \frac{N_o}{2}$$

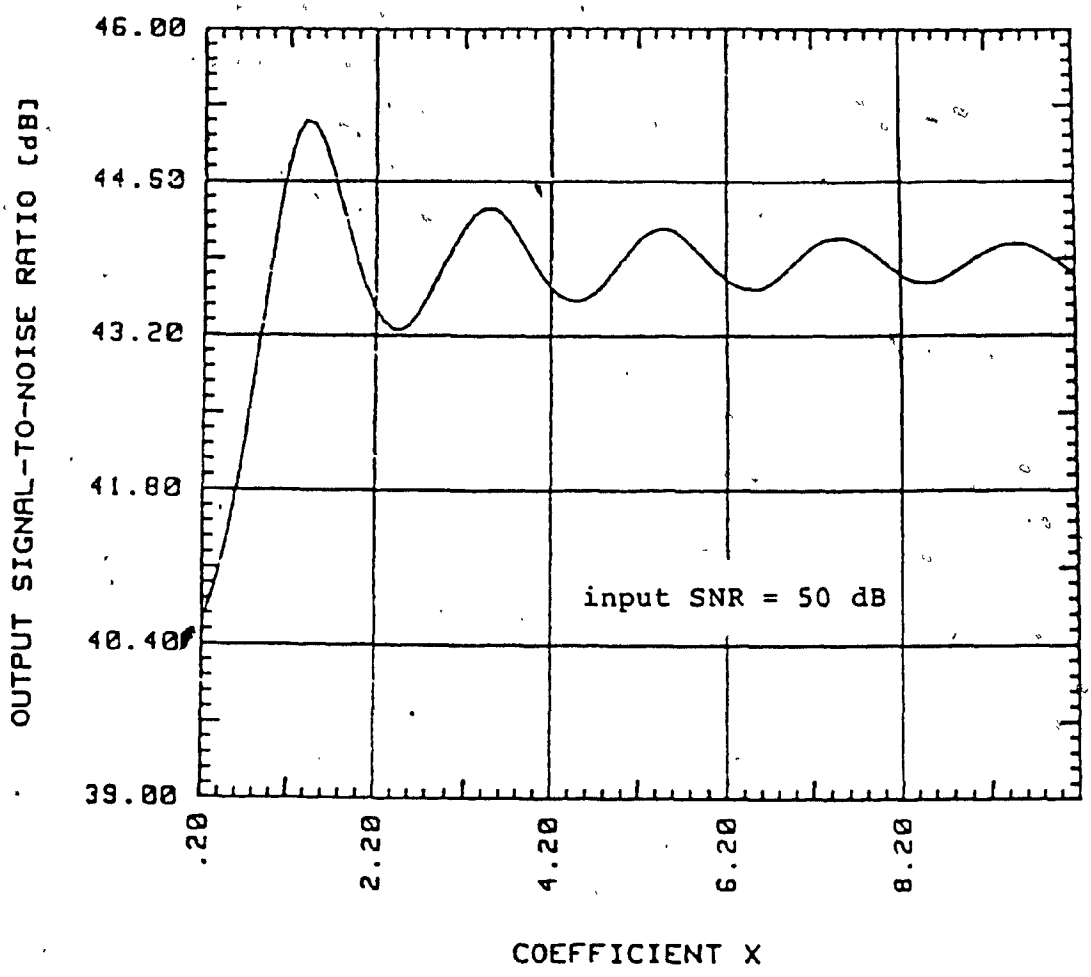

Fig. 5.13: Output SNR of FTF using ideal BPF's vs coefficient x_0

Therefore,

$$B_c = \frac{1}{2}\mathcal{F}^{-1}[F(w)c^*(jw)]\Big|_{\varepsilon=0} \tag{5.37}$$

In terms of the equivalent lowpass analog of the BPF's, it yields

$$B_c = \mathcal{F}^{-1}[F_1(jw)c_1^*(jw)]\Big|_{\varepsilon=0}$$

$$= \mathcal{F}^{-1}\left[\left(\frac{w_c}{w_c+jw}\right)^n \left(\frac{w_c}{w_c-jw}\right)^{2n}\right]\Big|_{\varepsilon=0} \tag{5.38}$$

The B_c of four different order synchronously tuned FTF's are shown in Table 5.2. The one-sided noise equivalent bandwidth of the cascaded BPF's, B_2, is also included in the table.

It is noted that B_c and B_2 increase as the bandwidth of the BPF increases for any order of the synchronous BPF. Certainly, if the bandwidth of the BPF increases, more noise will pass at $x_2(t)$ and more noise will be correlated.

It is known that the more is the filter cascaded, the less improvement in bandwidth. Thus, under the same noise bandwidth, B_2 increases with the order. However, it is interesting that B_c improves with the order. It is found that the cross-correlation of $n_1(t)$ and $n_2(t)$ decreases exponentially with the time difference. The decreasing rate and the correlation at zero time difference are reduced when the order of the BPF increases. In other words, the imagi-

nary power of the complex cross power spectral density increases at the expense of the real power. The B_c, compared to B_1, therefore, decreases as the order of the BPF increases. However, this is insignificant in the case of the second order.

Substituting B_c and B_2 into Eq.(5.26) and using the same definition of SNR_i in Eq.(5.28), the SNR_o of the synchronously-tuned FTF is computed. The result is tabulated in Table 5.3 and plotted in Figs.5.14 and 5.15. Compared to Fig.5.11, a similar performance in terms of SNR is found. Resulting from the slight improvement in B_c, the output SNR is better for third and fourth order FTF at high input SNR. The second order FTF shows inferior performance since it suffers from the increase in B_2 and no improvement in B_c.

5.3 Phase noise performance

White noise usually causes both phase and amplitude fluctuation of a sinusoidal signal. In some applications such as carrier recovery, outputs with clean phase is more critical than with stable amplitude response since the amplitude variation can be eliminated by a limiter but not the phase noise. Therefore, the effect of the phase noise, as a form of phase jitter in the time domain, on FTF is more significant for these applications. The study of the phase jitter of the FTF is thus of great interest, since it is designed to acquire and track the phase of a signal. When

Order	n	B_2	B_c	B_L
First	1	$\frac{1}{2}B_1$	$\frac{1}{2}B_1$	$\frac{5}{2}B_1$
Second	2	$\frac{5}{8}B_1$	$\frac{1}{2}B_1$	$\frac{21}{8}B_1$
Third	3	$\frac{21}{32}B_1$	$\frac{7}{16}B_1$	$\frac{93}{32}B_1$
Fourth	4	$\frac{85.8}{128}B_1$	$\frac{3}{8}B_1$	$\frac{405.8}{128}B_1$

Table 5.2: Table of various one-sided equivalent noise bandwidth of four synchronously-tuned FTF

Order	n	SNR_O
First	1	$\frac{18\eta^3}{113\eta^2+150\eta+32}$
Second	2	$\frac{72\eta^3}{457\eta^2+620\eta+138}$
Third	3	$\frac{576\eta^3}{3490\eta^2+4483\eta+959}$
Fourth	4	$\frac{1152\eta^3}{6637\eta^2+8012\eta+7194}$

Table 5.3: Output SNR of four synchronously-tuned FTF in terms of output SNR of BPF1, η

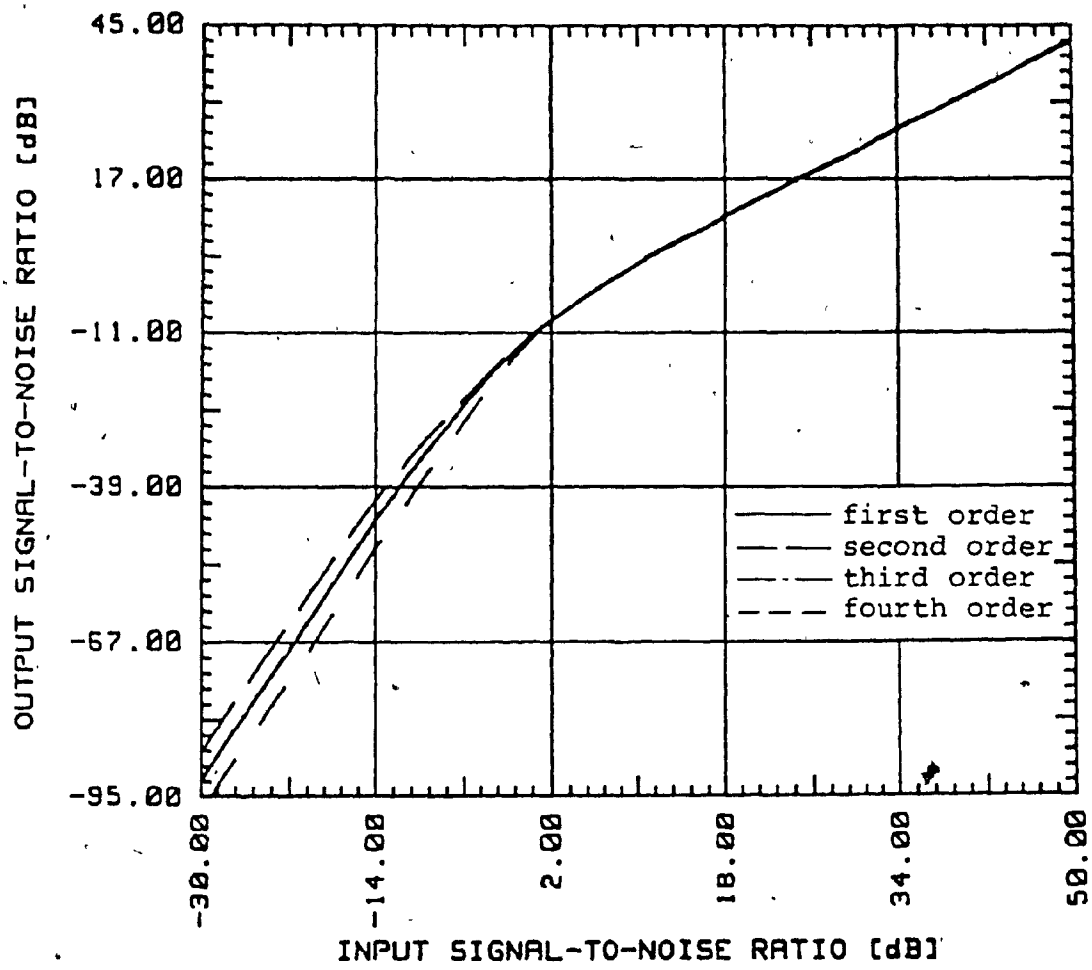

Fig. 5.14: Output SNR of continuous FTF's vs output SNR of BPF1 (general case)

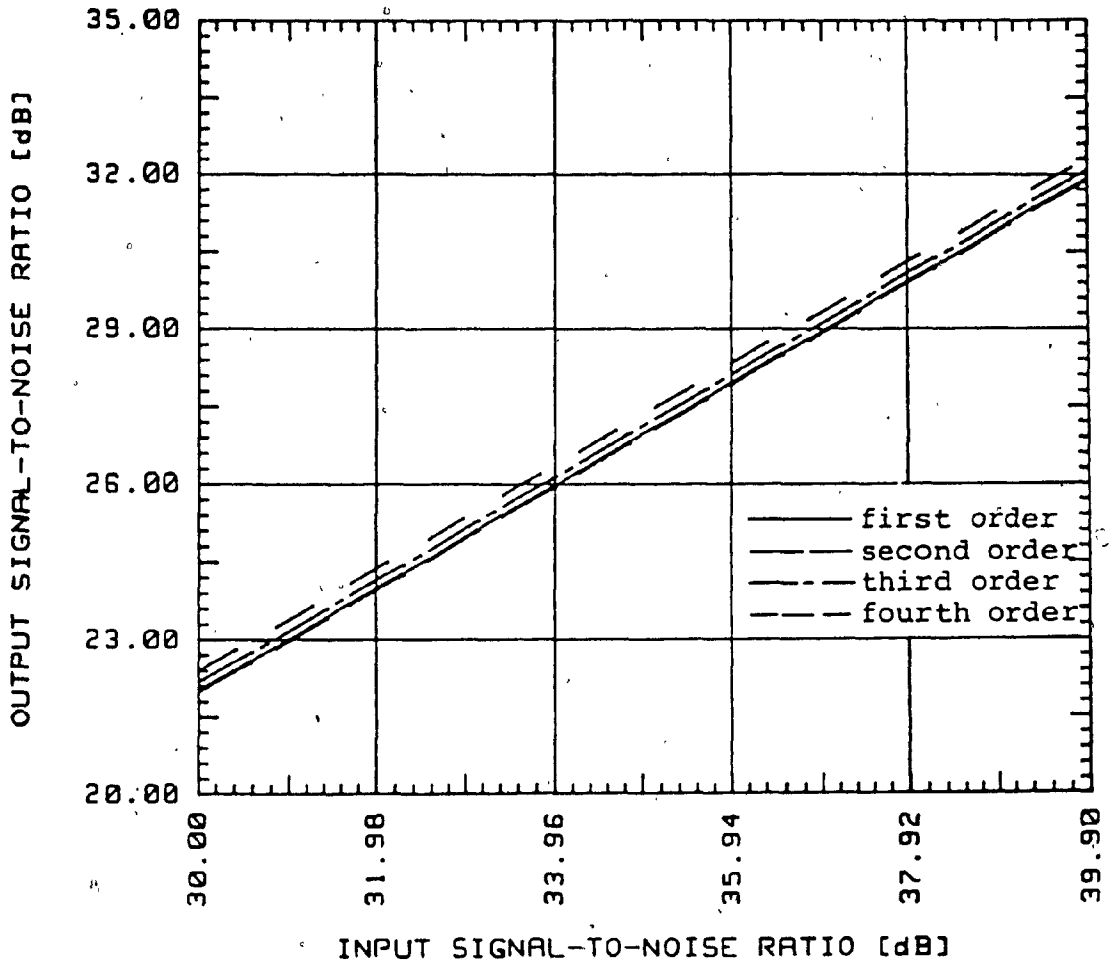

Fig. 5.15: Output SNR of continuous FTF's vs output SNR of BPF1 at high SNR

the phase jitter exceeds a certain value, a statistical phenomenon known as cycle skipping occurs. A brief study of this phenomenon is given in order to gain a better understanding.

5.3.1 Phase jitter analysis

To analyze the phase jitter of the FTF, an IF filter and a limiter are assumed to be placed before the FTF, and the baseband model is used for the baseband phase input. Let

$$r(t) = s(t) + n(t) \tag{5.39}$$

be the output of the IF filter. Here

$$s(t) = A\cos(w_o t+\theta)$$

is the input signal and $n(t)$ is the bandpass Gaussian noise process. $n(t)$ can be expressed as,

$$n(t) = n_c(t)\cos(w_o t+\theta) + n_s(t)\sin(w_o t+\theta) \tag{5.40}$$

$n_c(t)$ and $n_s(t)$ are the in-phase and quadrature component of the noise process $n(t)$. It can be shown that [13]

$$E[n_c(t)] = E[n_s(t)] = E[n(t)] = 0 \tag{5.41}$$

and

$$Var[n_c(t)] = Var[n_s(t)] = Var[n(t)] = N_o B_{IF} \tag{5.42}$$

where B_{IF} is the one-sided noise equivalent bandwidth of the IF filter and Var[X] is the variance of a random variable X.

The received signal of Eq.(5.39) can be rewritten as

$$r(t) = [A+n_c(t)]\cos(w_o t+\theta) + n_s(t)\sin(w_o t+\theta)$$
$$= R(t)\cos(w_o t+\theta+\varphi) \qquad (5.43)$$

where

$$R(t) = \sqrt{[A+n_c(t)]^2 + n_s^2(t)} \qquad (5.44)$$

$$\varphi(t) = \tan^{-1}\left(\frac{n_s(t)}{A + n_c(t)}\right) \qquad (5.45)$$

R(t) in Eq.(5.44) is the amplitude fluctuation which is removed by the limiter. Eq.(5.45) represents the input phase jitter to the FTF. When there is a high signal-to-noise ratio at the output of the IF filter preceding the limiter, the terms $n_c(t)$ and $n_s(t)$ will be much smaller than A, that is

$$|n_c(t)| , |n_s(t)| << A \qquad (5.46)$$

The phase jitter term $\varphi(t)$ can then be replaced by

$$\varphi(t) = n_s(t)/A \qquad (5.47)$$

If B_{IF} is much bigger than B_L, $\varphi(t)$ becomes a white Gaussian noise process with zero mean and power density

$$\text{Var}[\varphi(t)] = E[\frac{n_s^2(t)}{A^2}] = \frac{N_o}{2A^2} \qquad (5.48)$$

The output of the FTF in response to this phase jitter $\varphi(t)$ is

$$\theta_j(t) = \int_{-\infty}^{\infty} h(\lambda)\varphi(t-\lambda)d\lambda \tag{5.49}$$

where $h(t) = \mathcal{F}^{-1}[H(f)]$.

Clearly, the output phase jitter $\theta_j(t)$ of the linear baseband model of the FTF is a Gaussian process and its mean is zero. The variance of the output phase noise (jitter) then is

$$\sigma^2 \triangleq E[\theta_j^2(t)] = \int_{-\infty}^{\infty} |H(f)|^2 \Phi(f)df = \frac{1}{2\rho} \tag{5.50}$$

where $\Phi(f) = \mathcal{F}[\varphi(t)] = N_o/2A^2$,

$$\rho = A^2/2N_oB_L \tag{5.51}$$

and B_L is the one-sided lowpass equivalent noise bandwidth of the FTF, i.e.

$$B_L = \int_0^{\infty} |H(f)|^2 df \tag{5.52}$$

ρ in Eq.(5.51) is considered as the SNR in the FTF. The expression in Eq.(5.50) is expected as the baseband model of the FTF has the characteristics of a PLL assumed as a linear system. Therefore, the root mean square value of the phase jitter is, the same as the PLL, inversely proportional to the square root of the SNR in the loop. Table 5.2 shows the B_L for different orders of the synchronously tuned FTF. It can be seen that the output phase jitter increases with the bandwidth of the BPF. It also increases with the order of the BPF under the same B_1.

Furthermore, the first and second moments (mean and variance) are sufficient to specify the Gaussian process $\theta_j(t)$. The probability density function of the phase error due to the phase jitter is then found as [13]

$$P_e(\theta_j) = \frac{1}{\sqrt{\pi/\rho}} e^{-\theta_j^2 \rho} \tag{5.53}$$

where ρ is defined in Eq.(5.51). Eq.(5.53) also resembles the error probability of the PLL with high input SNR [1,2].

5.3.2 Cycle skipping in FTF

At low input SNR, a phenomenon called cycle skipping is observed in PLL and also in the feedforward quadrupler [7]. This is a random occurance, with low probability at high SNR, but with an increasing probability when the SNR decreases. For each cycle of the input there must be a corresponding cycle of the output. A cycle skip event happens if the output of the tracking filter advances or recedes a phase of 2π with respect to the input phase. This phenomenon in the PLL has been extensively studied in the literature [2,10,14]. Due to the periodic characteristics of the phase error of the PLL, the VCO skips one or several cycles with respect to the input phase when the VCO phase variance becomes too large. If the additive noise is the only cause of the phase variance, that is, if the input

signal is not modulated and its frequency is equal to the VCO central frequency, the probability of skipping a cycle either in a plus or minus direction is the same. However, the PLL skips cycle, even in the absence of additive noise, when the input signal frequency is not equal to the VCO central frequency (this phenomenon is well described by the phase plane trajectory method [2,10]). Therefore, a higher probability of cycle skipping is found when the PLL is required to acquire a large frequency step input.

A similar phenomenon of cycle skipping is also observed in the FTF. The additive noise is the only source of this random occurance. Contrasting to the slow feedback correction of the phase error modulo 2π, the feedforward compensation scheme allows any value of the phase error ($-\infty$ to $+\infty$) at the output of the first BPF, and as a result, there is only one asymptotic stable operating node in the FTF. Therefore, the phase error at the output of the first BPF caused by the frequency step will vanish eventually without exhibiting any cycle skipping. Although the multiplier in the FTF has a phase characteristics of modulo 2π, the phase error caused by the frequency step is not restricted by this periodicity.

As the additive noise is the only cause of the cycle skipping, to simplify the situation and, in fact, supported by experimental results, Hess [15] proposed that the output

of the PLL skips a cycle when the input contains a step of $\pm 2\pi$. The idea is similar to the "click" in the FM (Frequency Modulation) receiver. It is also applicable for the FTF. When the noise induces a $\pm 2\pi$ phase step at the input, a cycle is skipped if the FTF tracks this $\pm 2\pi$ phase. With reference to Fig.5.1, whenever a phase jump of $\pm 2\pi$ at $x_1(t)$, at $x_2(t)$ or at $z(t)$ occurs, a cycle skip event will also be induced at the output of the FTF. It is more likely that phase jump happens at the output of the doubler $z(t)$ since there is a degradation of 6 dB in SNR due to the nonlinear operation. On the contrary, it is less likely at the output of the cascaded BPF's $x_2(t)$. Although the doubler will likely increase the cycle skipping rate as a result of decreased SNR, it eliminates the cycle skipping due to the phase ambiguity introduced by the frequency divider used in the feedforward quadrupler [7]. It is verified expermemtally that the cycle skipping rate of the FTF is better than that in [7] even with the cycle skipping correction circuit.

The expression of average cycle skipping rate of the FTF is desirable. The determination of number of 2π phase step, tracked by FTF, yields the solution. Assuming the additive noise is white, an expression of the average cycle skipping rate can be shown as [15]

$$N_c = \gamma \operatorname{erfc}[SNR_i] \qquad (5.54)$$

where γ is the radius of gyration of narrowband noise defined as

$$\gamma = \frac{\sqrt{\int_{-\infty}^{\infty} f^2 \, F_1(f)df}}{\sqrt{\int_{-\infty}^{\infty} F_1(f)df}} \qquad (5.55)$$

and

$$\text{erfc}(x) = \frac{2}{\sqrt{\pi}} \int_{x}^{\infty} e^{-u^2} du \qquad (5.56)$$

Eq.(5.54) shows that the average cycle skipping rate depends on the output SNR of the first BPF of the FTF, SNR_i. Higher the SNR, the less occurance of cycle skipping.

In summary, the bandpass model of the FTF exhibits nonlinear characteristics. As a consequence, the output SNR is degraded with respect to that of the first BPF in order to achieve tracking ability. As far as the phase is concerned, the FTF is a linear system having the characteristics of a second order PLL which is assumed to be linear. The cause of the cycle skipping in the FTF is only due to the additive noise. We have shown that the average cycle skipping rate decreases if the bandwidth of the BPF's in use is reduced.

CHAPTER 6

A COMPARATIVE STUDY OF FTF WITH OTHER TRACKING FILTERS

In this chapter, an attempt is made to compare the FTF with a PLL and a single-tuned BPF with an AFC loop [17,18]. The comparison is made with the following considerations:

1) tracking behaviour
2) transient behaviour and acquisition time
3) non-linear behaviour
4) noise performance
5) hang-up

6.1 Comparison with the PLL

Throughout this thesis, the PLL has been compared to the FTF. It has been shown that the baseband model of the FTF has the linear characteristics of the PLL. The first order synchronous FTF has the characteristics of the second order PLL with infinite DC loop gain, and the second order FTF has the characterisitics of the fourth order PLL having two imperfect integrators. Their transient behaviours are therefore similar. Compared to the theoretical results in Figs.3.8, 3.9 and the experimental results in Figs.3.13 and 3.16, the measured results of the transient behaviour of a second order PLL with critical damping and natural frequency of 100KHz in Figs.6.1 and 6.2 are analogous to that of the FTF. Note that the acquisition time of the PLL is 6 times

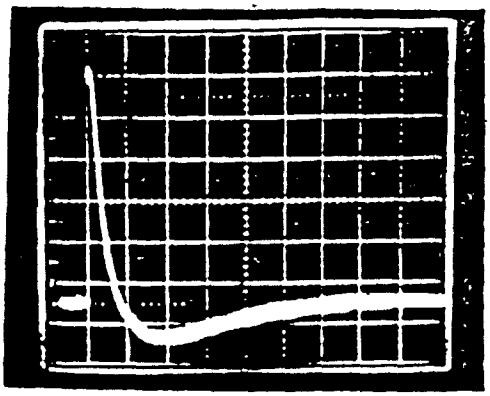

Vertical scale:20mV/div
Horizontal scale:10μs/div

$e_{ss}=0$

$t_{acq}=65\mu s$

Fig. 6.1: Measured phase step transient phase error of a critically damped PLL with natural frequency 100kHz

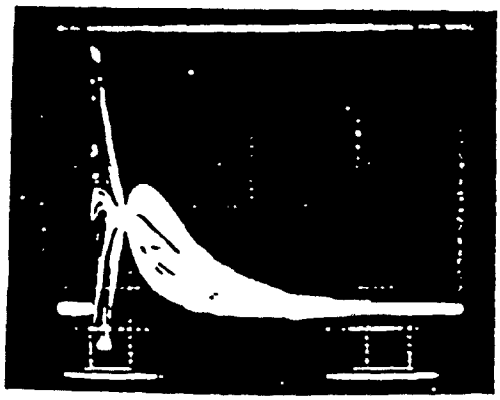

(a) Multiple traces

Vertical scale:50mV/div
Horizontal scale:10μs/div

$e_{ss}=0$

$t_{acq}=65\mu s$

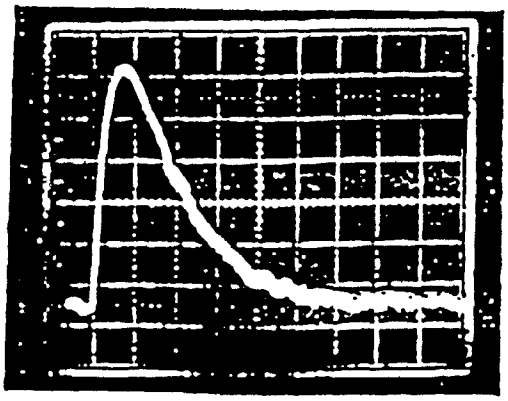

(b) Single trace

Vertical scale:20mV/div
Horizontal scale:10μs/div

Fig. 6.2: Measured frequency step transient phase error of a critically damped PLL with natural frequency 100kHz

longer than that of the single-tuned FTF. However, the equivalent "natural frequency" of the single-tuned FTF is approximately 500KHz which is 5 times larger than that of this PLL. A comparable acquisition time is expected as both tracking filters have the same characterisitics.

Similar to the acquisition behaviour, the tracking behaviour are similar in both cases. In constrast to the ideal fourth order PLL, the second order FTF cannot track any input with frequency velocity or frequency acceleration. This incapability is, however, associated with the fourth order PLL having two imperfect integrators.

Regarding the nonlinear operation of the circuits, both tracking filters represented by their bandpass models are nonlinear systems. For FTF, it has been shown that a narrower bandwidth is obtained due to the nonlinearity (Chapter 4), which is not beneficial, however, when noise is taken into account (Chapter 5). The nonlinearity of the PLL in its bandpass model is not described in the literature while the nonlinearity in its lowpass equivalent model is described in detail. The nonlinear periodic characteristics of the phase detector of the PLL is identified as the cause of the nonlinear operation of the PLL. Associated with this nonlinearity are phenomenons such as cycle skip and hangup. On the contrary, the lowpass equivalent model of the FTF is strictly linear. Thus, FTF is free from these notorious phenomenons (cycle skip due to phase jump in the FTF is not

included), an advantage over the PLL.

Fig.6.3 shows a typical spectrum of a PLL (critically damped with natural frequency is 100kHz) in the presence of white noise. A narrower bandwidth and better close-in noise spectrum are found when compared to the spectrum of the FTF in Fig.5.10. The improvement is primarily due to the negative feedback configuration. As far as phase noise is concerned, PLL is further perturbed by the short term instability or phase jitter of the VCO while FTF is only disturbed by the input phase noise. Hence, FTF has an advantage of being free from the phase jitter caused by the VCO. In fact, the output phase jitter of the FTF is equivalent to that of the linear PLL with an ideal and stable VCO. This is also the case when the input has high SNR. At low input SNR, the linear operation of the PLL is no longer valid and the phase error variance of the PLL is worse than that of the FTF. However, it is anticipated that the doubler in the FTF will cause some modulation dependent interference called pattern noise if the input is modulated and bandlimited. As is phase jitter of the VCO in PLL, this pattern noise will disperse the output spectrum of the FTF. Moreover, cycle skip of the FTF due to phase jump of 2π is similar to that of the first order PLL, but further study is needed to analyze and characterize this phenomenon in FTF.

Finally, it is rare that a PLL higher than third order is constructed because there has been little need for high

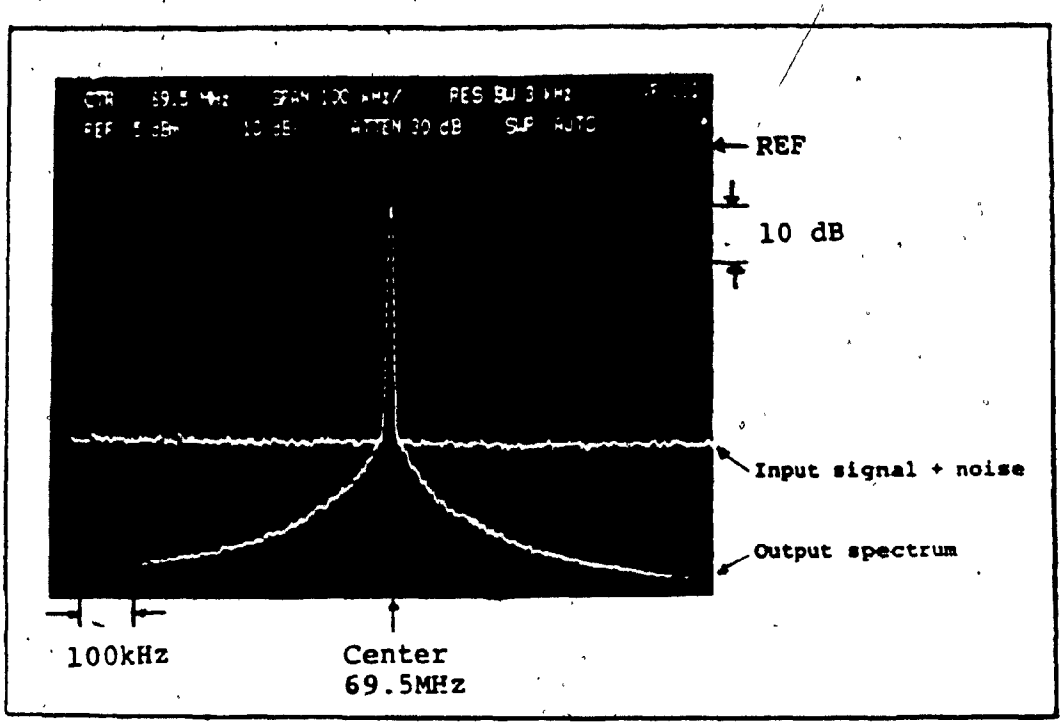

Fig. 6.3: Amplitude response of a critically damped PLL with natural frequency 100kHz in response to sinusoial signal plus noise

order PLL in common applications. It is also hard to design a stable high order PLL. On the contrary, FTF is unconditionally stable as long as the BPF's used are stable.

6.2 Comparison with an AFC loop

As mentioned in Chapter 1, this loop is an alternate of PLL as a tracking filter for fast acquisition. Refering to Fig.1.2, a narrowband BPF is adopted to serve for two purposes: producing an error signal linearly proportional to the input frequency offset and limiting input noise power. Unlike the FTF, the BPF can only have a maximum of 2π of phase variation over the entire bandwidth in order to obtain one-to-one correspondence between the frequency offset and the error signal. In reference [17], a single-tuned BPF satisfying this restriction is used. Assuming the loop is in the linear operation, this loop was shown to have second order PLL characteristics and to be able to track a phase step input. There exists, however, a steady-state error or static error if a frequency step input is applied. Increasing the DC gain of the loop can reduce the static error. This is analogous to the PLL such that an infinite loop DC gain is preferable to be insensitive to the input phase variation.

A computer simulation of the transient response is provided in [17]. From the simulation result, it is seen

that the acquisition time is incredibly short, only a fraction of the time constant of the single-tuned BPF. This result is questionable because the transient seems to vanish as fast just when only a single-tuned BPF is used.

The AFC loop has been modified by Weaver [18] to apply in a carrier recovery subsystem of a TDMA system. Instead of phase detector, frequency detector is used in Weaver's circuit which is referred to as Frequency Locked Loop (FLL). As in the AFC loop, a single-tuned BPF is also used in FLL. In Weaver's analysis, several exact differential equations are derived for different models to calculate the transient responses. The results show that the linear model of the FLL is applicable to predict the acquisition performance of the loop. In agreement with the result of [17], there also exists a static error which depends on the DC loop gain and the bandwidth of the single-tuned BPF. It is obvious that FTF is superior in tracking step inputs although negative feedback is not employed. From the linear model of the FLL, the acquisition time of a frequency step input is found to be short, between 2 to 10 times the time constant of the single-tuned BPF. Under the same noise bandwidth of the BPF's, this acquisition time is comparable with the first order and the second order FTF.

Since both AFC and FLL adopt negative feedback to track the input signal, their structure are very similar to that of the PLL (the linear model of the FLL is clearly seen

to have the structure of the PLL). The nonlinearity associated with the PLL is expected to be found in these two loops. For example in Weaver's model, the input frequency deviation must be small compared to the bandwidth of the single-tuned BPF so that the linear relation of the input and output of the single-tuned BPF is valid. If the input has large frequency offset, the acquisition performance may be degraded. On the contrary, FTF can handle large input frequency offset without upsetting the linear input and output relationship. Moreover, the idea of solving the hang-up problem in AFC loop is different from that of the FTF. Instead of completely removing the nonlinearity of the phase detector to solve the hangup, AFC loop or FLL restricts the phase error signal within $\pm\pi/2$ so that the phase error will not fall near the separatrix (Fig.3.32) of the phase plane. This helps to reduce the chance of the loop to have hangup. From this point of view, the double-tuned BPF cannot be applied in these two circuits if solving the hangup problem is the objective because the total phase variation of the double-tuned BPF is $\pm\pi$, unless the input frequency offset is restricted to be very small.

The performance of the AFC loop in the presence of noise has not been studied but the noise performance of the FLL is analyzed. The analysis shows that limiter can improve the acquisition and tracking performance, which is also the case in the FTF. Furthermore, the FLL in the analysis is treated as a special case of the Frequency

Modulation Feedback Demodulator (FMFB). The rate of frequency "click", similar to the cycle skipping rate of the FTF, has been calculated. As in cycle skipping rate of the FTF, the rate of click also depends on the input SNR. More information is still needed in order to have a overall comparison with the FLL and the AFC loop.

In summary, it is seen that the infinite DC gain is preferred in feedback control tracking circuit while unit DC gain is sufficient and necessary in the feedforward control tracking circuit. Moreover, the acquisition time of any tracking filter depends on the loop bandwidth or the bandwidth of the BPF used. The narrower the bandwidth, the longer the acquisition time. From this comparison, we can further confirm that the feedforward compensation scheme can undoubtedly achieve good tracking performance, fast and reliable acquisition compared to the feedback correction scheme.

CHAPTER 7

AN APPLICATION OF FTF TO A CARRIER RECOVERY SYSTEM

The demand of speed and efficiency of digital communications systems has led to the extensive use of TDMA and QPSK techniques. Use of QPSK allows transmission of two bits per symbol, or twice the information rate of binary transimission in the same bandwidth. TDMA, characterized by burst-mode operation, allows many users to share a common channel. The data from one user occurs in a short burst, followed closely by a short burst from another user, then another and so on. To efficiently use the transmission capacity, there is a very short guard time between bursts and a small number of symbols at the start of each burst is used for synchronizing the carrier. Therefore, the receiver must quickly establish correct phase for each burst to perform reliable coherent demodulation. The demonstrated fast acquisition speed and hangup free characteristics of the FTF can be applied to meet this special high-speed operating requirement. In this chapter, the application of the FTF to a carrier recovery system of a TDMA burst-mode modulator/demoulator (modem) is described. The effects of the acquisition, tracking behaviour and the noise performance of the FTF on the modem bit error rate (BER) performance are presented.

7.1 Tuned-filter synchronzer

Quadrupler, Remodulator and Costas loop are three current popular carrier recovery (CR) circuits used in QPSK digital communication systems. In high-speed TDMA systems, PLL is disqualified from this application because of its natural problem of hangup. The imbedded PLL structure of the Costas loop is also not used. A 'serial' tuned-filter carrier recovery circuit shown in Fig.7.1 is key to meeting the high-speed operating requirements [4]. The essential elements of this synchronzier include a nonlinear carrier regenerator, a tracking bandpass filter and a limiter.

The nonlinear regenerator is used to extract the suppressed carrier from the received modulation signal. "X4 multiplier" and "remodulator" are the nonlinear devices used in the Quadrupler and the Remodulator CR circuits respectively.

The tracking bandpass filter serves two purposes: filtering the carrier from the accompanying disturbance caused by the additive noise and the data dependent pattern noise; phase and frequency tracking to compensate for the repeater drift and the Doppler drift.

The limiter is used to obtain constant output amplitude.

Fig. 7.1: Tuned-filter synchronizer for TDMA application

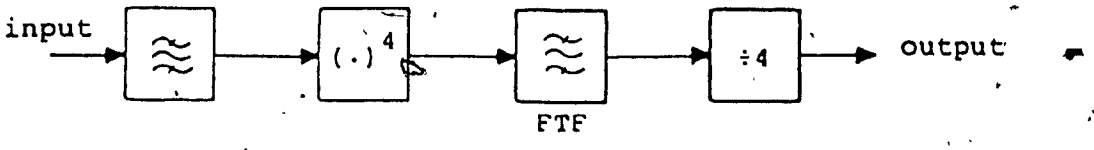

(a) Quadrupler

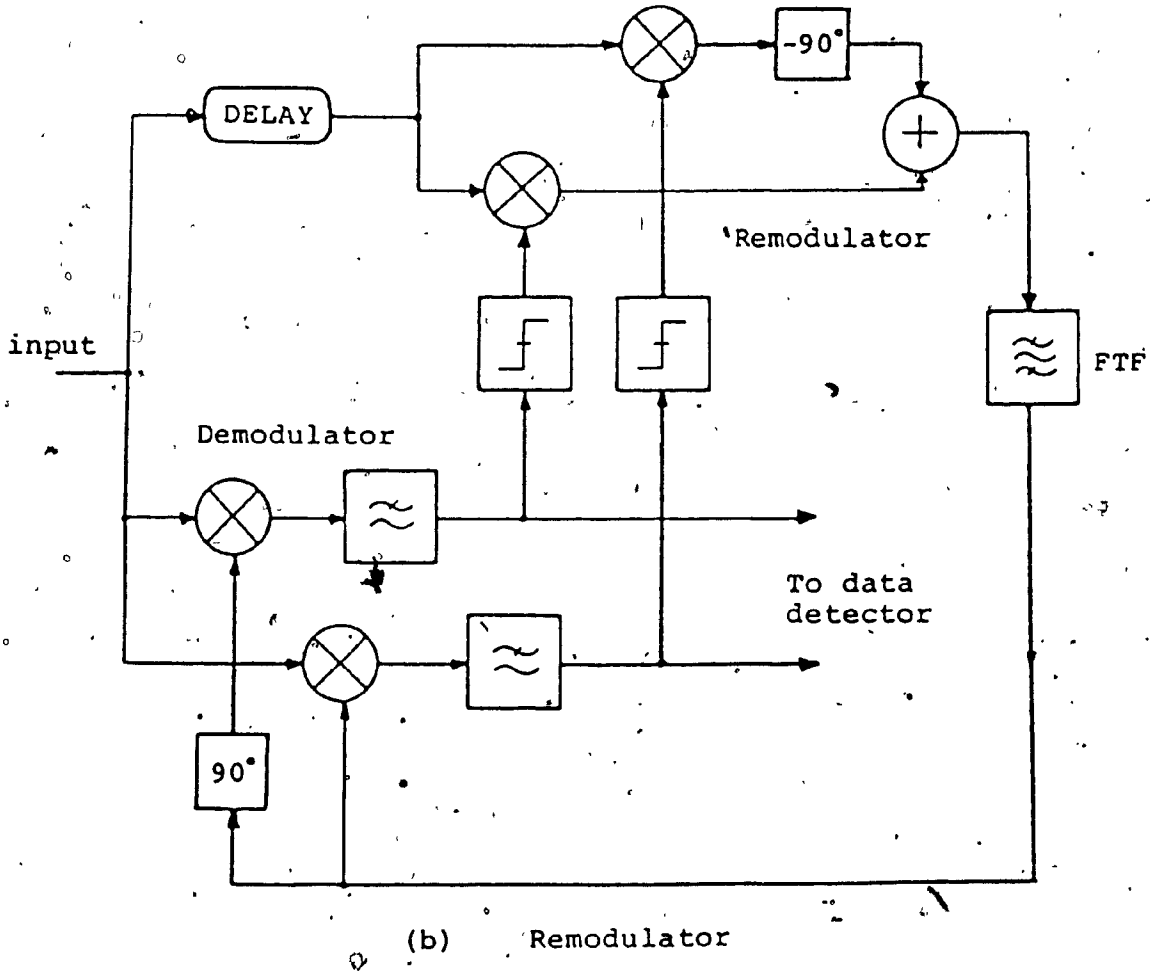

(b) Remodulator

Fig. 7.2: Application of FTF to carrier synchronizer for QPSK scheme

Fig.7.2 shows the application of the FTF to two CR circuits, the Quadrupler and the Remodulator. The merit and drawback of choosing these two schemes depend on the specific requirements of the systems [19]. In constrast to the PLL, the schemes arranged in Fig.7.2 can provide extremely fast acquisition, and the use of FTF can further provide better steady-state data recovery performance than that of AFC loop.

7.2 Application of FTF to Remodulator CR circuit

An experimental set-up of a Remodulator utilizing FTF is shown in Fig.7.3. The suppressed carrier is regenerated by removing the modulation from the modulated signal in the remodulator. The modulated signal is cross-multiplied by the demodulated and limited baseband components (in-phase and quadrature). The difference of the cross-products is the desired carrier (point Ⓒ) which is filtered and tracked by the FTF. The output of FTF containing a properly phased carrier (point Ⓓ) is then used for coherent demodulation. The waveforms multiplied together at the balanced mixers must be aligned in time. Otherwise the respective modulations are not well correlated to be properly removed. For this reason, a delay is needed to be placed before the remodulator for compensating the propagation delay due to the mixers and lowpass filters (point Ⓐ and Ⓑ). The delay also includes the extra delay due to the symbol timing recovery (STR) because an additional decision directed

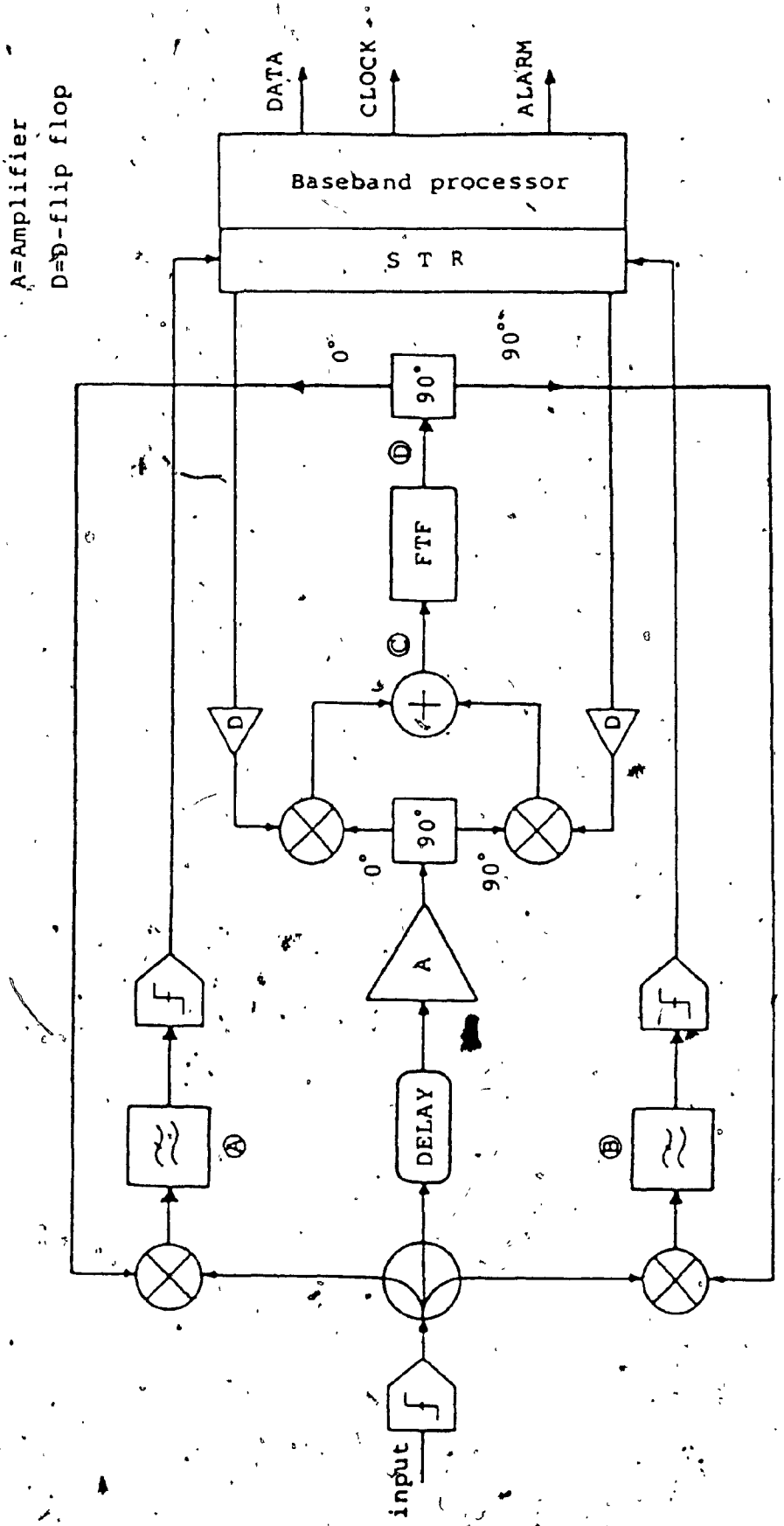

Fig. 7.3: Experimental set-up of a demodulator using FTF for carrier recovery application

technique is used to improve the demodulation performance in this specific remodulator.

Let the noise-free received signal to the remodulator be represented by

$$r(t) = [x_I(t) + jx_Q(t)]e^{jw_o t} \tag{7.1}$$

where $x_I(t)$ and $x_Q(t)$ are the in-phase and quadrature components of the received QPSK signal $r(t)$ and w_o is the carrier frequency. The regenerated carrier at the output of the remodulator can be written as [19,20]

$$c_R(t) = [a_R(t) + jb_R(t)]e^{jw_o t} \tag{7.2a}$$

where

$$a_R(t) = |x_I(t)| + |x_Q(t)| \tag{7.2b}$$

$$b_R(t) = x_I(t)\ \text{sign}[x_Q(t)] - x_Q(t)\ \text{sign}[x_I(t)] \tag{7.2c}$$

and $\text{sign}[x] = \frac{|x|}{x} = \frac{x}{|x|}$

The amplitude of the regenerated carrier is represented by A_R which is the mean of a_R whereas $[a_R(t)-A_R]$ and b_R are considered as AM and PM sidebands representing the in-phase and quadrature pattern noise components respectively. Under high input SNR, pattern noise is the dominant source of phase disturbance in the recovered carrier.

Figs.7.4b and 7.5b show the actual outputs of the remodulator before and after FTF (point © and ⓓ in Fig.7.3).

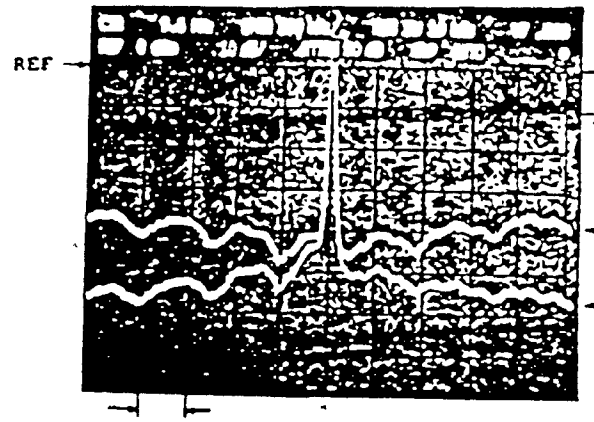

(a) output with a single-tuned BPF which cannot track frequency step

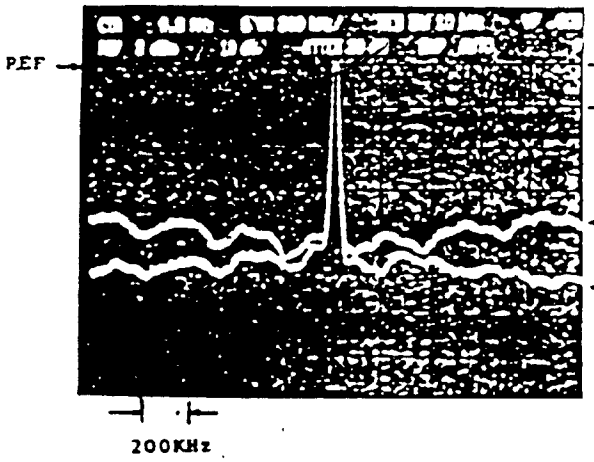

(b) Output with a single-tuned FTF which can track frequency step

Fig. 7.4: Output of a remodulator using single-tuned FTF

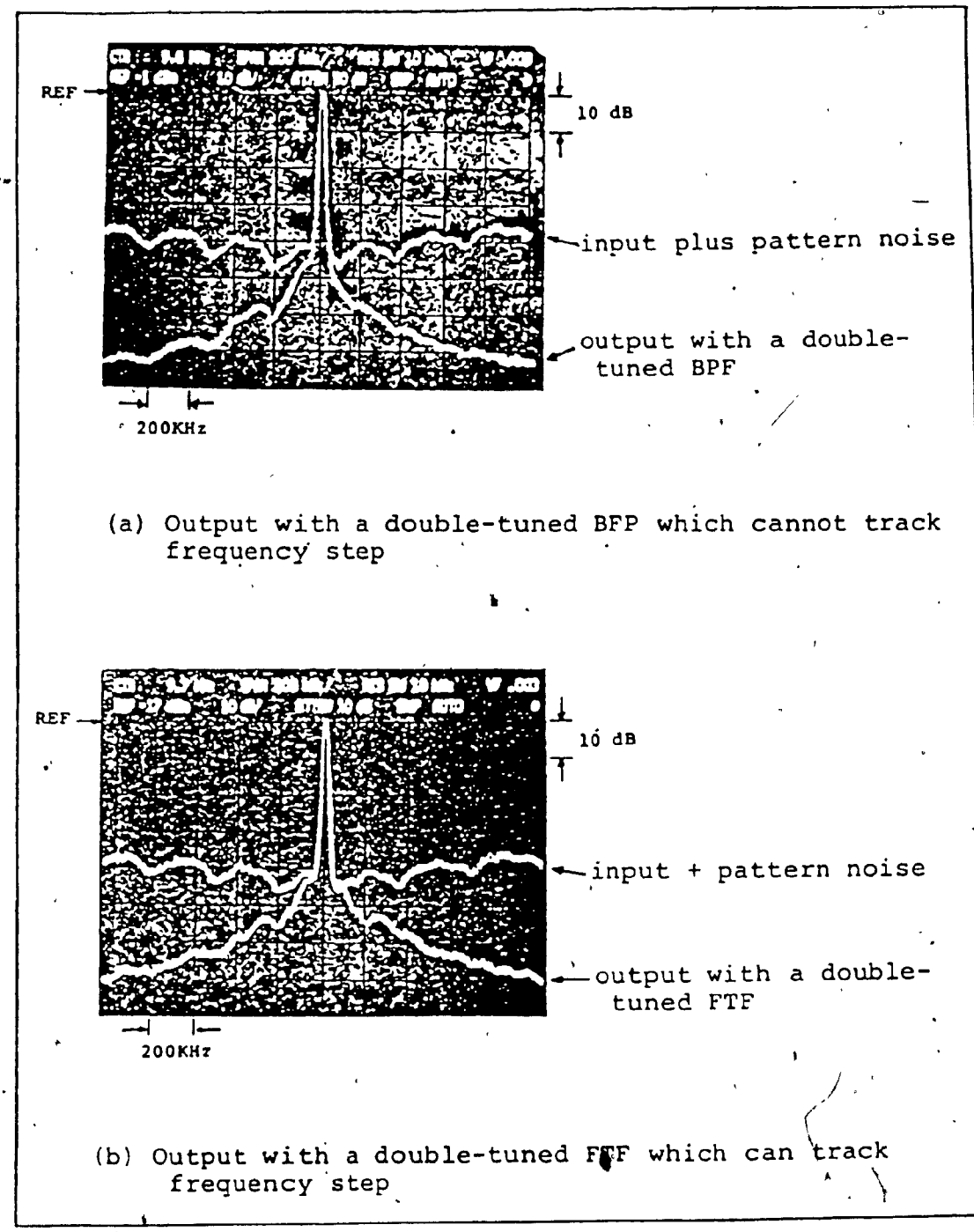

(a) Output with a double-tuned BFP which cannot track frequency step

(b) Output with a double-tuned FTF which can track frequency step

Fig. 7.5: Output of a remodulator using double-tuned FTF

The pattern noise are shown around the recovered carrier and is filtered expectedly by the FTF. Comparing with the outputs of only a single-tuned and a double-tuned BPF, Figs. 7.4a and 7.5a respectively, the output SNR of the FTF has suffered slightly in order to attain the non-existent frequency tracking capability of the BPF's. The performance analysis of FTF in an AWGN environment given in Chapter 5 has indicated that the output SNR degrades because of the nonlinear elements of the FTF. The analysis has also shown that, under the same noise bandwidth of the BPF, the SNR of the double-tuned FTF is no better than that of the single-tuned FTF. The better noise rejection in the experimental double-tuned FTF is due to its 3dB bandwidth being two times narrower than that of the single-tuned FTF. Furthermore, it is experimentally found that close-in noise is more harmful than the far field noise to the error probability of the demodulatior. Figs.7.6a and b show the near-field region of the measured spectra of the recovered carrier signals at the input and output of the double-tuned BPF and double-tuned FTF respectively. If phase and frequency tracking are not essential, the double-tuned BPF having better noise rejection will be desirable. By contrast, slight degradation from close-in noise has to be paid in order to have FTF track the frequency.

In the continuous mode operation, aside from the SNR affecting the performance of the CR circuit, there are two additional factors considered to evaluate the CR perfor-

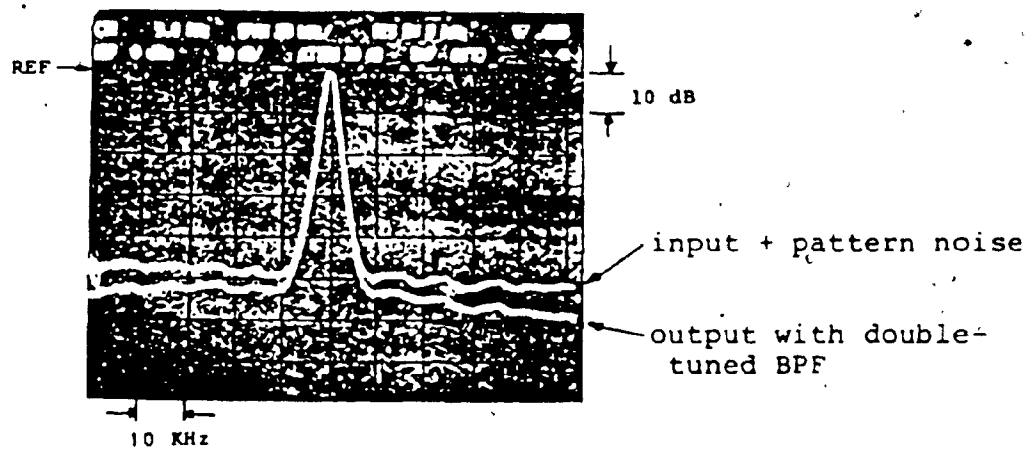

(a) Output with a double-tuned BPF which cannot track frequency step

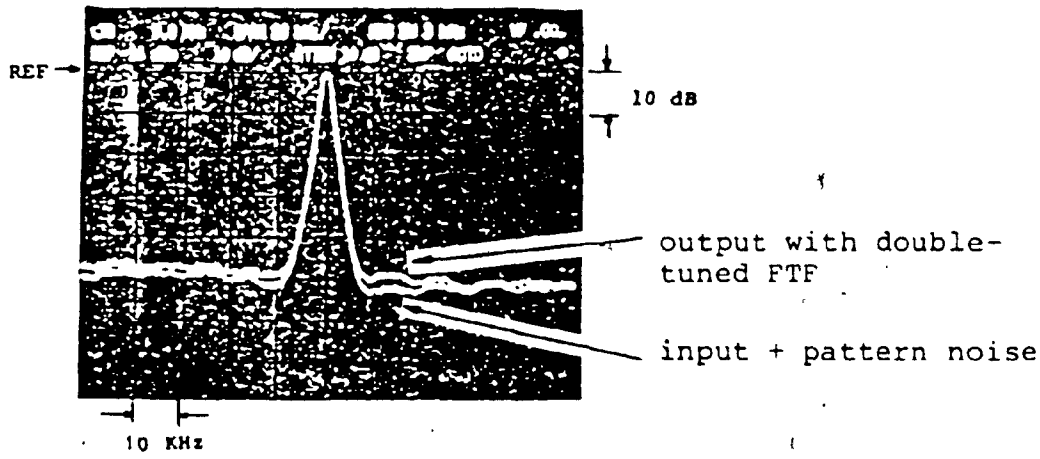

(b) Output with a double-tuned FTF which can track frequency step

Fig. 7.6: Near field of output of a remodulator using double-tuned FTF

mance [6]:

a) static phase error degradation, and

b) phase perturbation due to transient effects.

It is known that these two factors have a tradeoff with the equivalent noise bandwidth of the FTF. In Chapter 3, it is shown that the double-tuned FTF can lock within 10μs given the single-tuned BPF centered at 10MHz with Q=60. After this extreme short acquisition time, the phase perturbation due to the transient becomes negligible. Chapter 4 reveals the fact that FTF has a superior tracking ability. In case of perfectly matched BPF's, there is no steady-state error due to a phase or a frequency offset. Even with mis-matched BPF's, the static phase error is only a few degrees which contribute very minor degradation in the performance of the CR circuit.

In the burst-mode operation, the phase perturbation due to IBI of the FTF is included in the consideration. Without any penalty in the acquisition time, the transient of FTF due to IBI vanishes as fast as FTF operates at zero initial state. The method of quenching [4] is not necessary to improve the acquisition in this case.

Under the consideration of the CR using FTF, FTF can undoubtedly be applied in high-speed operating environment that requires precise tracking and rapid acquisition performance.

The above discussions are reflected in the BER performance of the demodulator. Assuming the demodulator is corrupted by additive white noise only, from Eq.(5.53), the probability of error due to phase jitter θ_j is

$$P_e(\theta_j) = \frac{1}{\sqrt{\pi/\rho}} e^{-\theta_j^2 \rho} \tag{7.3}$$

where ρ is the SNR in the FTF. The value of $\rho \triangleq \beta E_b/N_o$, where E_b is the bit energy and β is a correction factor of the SNR when QPSK modulation is present [21]. β depends on the symbol duration, E_b/N_o, equivalent noise bandwidth of FTF and IF filter preceding the remodulator.

The probability of a symbol error in the QPSK detector is the probability that the in-phase and quadrature noise components cause the resultant vector to cross the boundaries as shown in Fig.7.7.

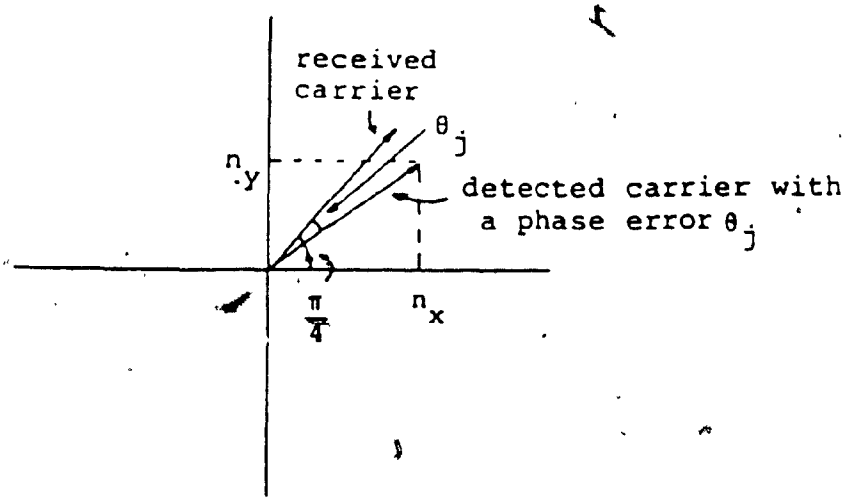

Fig. 7.7: Symbol error boundaries for QPSK

Therefore, a symbol error is caused if

$$n_x > E_s \cos(\frac{\pi+\theta_j}{4})$$

or $$n_y > E_s \sin(\frac{\pi+\theta_j}{4})$$

where symbol energy $E_s = 2E_b$.

The probability of a symbol error is then [21],

$$P_s = \frac{1}{2}E\left[\text{erfc}[\frac{\sqrt{E_s}}{N_o}\cos(\frac{\pi+\theta_j}{4})] + \text{erfc}[\frac{\sqrt{E_s}}{N_o}\sin(\frac{\pi+\theta_j}{4})]\right] \qquad (7.4)$$

where E is the expectation operator and erfc[X] is the complementary error function defined in Eq.(5.56). For low symbol error rate, i.e. $P_s << 1$, then the probability of bit error is

$$P_b \simeq P_s/2 \qquad (7.5)$$

The desired probability of bit error of a QPSK demodulator using FTF is then calculated as

$$P_b = \int_{-\pi}^{\pi} \frac{\exp(-\theta_j^2\rho)}{2\sqrt{\pi/\rho}} \left\{\text{erfc}[\frac{\sqrt{E_s}}{N_o}\cos(\frac{\pi+\theta_j}{4})] + \text{erfc}[\frac{\sqrt{E_s}}{N_o}\sin(\frac{\pi+\theta_j}{4})]\right\} d\theta_j \qquad (7.6)$$

Eq.(7.6) shows the effect of the carrier phase jitter of the FTF on the BER performance of the demodulator. Experimentally, the BER of the demodulator with FTF operating in continuous mode is measured. The results are compared with the

BER due to a BPF alone (Figs.7.8 and 7.9). It is noted that, in both single-tuned and double-tuned FTF, the extra SNR required to achieve tracking ability of the FTF is reflected in BER performance. With narrower bandwidth, the BER performance is improved in double-tuned FTF. As shown in Fig.7.10, the more filters in cascade, the more improvement in the BER. This is also valid when higher order FTF is employed but minor degradation will be expected. Moreover, it is known that longer acquisition time will result from narrower bandwidth. This is shown in the BER measured in burst-mode operation (Fig.7.11). The BER of the four single-tuned BPF's in cascade diverges because the narrow bandwidth 71KHz of this BPF requires more than 20μs, the maximum time for synchronization, to lock up. The error increases as a result of the increased phase error of the recovered carrier. Similarly, when the BER using FTF in burst-mode is measured, a similar performance as that of the continuous-mode operation is obtained with a 0.5dB degradation. This degradation may be assoicated with the nonlinearity of the remodulator and with the SNR transient introduced by IBI. Nonetheless, hangup phenomenon is not found during the measurement although the FTF locks up within 20μs.

Overall, FTF applied in the tuned-filter synchronizer satisfies the high-speed operating requirement of TDMA and QPSK digital systems. Its superior tracking and rapid acquisition abilities lend itself to be a good candidate for

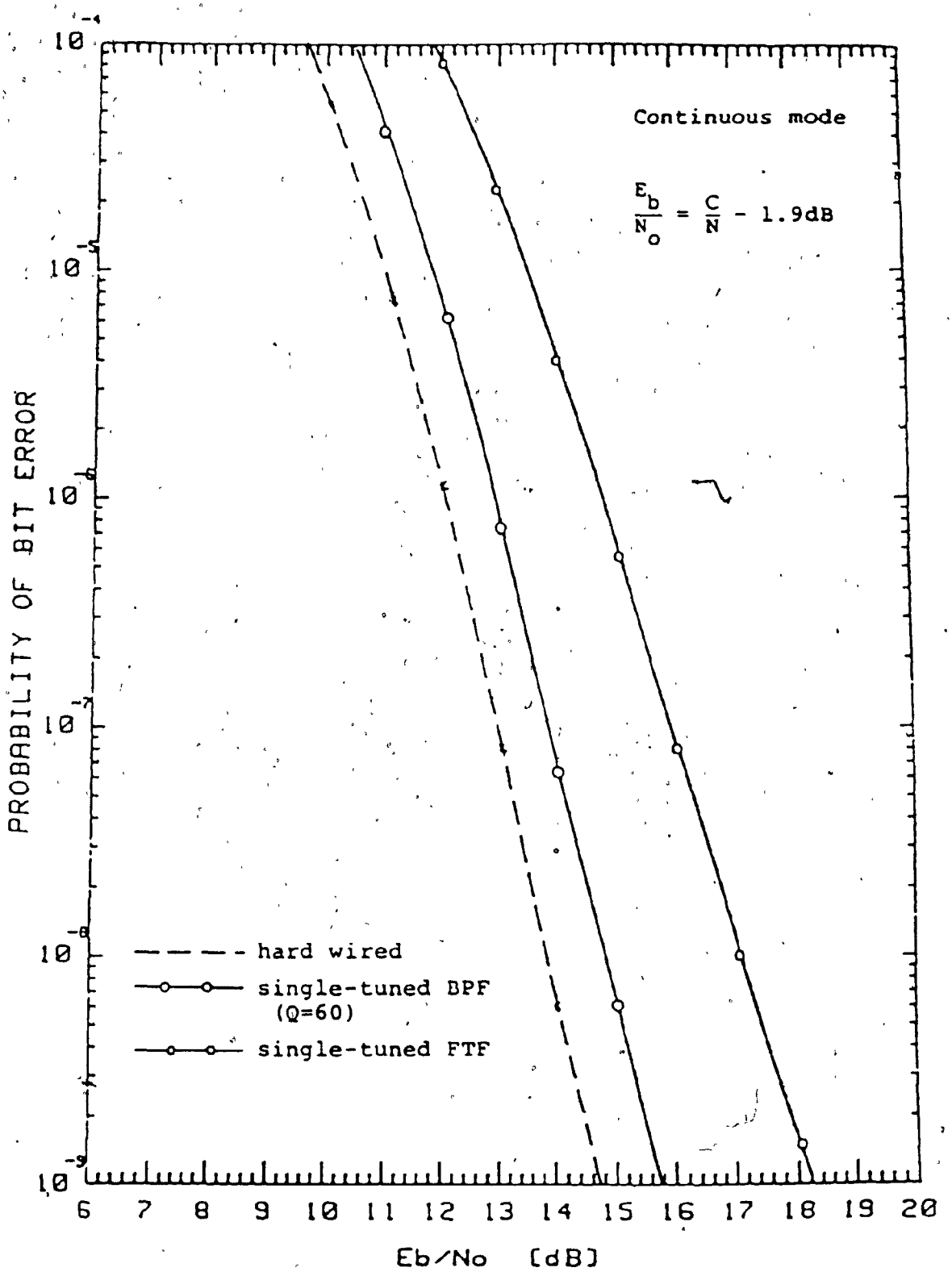

Fig. 7.8: BER of a demodulator using single-tuned FTF for carrier recovery (continuous mode)

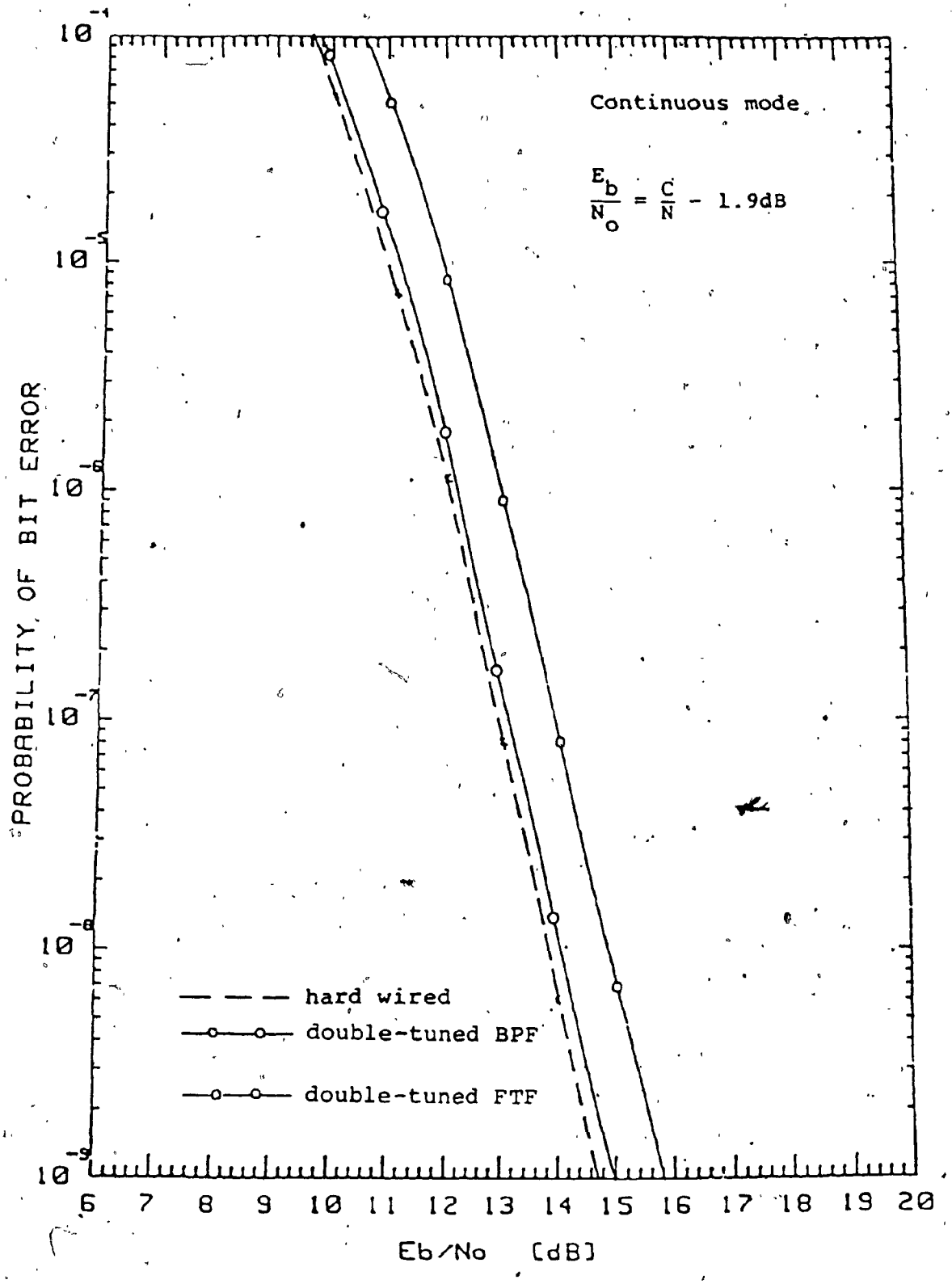

Fig. 7.9: BER of a demodulator using double-tuned FTF for carrier recovery (continuous mode)

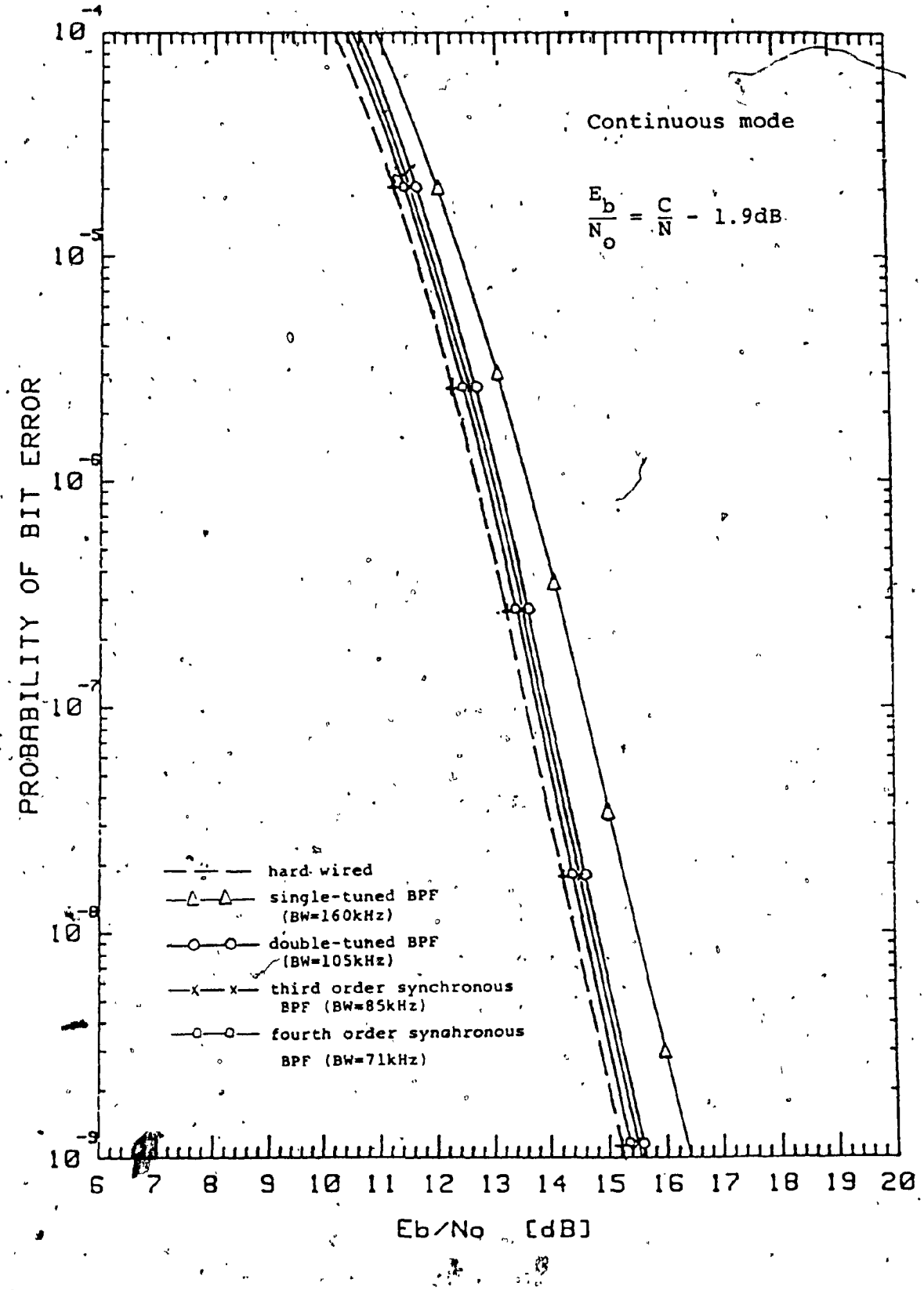

Fig. 7.10: Comparison of BER of a demodulator using synchronously-tuned BPF's (continuous mode)

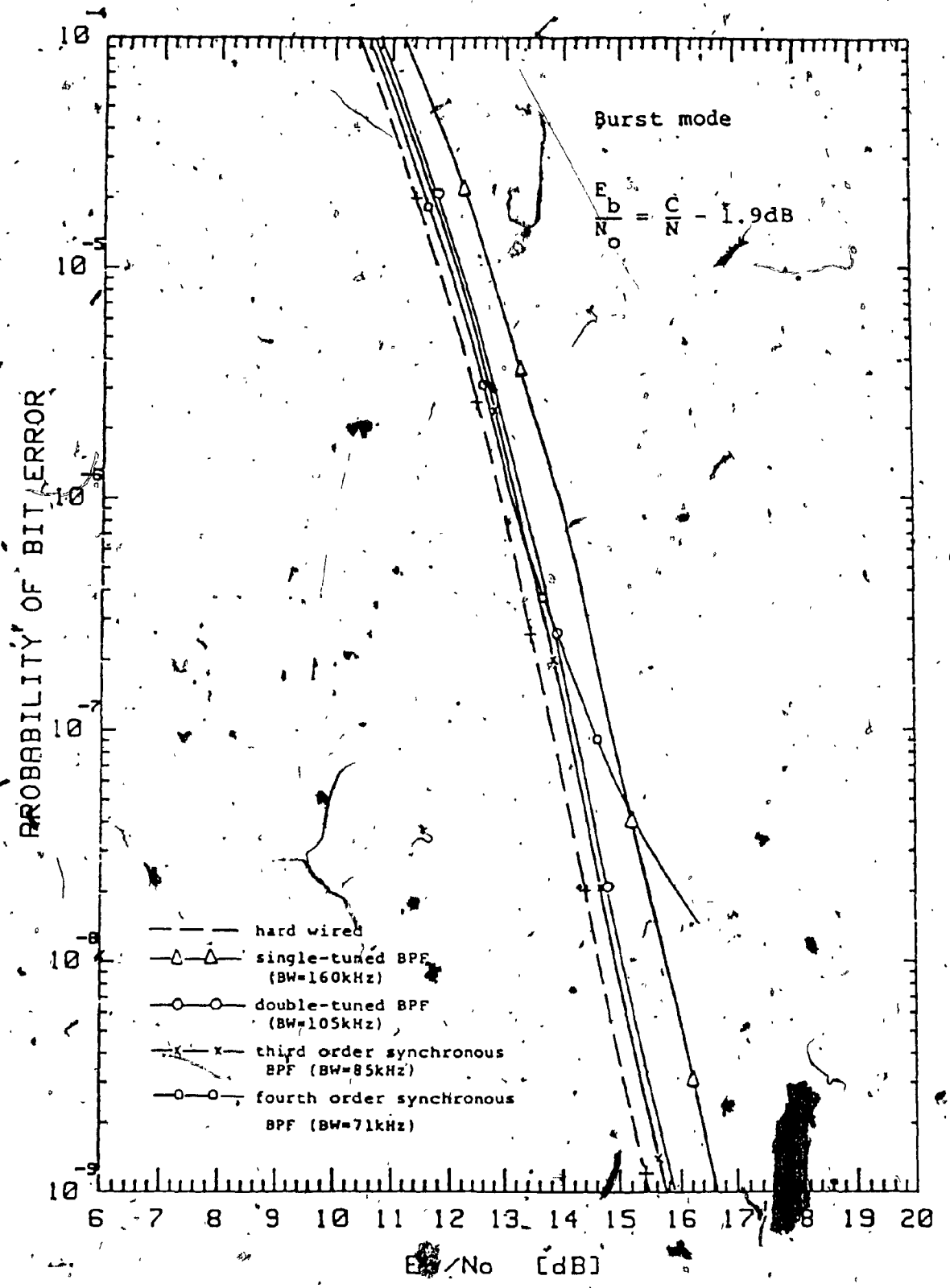

Fig. 7.11: Comparison of BER of a demodulator using synchronously-tuned BPF's (burst mode)

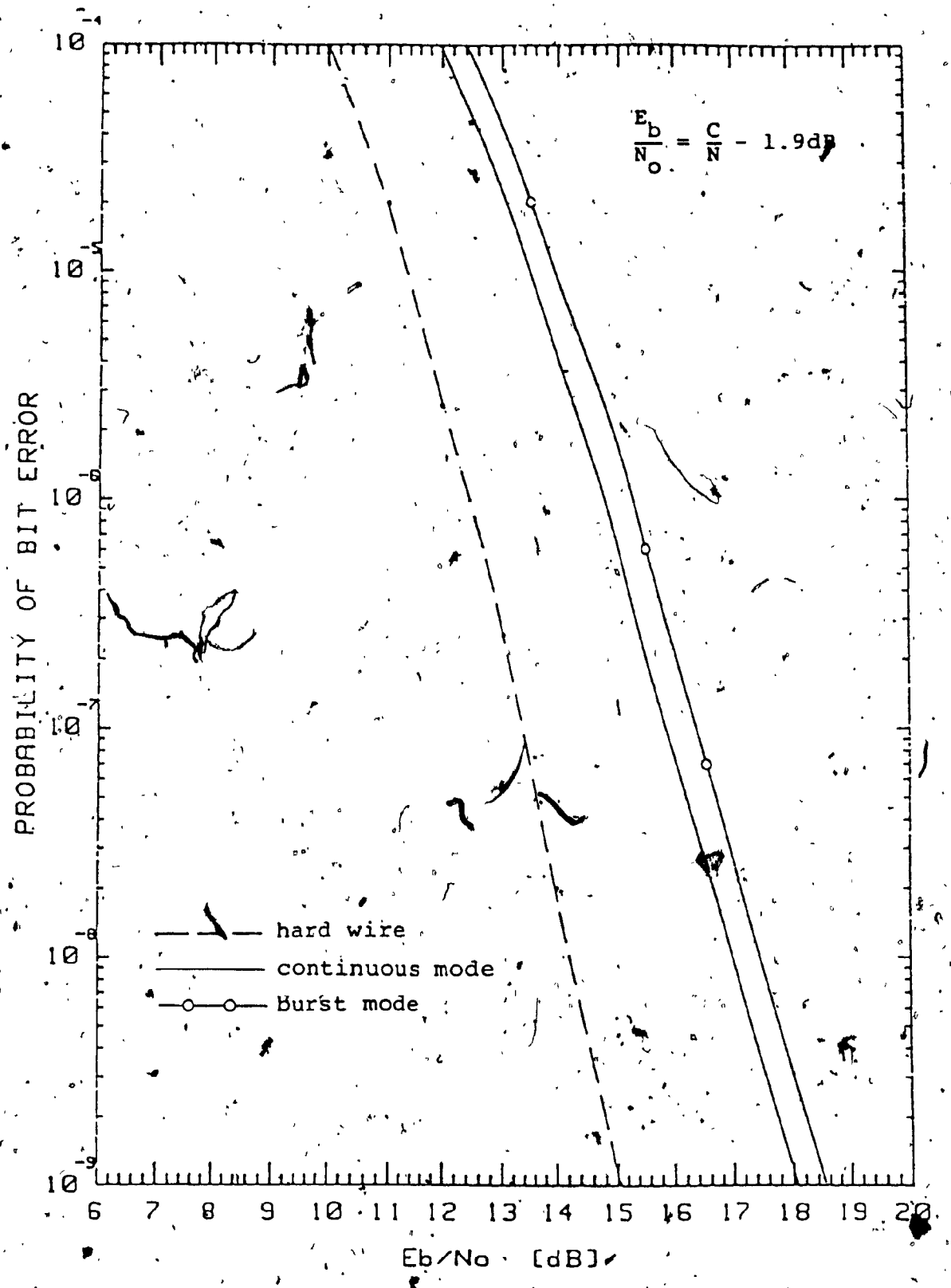

Fig. 7.12: BER of a demodulator using single-tuned FTF (burst mode)

this application. Its advantageous hangup-free characteristics is important for reliable and high capacity communication systems.

CHAPTER 8

CONCLUSIONS AND SUGGESTIONS FOR FURTHER STUDY

8.1 Conclusions

A tracking bandpass filter using a novel feedforward compensation scheme has been introduced and studied. From its lowpass equivalent model, this feedforward tracking filter (FTF) using synchronous BPF's is shown to have the characteristics of the phase-locked loop (PLL) although the feedback correction is not adopted. Generally, the tracking ability of the FTF is not restricted by any particular phase response characteristics of the BPF used. A comparative study has shown that synchronous type of BPF in the continuous FTF while the symmetrical transversal filters with the apodized weight coefficients in the discrete FTF gives the fastest acquisition. For continuous FTF, the rapid and reliable acquisition is achieved in six times of the time constant of a single-tuned BPF from zero or non-zero state. In the case of discrete FTF, the acquisition time is less than two times of the propagation delay of a transversal filter. The comparison further shows that, under the same equivalent noise bandwidth, the double-tuned FTF has the best acquisition performance among the continuous and discrete FTF's considered. Since the baseband model of the FTF is strictly linear, the feedforward compensation scheme is shown to be capable of solving the hangup problem. The attractive tracking abilities of phase step

and frequency step with zero steady-state error are also found in both continuous and discrete FTF, however, with limitation of tracking frequency velocity and frequency acceleration inputs.

The nonlinear behaviour of the FTF in the AWGN environment has been investigated. The spectral analysis of the nonlinear behaviour shows that the output contains a mixture of signal intermodulation product and noise product terms which is not linearly dependent on the input signal and input noise. It is demonstrated that a penalty of 6 to 7 dB of SNR is imposed for attaining the tracking ability in the feedforward scheme, in both discrete and continuous FTF. As far as phase noise is concerned, same phase jitter performace of the PLL is obtained. Cycle skipping phenomenon is also found in the FTF, which is dependent mainly upon the output SNR of the doubler.

Compared to other tracking bandpass filters using feedback correction scheme, FTF is proven to be unconditionally stable. In addition, without the negative feedback, FTF only needs BPF of unit gain. Moreover, its rapid acquisition is not hindered by the hangup phenomenon.

8.2 Suggestions for further study

Although the acquistion and tracking performance and

the noise performance of the FTF were extensively studied, there are certainly some other interesting aspects which were not covered. The following tasks are suggested for further investigation:

1) Analysis of the nonlinear behaviour of the FTF with the pattern noise: The results of this analysis will be desirable when FTF is applied into a CR circuit. The effect of the phase noise on the BER performance can be predicted more accurately.

2) Characterization of the cycle skipping in the FTF: The source and the properties of this phenomenon in the FTF are recommended for further investigation. Method of reducing the cycle skipping event will be beneficial.

3) Study of the Feedforward Phase Compensator: An alternative feedforward compensation scheme depicted in Fig. 8.1 has been shown to have similar acquisition and tracking performance as that of FTF [30]. Analysis of its performance in the presence of noise is interesting and desirable.

4) Study of FTF with modulated input signals: The input is assumed to be a pure sinusoidal signal with random phase throughout the studies. It is interesting to understand the nonlinear operation of the FTF on the modulated inputs.

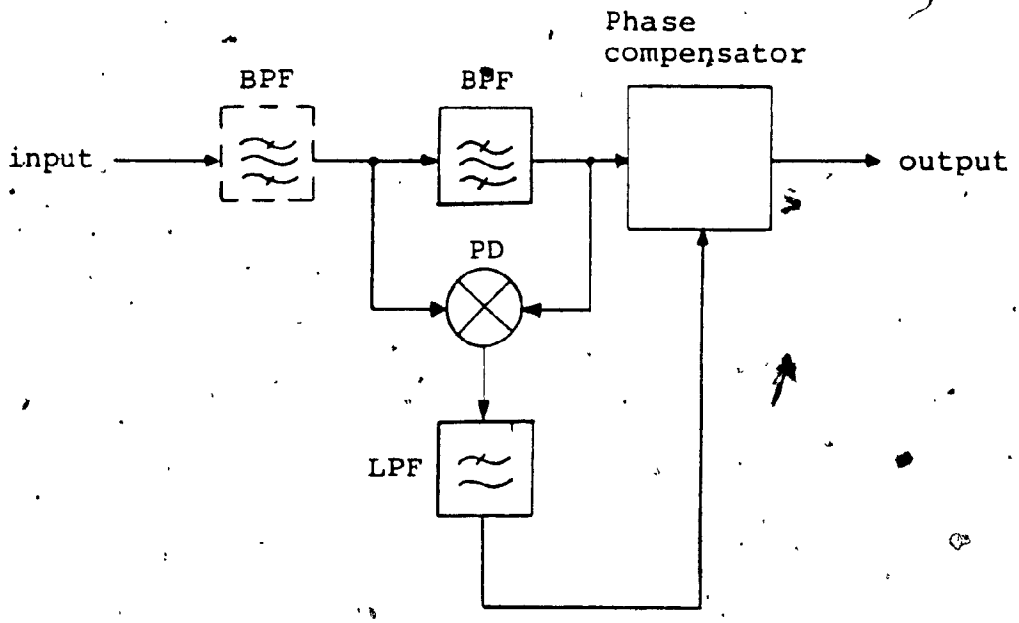

Fig. 8.1: Feedforward phase compensator

REFERENCES

[1] F.M. Gardner, Phaselock Technique, 2nd ed., John Wiley and Sons Inc., 1979.

[2] A. Blanchard, Phase-Locked Loop, Application to Coherent Receiver Design, John Wiley and Sons Inc., 1976.

[3] F.M. Gardner, "Hangup in Phase-Lock Loops", IEEE Trans. on Comm., Vol. COM-25, pp. 1210-1214, Oct. 1977.

[4] F.M. Gardner, Carrier and Clock Synchronization for TDMA Digital Communications, Eur. Space Agency Rep. ESA TM-169 (ESTEC), Dec., 1976.

[5] D.K. Frederick and A.B. Carlson, Linear Systems in Communication and Control, John Wiley and Sons Inc., 1971.

[6] C.J. Wolejsza and D. Chakraborty, "TDMA Modem Design Criteria", COMSAT Tech. Rev., Vol.9, No.2A, pp. 413-444 Fall 1979.

[7] H. Kurihera, T. Katon, H. Komizo and H. Nakamura, "Carrier Recovery with Low Cycle Skipping Rate for CPSK/TDMA Systems", 5th Int'l. Conference on Digital Satellite Comm., Genoa, Italy, pp.319-324 23-26 Mar., 1981.

[8] P.H. Lewis and W.E. Weingarten, "A Comparison of Second, Third and Fourth Order Phase-Locked Loops", IEEE Trans. on AES, Vol. AES-3, No.4, pp. 720-727, July 1967.

[9] C.H. Feng, S.X. Xiong and L.D. Ge, "Some Discussions on

Fourth Order Phase-Locked Loops in Narrow Band Tracking", Vol.3, 4th World Telecom., Forum, Geneva, Oct.29 to Nov.1, 1983.

[10] A.J. Viterbi, Principle of Coherent Communications, McGraw-Hill, 1966.

[11] D. Middleton, An Introduction to Statistical Communication Theory, McGraw-Hill, 1960.

[12] W.B. Davenport,Jr. and W.L. Root, An Introduction to the Theory of Random Signals and Noise, McGraw-Hill, 1958.

[13] A. Papoulis, Probability, Random Variables, and Stochastic Processes, McGraw-Hill, 1965.

[14] G. Ascheid and H. Meyr, "Cycle Slips in Phase-Locked Loops: A Tutorial Survey", IEEE Trans. on Comm., Vol. COM-30, No.10, pp. 2228-2241, Oct. 1982.

[15] D.T. Hess, "Cycle Slipping in a First-Order Phase-Locked Loop", IEEE Trans. on Comm. Tech., Vol. COM-16, No.2. April 1968, pp. 255-260.

[16] E. Volterra and E.C. Zachmanoglou, Dynamics of Vibration, Chapter 5, C.E. Merrill Books, Inc., 1965.

[17] M. Asahara, N. Toyonaga, S. Sasaki and T. Miyo, "Analysis of Carrier Recovery Adopting a Narrow Band Passive Filter with AFC loop", Proc. of Third Int'l. Conference on Digital Satellite Comm., Kyoto, Japan, 11-13 Nov., 1975, pp. 99-104.

[18] C.F. Weaver, "An Analysis of A Fast Carrier Recovery System for TDMA", CRL Internal Report Series No.CRL-88, McMaster University, Hamilton, Ontario, Nov., 1981.

[19] T. Le-Ngoc and M. Roux, "Comparative Performance of Four-Phase Carrier Synchronizers in the presence of Static Phase Error", Int'l Conference on Energy and Communication, Montreal, Canada, Oct., 1984.

[20] T. Le-Ngoc, "A Class of Power and Bandwidth Efficient Transmission Techniques for Digital Radio Communications Systems", Ph.D. thesis, University of Ottawa, 1983.

[21] J.J. Spilker, Digital Communications by Satellite, Prentice-Hall Inc., 1977.

[22] R.W. Sanneman and J.R. Rowbotham, "Unlock Characteristics of the Optimum Type II Phase-Locked Loop", IEEE Trans. on Aerospace and Navigational Eletronics, ANE-11, Mar. 1984, pp. 15-24.

[23] B. Noble and J.W. Daniel, Applied Linear Algebra, 2nd ed., Prentice-Hall Inc., 1977.

[24] J.G. Proakis, Digital Communication, McGraw-Hill Inc., 1983.

[25] V.K. Bhargava, D. Haccoun, R. Matyas and N. Nuspl, Digital Communications by Satellite, John Wiley and Sons Inc., 1981.

[26] H. Matthew, Surface Wave Filters, John Wiley and Sons Inc., 1977.

[27] A. Antoniou, Digital Filters: Analysis and Design, McGraw-Hill Inc., 1979.

[28] K. Steiglitz, An Introduction to Discrete Systems, John Wiley and Sons Inc., 1974.

[29] A.B. Williams, Electronic Filter Design Handbook, McGraw-Hill Book Co., 1981.

[30] T. Le-Ngoc, "A New Feedforward Filter for Fast Recovery System", submitted to ISCAS 1985.

APPENDIX A

STATISTICS OF NARROWBAND NOISE PROCESSES $n_1(t)$ and $n_2(t)$ of FTF

This appendix derives the statistical properties of two narrowband processed, $n_1(t)$ and $n_2(t)$, of FTF defined in Chapter 5. The mean and variance functions of the noise processes are evaluated in section A.1. Section A.2 describes the properties of the cross-correlation function of the two processes. Section A.3 computes the higher order joint moments of the noise processes in terms of the first and second moments obtained in sections A.1 and A.2.

A.1 Mean and variance

Repeating the definition of $n_1(t)$ and $n_2(t)$,

$$n_1(t) = \int_{-\infty}^{\infty} f(\vartheta)n(t-\vartheta)d\vartheta \qquad \text{(A.1a)}$$

$$n_2(t) = \int_{-\infty}^{\infty} c(\vartheta)n(t-\vartheta)d\vartheta \qquad \text{(A.1b)}$$

where $f(t) = \mathcal{F}^{-1}[F(f)]$ and $c(t) = \mathcal{F}^{-1}[F^2(f)]$.

$\mathcal{F}^{-1}[X]$ denotes the inverse Fourier transform of function X. $n_1(t)$ and $n_2(t)$ are wide-sense stationary Gaussian random processes because the input noise process n(t) is a wide-sense stationary process, and the BPF's are linear time invariant systems. To specific a Gaussian random process, only the mean and the autocovariance functions are needed to be determined. Following is the derivation of these two

functions.

The mean function of the process $n_1(t)$ is given by

$$E[n_1(t)] = \int_{-\infty}^{\infty} f(\vartheta)E[n(t-\vartheta)]d\vartheta = 0 \qquad (A.2)$$

since $E[n(t)] = 0$. Similarly, $E[n_2(t)] = 0$.

From Eq.(A.2), the autocovariance of $n_1(t)$ is then found as

$$\mu_1(t_1,t_2) = E[n_1(t_1),n_1(t_2)] = R_{n_1n_1}(\epsilon) \qquad (A.3)$$

where $R_{n_1n_1}(\epsilon)$ is the autocorrelation function of $n_1(t)$. If $\epsilon=0$, the autocovariance function becomes the variance function of $n_1(t)$, i.e.

$$\begin{aligned} Var[n_1(t)] &= E[n_1^2(t)] = R_{n_1n_1}(0) \\ &= \int_{-\infty}^{\infty} S_{n_1n_1}(f)df = \int_{-\infty}^{\infty} |F(f)|^2 N_o df \\ &= N_o B_1 \end{aligned} \qquad (A.4)$$

where

$$B_1 = \int_0^{\infty} |F(f)|^2 df \qquad (A.5)$$

which is known as the one-sided noise equivalent bandwidth of the BPF1, $F(f)$.

Using the same approach, the autocovariance function and variance of $n_2(t)$ is found respectively as

$$\mu_2(t_1,t_2) = R_{n_2n_2}(\epsilon) \qquad (A.6)$$

$$Var[n_2(t)] = N_o B_2 \qquad (A.7)$$

where

$$B_2 = \int_0^\infty [|F(f)|^2]^2 df \qquad (A.8)$$

which is the one-sided noise equivalent bandwidth of the BPF1 and BPF2 in cascade, C(f). Usually $B_2 < B_1$, the equality holds when the BPF's are ideal.

A.2 Cross-correlation function

The cross-correlation of $n_1(t)$ and $n_2(t)$ is defined as [11,13]

$$R_{n_1 n_2}(\epsilon) = E[n_1(t)n_2(t+\epsilon)]$$

$$= \int_{-\infty}^{\infty}\int_{-\infty}^{\infty} f(\upsilon)c(\xi)E[n(t-\upsilon)n(t+\epsilon-\xi)]d\upsilon d\xi \qquad (A.9)$$

where

$$E[n(t-\upsilon)n(t+\epsilon-\xi)] = R_{nn}(\epsilon+\upsilon-\xi) = \frac{N_o}{2}\delta(\epsilon+\upsilon-\xi) \qquad (A.10)$$

Therefore, Eq.(A.9) shows that $n_1(t)$ $n_2(t)$ are correlated because they are derived from the same source. Moreover, it can be shown that

$$R_{n_1 n_2}(\epsilon) = R_{n_1 n_2}(-\epsilon) \qquad (A.11)$$

Taking the Fourier transform of Eq.(A.9), the cross-spectral density can be obtained as [11]

$$S_{n_1 n_2}(f) = F(jw)C(jw)^* S_{nn}(f) \qquad (A.12a)$$

$$S_{n_2 n_1}(f) = F(jw)^* C(jw) S_{nn}(f) \qquad (A.12b)$$

where $j=\sqrt{-1}$ and $S_{nn}(f)$ is the spectral density of n(t).

Substituting $S_{nn}(f)$ and $C(jw)$ into Eqs.(A.1), it yields

$$S_{n_1n_2}(f) = \frac{N_o}{2}|F(f)|^2F(f)^* = \frac{N_o}{2}|F(f)|^3e^{-j\theta(f)} \quad (A.13a)$$

$$S_{n_2n_1}(f) = \frac{N_o}{2}|F(f)|^2F(f) = \frac{N_o}{2}|F(f)|^3e^{j\theta(f)} \quad (A.13b)$$

if $F(f) = |F(f)|e^{j\theta(f)}$.

Eqs.(A.13), representing the cross-spectral density of $n_1(t)$ and $n_2(t)$, is a complex quantity and depends on the BPF's in use. It can be noted that $S_{n_1n_2}(f)$ and $S_{n_2n_1}(f)$ have the same modulus but their phase is opposite in sign. Since f(t) is real, F(f) is an even function of f and $\theta(f)$ is an odd function. If we define the real and imaginary parts of $S_{n_1n_2}(f)$ respectively as

$$S^{real}_{n_1n_2}(f) = \frac{1}{2}[S_{n_1n_2}(f) + S_{n_1n_2}(f)^*] \quad (A.14a)$$

$$S^{imag}_{n_1n_2}(f) = \frac{1}{2j}[S_{n_1n_2}(f) - S_{n_1n_2}(f)^*] \quad (A.14b)$$

then they can be expressed as

$$S^{real}_{n_1n_2}(f) = \frac{N_o}{2}|F(f)|^3\cos\theta(f) \quad (A.15a)$$

$$S^{imag}_{n_1n_2}(f) = -\frac{N_o}{2}|F(f)|^3\sin\theta(f) \quad (A.15b)$$

Therefore, $S^{real}_{n_1n_2}(f)$ is an even function of f and $S^{imag}_{n_1n_2}(f)$ is an odd one. The total cross-correlation power is

$$R_{n_1n_2}(0) = R_{n_2n_1}(0) = \int_{-\infty}^{\infty} S_{n_1n_2}(f)df$$

$$= \int_{-\infty}^{\infty} S^{real}_{n_1n_2}(f)df = N_oB_c \quad (A.16)$$

where

$$B_c = \int_0^{\infty} |F(f)|^3\cos\theta(f)df \quad (A.17)$$

as the one-sided equivalent noise-correlation bandwidth.

The next step is to find the convolution of $S_{n_1n_2}(f)$ and $S_{n_2n_1}(f)$, i.e.

$$S_{n_1n_2}(f)*S_{n_2n_1}(f) = S_{n_1n_2}(f)*S_{n_1n_2}(f)^*$$

$$= \int_{-\infty}^{\infty}[S^{real}_{n_1n_2}(\lambda)-jS^{imag}_{n_1n_2}(\lambda)]\,[S^{real}_{n_1n_2}(f-\lambda)+jS^{imag}_{n_1n_2}(f-\lambda)]\,d\lambda \quad (A.18)$$

Since $S^{real}_{n_1n_2}(f)$ is even and $S^{imag}_{n_1n_2}(f)$ is odd, the convolution is

$$S_{n_1n_2}(f)*S_{n_2n_1}(f) = S^{real}_{n_1n_2}(f)*S^{real}_{n_1n_2}(f)+S^{imag}_{n_1n_2}(f)*S^{imag}_{n_1n_2}(f) \quad (A.19)$$

which is a real quantity.

A.3 Moments of multivariate Gaussian random variables

In Chapter 5, the calculation of the noise power involves the high order moment function of the Gaussian noise processes. In general, the high order moment function is found by taking the expectation of the n random variables considered. Therefore, using the characteristics function of the n random variables, the expectation of the n random variables can be shown as [13]

$$E[x_1,x_2,\ldots,x_n] = j^{2n}\,\frac{\partial^n\psi(v_1,jv_2,\ldots,jv_n)}{\partial v_1,\partial v_2,\ldots,\partial v_n} \quad (A.20)$$

where $\psi(jv_1,jv_2,\ldots,jv_n)$ is the characteristic function of the n random variables $x_1,x_2,\ldots,x_n$. For Gaussian random variables, the characteristic function is given as

$$\psi(jv_1, jv_2, \ldots, jv_n) = \exp\left[-\frac{1}{2}\sum_{k=1}^{n}\sum_{\ell=1}^{n}\lambda_{k\ell}v_k v_\ell\right] \qquad (A.21)$$

where $\lambda_{k\ell}=\lambda_{\ell k}$ is the covariance of random variables x_k and x_ℓ. In our application, n=2,3,4,5 and 6 are of interest and these results are summarized in Table A.1.

n	$E[x_1x_2\ldots x_n]$
2	$E[x_1x_2]$
3	0
4	$E[x_1x_2]E[x_3x_4] + E[x_1x_3]E[x_2x_4] + E[x_1x_4]E[x_2x_3]$
5	0
6	$E[x_1x_4]E[x_2x_3]E[x_3x_6] + E[x_1x_3]E[x_2x_4]E[x_5x_6]$ $+ E[x_1x_2]E[x_3x_4]E[x_5x_6] + E[x_1x_6]E[x_2x_5]E[x_3x_4]$ $+ E[x_1x_5]E[x_2x_6]E[x_3x_4] + E[x_1x_6]E[x_2x_4]E[x_3x_5]$ $+ E[x_1x_4]E[x_2x_6]E[x_3x_5] + E[x_1x_5]E[x_2x_4]E[x_3x_6]$ $+ E[x_1x_3]E[x_2x_6]E[x_4x_5] + E[x_1x_2]E[x_2x_6]E[x_4x_5]$ $+ E[x_1x_5]E[x_2x_3]E[x_4x_6] + E[x_1x_3]E[x_2x_5]E[x_4x_6]$ $+ E[x_1x_2]E[x_3x_5]E[x_4x_6]$

Table A.1: Moments of multivariate Gaussian random variables

APPENDIX B

EVALUATION OF CERTAIN CONVOLUTION INTERGRALS

In this appendix, four particular convolution integrals are evaluated. These four convolution integrals are important in the spectral analysis of the output of the FTF.

B.1 Convolution of two rectangular pulses

$$u(t) = \begin{cases} A_1 & , \ 0 < t < T \\ 0 & , \ \text{otherwise} \end{cases} \tag{B.1a}$$

and

$$v(t) = \begin{cases} A_2 & , \ 0 < t < T \\ 0 & , \ \text{otherwise} \end{cases} \tag{B.1b}$$

Eqs.(B.1) represent two rectangular pulses with the same period. The result of the convolution of these two pulses is a triangular pulse of twice the period of u(t) as shown in Eq.(B.2). and Fig.B.1.

$$c_1(t) = u*v = \int_{-\infty}^{\infty} u(\xi)v(t-\xi)d\xi$$

$$= \begin{cases} A_1A_2t & , \ 0 < t < T \\ A_1A_2(2T-t) & , \ T < t < 2T \\ 0 & , \ \text{otherwise} \end{cases} \tag{B.2}$$

B.2 Convolution of a rectangular pulse with a triangular pulse

Using the triangular pulse u(t) in Eq.(B.2) and the

rectangular pulse in Eq.(B.3) which is

$$v(t) = \begin{cases} A_3 & , \ 0 < t < T \\ 0 & , \ \text{otherwise} \end{cases} \tag{B.3}$$

the result of the convolution is found as

$$c_2(t) = \begin{cases} \frac{1}{2}A_1A_2A_3t^2 & , \ 0<t\leq T \\ -A_1A_2A_3(t-\frac{3T}{2})^2+\frac{3}{4}A_1A_2A_3T^2 & , \ T<t\leq 2T \\ \frac{1}{2}A_1A_2A_3(t-3T)^2 & , \ 2T<t\leq 3T \end{cases} \tag{B.4}$$

This result, shown in Fig.B.2, is symmetrical about t=3T/2. Between the first period $0<t\leq T$, the result is a parabola with base at (0,0). An inverted parabola with the base at $(3T/2, \ 3A_1A_2A_3T^2/4)$ is found within the period $T<t\leq 2T$. The parabola at the third period $2T<t\leq 3T$ is a mirror image of the first period. The overall period of the $c_2(t)$ is three times as that of v(t).

B.3 Convolution of a truncated sinusoidal pulse with a rectangular pulse

In this case, the truncated sinusoidal pulse is defined as

$$u(t) = \begin{cases} A_1\cos(bt) & , \ -\frac{T}{2}\leq t\leq \frac{T}{2} \\ 0 & , \ \text{otherwise} \end{cases} \tag{B.5}$$

where b is a constant, and the rectangular pulse is

$$v(t) = \begin{cases} A_2 & , \ -\frac{T}{2}\leq t\leq \frac{T}{2} \\ 0 & , \ \text{otherwise} \end{cases} \tag{B.6}$$

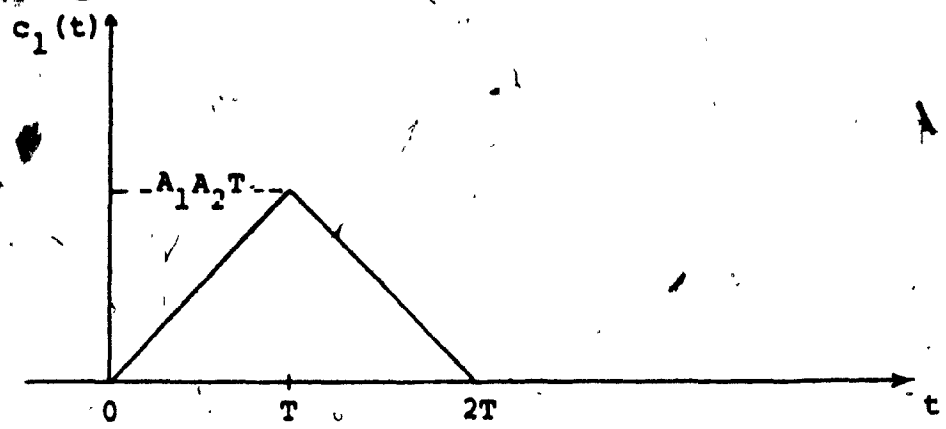

Fig. B.1: Resuls of convolution of two rectangular pulse

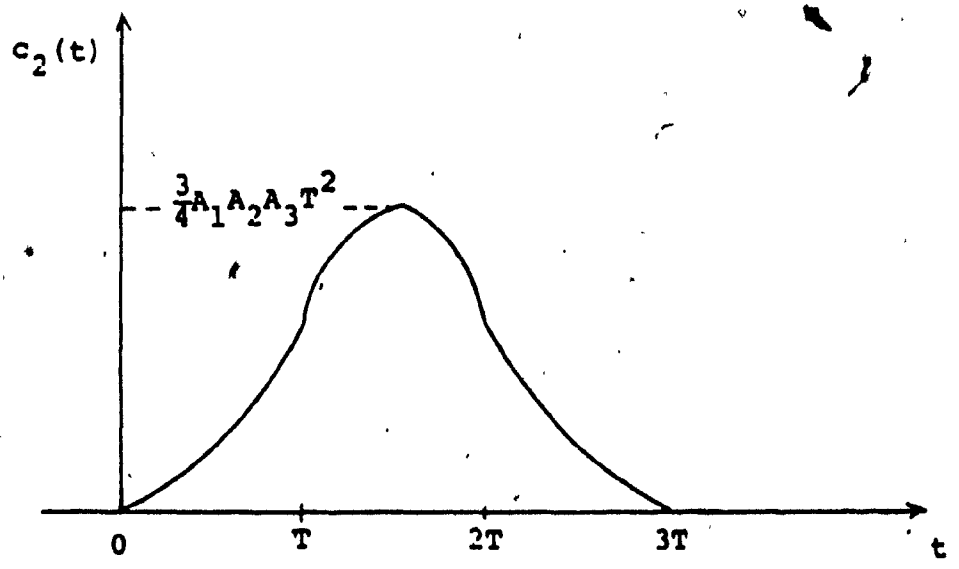

Fig. B.2: Result of convolution of a rectangular pluse with a triangular pulse

Convolving u(t) and v(t) in Eq.(B.5) and (B.6) respectively, we obtain

$$c_3(t) = \frac{A_1A_2}{b}[\sin b(\frac{T}{2} - |t|) + \sin\frac{bT}{2}] \quad ,0 < |t| < T \qquad (B.7)$$

The convolution result of Eq.(B.7) shows that it is symmetrical about 0, and its period is twice as wide as the period of the v(t) in Eq.(B.6). The shape of the results is determined by the value of b.

B.4 Convolution of two truncated sinusoidal pulses

Two cases of truncated sinusoidal pulses are considered. The first case is the pulse u(t) defined by Eq.(B.5) and the other pulse is given by Eq.(B.8).

$$v(t) = \begin{cases} A_1 \sin(bt) & , -\frac{T}{2} < t < \frac{T}{2} \\ 0 & , \text{otherwise} \end{cases} \qquad (B.8)$$

The result of the convolution of the pulse with itself is evaluated respectively as

$$c_4(t) = \begin{cases} \frac{A_1^2}{2}\{\frac{1}{b}\sin[b(T-|t|)] + (T-|t|)\cos(bt)\}, & -T<t<T \\ 0 \quad , \text{ otherwise} \end{cases} \qquad (B.9)$$

and

$$c_5(t) = \begin{cases} \frac{A_1^2}{2}\{\frac{1}{b}\sin[b(T-|t|)] - (T-|t|)\cos(bt)\}, & -T<t<T \\ 0 \quad , \text{ otherwise} \end{cases} \qquad (B.10)$$

The sum of $c_4(t)$ and $c_5(t)$ gives

$$c_6(t) = \begin{cases} \frac{A_1^2}{2}\left\{\frac{1}{b}\sin[b(T-|t|)]\right\} & , -T < t < T \\ 0 \quad , \quad \text{otherwise} \end{cases} \qquad (B.11)$$

which is also a sinusoidal pulse and its shape is dependent on the parameter b. Again, the period of the convolution result is twice as that of the individual u(t) and v(t).

APPENDIX C

CHARACTERISTICS OF SYNCHRONOUSLY-TUNED AND SAW BPF'S

C.1 Characteristics of single-tuned and synchronously-tuned BPF's

C.1.1 Parallel resonance single-tuned BPF

A single-tuned or first-order BPF can be realized by series or parallel LCR circuit. In the experiment, a parallel LCR circuit shown in Fig.C.1 is used.

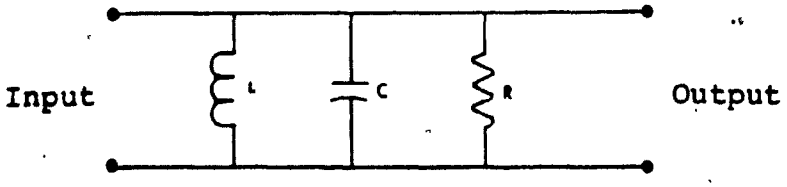

Fig.C.1: Parallel LCR configuration of single-tuned BPF

This circuit is a second order system with transfer function

$$F(jw) = \frac{j\frac{ww_o}{Q}}{w_o^2 + j\frac{ww_o}{Q} - w^2} \qquad (C.1)$$

where the center frequency is

$$w_o = 1/\sqrt{LC} \qquad (C.2)$$

and the quality factor is

$$Q = R\sqrt{C/L} \qquad (C.3)$$

It can be shown that the bandwidth of a single-tuned BPF is

$$BW_{3dB} = w_o/Q \tag{C.4}$$

and the one-sided equivalent noise bandwidth is

$$B_N = \frac{\pi}{2} BW_{3dB} \tag{C.5}$$

For high Q case (Q>5), Eq.(C.1) is approximated as

$$F(jw) = \frac{1}{\sqrt{1+4Q^2\frac{\Delta w^2}{w_o^2}}} \tag{C.6}$$

where $\Delta w = w - w_o$ and the phase of the filter is

$$\theta(w) = -\tan^{-1}(2Q\frac{\Delta w}{w_o}) \tag{C.7}$$

Both the amplitude and the phase of a single-tuned with Q of 60 and center frequency of 10MHz are plotted in Fig.C.2.

C.1.2 Synchronously-tuned BPF

There are several ways to implement the high order resonant BPF. Synchronously-tuned filters are the most basic filter type and the easiest to construct and align. They are realized by cascading a number of single-tuned filters with each filter having the same center frequency and Q. Each filter must be isolated from the previous stage, for example a buffer is placed between each stage.

The overall Q of an n^{th} order synchronously-tuned BPF

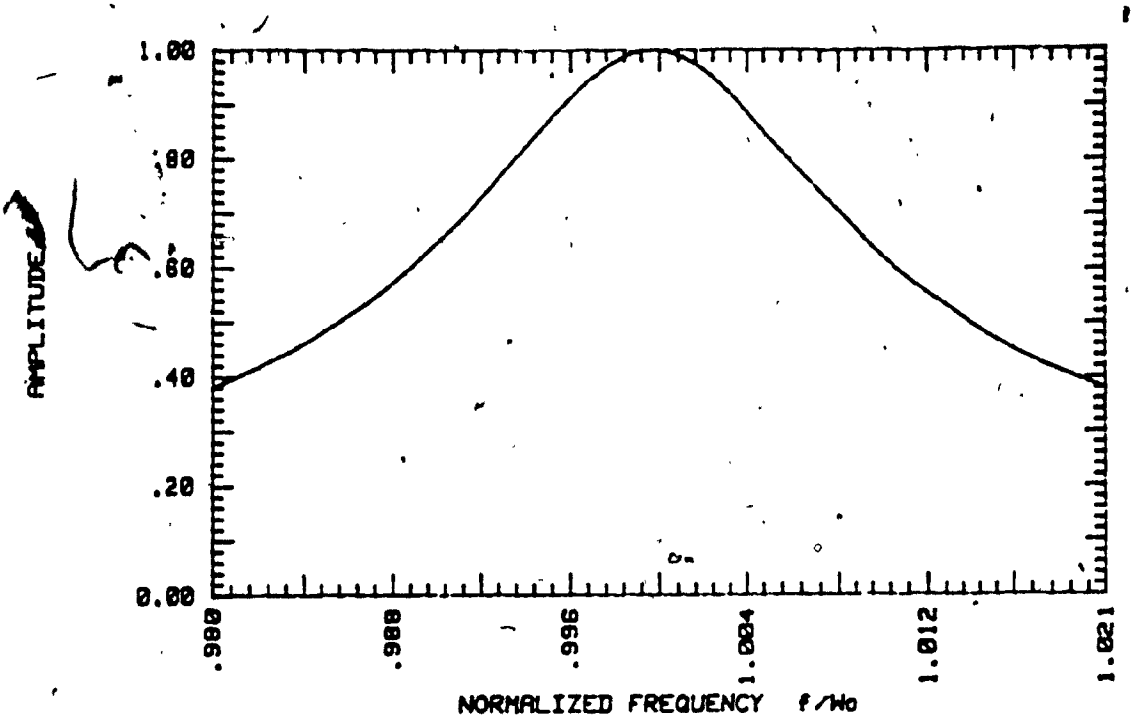

(a) Amplitude response

(b) Phase response

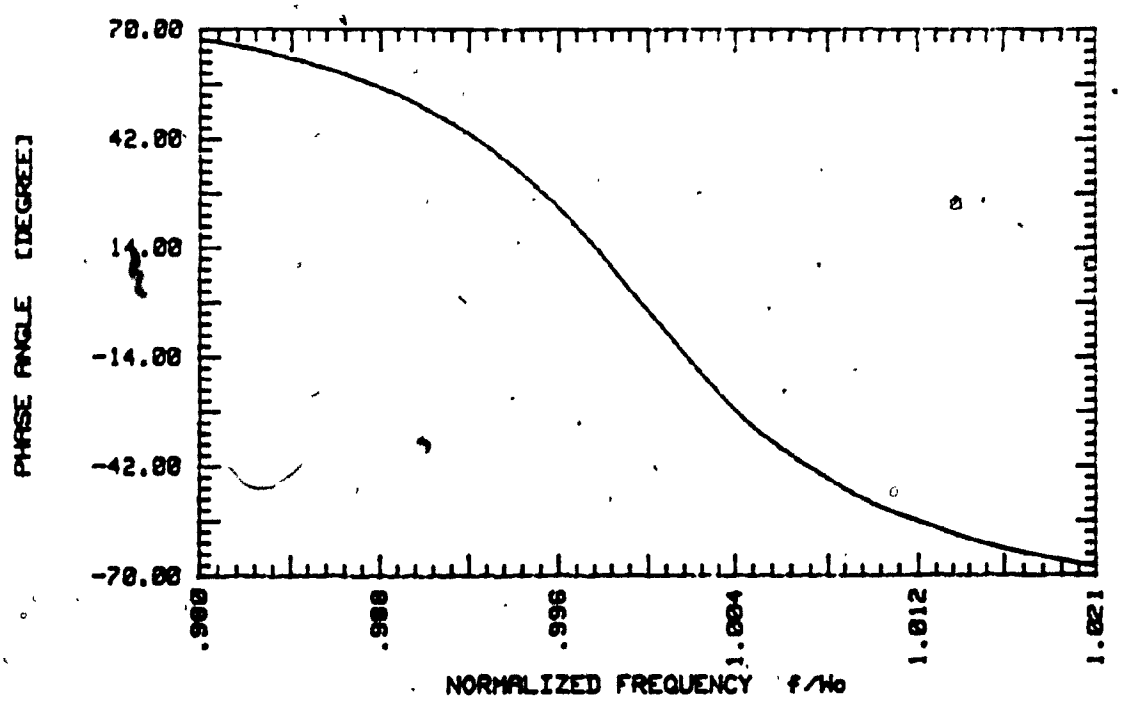

Fig. C.2: Frequency response of a single-tuned BPF with Q=60, center frequency=10MHz

is given by [29]

$$Q_{overall} = \frac{1}{\sqrt{2^{\frac{1}{n}}-1}} Q_{stage} \tag{C.8}$$

where

$$Q_{stage} = \frac{w_o}{BW_{3dB}} \tag{C.9}$$

From Eq.(C.8), the overall 3dB bandwidth can be found as

$$BW_{overall} = \sqrt{2^{\frac{1}{n}}-1}\, BW_{3dB} \tag{C.10}$$

The one-sided noise equivalent bandwidth for high Q case is calulated by

$$B_N = 2\int_0^{\infty} \left[\frac{w_c^2}{(2\pi f)^2+w_c^2}\right]^n df = \frac{(-1)^{n-1}\sqrt{\pi}\,\pi}{2(n-1)!\,\Gamma(1/2-n+1)} B_{3dB} \tag{C.11}$$

where $w_c=\pi B_{3dB}$ is the cutoff frequency of each stage. $\Gamma(x)$ is Gamma function of x.

Figs.C.3 and C.4 show the transient response of a single-tuned and double-tuned BPF due to a phase step and frequency step. It is noted that the phase error is zero with respect to a phase step input, whereas the phase error is resulted for a frequency step input because of the steep slope phase response of the filter. Besides, the phase error is doubled in case of the double-tuned BPF whose noise bandwidth is half of the single-tuned BPF.

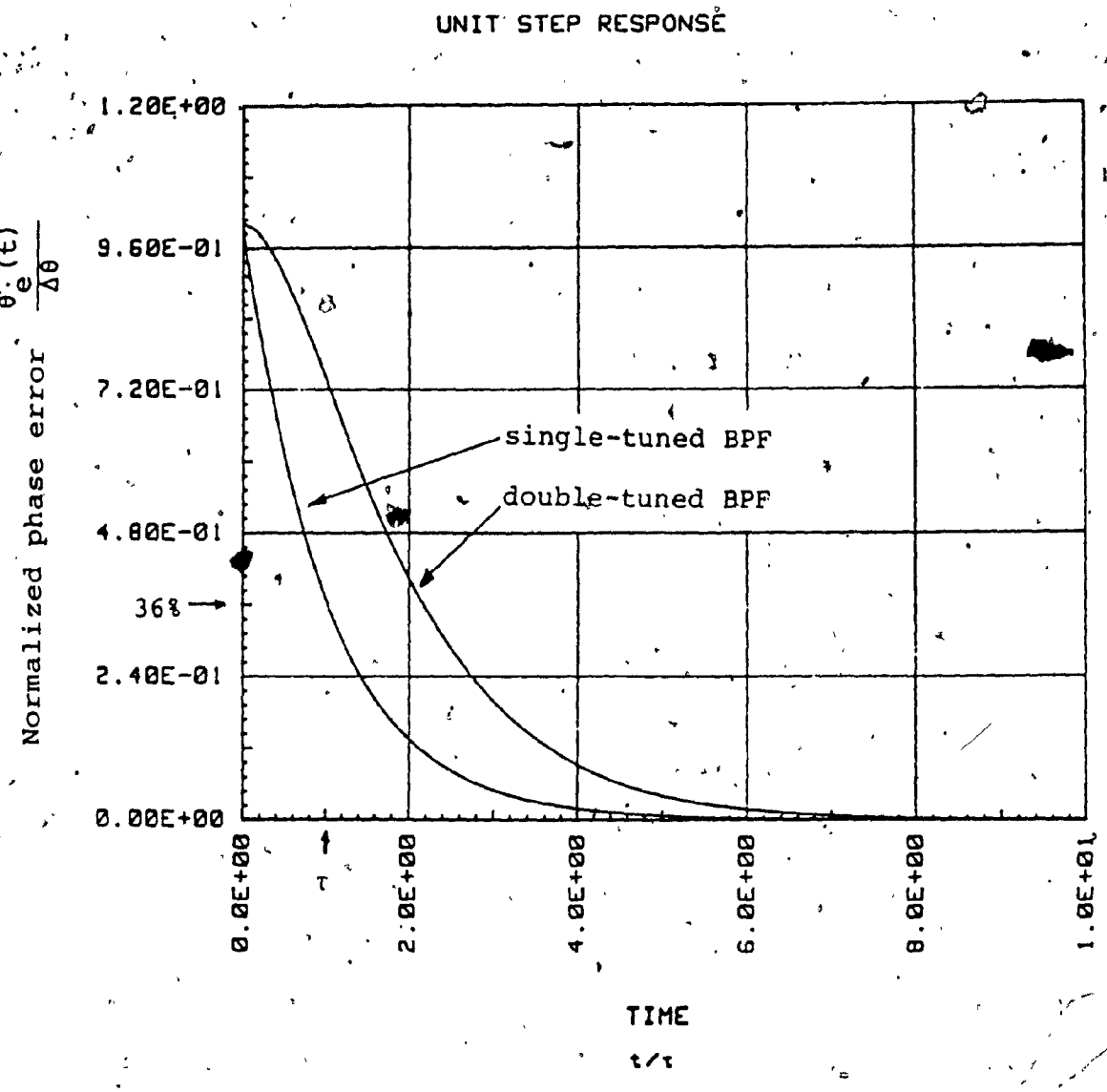

Fig. C.3: Calculated phase step transient phase error of a single-tuned BPF and a double-tuned BPF.

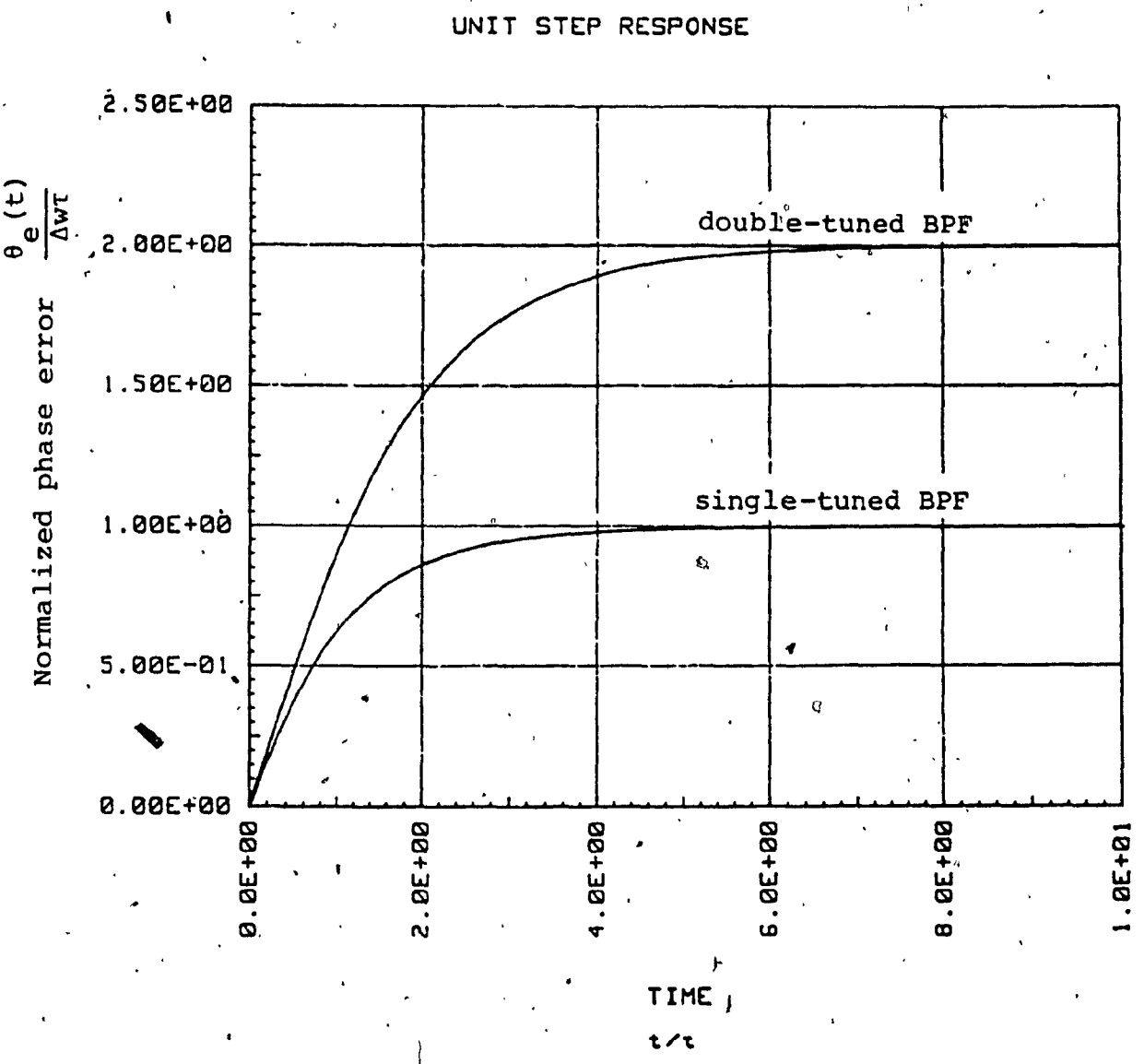

Fig. C.4: Calculated frequency step transient phase error of a single-tuned BPF and a double-tuned BPF

C.2 Characteristics of SAW BPF

A digital BPF is employed in the discrete FTF, which is known as Surface Wave Acoustic (SAW) filter, belonging to a class of filters called transversal filters [26]. In terms of digital filter terminology, transversal filters are also known as non-recursive or moving average filters [27]. Filtering of the transversal filter is achieved by passing the input signal through a number of attenuated delay paths and adding these delayed signals. A schematic diagram of this filter is shown in Fig.C.5. The filter consists of N taps separated by delays and each tap is attenuated by a coefficient a_n. The total delay of the transversal filter is equal to the sum of each delay element T_n. The number of delays and the coefficients determine the desired passband, stopband and the rolloff of the frequency response of the filter.

The output Y(k) of the transversal filter is given as

$$Y(k) = \sum_{n=0}^{N-1} a_n X(k-n) \qquad (C.12)$$

and using the z-transform, the transfer function of the filter is found as

$$F(z) = \sum_{n=0}^{N-1} a_n z^{-n} \qquad (C.13)$$

Taking $z^{-(N-1)}$ out and factorizing the polynomial of

Eq.(C.13), it yields

$$F(z) = z^{-(N-1)} \prod_{i=0}^{N-1} z - z_i \qquad (C.14)$$

Therefore, the transfer function of a transveral filter depends solely on its zeros. If a symmetrical restriction of the coefficients is imposed such that

$$a_n = a_{N-1-n} \qquad (C.15)$$

the frequency response of this filter is as summarized in Table C.1. It is clearly seen that the phase of the symmetrical transversal filter is a linear function of the angular frequency w. Three special cases

1) apodized coefficient [sin(k/2)]/(k/2),
2) apodized coefficient [sin(k/6)]/(k/6) and
3) normalized uniform coefficient

are illustrated in Figs.C.6-8. Their corresponding frequency response are also plotted in both linear and logarithmic scale in Figs.C.9-11. The case of apodized coefficient has better rolloff and rejection in the stopband. These three cases illustrate that the characteristics of the frequency response of the transversal filter depend on the number of taps and coefficients.

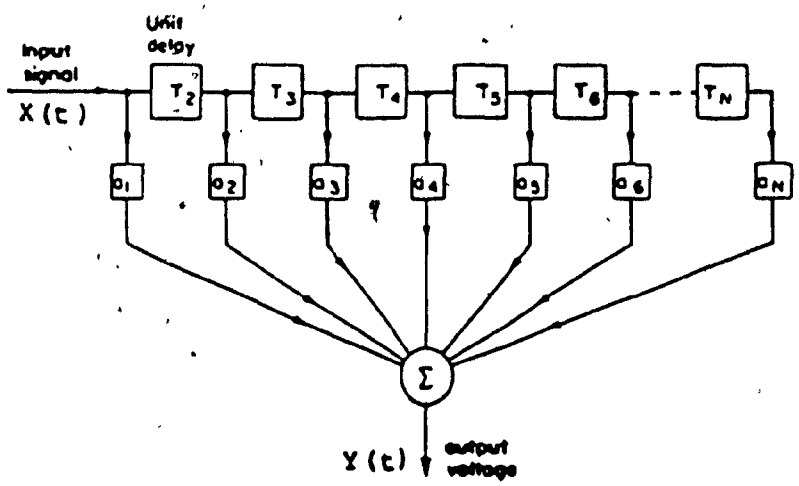

Fig.C.5: Schematic diagram of a transversal filter

N	$F(e^{jwT})$
odd	$e^{-jw(N-1)T/2} \sum_{k=0}^{(N-1)/2} b_k \cos wkT$
even	$e^{-jw(N-1)T/2} \sum_{k=1}^{N/2} c_k \cos[w(k-1/2)T]$
where $b_o = a[\frac{(N-1)T}{2}]$ $b_k = 2a[(\frac{N-1}{2}-k)]$ $c_k = 2a[(\frac{N}{2}-k)T]$	

Table C.1: Frequency response of symmetrical transversal filter

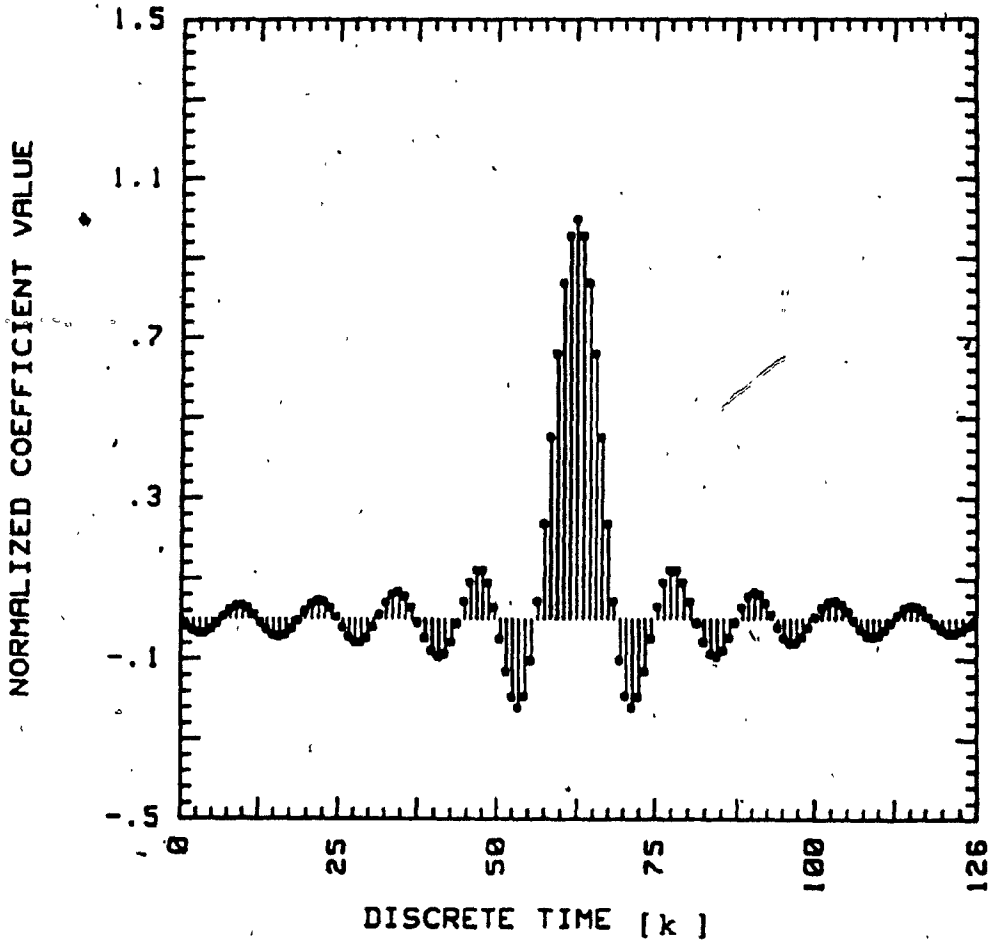

Fig. C.6: The apodized coefficient value [sin(k/2)]/(k/2) of a SAW BPF with 127 taps

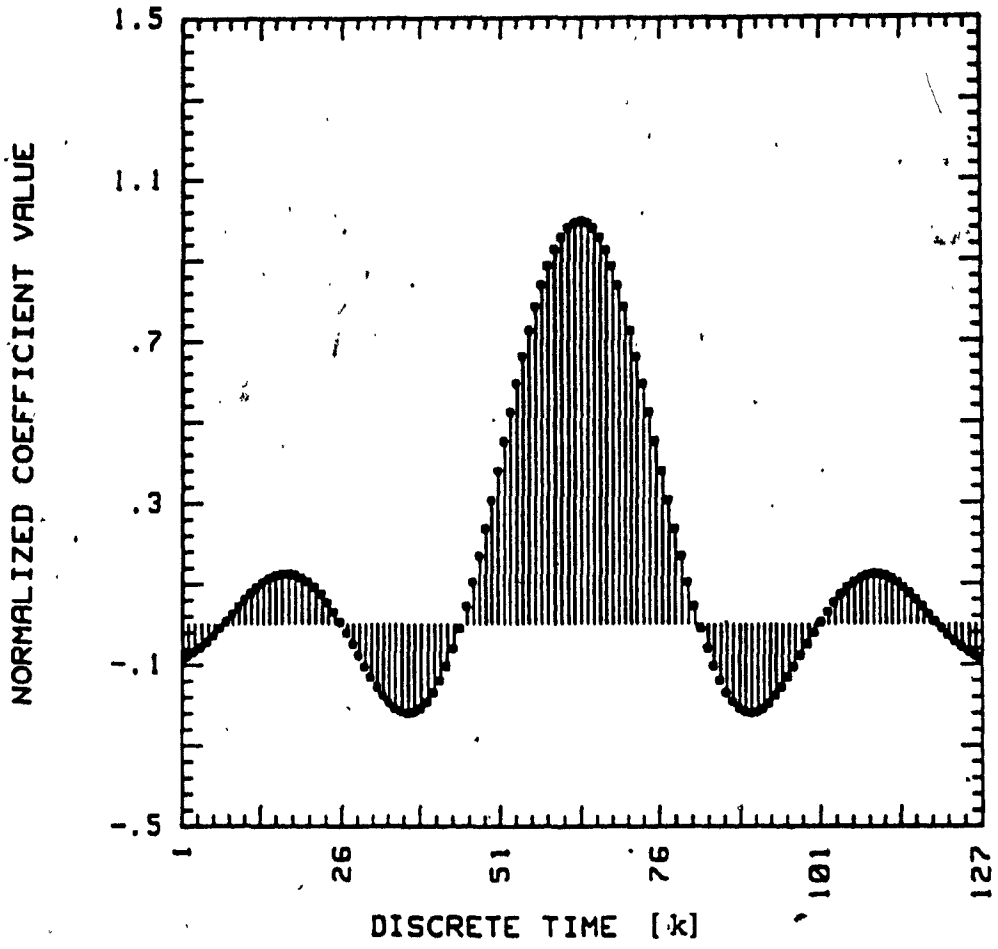

Fig. C.7: The apodized coefficient value, [sin(k/6)]/(k/6) , of a SAW BPF with 127 taps

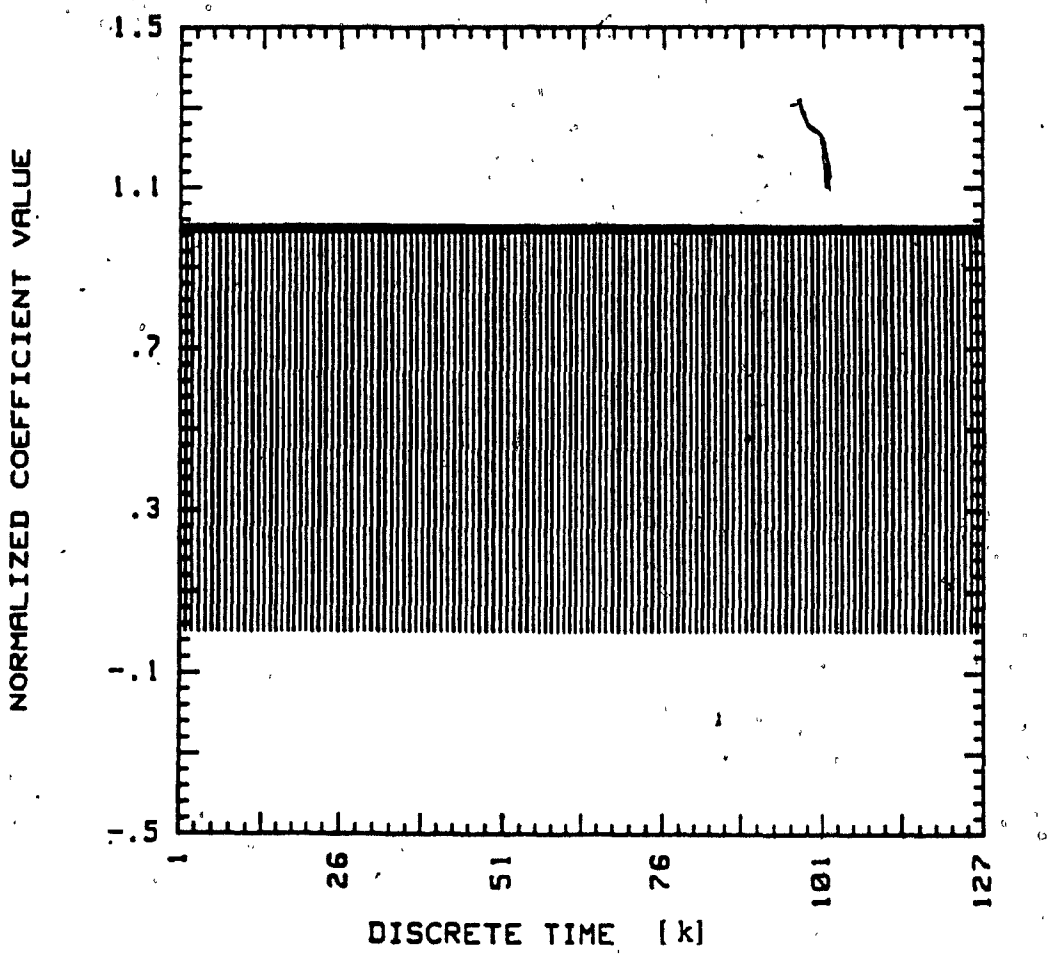

Fig. C.8: The uniform coefficient value of a SAW BPF with 127 taps

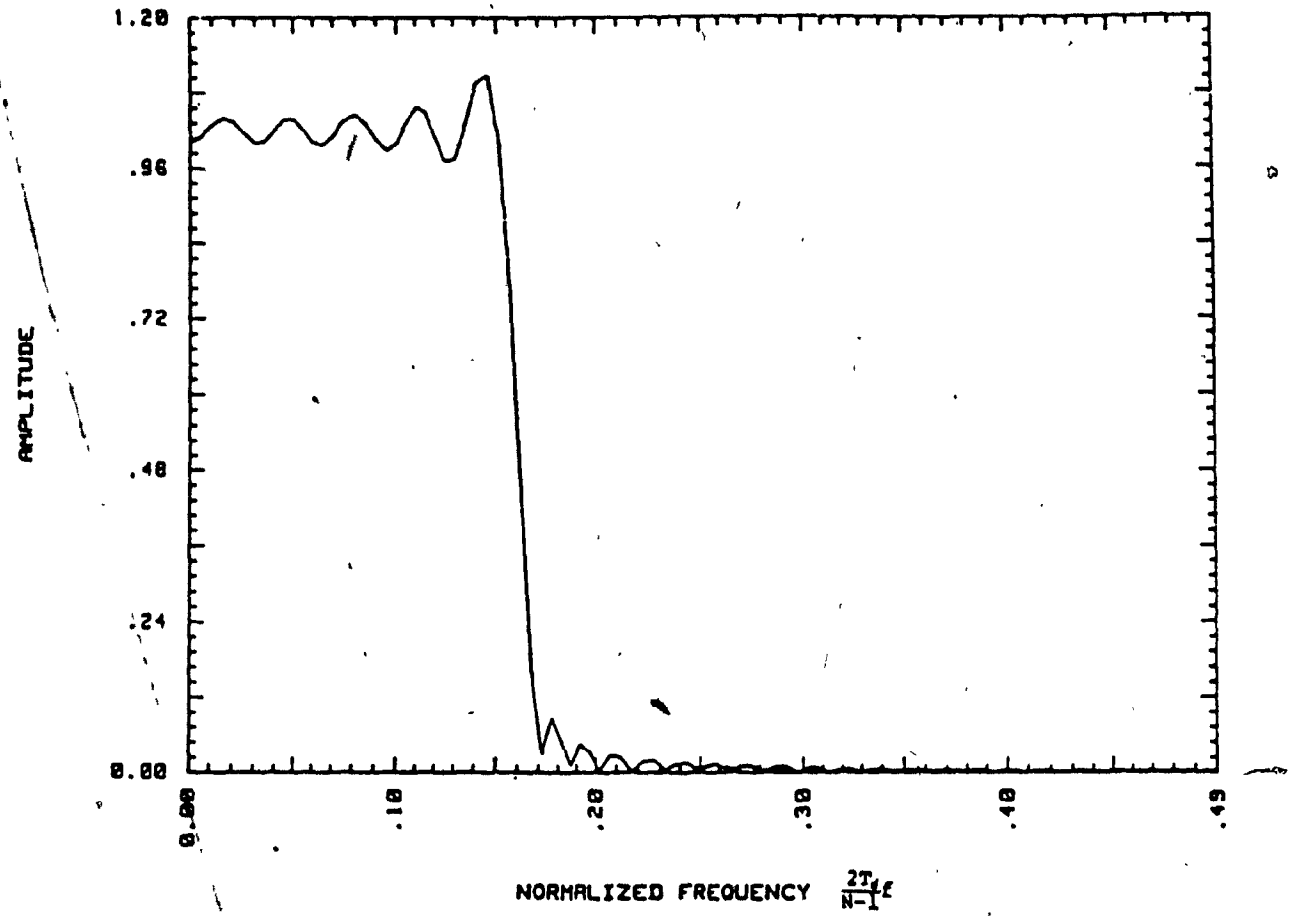

Fig. C.9: Amplitude response (linear scale) of a SAW BPF with coefficient values of Fig. C.6

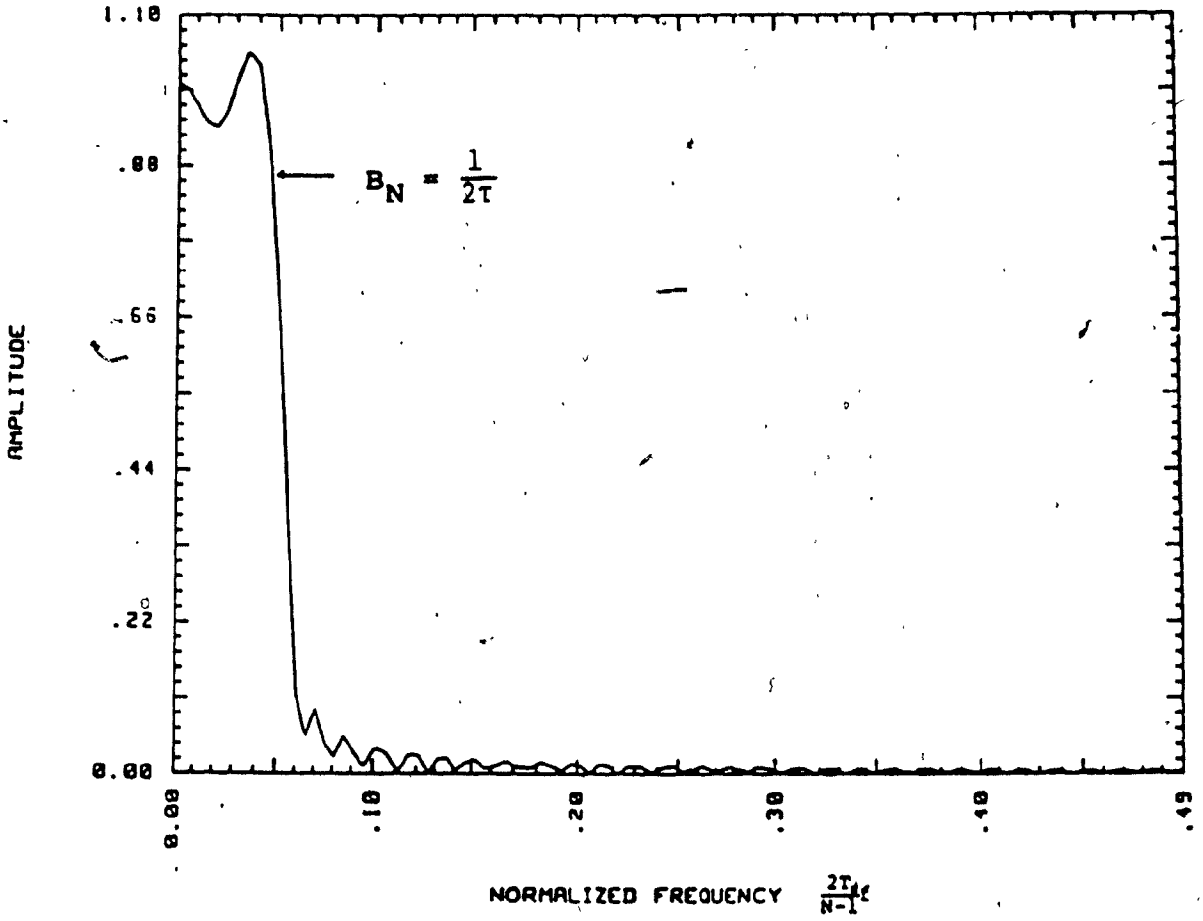

Fig. C.10: Amplitude response (linear scale) of a SAW BPF with coefficient values in Fig. C.7

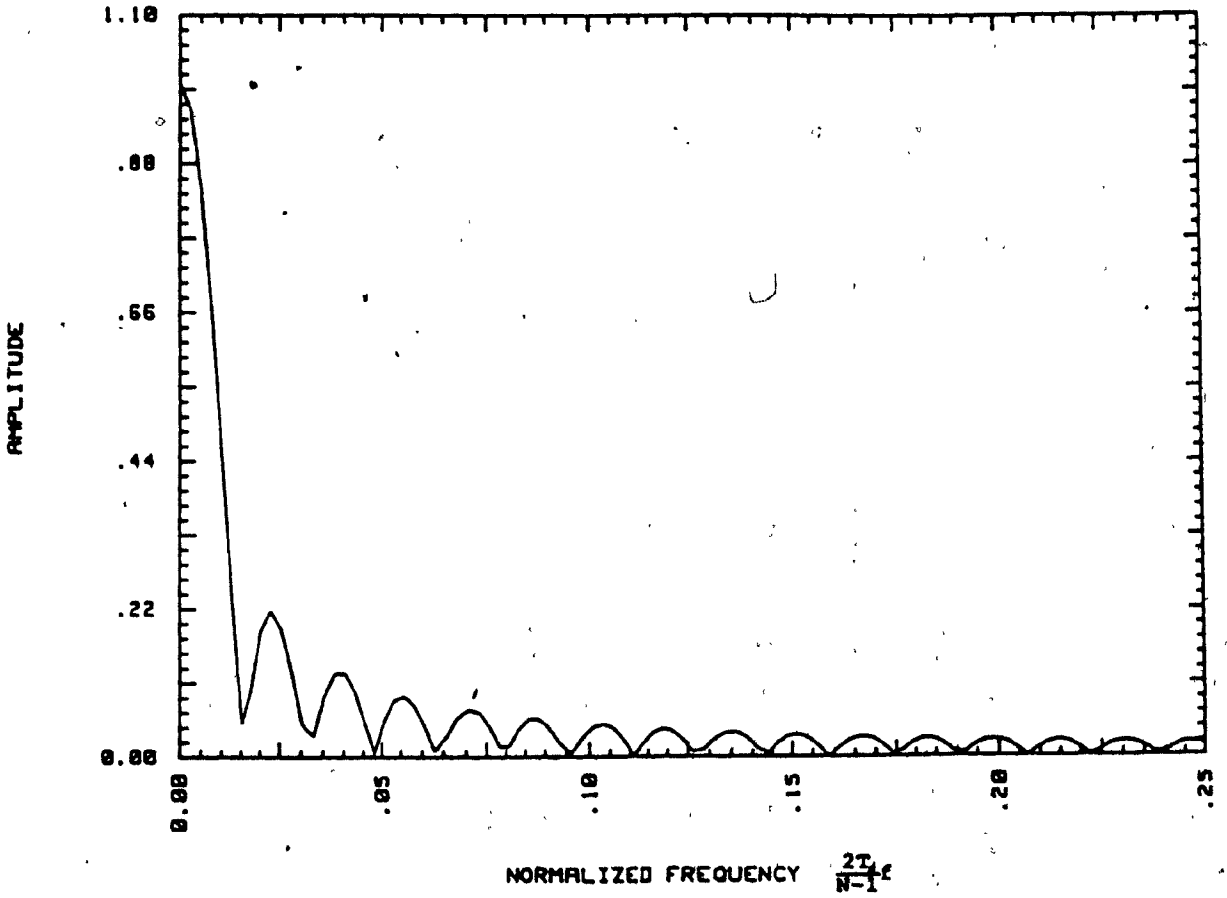

Fig. C.11: Amplitude response (linear scale) of a SAW BPF with coefficient values in Fig. C.8

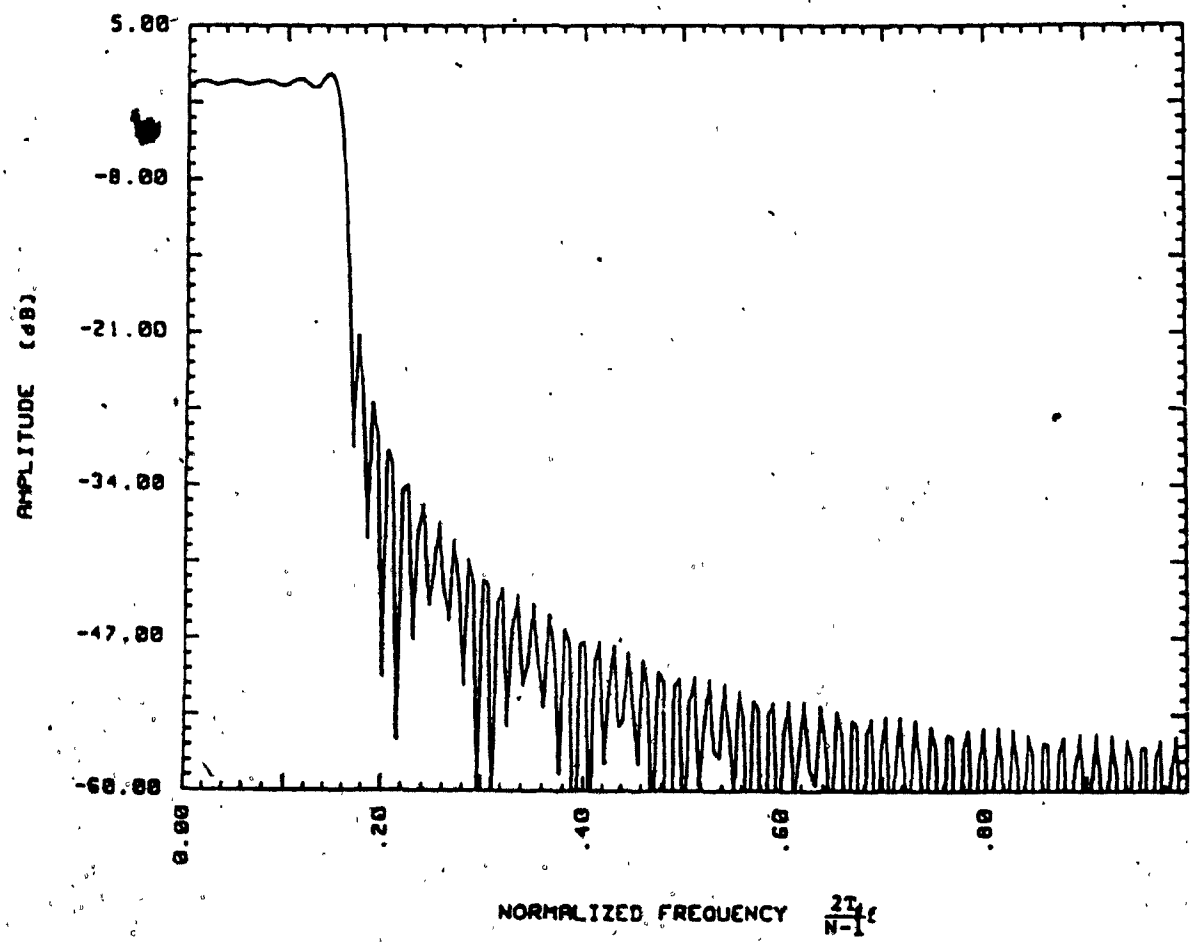

Fig. C.12: Amplitude response (log scale) of a SAW BPF with coefficient values in Fig. c.6

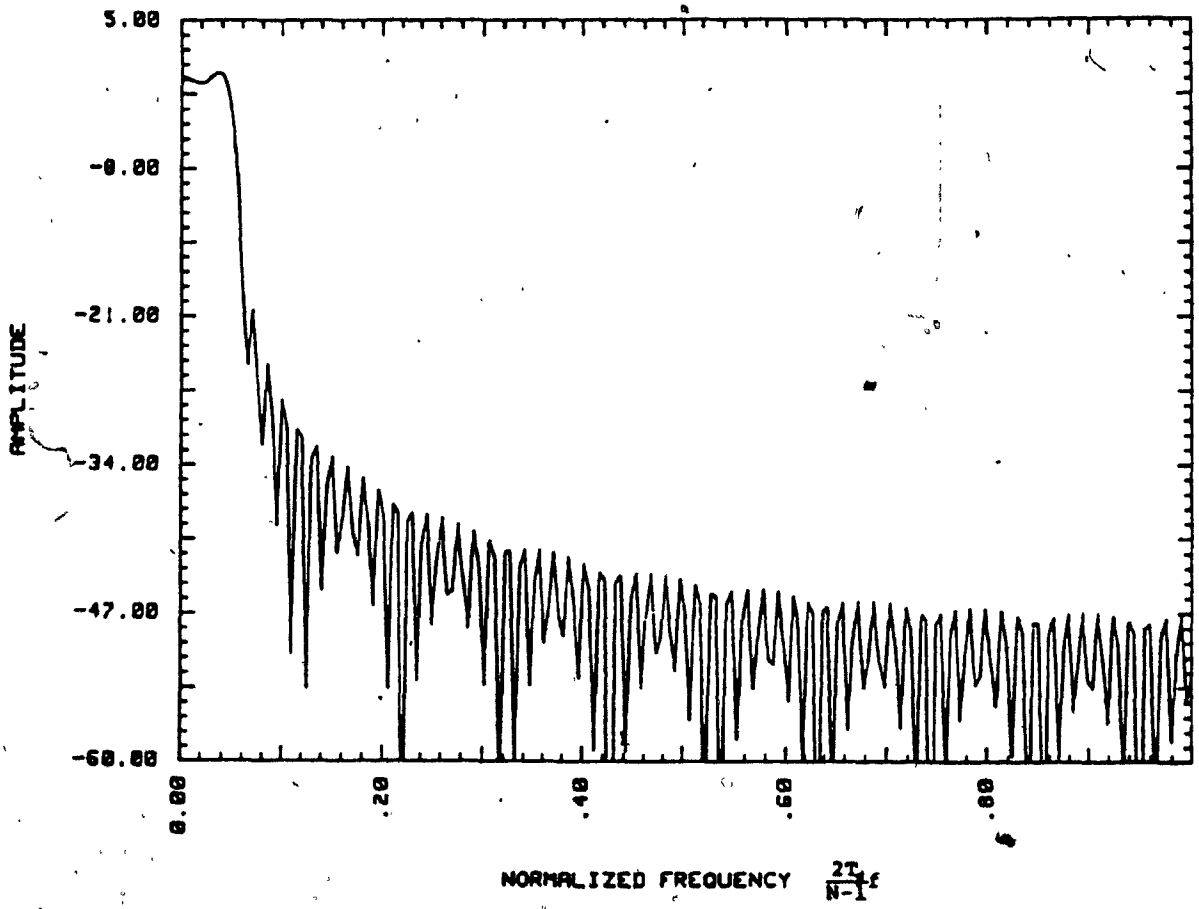

Fig. C.13: Amplitude response (log scale) of a SAW BPF with coefficient value in Fig. C.7

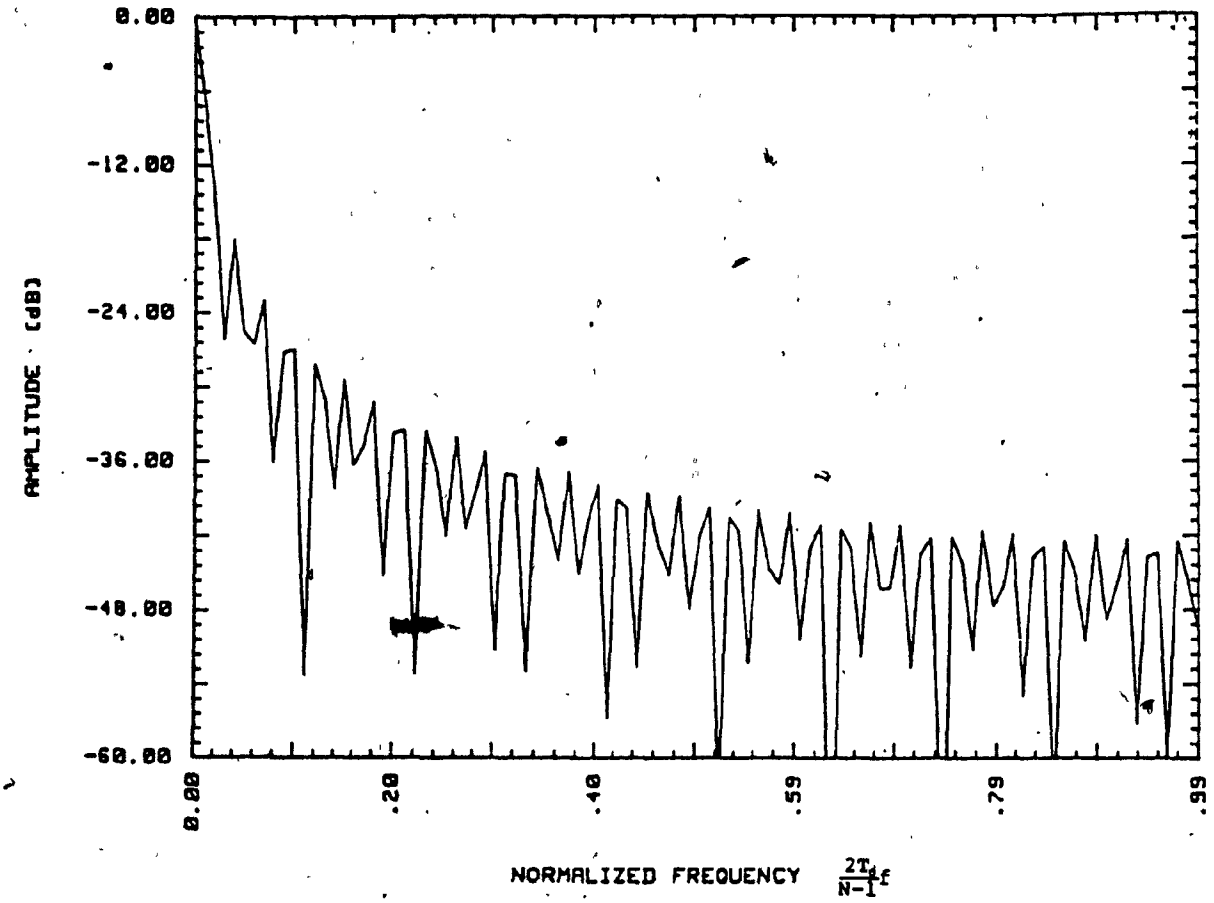

Fig. C.14: Amplitude response (log scale) of a SAW BPF with coefficient values in Fig. C.8

APPENDIX D

EXPERIMENTAL SET-UP

The experimental set-ups to measure the steady-state and transient responses of the FTF are described briefly in this appendix.

Fig.D.1 illustrates the practical realization of the discrete FTF. Limiters are used to eliminate the amplitude variation of the input signal. The amplifier in the BPF block (dotted line) is necessary to compensate the insertion loss of the passive SAW BPF in order to have the desired unity gain. The lowpass filter followed the second BPF block is used to filter out the harmonics due to the amplification. The other lowpass filter after the multiplier, for the same reason, is used to eliminate the harmonics resulted from the nonlinear operation of the multiplier.

The single-tuned FTF has the same block diagram as in Fig.D.1 except that the BPF block is replaced by the single-tuned BPF in Fig.D.2. Cascading the single-tuned BPF and substituting into the BPF block, higher order FTF is obtained. Some minor modifications of the block diagram shown in Fig.D.1 have to be carried out in order to have satisfactory performance. Those modifications, for example, are the attentuation pads and the amplifier gain.

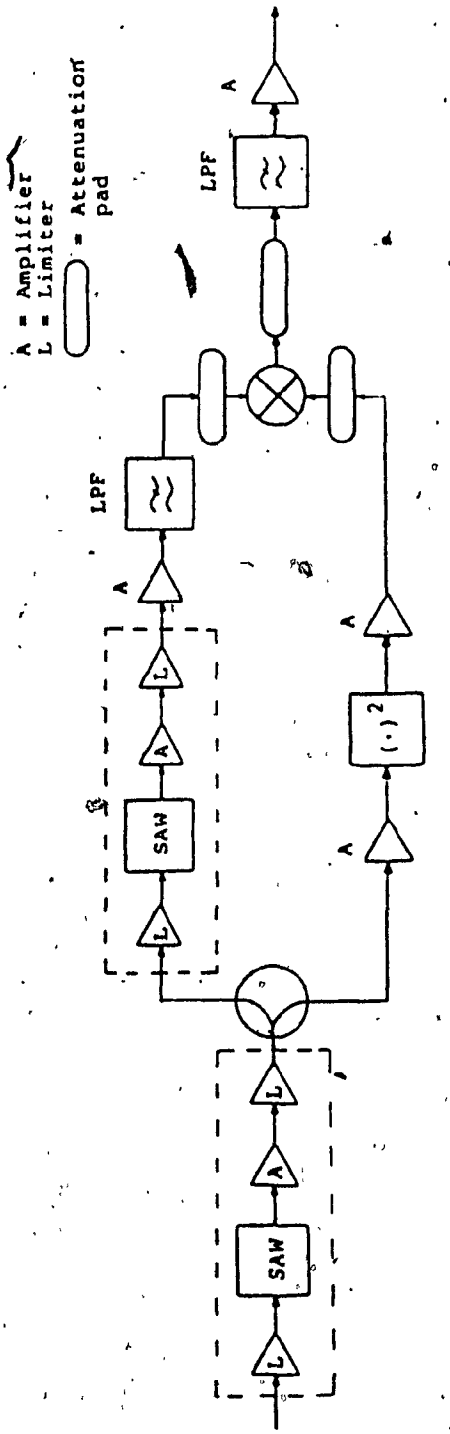

Fig. D.1: Experimental set-up of a discrete FTF using SAW BPF's

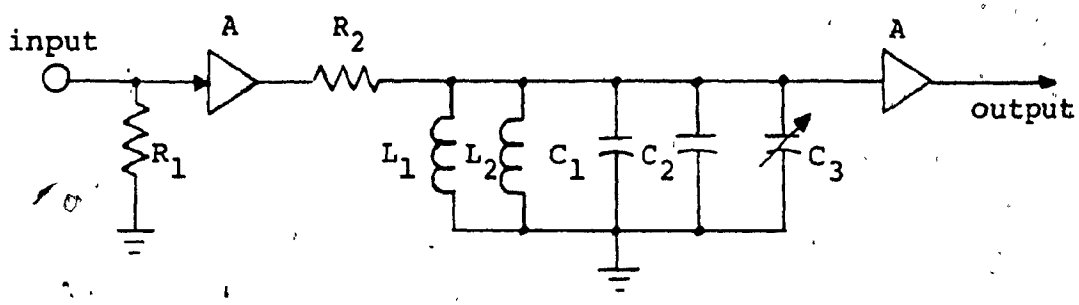

Fig. D.2: Schematic diagram of an experimental single-tuned BPF

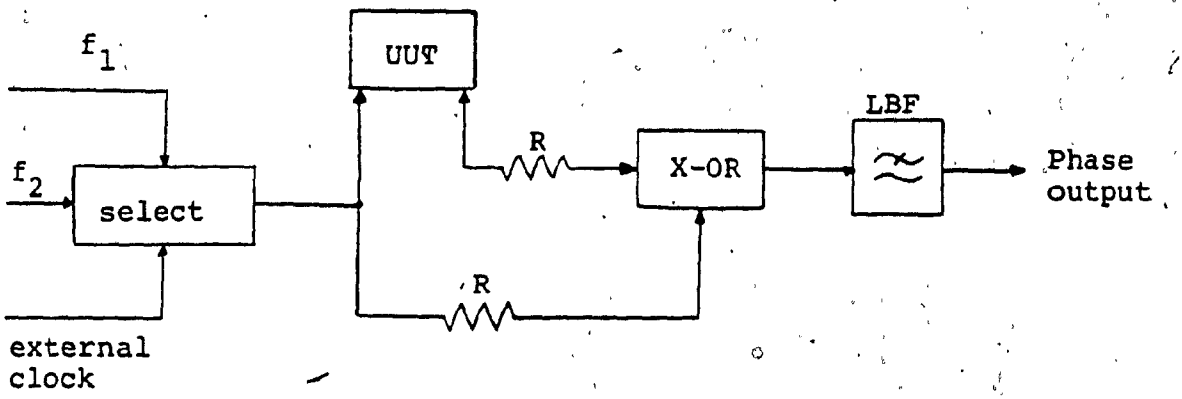

Fig. D.3: Schematic diagram of the transient test-jig

A test-jig is constructed for the purpose of measuring the phase transient response of the FTF. In general, this test-jig shown in Fig.D.3 can be used to measure the transient response of any device. It can be seen that two inputs are fed and selected by a switch controlled by an external clock. These inputs are splitted and processed by a unit under test (UUT) and a resistive path. The resistive path without any phase alternation is used as a reference to compare with the output of the UUT. The output of the phase detector (an exclusive-OR gate) is the result of the comparison and is equivalently the phase difference between the input and output of the UUT. The exclusive-OR gate is chosen so as to have a linear characteristics of the phase difference of the input and output of the UUT. A lowpass filter follows the phase detector to filter the harmonics. The bandwidth of this filter cannot be too narrow, otherwise the transient time required for this filter may be incorporated into the measured transient response, as a result an inaccurate measurement is obtained.

Figs.D.4 and D.5 show the use of the test-jig to measure the phase and frequency step transient response of the FTF.

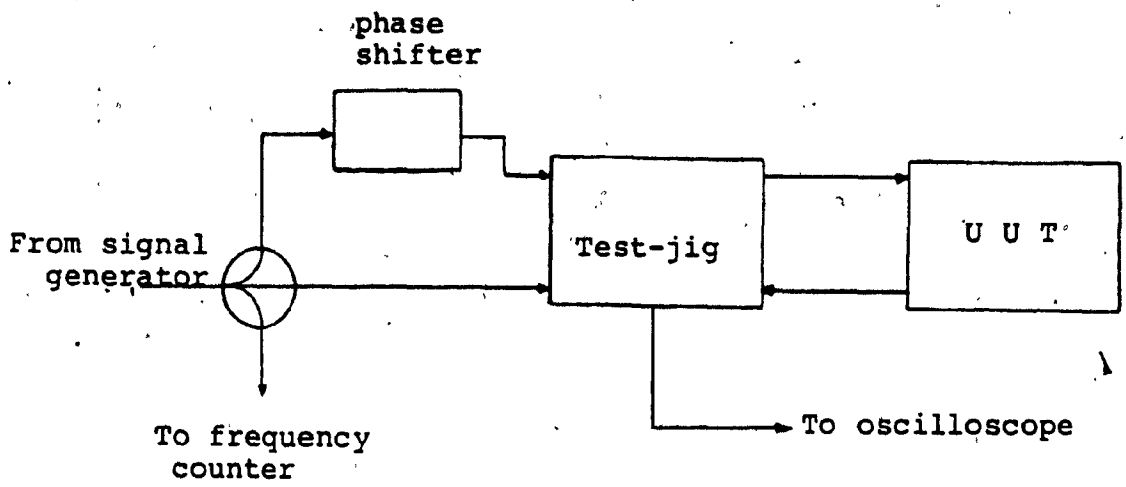

Fig. D.4: Set-up for phase step transient measurement

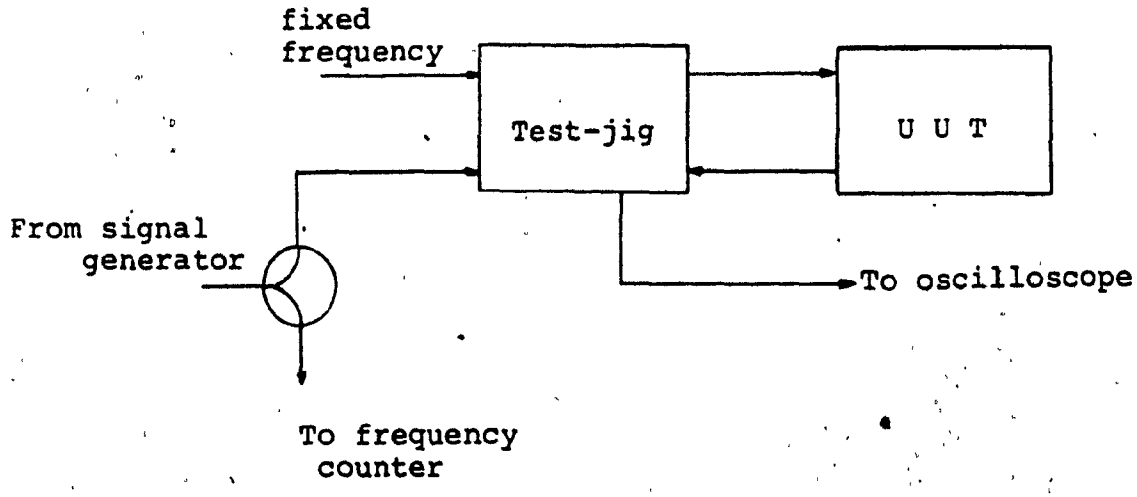

Fig. D.5: Set-up for frequency step transient measurement